QA: QA

Civilian Radioactive Waste Management System
Management & Operating Contractor

Waste Package Degradation Process Model Report

TDR-WIS-MD-000002 REV 00 ICN 01

June 2000

Prepared for:

U.S. Department of Energy
Yucca Mountain Site Characterization Office
P.O. Box 30307
North Las Vegas, Nevada 89036-0307

Prepared by:

TRW Environmental Safety Systems Inc.
1180 Town Center Drive
Las Vegas, Nevada 89144-6352

WM-11
NM5507

Under Contract Number
DE-AC08-91RW00134

DISCLAIMER

This report was prepared as an account of work sponsored by an agency of the United States Government. Neither the United States Government nor any agency thereof, nor any of their employees, nor any of their contractors, subcontractors or their employees, makes any warranty, express or implied, or assumes any legal liability or responsibility for the accuracy, completeness, or any third party's use or the results of such use of any information, apparatus, product, or process disclosed, or represents that its use would not infringe privately owned rights. Reference herein to any specific commercial product, process, or service by trade name, trademark, manufacturer, or otherwise, does not necessarily constitute or imply its endorsement, recommendation, or favoring by the United States Government or any agency thereof or its contractors or subcontractors. The views and opinions of authors expressed herein do not necessarily state or reflect those of the United States Government or any agency thereof.

AMRs Supporting the Waste Package Degradation PMR

AMR	I.D.	Document Number
Aging and Phase Stability of Waste Package Outer Barrier	W0020	ANL-EBS-MD-000002 Rev.00
General Corrosion and Localized Corrosion of Waste Package Outer Barrier	W0035	ANL-EBS-MD-000003 Rev.00
Abstraction of Models for Pitting and Crevice Corrosion of Drip Shield and Waste Package Outer Barrier	W0040	ANL-EBS-PA-000003 Rev.00
Abstraction of Models of Stress Corrosion Cracking of Drip Shield and Waste Package Outer Barrier and Hydrogen Induced Corrosion of Drip Shield	W0045	ANL-EBS-PA-000004 Rev.00
WAPDEG Analysis of Waste Package and Drip Shield Degradation	W0050	ANL-EBS-PA-000001 Rev.00
FEPs Screening of Processes and Issues in Drip Shield and Waste Package Degradation	W0055	ANL-EBS-PA-000002 Rev.00
Environment on the Surfaces of the Drip Shield and Waste Package Outer Barrier	W0070	ANL-EBS-MD-000001 Rev.00
Analysis of Mechanisms for Early Waste Package Failure	W0075	ANL-EBS-MD-000023 Rev.01
General Corrosion and Localized Corrosion of the Drip Shield	W0085	ANL-EBS-MD-000004 Rev.00
Stress Corrosion Cracking of the Drip Shield, the Waste Package Outer Barrier and the Stainless Steel Structural Material	W0095	ANL-EBS-MD-000005 Rev.00
Hydrogen Induced Cracking of Drip Shield	W0105	ANL-EBS-MD-000006 Rev.00
Degradation of Stainless Steel Structural Material	W0115	ANL-EBS-MD-000007 Rev.00
Abstraction of Models for Stainless Steel Structural Material Degradation	W0120	ANL-EBS-PA-000005 Rev.00
Incorporation of Uncertainty and Variability of Drip Shield and Waste Package Degradation in WAPDEG Analysis	W0140	ANL-EBS-MD-000036 Rev.00

Civilian Radioactive Waste Management System
Management & Operating Contractor

Waste Package Degradation Process Model Report

TDR-WIS-MD-000002 REV 00 ICN 01

June 2000

Prepared by:

V. Pasupathi, PMR Lead
Waste Package Materials

6/16/00
Date

Checked by:

M.J. Plinski
Waste Package Department

6/16/00
Date

Approved by:

David Stahl, Manager
Waste Package Materials

6/16/00
Date

AUTHORS

Process Model Report Leads

J.C. Farmer
V. Pasupathi

Process Model Report

J.C. Farmer
T.E. Summers
D.E. Shoesmith
G.M. Gordon
G. Gdowski
S. Lu
P.L. Andresen
P. Macheret

FEPs and Model Abstractions

J.H. Lee
B.E. Bullard
K.G. Mon

Support Sections

V. Pasupathi
J.C. Farmer
A.M. Haghi
G.C. De

INTENTIONALLY LEFT BLANK

CHANGE HISTORY

Revision Number	Interim Change Number (ICN)	Description of Change
00	00	Initial issue
00	01	Substantive technical changes are limited to Section 3.1.7 (stress corrosion cracking) and WAPDEG Analysis (Sections 3.2.1, 3.2.4, and 3.2.5) results. Stress threshold and uncertainty ranges in the stress corrosion cracking model were changed in response to DOE review comments. Minor changes are primarily nontechnical editorial changes throughout the document including reference citations and clarification statements. Changes are designated by a change bar in the right margin.

INTENTIONALLY LEFT BLANK

EXECUTIVE SUMMARY

A crucial element of the long-term postclosure safety strategy for the potential monitored geologic repository at Yucca Mountain is to contain high-level radioactive waste (HLW), and to keep that waste and its container as dry as possible. This report is one of nine Process Model Reports (PMRs) developed to address the technical basis supporting the Total System Performance Assessment (TSPA) model. These PMRs are supported by Analysis and Model Reports (AMRs) that contain more detailed technical information.

The waste package (WP) is a major component of the engineered barrier system (EBS) and contributes to isolation of HLW during the preclosure and postclosure periods. It also reduces the uncertainties associated with performance of the repository. As a result, the integrity of the WP and the drip shield (DS) have been designated as "Principal Factors" important to the repository safety strategy. The WP, protected by a DS, will be subjected to degradation processes in the repository that will eventually impact postclosure performance. Some of the important conditions contributing to WP degradation include: humidity and temperature in the emplacement drift; chemistry of the dripping water; and the corrosion susceptibility of the WP materials. Eight process-level models or analyses, four abstraction models, and two engineering calculations were developed and documented in individual AMRs or Calculations. This PMR provides a summary of process-level and abstraction models, as well as a summary of their utilization in the integrated WP degradation model contained in the WAPDEG code.

This report also includes discussions on the features, events, and processes (FEPs) relevant to the performance of the WP materials. These FEPs that are deemed important to repository performance are evaluated, either as components for the TSPA, or as separate analyses in the AMRs.

In addition to describing the process-level and abstraction models, this PMR addresses two of the Key Technical Issues (KTIs) in the Issue Resolution Status Report (IRSR) prepared by the U.S. Nuclear Regulatory Commission (NRC). These issues are the Container Life and Source Term (CLST) and the TSPA and Integration (TSPAI). Several subissues that relate directly to the WP are discussed in this PMR, along with the approach used by the Yucca Mountain Site Characterization Project (YMP) to meet the acceptance criteria for each of the KTIs.

This PMR also addresses relevant issues identified by other agencies and organizations, including the Nuclear Waste Technical Review Board (NWTRB).

The integrated WP model incorporated into the WAPDEG code was used to develop the results documented here. The analyses have shown that both the DS and WPs do not experience significant failures within the regulatory time period (10,000 years).

The materials selected for the DS and WP outer barrier, Titanium Grade 7 and Alloy 22, respectively are highly corrosion resistant under the repository exposure conditions. Both the DS and WP degrade by general corrosion (GC) at very low rates. However, degradation modes such as localized corrosion (LC) (pitting and crevice corrosion), stress corrosion cracking (SCC), and hydrogen-induced cracking (HIC) could lead to premature failure of the WP or DS, if any degradation is initiated. Fortunately, the selected materials appear to be immune to LC under

repository-relevant conditions. With appropriate processing, the initiation of SCC and HIC (in the case of Titanium Grade 7) are delayed to a point where acceptable repository performance is achieved. To preclude SCC, post-weld stress mitigation processes will be implemented on the closure welds of the dual-closure-lid WP. The compressive layer that is needed to preclude SCC is produced by either one of two post-weld stress mitigation processes, laser peening or localized induction annealing. The life of the WP is determined by the time required to remove the mitigated layer of material at each weld by GC.

CONTENTS

CONTENTS (Continued)

FIGURES

FIGURES (Continued)

Page

FIGURES (Continued)

Page

FIGURES (Continued)

Page

FIGURES (Continued)

Page

FIGURES (Continued)

Page

TABLES

INTENTIONALLY LEFT BLANK

ACRONYMS AND ABBREVIATIONS

AFM	atomic force microscope or microscopy
AMR	Analysis and Model Report
APC	aqueous phase corrosion
ASTM	American Society for Testing and Materials
BSW	basic saturated water
BWR	boiling water reactor
CAM	corrosion allowance material
CDF	cumulative distribution function
CLST	container life and source term
CP	cyclic polarization
CRM	corrosion resistant material
CRWMS	Civilian Radioactive Waste Management System
DCPD	direct current potential drop
DIRS	Document Input Reference System
DIS	Data Inventory Sheet
DOE	U.S. Department of Energy
DOX	dry oxidation or dry air oxidation
DS	drip shield
DTN	data tracking number
EBS	engineered barrier system
EDA	Enhanced Design Alternative
FEP	features, events, and processes
GB	grain boundary
GC	general corrosion
HAC	humid air corrosion
HAZ	heat-affected zone
HIC	hydrogen-induced cracking
HLW	high-level radioactive waste
IRSR	Issue Resolution Status Report
J-13	Water from Well No. J-13
KTI	key technical issue
LADS	license application design selection
LC	localized corrosion
LLNL	Lawrence Livermore National Laboratory

ACRONYMS AND ABBREVIATIONS (Continued)

LRO	long-range order (or ordering)
LTCTF	Long-Term Corrosion Test Facility
M	molarity
MIC	microbiologically influenced corrosion
M&O	Management and Operating Contractor
N	normality
NDE	nondestructive examination or evaluation
NFE	near-field environment
NG	Nuclear Grade
NRC	U.S. Nuclear Regulatory Commission
NWTRB	Nuclear Waste Technical Review Board
OCRWM	Office of Civilian Radioactive Waste Management
PA	Performance Assessment
PMR	Process Model Report
PND	probability of nondetection
ppm	parts per million
PT	Penetrant testing
QA	Quality Assurance
QARD	Quality Assurance Requirements and Description Document
RH	relative humidity
RT	radiographic testing
SAW	simulated acidic concentrated water
SCC	stress corrosion cracking
SCE	saturated calomel electrode
SCW	simulated concentrated water
SDW	simulated dilute water
SEM	scanning electron microscopy
SNF	spent nuclear fuel
SSW	simulated saturated water
TBD	to be determined
TBV	to be verified
TDMS	Technical Data Management System
TEM	transmission electron microscope
TSPA	Total System Performance Assessment
TSPA-VA	Total System Performance Assessment-Viability Assessment
TTT	time-temperature-transformation diagram

ACRONYMS AND ABBREVIATIONS (Continued)

UNS	Unified Numbering System for Metals and Alloys
UT	ultrasonic testing
UVa	University of Virginia
VPC	vapor phase corrosion
WAPDEG	waste package degradation code
WF	waste form
WP	waste package
WPOB	waste package outer barrier
wt. %	weight percent
XRD	X-ray diffraction
YMP	Yucca Mountain Site Characterization Project
YS	yield stress

INTENTIONALLY LEFT BLANK

1. INTRODUCTION

A crucial element of the long-term postclosure safety strategy for the potential monitored geologic repository at Yucca Mountain is to contain high-level radioactive waste (HLW), and to keep that waste and its container as dry as possible. There are several degradation processes that could impact the performance of the engineered barrier system (EBS). The role of this PMR is to describe one of the process-level models (Waste Package Degradation) utilized to evaluate these degradation processes. To evaluate the postclosure performance of the monitored geologic repository proposed for construction at Yucca Mountain, a Total System Performance Assessment (TSPA) will be conducted. A set of nine Process Model Reports (PMRs), of which this document is one, is being developed to summarize the technical basis for process-level models supporting the TSPA model. These reports cover the following areas:

- Integrated Site Model
- Unsaturated Zone Flow and Transport
- Near-Field Environment (NFE)
- EBS Degradation, Flow, and Transport
- Waste Package Degradation
- Waste Form Degradation
- Saturated Zone Flow and Transport
- Biosphere
- Disruptive Events.

These PMRs are supported by several Analysis and Model Reports (AMRs) that contain more detailed technical information. This technical information consists of data, analyses, models, software, and other documentation necessary to defend the applicability of each model for its intended purpose. The PMR is intended to ensure the traceability of waste package degradation information from its various sources through the AMRs, PMRs, and eventually in TSPA.

As described in the *Monitored Geologic Repository Project Description Document*, the recommended waste package design is *Enhanced Design Alternative II* (CRWMS M&O 1999a, Section 1.1.2).

The Enhanced Design Alternative II (EDA II) waste package design is the reverse of the Viability Assessment (VA) design. In EDA II, the corrosion-resistant material protects the underlying structural material from corrosion, while the structural material supports the thinner, more expensive corrosion-resistant material. As shown in Figure 1-1, this design includes a double-wall waste package (WP) made from Alloy 22 and 316 nuclear grade (NG) stainless steel. The WP is placed underneath a protective drip shield (DS) made of a titanium-based alloy, as shown in Figure 1.2.

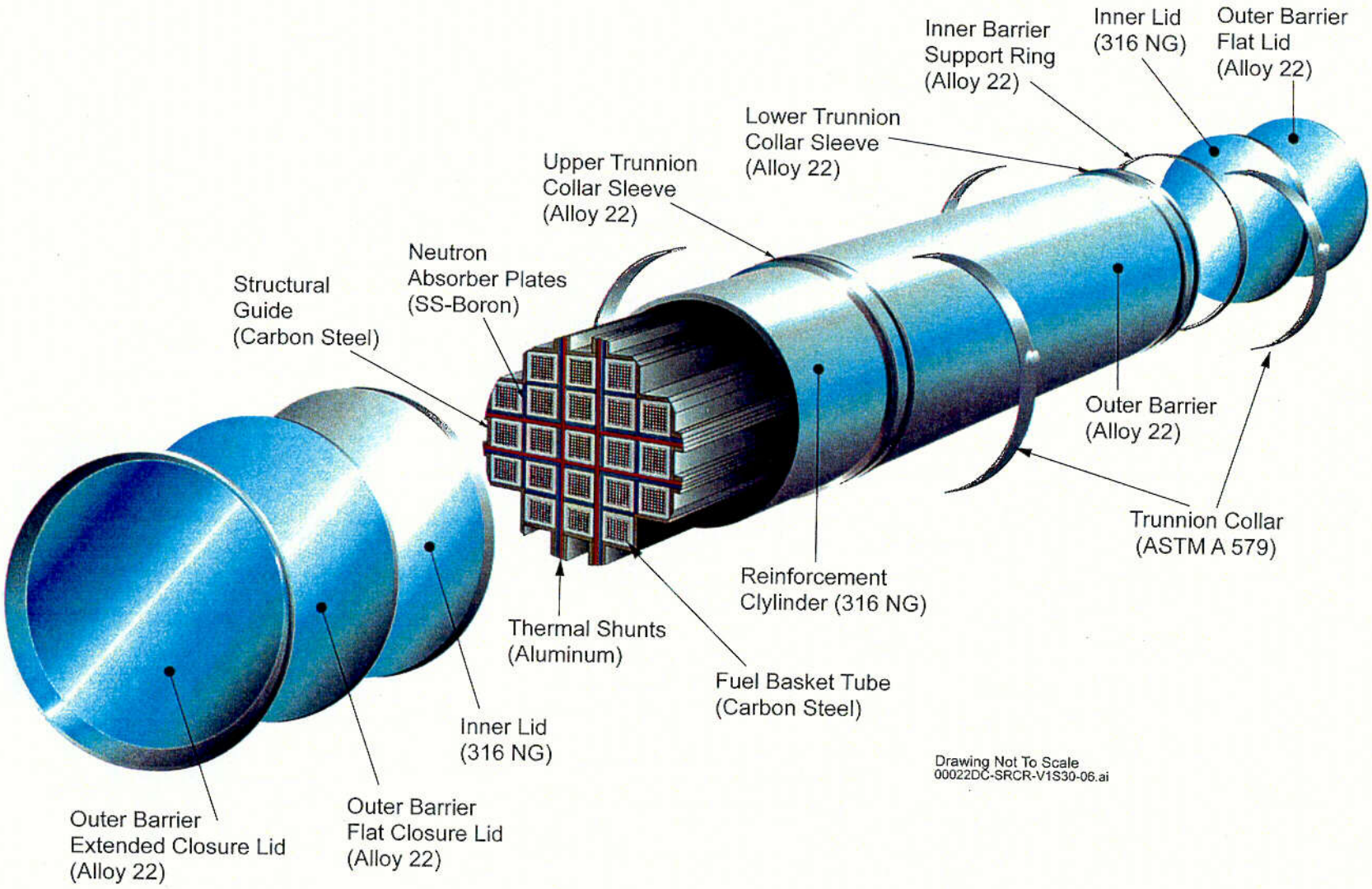

Figure 1-1. Waste Package

EDA II uses thermal management features (line loading, ventilation, and blending) to limit peak temperatures of cladding, the waste package shell, and the drift wall. This produces more uniform temperature along the drifts, and margin in meeting requirements for cladding integrity, drift stability, and avoidance of phase instability in the waste package materials. Figure 1-2 shows a typical layout of an in-drift placement of three types of waste packages. Note that DSs will be placed over the waste packages just before repository closure to provide protection from dripping water and rock fall.

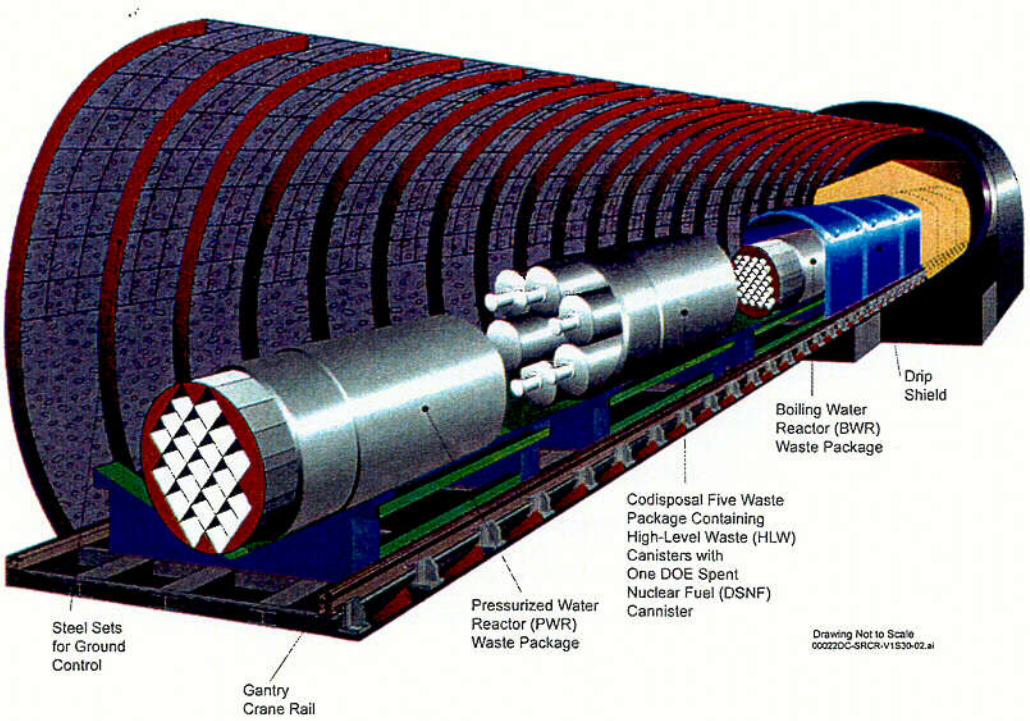

Figure 1-2. A View of a Typical In-Drift Placement of Waste Packages

The purpose of this PMR is to account for the degradation of WP materials under conditions expected at the Yucca Mountain site, which is being evaluated as a possible geologic repository for the disposal of HLW waste. Data pertaining to WP material degradation are presented in supporting AMRs. Functional summaries of the component models and their respective output are provided in Section 1.4. This report was developed in accordance with the technical product development plan *Development Plan for Waste Package Degradation Process Model Report* (CRWMS M&O 1999b).

Each of the process-level models described in the Waste Package Degradation PMR accounts for a different degradation process, all of which are integrated in the waste package degradation code (WAPDEG) (CRWMS M&O 2000g). Each model was developed using unique methodologies and inputs, with the determination of that model dependent on the functional requirements of the waste package component being represented.

In January 2000, the Project modified the repository design. The changes instituted involve removing backfill from the reference design and reorienting the drifts to minimize the impacts of the rockfall. Preparation of this PMR and the supporting AMRs preceded this design change and

C-2

do not, therefore, include the impact of that change. However, a qualitative assessment has been made to evaluate the effect of no backfill on the results presented in this PMR and the supporting AMRs. AMRs impacted by the removal of the backfill include those that describe:

- Stress corrosion cracking (SCC) of the drip shield (DS), the waste package outer barrier (WPOB) and the Stainless Steel Structural Material.
- Abstraction of Models for the SCC of DS and WPOB and hydrogen-induced cracking (HIC) of DS.
- WAPDEG Analysis of WP and DS Degradation.

At this time, the AMR on the SCC assumes that the DS is protected by backfill from rockfall-induced stress and therefore, no SCC. Removal of the backfill may subject the DS to localized stress due to rockfall, thereby increasing the susceptibility to SCC. The abstraction AMR on SCC and the WAPDEG analysis AMR are similarly affected. While a more detailed analysis is required to quantify the impact of the design change, preliminary analyses indicate that any stress corrosion cracks in the DS will not result in the direct dripping of water on the waste package since it is believed that the cracks will become plugged with corrosion products. While this cracking constitutes failure of the DS, it is expected to continue to maintain its function of keeping the water away from the WP. These issues are planned to be addressed in the next revisions of the specific AMRs.

In addition to the increased susceptibility to SCC, the DS may also be subjected to increased corrosion due to rockfall-induced cold-worked regions. Preliminary review of the literature indicates that this is not a significant issue.

It is planned to address these issues in the next versions of the AMRs.

1.1 OBJECTIVES

1.1.1 Objectives of this Report

The objectives of this report are to document degradation models for the waste package and DS material with specific regard to the data input methodologies used to construct the model, uncertainties and limitations of the modeling results, and validation of the model. This report summarizes the following:

- Sources of data input
- Methodologies used to construct the model components
- Modeling results, uncertainties, and limitations.

Assumptions that are specific to the individual models are listed in Chapter 3. Additional details of model assumptions can be found in Chapter 5 of the individual AMRs.

1.1.2 Purpose of the Analysis and Model Reports

The primary purpose of the supporting AMRs is to provide detailed documentation of the process-level models necessary for predicting the performance of the WP and DS materials in environments relevant to Yucca Mountain. These models enable engineers and scientists to predict the release of radionuclides from the WP, and their transport in the saturated and unsaturated zones. Figure 1-3 shows the model inputs, outputs and the laboratory test information that forms the bases for the confidence in the model results.

At the base of the model confidence foundation are the data generated from various testing programs; then, data along with other input parameters related to the repository design and expected environment are used in the development of degradation process models. The output from these models are calculated lifetimes for the waste package and drip shields.

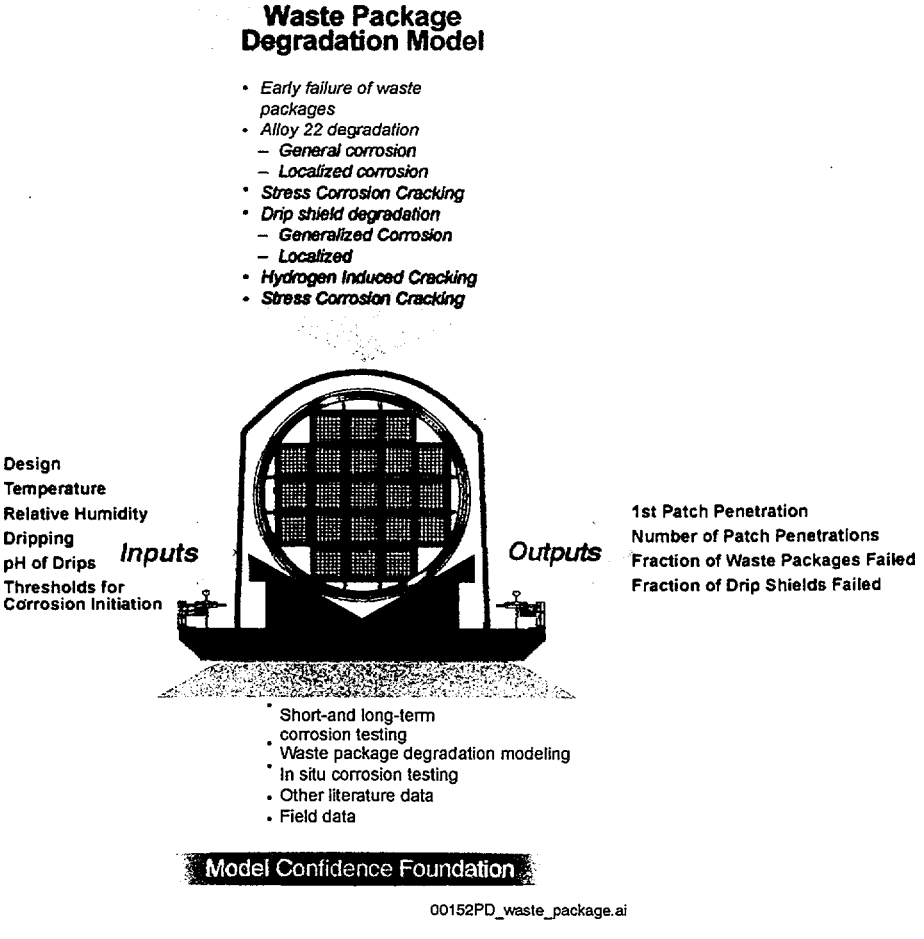

Figure 1-3. Model Confidence Foundation

1.2 SCOPE

The Waste Package Degradation PMR describes processes that will lead to degradation of the waste package components within the near-field environment (NFE). Specific technical information contained in the Waste Package Degradation PMR consists of data, analyses, models, software, and supporting documents. This report also provides a technical basis for the applicability of the overall integrated model for its intended purpose of evaluating postclosure performance of the Yucca Mountain repository system.

The Waste Package Degradation PMR provides information about important factors that affect WP and DS lifetimes. This PMR uses inputs from companion documents, including the license application design selection (LADS) report, which describes the EDA II design and expected temperature history for the waste package in the repository.

Chapter 2 of this PMR describes the evolution of the waste package degradation model. Details of the individual models and analyses are provided in Chapter 3. Chapter 4 describes the NRC IRSR, which serves as a driver for much of the work that is discussed. Acceptance criteria and responses to these criteria are addressed in this chapter. Summary and conclusions are provided in Chapter 5.

1.3 PRINCIPAL FACTORS AND OTHER FACTORS CONSIDERED

The magnitude of the Yucca Mountain Site Characterization Project (YMP) and the complexities associated with both the natural and engineered barrier systems dictate that the YMP prioritize its activities and focus on the factors most important to performance, hereafter named the Principal Factors. The *Repository Safety Strategy: U.S. Department of Energy's Strategy to Protect Public Health and Safety After Closure of a Yucca Mountain Repository* (CRWMS M&O 2000w) has identified seven Principal Factors and twenty Other Factors of second-order importance. The selection of the Principal Factors was based on preliminary TSPA analyses and expert judgment, which showed that these factors significantly affect the performance of the potential repository. The Other Factors were deemed to have minimal impact on the repository performance in terms of dose to the accessible environment. Table 1-1 lists the seven Principal Factors, the twenty Other Factors, and the PMRs that address each factor. Specific Principal Factors discussed in this report are:

- Performance of the DS
- Performance of the WP barriers.

Performance of the DS is a principal factor since it represents the diversion of seepage away from the WP. This factor defines the timing and amount of water transmitted through the DS.

Performance of the WP barriers is a principal factor for the postclosure safety case because it defines the timing and amount of water transmitted into the WP, and thereby controls the rate of release of radionuclides.

Table 1-1. Principal Factors, Other Factors, and the PMRs Where Addressed

Principal Factor (Nominal Scenario)	Process Model Report
Seepage into drifts	Unsaturated Zone Flow and Transport
Performance of the DS	Waste Package Degradation
Performance of the WP barriers	Waste Package Degradation
Solubility limits of dissolved radionuclides	Waste Form (WF) Degradation
Retardation of radionuclide migration in the unsaturated zone	Unsaturated Zone Flow and Transport
Retardation of radionuclide migration in the saturated zone	Saturated Zone Flow and Transport
Dilution of radionuclide concentrations during migration	Saturated Zone Flow and Transport
Other Factors (Nominal Scenario)	
Climate	Unsaturated Zone Flow and Transport
Net Infiltration into the mountain	Unsaturated Zone Flow and Transport
Unsaturated zone flow above the repository	Unsaturated Zone Flow and Transport
Coupled processes - effects on unsaturated zone flow	Unsaturated Zone Flow and Transport
Coupled processes - effects on seepage	NFE
Environments on the DS	EBS Degradation, Flow, and Transport
Environments on the waste package	EBS Degradation, Flow, and Transport
Environments within the waste package	WF Degradation
CSNF WF performance	WF Degradation
DHLW glass WF performance	WF Degradation
DSNF, Navy fuel, Pu disposition WF performance	WF Degradation
Colloid-associated radionuclide concentrations	WF Degradation
In-package radionuclide transport	WF Degradation
Transport through the drift invert	EBS Degradation, Flow, and Transport
Advective pathways in the unsaturated zone	Unsaturated Zone Flow and Transport
Colloid-facilitated transport in the unsaturated zone	Unsaturated Zone Flow and Transport
Coupled processes – effects on unsaturated zone transport	Unsaturated Zone Flow and Transport
Advective pathways in the saturated zone	Saturated Zone Flow and Transport
Colloid-facilitated transport in the saturated zone	Saturated Zone Flow and Transport
Biosphere transport and uptake	Biosphere
Factors For Disruptive Event Scenarios	
To be determined; see Section 3.5 for preliminary considerations (CRWMS M&O 2000w)	Disruptive Events

General guidelines dictate that the YMP bound the effects of the Other Factors, when possible, and perform analyses that are conservative. Principal Factors are to be studied and evaluated more thoroughly, using both realistic evaluations and bounding analyses.

1.4 QUALITY ASSURANCE

The Quality Assurance (QA) program applies to this analysis. All types of WP designs were classified as per *Classification of Permanent Item,* QAP-2-3 as Quality Level 1. This report applies to all of the WP designs included in the Monitored Geologic Repository Classification Analyses. *Classification of the MGR Uncanistered Spent Nuclear Fuel Disposal Container System* (CRWMS M&O 1999c) is cited as an example of a waste package type. The development of this report is conducted under the activity evaluation *1101213PM7 Waste Package Analyses & Models - PMR* (CRWMS M&O 1999d), which was prepared per QAP-2-0, *Conduct of Activities.* The results of this evaluation indicate that the activity is subject to the *Quality Assurance Requirements and Description* (DOE 2000) requirements.

The Waste Package Degradation PMR was prepared in accordance with AP-3.11Q, *Technical Reports,* and reviewed in accordance with AP-2.14Q, *Review of Technical Products.* The AMRs that support this PMR were prepared in accordance with AP-3.10Q, *Analyses and Models.*

The status of the data supporting this PMR is included in the supporting AMRs and in the Document Input Reference System (DIRS) database. The data are incorporated in the Technical Data Management System (TDMS). Data verification and qualification were carried out in accordance with procedures AP-3.15Q, *Managing Technical Product Inputs* and AP-SIII.2Q, *Qualification of Unqualified Data and the Documentation of Rationale for Accepted Data,* respectively.

No software codes were used directly in the development of this PMR. However, this report does include the results from software codes used in the supporting AMRs.

ANSYS, Version 5.3, which is a finite element analysis code used for thermal and stress analyses, was used to develop data cited in SCC AMR (CRWMS M&O 2000f).

pcCRACK, Version 3.1, is a fracture mechanics code used for stress intensity and crack growth simulation analyses. This code was also used to develop data cited in the SCC AMR (CRWMS M&O 2000f).

WAPDEG, Version 4.0, is used to determine waste package and DS failure fractions as a function of time. Details of the use of this code are provided in the AMR on WAPDEG Analysis (CRWMS M&O 2000g).

1.5 WASTE PACKAGE DEGRADATION PROCESS AND ABSTRACTION MODELS

The integrated model for WP and DS degradation consists of several individual process-level and abstraction models, as well as some numerical analyses.

In all, eight (8) process-level models, six (6) abstraction models, and two (2) engineering calculations were developed and documented in individual AMRs or Calculations. These are listed below.

Process-Level Model Analyses:

- *Analysis of Mechanisms for Early Waste Package Failure*, Document Identifier DI # ANL-EBS-MD-000023 (CRWMS M&O 2000m)
- *Environment on the Surface of the Drip Shield and Waste Package Outer Barrier*, DI # ANL-EBS-MD-000001 (CRWMS M&O 2000a)
- *Aging and Phase Stability of Waste Package Outer Barrier*, DI # ANL-EBS-MD-000002 (CRWMS M&O 2000b)
- *General Corrosion and Localized Corrosion of Waste Package Outer Barrier*, DI # ANL-EBS-MD-000003 (CRWMS M&O 2000c)
- *General Corrosion and Localized Corrosion of Drip Shield*, DI # ANL-EBS-MD-000004 (CRWMS M&O 2000d)
- *Stress Corrosion Cracking of the Drip Shield, the Waste Package Outer Barrier and the Stainless Steel Structural Material*, DI # ANL-EBS-MD-000005 (CRWMS M&O 2000f)
- *Hydrogen Induced Cracking of Drip Shield*, DI # ANL-EBS-MD-000006 (CRWMS M&O 2000h)
- *Degradation of Stainless Steel Structural Material*, DI # ANL-EBS-MD-000007 (CRWMS M&O 2000e)

Abstraction Models and Calculations:

- *WAPDEG Analysis of Waste Package and Drip Shield Degradation*, DI # ANL-EBS-PA-000001 (CRWMS M&O 2000g)
- *Abstraction of Models of Stress Corrosion Cracking of Drip Shield and Waste Package Outer Barrier and Hydrogen Induced Corrosion of Drip Shield*, DI # ANL-EBS-PA-000004 (CRWMS M&O 2000j)
- *FEPs Screening of Processes and Issues in Drip Shield and Waste Package Degradation*, DI # ANL-EBS-PA-000002 (CRWMS M&O 2000s)
- *Abstraction of Models for Pitting and Crevice Corrosion of Drip Shield and Waste Package Outer Barrier*, DI # ANL-EBS-PA-000003 (CRWMS M&O 2000n)
- *Calculation of Probability and Size of Defect Flaws in Waste Package Closure Welds to Support WAPDEG Analysis*, DI # CAL-EBS-PA-000003 (CRWMS M&O 2000k)

- *Calculation of General Corrosion Rate of Drip Shield and Waste Package Outer Barrier to Support WAPDEG Analysis*, DI # CAL-EBS-PA-000002 (CRWMS M&O 2000i)

- *Abstraction of Models for Stainless Steel Structural Material Degradation*, DI # ANL-EBS-PA-000005 (CRWMS M&O 2000o)

- *Incorporation of Uncertainty and Variability of Drip Shield and Waste Package Degradation in WAPDEG Analysis*, DI # ANL-EBS-MD-000036 (CRWMS M&O 2000p)

Results from the last two AMRs (CRWMS M&O 2000o and CRWMS M&O 2000p) are not being used as input to the Waste Package Degradation Nominal Case Analysis. These two reports are omitted as input since the stainless steel inner shell is not considered to be a corrosion barrier. Thus, it is not assigned any performance credit. The AMR on uncertainty and variability requires additional data to further develop the model, and will be included in the next major revision of the PMR. For this PMR, uncertainty and variability are included in the bounding approach used for process-level and abstraction models.

Figure 1-4 shows the elements of the integrated model, and interrelationships among the various process-level models and the AMRs that comprise it. Related phenomena are logically grouped in the process-level models. For example, the process-level model for general corrosion (GC) and localized corrosion (LC) of the waste package outer barrier (WPOB) includes dry oxidation (DOX), humid air corrosion (HAC), and expected environment on the surface. A brief overview of each of these models is presented below. Details of the process-level and abstraction models are presented in the AMRs and in Chapter 3.

1.5.1 Environment on the Surface of Drip Shield and Waste Package Outer Barrier

Information on the surface environment provided below is based on the parent AMR (CRWMS M&O 2000a, Section 1.2) and is discussed in greater detail in Section 3.1.3. This process-level model addresses the evolution of the chemistry of the water film on the DS and WPOB as a function of temperature and relative humidity (RH). The concentrations of aqueous salt solutions that can form on the hot waste package surface are being determined experimentally and theoretically (based upon chemical thermodynamics). These concentrations define the medium for testing WP materials under a worst-case scenario. An example is the development of a simulated saturated J-13 water (SSW) with an elevated boiling point (120-127°C). Hygroscopic salts may be deposited on surfaces by seepage water and episodic water flow, as well as by dust and aerosols entrained in ventilation air. The deliquescence point of these salts determines the RH at which humid-air and aqueous-phase corrosion commences.

Abstracted models are developed for the evolution of environments on the exposed surfaces of the DS and WPOB as a function of time and location within the repository. These abstracted models are in forms that are suitable as inputs to the WAPDEG analysis and include the uncertainty and variability of exposure conditions. Additional information on the WAPDEG code is presented in Section 2.2.

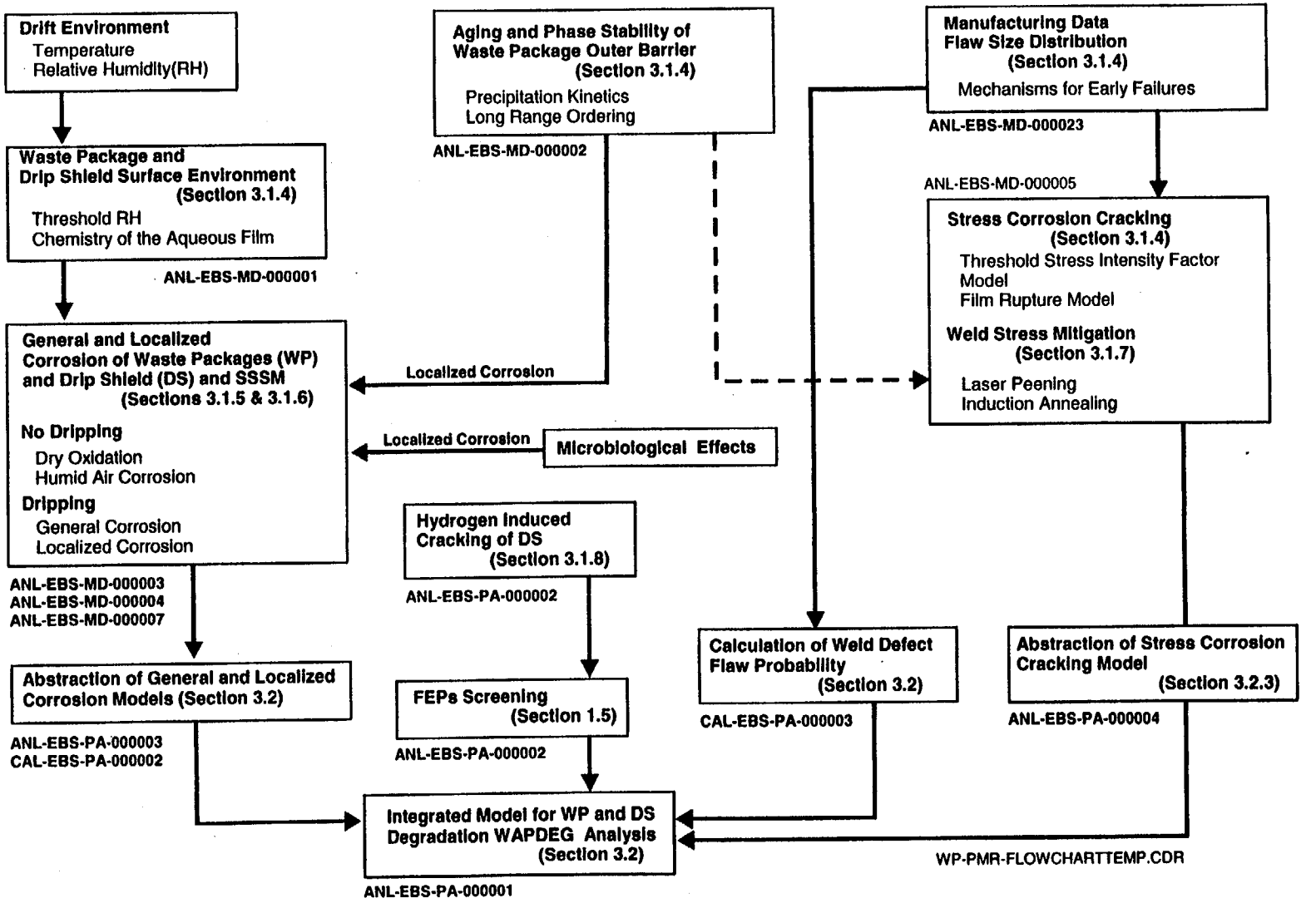

Figure 1-4. Schematic Representation of the Elements of Process Models Interrelationships Among the Process Models and the AMRs Containing These Models

1.5.2 Mechanisms for Early Failures and Manufacturing Defects

Information on early failures provided below is based on the parent AMR (CRWMS M&O 2000m, Section 6) and is described in greater detail in Section 3.1.2. This analysis addresses the potential for early failures of the waste package due to material defects, as well as defects from waste package fabrication processes. These fabrication processes include welding. The probability of waste package fabrication defects, their uncertainty and variability, and the consequences of the defects on waste package failure times (e.g., number of potential failure sites and flaw size distribution) are discussed.

Abstracted calculations are developed for the occurrence and size distribution of defect flaws from material and manufacturing defects in the waste package. Abstracted calculations include uncertainty and variability of the above properties.

1.5.3 Aging and Phase Stability of Waste Package Outer Barrier

Information on aging and phase stability provided below is based on the parent AMR (CRWMS M&O 2000b, Section 6) and is described in greater detail in Section 3.1.4. This process-level model addresses degradation of the WPOB resulting from exposure to elevated temperatures. In the case of Alloy 22 and related materials, such thermal histories can result in the formation of precipitates (μ, P, σ) and other undesirable phases. The precipitates can form within the individual grains or at grain boundaries. Precipitation can cause embrittlement, thereby increasing susceptibility to damage by rockfall and impact. Since these precipitates may be rich in molybdenum and chromium, two of the alloying elements responsible for the high degree of passivity of Alloy 22, aging can also result in increased susceptibility to general and LC, as well as to SCC. The time-temperature-transformation (TTT) curve and an expression for estimating the volume fraction of precipitates in the grain boundary (GB) have been developed for Alloy 22. Estimates of uncertainty are made. The effect of aging on corrosion has been addressed, and has been determined to be a corrosion enhancement factor of approximately 2.5 for the fully aged material.

1.5.4 General Corrosion and Localized Corrosion

Information on corrosion provided below is based on three separate AMRs (CRWMS M&O 2000c Section 6, 2000d Section 6, and 2000e Section 6) and is described in greater detail in Sections 3.1.5 and 3.1.6. Three separate process-level models were developed to address general corrosion and localized corrosion of the DS, WPOB, and stainless steel structural support respectively. The current design uses Titanium Grade 7 as the DS, Alloy 22 as the WPOB, and 316NG stainless steel as the inner structural material. Each of these models includes sub-models for DOX, HAC, GC in the aqueous phase, and LC in the aqueous phase. Note that "dry oxidation" and "dry air oxidation" are synonymous terms. While the stainless steel structural material is not specifically intended to be a corrosion barrier, it may affect the chemistry of water entering the waste package and retard the rate of radionuclide release from the breached waste package. Given the limited availability of data for 316NG stainless steel, data for 316L stainless steel are used as representative. This is appropriate since the compositions of these two materials are very similar, and since their susceptibilities to corrosion are known to be similar. Microbial corrosion is addressed in the section devoted to LC (Section 3.1.6.8).

1.5.4.1 Dry Oxidation

The process-level model for corrosion of the DS and WP materials includes a sub-model for DOX. It is assumed that DOX can be treated as a type of GC, with uniform attack. The rates of DOX are estimated as a function of temperature, to the extent possible.

1.5.4.2 Humid Air Corrosion & Vapor Phase Corrosion

The process-level model for corrosion of the DS and waste package materials accounts for humid air and vapor phase corrosion. These modes of corrosion are also treated as a type of GC. To the extent possible, rates of humid air and vapor phase corrosion (VPC) are estimated as a function of temperature.

1.5.4.3 Aqueous Phase Corrosion

The process-level model for aqueous phase corrosion (APC) of the DS and WP accounts for both general and localized attack. Two models for the initiation of LC are considered (Methods A and B). In Method A, the threshold potential for localized attack of the material is determined from experimentally determined cyclic polarization (CP) data obtained with relevant test environments. These environments include simulated dilute water (SDW), simulated concentrated water (SCW) and simulated acidic concentrated water (SAW) at 30, 60, and 90°C, as well as SSW at 100 and 120°C. The compositions of SDW and SAW are 10X and 1,000X concentrations of J-13 well water, respectively. More recently, basic saturated water (BSW) has been included in the set of standard test media. Published rates for LC are invoked when the expected open circuit corrosion potential exceeds the threshold potential. Since pitting has not been observed in laboratory experiments at LLNL, the primary mode of LC is expected to be crevice corrosion. If the threshold for LC is not exceeded, it is assumed that the mode of attack is GC. GC rates are estimated from various sources of available test data, including weight loss measurements from the Long Term Corrosion Test Facility (LTCTF). In Method B, a threshold temperature for localized attack at the open circuit corrosion potential is determined from published literature data or from tests at elevated temperature and pressure. The same rates of LC are used in Method B as used in Method A. This APC model will be applied to each unit area of the WP exterior surface.

Abstracted models have been developed to account for GC of the DS and WP materials. These abstractions are very similar to the process-level models. The abstracted models include thresholds for initiation of various modes of corrosion, as well as the corresponding rates of penetration. The abstracted models are in forms that are suitable for input to the WAPDEG analysis. The RH threshold for initiation of HAC and APC are included, as well as the electrochemical potential for initiation of localized attack during APC. In the case of the DS and WPOB, distributions of GC rates are based upon data from the LTCTF, while published data are used as the basis of estimating LC rates. Both general and localized corrosion rates of 316NG stainless steel are based upon published data. Estimates of the uncertainty and variability of each quantity are provided. When LC occurs, it is assumed to occur over an entire WAPDEG patch (element).

1.5.5 Stress Corrosion Cracking

The process-level model for the SCC is documented in the corresponding AMR (CRWMS M&O 2000f, Section 6) and is described more fully in Section 3.1.7. SCC of materials may occur when an appropriate combination of material susceptibility, tensile stress and environment are present. This process-level model accounts for the possibility of SCC of the DS, the WPOB, and the stainless steel structural material. This model also evaluates two alternative methods: Method A which is based on threshold stress intensity factor criterion for initiation of SCC ($K_I > K_{ISCC}$); and Method B which is based upon a threshold stress and a finite rate of SCC propagation. The rate of SCC propagation is dependent upon the local environment and the stress intensity factor at the crack tip. The stresses for initiation and propagation of SCC are due to unannealed closure welds, deformation caused by rock fall, and the weight of the WP. This particular analysis requires appropriate stress analysis models and measurements for calculation of the through-wall stress distribution for representative cross sections of the WP, including unwelded base metal and unannealed welds. This stress distribution is used to calculate a corresponding stress intensity factor distribution for flaws that range in size from zero to the entire thickness of the wall including the welded region. This stress intensity factor distribution is used as input for both Methods A and B. In Method A, SCC initiates at pre-existing flaws that develop during fabrication of the waste package, or at flaws that develop during LC. Values of K_{ISCC} are based upon data published in the technical and scientific literature, or measurements made with the double cantilever and compact tensions beam techniques. In Method B, SCC is initiated if the threshold stress is exceeded on a smooth surface. Then, the SCC propagation rate is calculated as a function of local environment and stress intensity factor. The time-to-failure is determined by integrating the calculated propagation rate. As previously discussed, relevant test environments include SDW, SCW, and SAW at 30, 60, and 90°C, SSW at 100 and 120°C, and BSW at 110°C.

Abstracted models have been developed for SCC of the WPOB (Alloy 22). These abstracted models include: (1) a threshold stress for initiation; (2) a crack growth rate as a function of stress and local exposure conditions, including temperature; (3) crack density; and (4) crack morphology. Crack morphology includes a description of the size of openings. The abstracted models are in a form that is suitable for input to the WAPDEG analysis, and include the uncertainty and variability of the above processes.

Post-weld stress mitigation techniques are being employed to delay the initiation of SCC. The techniques under consideration include laser peening and localized induction annealing. These processes are accounted for in the model presented here.

1.5.6 Hydrogen-Induced Cracking of Drip Shield

This process-level model establishes the conditions under which the DS (Titanium Grade 7) will experience hydrogen uptake, thereby leading to the threat of hydrogen embrittlement and hydrogen-induced cracking (HIC). This mode of failure is not believed to be a credible threat to Alloy 22 and has been, excluded as shown in Section 1.6 below. This is based on the design, which includes backfill, and the rate of hydrogen pick up is very low. HIC may be a greater threat without backfill, since the titanium DS can be galvanically coupled to carbon steel rock

bolts and mesh. Analysis of the galvanic effects and hydrogen pick up is planned to be included in the next version of the AMR.

1.6 SCREENING OF FEATURES, EVENTS, AND PROCESSES

The initial set of features, events and processes (FEPs) has been developed for the YMP TSPA by combining lists of FEPs identified as relevant to the YMP. This combined list consists of 1,261 FEP entries from the Nuclear Energy Agency working group, 292 FEPs from YMP literature and site studies, and 82 FEPs identified during YMP project staff workshops. The FEPs have been identified by a variety of methods including expert judgement, informal elicitation, event tree analysis, stakeholder review, and regulatory stipulation. All potentially relevant FEPs have been included, regardless of origin. The compilation included FEP entries mentioned above and 151 layers, categories and headings. It resulted in a FEP list of 1786 entries. This approach has led to considerable redundancy in the FEP list, because the same FEPs are frequently identified by multiple sources, but it also ensures that a comprehensive review of narrowly defined FEPs will be performed.

Each FEP has been classified as either a Primary or Secondary FEP. The classification resulted in the identification of 310 Primary FEPs. Primary FEPs are those for which detailed screening arguments are developed. The classification and description of Primary FEPs strives to capture the essence of all the Secondary FEPs that map to the primary. Secondary FEPs are either FEPs that are completely redundant or that can be aggregated into a single Primary FEP. The Primary FEPs have been assigned to associated PMRs. The assignments were based on the nature of the FEPs so that the analysis and resolution for screening decisions reside with the subject-matter experts in the relevant disciplines. The resolution of other system-level FEPs are documented in AMRs prepared by the responsible PMR groups. This section summarizes the screening decisions associated with the FEPs for the waste package and DS PMR group. Details of the screening processes are documented in the associated AMR.

The scope of the FEPs screening is to identify the treatment of the Primary FEPs affecting waste package and DS degradation. The FEPs that are deemed potentially important to repository performance are evaluated, either as components for the TSPA or as separate analyses in the AMR. The scope for this activity involves the following two tasks:

Task 1: Identify FEPs that are considered explicitly in the TSPA (called included FEPs) and the AMRs in which these FEPs are addressed

Task 2: Identify FEPs not included in TSPA (called excluded FEPs) and provide justification for why these FEPs do not need to be a part of the TSPA model.

Of the original list of FEPs, twenty-eight have been identified as Primary FEPs in relationship to waste package and DS degradation. The approach used for this analysis is a combination of qualitative and quantitative screening. The analyses are based on the criteria provided by the NRC in the proposed 10 CFR Part 63 (Dyer 1999) and by the U.S. Environmental Protection Agency in the proposed 40 CFR Part 197 (64 FR 46976) to determine whether or not each FEP should be included in the TSPA. For FEPs that are excluded from the TSPA based on NRC or U.S. Environmental Protection Agency criteria, the screening argument includes a summary of

the basis and results that indicate either low probability or low consequence. As appropriate, screening arguments cite work performed outside this activity, such as in other AMRs. For FEPs that are included in the TSPA, the TSPA disposition includes a reference to the AMR that describes how the FEP has been incorporated in the process models or the TSPA abstraction models.

The FEPs screening analysis results for the twenty-eight Primary FEPs relevant to waste package and DS degradation processes are summarized in Table 1-2. This table shows the FEP number, FEP name, screening decision (include/exclude), and a synopsis of the screening argument. Details of the screening processes and arguments are planned to be included in the next revision of the FEPs AMR.

1.7 RELATIONSHIP TO OTHER PROCESS MODEL REPORTS AND DOCUMENTS

This PMR provides information about important factors affecting waste package lifetime such as the thermal, hydrologic, and geochemical processes acting on the waste package surface. The PMR uses inputs from other documents such as LADS report (EDA II design) and thermal analyses. The emphasis of the discussion of model inputs and outputs is on information needed for the assessment of postclosure performance. The waste package degradation PMR supports the TSPA and other major Project milestones, such as the Site Recommendation (SR) and the License Application (LA).

While the scope of this PMR is to address degradation of the WP and the DS, other PMRs (such as the EBS PMR) address other aspects of DS and EBS component performance.

Table 1-2. Primary FEP Summary for Waste Package and Drip Shield Degradation

FEP Number	FEP Title	Screening Decision	Reason for Include/Exclude Decision
1.1.03.01.00	Error in waste or backfill emplacement	Exclude	Exclude based on low probability constrained by the design requirements. The design requirements assume that the repository will be constructed, operated, and closed according to the regulatory requirements applicable to the construction, operation, and closure period and that deviations from design will be detected and corrected. Details of the basis will be documented in the next revision of FEPs AMR.
1.2.02.03.00	Fault movement shears waste container	Exclude	Exclude based on Low probability. Detailed description of the basis for the screening decision is given in the Disruptive Events FEPs AMR (CRWMS M&O 2000v).
1.2.03.02.00	Seismic vibration causes container failure	Exclude	Exclude based on low consequence constrained by the design requirements of WP and DS. This FEP was originally directed at vertical emplacement of containers in boreholes. The current design is to place large containers horizontally in the drifts with drip shield and backfill over the drip shield. This design removes the possibility of container-rock wall contact due to seismic activity. In addition, preliminary analyses indicate that even under most severe seismic vibration, the WP will not undergo failure. Details of the basis will be documented in the next revision of FEPs AMR. For the DS, the design criteria require that the DS be designed to withstand a Category 2 design basis earthquake without rupturing or parting between individual DS units and without contacting waste packages (CRWMS M&O 2000t, System Design Criteria 1.2.1.16 and 1.2.1.17). This FEP is also addressed in the Disruptive Events FEPs AMR (CRWMS M&O 2000v). This FEP addresses CLST KTI IRSR Subissues 2 and 6 (see Table 4-1).
1.2.04.04.00	Magma interacts with waste	Include	Magma interactions with the waste are included in the TSPA as part of disruptive events analyses. This FEP is addressed in the Disruptive Events FEPs AMR (CRWMS M&O 2000v). This FEP addresses CLST KTI IRSR Subissues 2 (see Table 4-1).
2.1.03.01.00	Corrosion of waste containers	Include	Corrosion is the most likely process leading to degradation and failure of WPs and DSs in the repository. All significant corrosion modes are included in WP/DS corrosion modeling. These include dry-air oxidation, humid-air corrosion, and aqueous corrosion processes such as general corrosion, localized (pitting and crevice) corrosion, stress corrosion cracking, hydrogen-induced corrosion, and microbiologically influenced corrosion. WP/DS corrosion is modeled with the Waste Package Degradation computer code (WAPDEG) (CRWMS M&O 1999e). WAPDEG produces waste package/drip shield degradation profiles consisting of the fraction of waste packages/drip shields failed versus time and the average (per failed waste package/drip shield) number of penetration openings versus time. The degradation profiles are used as input into the TSPA model. This FEP is the subject of this PMR and addressed in Sections 3.1 and 3.2. This FEP addresses CLST KTI IRSR Subissues 1, 2 and 6 (see Table 4-1).

Table 1-2. Primary FEP Summary for Waste Package and Drip Shield Degradation (Continued)

FEP Number	FEP Title	Screening Decision	Reason for Include/Exclude Decision
2.1.03.02.00	Stress corrosion cracking of waste containers	Include for WP; Exclude for DS	Include for waste package. Because, among other exposure condition parameters, tensile stress is required to initiate stress corrosion cracking (SCC), and the WP closure welds are the only places with such tensile stresses, only the WP closure welds are considered for SCC (CRWMS M&O 2000f). The other fabrication welds of the WP will be fully annealed before waste is loaded into the disposal containers, and thus are not subject to SCC. WP SCC is modeled with the WP Degradation (WAPDEG) computer code (CRWMS M&O 1999e). The degradation profiles are used as input into the TSPA model (see FEP 2.1.03.01.00). Exclude for drip shield based on low consequence. All fabrication welds of the drip shield will be fully annealed before placed in the emplacement drift, and thus are not subject to SCC. Also, the major sources of stresses in the drip shield induced by backfill and earthquakes are not significant for SCC (CRWMS M&O 2000f, Section 5, Assumption 1). Additionally, even if it occurs, the SCC cracks in the drip shield, which are likely "tight" openings and filled with corrosion products and/or other precipitates, is not expected to compromise significantly the intended function of the drip shield (i.e., preventing the dripping water from contacting the waste package). This FEP is addressed in Section 3.1.7. This FEP addresses CLST KTI IRSR Subissues 1 and 2 (see Table 4-1).
2.1.03.03.00	Pitting of waste containers	Include	Localized (pitting and crevice) corrosion is one of a number of potential corrosion mechanisms that could lead to eventual compromise of WPs and/or DSs in the repository. As discussed in detail in the companion abstraction AMR, localized corrosion of WP outer barrier (Alloy 22) and DS is not likely to occur under repository-relevant exposure conditions (CRWMS M&O 2000n). Localized corrosion initiation and propagation models are included in TSPA as part of WP degradation analysis. Waste container localized corrosion is modeled with the Waste Package Degradation (WAPDEG) computer code (CRWMS M&O 1999e). The degradation profiles are used as input into the TSPA model (see FEP 2.1.03.01.00). This FEP is addressed in Section 3.1.7. This FEP addresses CLST KTI IRSR Subissues 1 and 2 (see Table 4-1).
2.1.03.04.00	Hydride cracking of waste containers	Exclude for DS; Exclude for WP	Exclude for drip shield based on low consequence. Hydrogen-induced cracking (HIC) of drip shield is a potential degradation mechanism that could cause catastrophic failure of drip shield if the hydrogen uptake in the titanium drip shield is greater than the critical hydrogen concentration (CRWMS M&O 2000h). In the repository design of backfill placed over the drip shield, crevice corrosion and passive general corrosion of the drip shield are two feasible processes in the repository that could lead HIC failure of the drip shield. Because the drip shield will not be subject to crevice corrosion under the exposure conditions anticipated in the repository (CRWMS M&O 2000n), general corrosion is the only mechanism that could cause HIC in the drip shield. Bounding analyses have shown that the time that the hydrogen uptake concentration reaches the critical hydrogen concentration under the exposure conditions anticipated in the repository (CRWMS M&O 2000h) is greater than the time required to initiate the drip shield breach by general corrosion (about 20,000 years) (see Section 3.2.5). Therefore, HIC is not a limiting degradation process that could affect the drip shield performance in the repository, and is excluded based on low consequence.

Table 1-2. Primary FEP Summary for Waste Package and Drip Shield Degradation (Continued)

FEP Number	FEP Title	Screening Decision	Reason for Include/Exclude Decision
2.1.03.04.00 (Cont'd)	Hydride cracking of waste containers	Exclude for DS; Exclude for WP	Exclude for waste package based on low probability. HIC of the waste container outer barrier (Alloy 22) is not considered a possible degradation mechanism under repository-relevant exposure conditions. Handbook data (ASM International 1987, pp. 650-651) indicate that fully annealed nickel-base alloys such as Alloy 22 may be immune to hydrogen-induced embrittlement (hydride cracking). The susceptibility to hydride cracking may be enhanced only when the strength level of this alloy is increased either by cold working or by aging at a temperature of 540°C at which ordering and/or grain-boundary segregation can occur. The susceptibility to cracking will be reduced with decreasing strength level and correspondingly with increasing aging temperature. However, since the waste package temperature will be sufficiently less than 540°C, the possibility of HIC in Alloy 22 will be very remote. Details of the basis will be documented in the next revision of FEPs AMR. Therefore, this FEP for the waste package outer barrier is excluded on the basis of low probability. This FEP is addressed in Section 3.1.8. This FEP addresses CLST KTI IRSR Subissue 1 (see Table 4-1).
2.1.03.05.00	Microbially-mediated corrosion of waste container	Include for WP; Exclude for DS	Include for waste package. Microbiologically influenced corrosion (MIC) is included in TSPA as part of waste package degradation analysis. The potential effect of MIC on waste container corrosion is analyzed with an enhancement factor approach, assuming MIC increases corrosion penetration rate. In this approach, the abiotic corrosion rate is multiplied by the enhancement factor when the exposure conditions in the emplacement drift warrant significant microbial activity (CRWMS M&O 2000c). Waste container microbiologically influenced corrosion is modeled with the Waste Package Degradation (WAPDEG) computer code (CRWMS M&O 1999e). The degradation profiles are used as input into the TSPA model (see FEP 2.1.03.01.00). Exclude for drip shield based on low consequence. Quantitative data on MIC of drip shield materials such as titanium (Ti) Grades 7 and 16 are not available from the literature. It is considered that the candidate titanium alloy is immune to MIC (CRWMS M&O 2000s). The MIC is excluded for the drip shield (Ti- Grade 7) corrosion modeling in the process model analysis (CRWMS M&O 2000d). This FEP is addressed in Sections 3.1.5 and 3.1.6. This FEP addresses CLST KTI IRSR Subissue 1 (see Table 4-1).
2.1.03.06.00	Internal corrosion of waste container	Exclude	Exclude based on low consequence. The waste container could be corrosively attacked from inside if corrosive condition exists in the inside. After being loaded with waste, the waste containers are to be filled with the inert gas (helium) prior to the closure, displacing water and oxygen inside the container. The helium gas-filled condition will provide an inert environment inside the container, and will maintain the environment for insignificantly low corrosion rates. Prior to the breach of the containers, there should be no or minimum corrosion because of the inert environment inside the container. The most likely cause of any possible internal corrosion is the residual moisture remaining in the waste package at the time of emplacement. The potential source of this moisture is believed to be primarily waterlogged failed fuel rods. Analyses have indicated that the amount of moisture available to cause internal corrosion is very limited and even with very conservative assumptions, the potential for degradation of the container materials is very remote (CRWMS M&O 2000s).

Table 1-2. Primary FEP Summary for Waste Package and Drip Shield Degradation (Continued)

FEP Number	FEP Title	Screening Decision	Reason for Include/Exclude Decision
2.1.03.07.00	Mechanical impact of waste container	Exclude	Excluded based on low consequence constrained by the design requirements. Mechanical damage of the waste container and drip shield by rockfall is discussed in greater detail under FEP 2.1.07.01.00 – Rockfall (large block). Additionally, the Emplacement Drift System design criteria require that the drip shield be designed to withstand a 13 metric tons rock falling onto the top of the backfill without rupturing the drip shield or parting between individual drip shield units and without contacting waste packages (CRWMS M&O 2000t, System Design Criteria 1.2.1.14 and 1.2.1.15). In view of the above rationale, this FEP is excluded based on low consequence. Mechanical damage of the waste container and drip shield by ground motion during seismic events is discussed in greater detail under FEP 1.2.03.02.00 – Seismic Vibration Causes Waste Container and Drip Shield Failure. In addition, the Emplacement Drift System design criteria require that the drip shield be designed to withstand a Category 2 design basis earthquake without rupturing or parting between individual drip shield units and without contacting waste packages (CRWMS M&O 2000t, System Design Criteria 1.2.1.16 and 1.2.1.17). In view of the above rationale, this FEP is excluded based on low consequence. A calculation of the maximum stresses developed in the waste package due to internal pressurization as a result of fuel rod rupture at 400°C is less than the ASME code (ASME 1995, Section II); requirements for the allowable tensile strength (CRWMS M&O 2000x, Table 6-3). Therefore, with the current robust waste container design, the pressurization of the internal gas under the expected repository condition would not cause mechanical damage to the waste container. In general, corrosion products have greater volume than the bare metal. When the corrosion products form in a tightly confined space, the volume increase by the corrosion products generates swelling pressure to the surrounding and thus could cause mechanical damage to the surrounding. In the current design of waste package and engineered barrier system in the emplacement drift, there is no possibility of forming such a tightly confined space such that the swelling corrosion products could cause mechanical damage to the Alloy 22 outer barrier. Therefore, mechanical damages by internal gas pressure and swelling corrosion products are excluded based on low consequence. This FEP addresses CLST KTI IRSR Subissue 2 (see Table 4-1).
2.1.03.08.00	Juvenile and early failure of waste containers	Include/exclude for WP; Exclude for DS	Include manufacturing and welding defects in waste container degradation analysis. The major effect of pre-existing manufacturing defects is to provide sites for crack growth by stress corrosion cracking (SCC), potentially leading to an early failure. Among other exposure condition parameters, tensile stress is required to initiate SCC (CRWMS M&O 2000f). Effect of manufacturing and welding defects on waste container failure is addressed by including the defect flaws in SCC analysis (CRWMS M&O 2000g). As discussed in FEP 2.1.03.02.00, only the closure welds are considered for SCC. Accordingly, the defects in the closure welds will be considered in TSPA analysis through the SCC analysis. Exclude manufacturing and welding defects in drip shield degradation based on low consequence. Because all the fabrication welds in drip shields will be fully annealed before placement in the emplacement drift, drip shields are not subject to SCC (CRWMS M&O 2000f). Also, other sources of stresses in the drip shield induced by backfill and earthquakes are insignificant to SCC (CRWMS M&O 2000f, Section 5, Assumption 1). Thus manufacturing defects in drip shield are excluded from TSPA analysis based on low consequence.

Table 1-2. Primary FEP Summary for Waste Package and Drip Shield Degradation (Continued)

FEP Number	FEP Title	Screening Decision	Reason for Include/Exclude Decision
2.1.03.08.00 (Cont'd)	Juvenile and early failure of waste containers	Include/exclude for WP; Exclude for DS	Exclude potential early failure of waste container and drip shield from improper quality control during the emplacement based on low probability. After emplacement the waste containers and drip shields will be inspected. If there is any damage, they would be retrieved (CRWMS M&O 1998b). Thus, the probability of having potential early failure of waste container and drip shield from improper quality control during the emplacement will be extremely small and is excluded from the TSPA analysis based on low probability. This FEP is addressed in Sections 3.1.2, 3.1.7, 3.2.3, and 3.2.4. This FEP addresses CLST KTI IRSR Subissues 1 and 2 (see Table 4-1).
2.1.03.09.00	Copper corrosion	Exclude	Exclude based on low probability. Copper is not considered for use as an engineered barrier at Yucca Mountain, and thus this FEP is not considered relevant for the Yucca Mountain TSPA. There will be zero probability to have a copper waste container in the repository.
2.1.03.10.00	Container healing	Exclude	Exclude based on low consequence. Plugging (or healing) of corrosion holes or pits in waste container by corrosion products and mineral precipitates is a potentially possible process in the repository. However, there are large uncertainties associated with the quantification of the effect of the process on water flow and radionuclide transport through the openings. Because of this, potential performance credit from the plugging (or healing) of the corrosion penetration openings are not taken into account in TSPA analysis. This FEP is not applicable to waste container corrosion.
2.1.03.11.00	Container form	Exclude	Exclude based on low consequence. The waste package/drip shield/repository design has been standardized for the Yucca Mountain Project (CRWMS M&O 1999a). While there is more than one waste package design expected to be used in the proposed repository, they are all similar in their design, the fabrication methodology used, and their dimensions (CRWMS M&O 2000u, p. 1). Therefore, there will be little variation in strength, dimensions, and shape of the waste packages used in the proposed repository. Effects of different waste forms (CSNF, DSNF, and DHLW) on heat dissipation and physical and chemical conditions in the vicinity the waste packages are indirectly included in the TSPA analysis through different thermal-hydrologic-geochemical responses and their impacts on corrosion processes. Waste package and drip shield degradation modes are modeled with the Waste Package Degradation computer code (WAPDEG) (CRWMS M&O 1999e, 2000g). The WAPDEG code makes use of thermal-hydrologic-geochemical "time histories" for a given simulation, which encompass the variability in exposure conditions that are due in part to different "container forms."
2.1.03.12.00	Container failure (long term)	Include	Long-term corrosion degradation and failure of waste containers and drip shields in the repository are included in TSPA as part of waste package degradation analysis. The analysis accounts for the major degradation mechanisms and processes that are likely in the repository. The waste container and drip shield corrosion are modeled with the Waste Package Degradation computer code (WAPDEG) (CRWMS M&O 1999e, 2000g). WAPDEG produces waste package degradation profiles consisting of the fraction of waste packages/drip shields failed versus time and the average (per failed waste package/drip shield) number of penetration openings versus time. The degradation profiles are used as input into the TSPA model. This FEP is the subject of this PMR and addressed in Sections 3.1 and 3.2. This FEP addresses CLST KTI IRSR Subissues 1, 2 and 6 (see Table 4-1).

Table 1-2. Primary FEP Summary for Waste Package and Drip Shield Degradation (Continued)

FEP Number	FEP Title	Screening Decision	Reason for Include/Exclude Decision
2.1.06.06.00	Effects and degradation of DS	Include/exclude	Include physical and chemical degradation processes in drip shield degradation. Physical and chemical degradation processes for the drip shield are included in TSPA as part of waste package and drip shield degradation analyses. The analyses accounts for the major degradation mechanisms and processes that are likely in the repository (CRWMS M&O 2000g; also see Section 3.2.5). This includes corrosion-induced and other degradation and failure processes. The waste container and drip shield degradation are modeled with the Waste Package Degradation computer code (WAPDEG) (CRWMS M&O 1999e, 2000g). The degradation profiles are used as input into the TSPA model (see FEP 2.1.03.01.00). In addition, the model is designed to account for the effect on the drip shield of non-corrosion degradation processes such as rockfall or seismic motion. These effects are considered for both the intact and degraded states of the drip shield. Exclude rockfall in drip shield degradation based on low consequence. Mechanical damage of the drip shield by rockfall is discussed in greater detail under FEP 2.1.07.01.00 – Rockfall (large block). In addition, the Emplacement Drift System design criteria require that the drip shield be designed to withstand a 13 metric tons rock falling onto the top of the backfill without rupturing the drip shield or parting between individual drip shield units and without contacting waste packages (CRWMS M&O 2000t, System Design Criteria 1.2.1.14 and 1.2.1.15). In view of the above rationale, this FEP is excluded based on low consequence. Exclude ground motion in drip shield degradation based on low consequence. Mechanical damage of the drip shield by ground motion during seismic events is discussed in greater detail under FEP 1.2.03.02.00 – Seismic Vibration Causes Waste Container and Drip Shield Failure. In addition, the Emplacement Drift System design criteria require that the drip shield be designed to withstand a Category 2 design basis earthquake without rupturing the drip shield or parting between individual drip shield units and without contacting waste packages (CRWMS M&O 2000t, System Design Criteria 1.2.1.16 and 1.2.1.17). In view of the above rationale, this FEP is excluded based on low consequence. This FEP is addressed in Sections 3.1.3, 3.1.5, 3.1.6, 3.1.8, and 3.2.5. This FEP addresses CLST KTI IRSR Subissues 1 and 2 (see Table 4-1).
2.1.06.07.00	Effects of material interfaces	Include	Waste container and drip shield corrosion degradation analysis includes the effects of material interfaces in the repository. The thermal-hydrologic-geochemical condition analyses in the repository include effects of materials present in the emplacement drift, including waste package, drip shield and backfill. The corrosion degradation analysis includes effect on corrosion processes of backfill gravel contacting the drip shield and waste container (CRWMS M&O 2000g). This FEP is addressed in Sections 3.1.3, 3.1.5, 3.1.6, and 3.2.5. This FEP addresses CLST KTI IRSR Subissue 1 (see Table 4-1).
2.1.07.01.00	Rockfall (large block)	Exclude	Exclude based on low consequence. This FEP is also addressed in the Disruptive Events FEPs AMR (CRWMS M&O 2000v) and excluded based on low consequence. The Emplacement Drift System design criteria require that the drip shield be designed to withstand a 13 metric tons rock falling onto the top of the backfill without rupturing the drip shield or parting between individual drip shield units and without contacting waste packages (CRWMS M&O 2000t, System Design Criteria 1.2.1.14 and 1.2.1.15). In view of the above rationale, this FEP is excluded based on low consequence. This FEP addresses CLST KTI IRSR Subissue 2 (see Table 4-1).

Table 1-2. Primary FEP Summary for Waste Package and Drip Shield Degradation (Continued)

FEP Number	FEP Title	Screening Decision	Reason for Include/Exclude Decision
2.1.07.05.00	Creeping of metallic materials in the EBS	Exclude	Exclude based on low consequence. Creep data were not found for Alloy 22 (ASTM B 575 N06022) or Titanium Grade 7. Screening argument is developed using the creep data for Alloy 625 (ASTM B 443 – 93e1.1995) whose composition is very similar to Alloy 22. Creep data for Alloy 625 are reported for temperatures of 1200°F (650°C) and higher (Haynes International 1993, p. 5). This temperature is well above the expected temperatures for repository operations. At the repository temperatures, the rate of creep is expected to be very low, because the stresses required to cause creep are not present (CRWMS M&O 2000s). This FEP addresses CLST KTI IRSR Subissue 2 (see Table 4-1).
2.1.09.03.00	Volume increase of corrosion products	Exclude	Exclude based on low consequence. For the waste package and EBS emplacement design considered for the repository, the volume increase by corrosion products from the corroding materials in the emplacement drift is not expected to affect the stress state of drip shields or waste containers, or other EBS materials in the drift. Therefore, this FEP is excluded based on low consequence. In addition, FEP 2.1.03.07.00 – Mechanical Impact on the Waste Container and Drip Shield also deals with corrosion products, namely, the internal and external forces caused by swelling. This portion of the FEP is also excluded. This FEP addresses CLST KTI IRSR Subissue 2 (see Table 4-1).
2.1.09.09.00	Electrochemical effects in waste and EBS	Exclude	Exclude based on low consequence. Electrochemical reactions between the materials in the emplacement drift could establish an electrical field within the drift. Both the Titanium Grade 7 used for the drip shield and Alloy 22 for the waste-container outer barrier are highly corrosion resistant. Thus significant perturbations to the electrochemical system in the drift are required to increase corrosion potential of the materials and to affect their corrosion behaviors (CRWMS M&O 2000c, 2000d). In the current design of the engineered barrier system in the emplacement drift, the potential electrical fields that could be set up in the drift is not expected to be large enough to induce unexpected corrosion behaviors of the drip shield or the waste-container outer barrier. Therefore, this FEP is excluded on the basis of low consequence.
2.1.10.01.00	Biological activity in waste and EBS	Include for WP; Exclude for DS	Include for waste package. Microbes can influence the initiation and rate of waste container corrosion. Alloy 22 (waste container outer barrier material) could be subject to microbiologically influenced corrosion (MIC) depending on the microbial activity in the repository. MIC is included in TSPA as part of waste package degradation analysis. The potential effect of MIC on waste container corrosion is analyzed with an enhancement factor approach, assuming MIC increases corrosion penetration rate. In this approach, the abiotic corrosion rate is multiplied by the enhancement factor when the exposure conditions in the emplacement drift warrant significant microbial activity (CRWMS M&O 2000c). Waste container MIC is modeled with the Waste Package Degradation (WAPDEG) computer code (CRWMS M&O 1999e, 2000g). The degradation profiles are used as input into the TSPA model (see FEP 2.1.03.01.00). Exclude for drip shield based on low consequence. Quantitative data on MIC of drip shield materials such as titanium (Ti) Grades 7 and 16 are not available from the literature. It is considered that the candidate titanium alloy is immune to MIC (CRWMS M&O 2000s). The MIC is excluded for the drip shield (Ti- Grade 7) corrosion modeling in the process model analysis (CRWMS M&O 2000d). Therefore, this FEP is excluded for drip shield based on low consequence. This FEP is addressed in Sections 3.1.5 and 3.1.6. This FEP addresses CLST KTI IRSR Subissue 1 (see Table 4-1).

Table 1-2. Primary FEP Summary for Waste Package and Drip Shield Degradation (Continued)

FEP Number	FEP Title	Screening Decision	Reason for Include/Exclude Decision
2.1.11.05.00	Differing thermal expansion of repository components	Exclude	Exclude based on low consequence. The current drift design minimizes the thermal gradient and temperatures where differential expansion occurs (due to differences in component/rock properties) will not be reached. To mitigate any possibility of thermal stresses as a result of differing thermal expansion coefficients of the waste package materials, the waste package barriers will be constructed with a gap up to 4 mm between the outer barrier (Alloy 22) and inner barrier (316 NG stainless steel) (CRWMS M&O 2000s). Therefore, this FEP is excluded based on low consequence. This FEP addresses CLST KTI IRSR Subissue 2 (see Table 4-1).
2.1.11.06.00	Thermal sensitization of waste containers increases fragility	Include	Alloy 22 is known to be subject to "aging" and phase instability when exposed to elevated temperatures. The processes involve precipitation of different secondary phases and restructuring of the microstructure. The affected material exhibits increased brittleness and decreased resistance to corrosion, especially to localized corrosion and stress corrosion cracking (SCC) (CRWMS M&O 2000b). Preliminary testing results have shown that the waste container outer barrier (Alloy 22) could be subject to aging and phase instability under repository thermal conditions (CRWMS M&O 2000b). Effects of potential thermal sensitization of the waste package outer barrier are included in TSPA as part of waste package degradation analysis. The effects are accounted for with a corrosion enhancement factor that is applied to the corrosion rate for the non-affected condition (CRWMS M&O 2000c). The waste container thermally induced corrosion mechanisms are modeled with the Waste Package Degradation (WAPDEG) computer code (CRWMS M&O 1999e, 2000g). The degradation profiles are used as input into the TSPA model (see FEP 2.1.03.01.00). This FEP is addressed in Sections 3.1.4, 3.1.5 and 3.1.6. This FEP addresses CLST KTI IRSR Subissues 1 and 2 (see Table 4-1).
2.1.12.13.00	Gas generation (H_2) from metal corrosion	Exclude	Exclude based on low consequence. The Yucca Mountain repository is in the unsaturated zone and expected to be connected to the atmosphere and to be operating under oxidizing conditions. Therefore any gases generated by metal corrosion would escape from the drifts. Hydrogen (H_2) gas could be generated from the reduction of water as a result of corrosion reactions underway (more likely under reducing conditions). This hydrogen gas generation would be less likely under oxidizing conditions that are assumed for the repository. Furthermore, the hydrogen gas generation rate, if occur, would be very low for the current repository design because of very low corrosion rates of Alloy 22 (waste container outer barrier) and titanium Grade 7 (drip shield). Alloy 22 and titanium Grade 7 were selected because of their excellent resistance to pitting and crevice corrosion and stress corrosion cracking. Additionally, the iron content in Alloy 22 is very low, therefore the issue of iron corrosion is not relevant to the current design. With the waste package materials, the hydrogen that may be produced from their corrosion in the

Table 1-2. Primary FEP Summary for Waste Package and Drip Shield Degradation (Continued)

FEP Number	FEP Title	Screening Decision	Reason for Include/Exclude Decision
2.1.13.01.00	Radiolysis	Exclude	Exclude based on low consequence. When significant radiation fields and stable "liquid" water exist on the surface of waste container and drip shield, radiolysis of water and some dissolved species in the water could produce highly oxidizing and corrosive fluids. Radiolysis due to gamma and neutron radiation is possible while the container is intact. Alpha and beta radiolysis will be of importance after canister failure, when water gets in close contact with the waste form matrix. Electrochemical testing results simulating the radiation exposure conditions that are expected in the repository have shown that the amount of the corrosion potential increase of Alloy 22 (waste container outer barrier) and Titanium Grade 7 (drip shield) from the radiolysis should not affect their localized corrosion behavior (CRWMS M&O 2000c, 2000d). Therefore, the radiolysis effect on waste-container outer barrier and drip shield is excluded in TSPA analysis based on low consequence. This FEP is addressed in Sections 3.1.5 and 3.1.6. This FEP addresses CLST KTI IRSR Subissue 1 (see Table 4-1).
2.1.13.02.00	Radiation damage in waste and EBS	Exclude	Exclude based on low consequence. The dose rate of gamma radiation at the surface of the waste package and drip shield is determined by the concentration of the various radioactive isotopes within the waste package (as functions of age, type, and length of time the fuel was in the reactor, etc.) and the attenuation provided by the engineered barriers (ASM International 1987, pp. 971-974; CRWMS M&O 2000s). However, the type and dose rates of radiation emitted from decaying wastes are not sufficient to degrade the metallurgical and mechanical properties of the waste package and drip shield materials, and their protective/passive layers (CRWMS M&O 2000s). The only significant effect of radiation will be the change in external environment due to groundwater radiolysis (ASM International 1987, pp. 971-974) (see FEP 2.1.13.01.00). Therefore, this FEP is excluded based on low consequence.

INTENTIONALLY LEFT BLANK

2. EVOLUTION OF THE PROCESS MODEL

2.1 BACKGROUND

The overall performance of the WP and DS materials has been identified as a principal factor in the performance of the repository. It is expected that the lifetime goals for the DS and WP may be increased in the future. Therefore, materials and designs that prolong service life are sought continuously.

The reference design used in the viability assessment (VA) has been estimated to experience first through-wall failure by pit penetration in about 2,700 years, with about 1% of the packages failing in approximately 10,000 years. This estimate is based upon the waste package degradation model (WAPDEG) used as input to *Total System Performance Assessment-Viability Assessment (TSPA-VA) Analyses Technical Basis Document* (CRWMS M&O 1998a, TSPA-VA, Chapter 5). However, the goals of the YMP have been continuously pushed towards longer WP lifetimes, thereby requiring that the repository exceed performance requirements of the VA design by a significant margin. Accordingly, a selection process for alternative materials and designs intended to provide higher levels of confidence for an extended WP lifetime was undertaken. As mentioned in the LADS report, this process resulted in the selection of a double-walled WP placed under a protective DS made of Titanium Grade 7 (CRWMS M&O 1999a). The outer wall of the WP is corrosion-resistant Alloy 22, with an inner wall of stainless steel (316NG) that serves as a structural support. This new design is known as EDA II (CRWMS M&O 1999a). The selection of this new design configuration, coupled with the selection of new materials, has necessitated the development of new models to predict penetration rates. Individual component models (sub-models) are documented in the individual Analysis and Model Reports (AMRs) (see Section 1.5 for the topics in each AMR). Each AMR is provided as an input to the WP Degradation PMR, as well as to the TSPA for Site Recommendation.

2.2 PREVIOUS TREATMENT OF WASTE PACKAGE DEGRADATION MODELING

Modeling of WP degradation has evolved over the past decade along with changes in materials selected for its containment barriers. Early WP designs consisted of thin-walled stainless steel canisters with heavy-walled carbon steel overpacks, and were designed for emplacement in salt, basalt or tuff repositories. The design thickness of the overpack component was the sum of the required structural thickness, plus the corrosion allowance necessary to assure that the required structural thickness will survive the required containment period. The corrosion allowance was established on the basis of the calculated temperature profile of the WP surface during the containment period, the unexpected presence of an unlimited quantity of anoxic brine, and the resulting corrosion rate.

In late 1987, the U.S. Congress passed *The Nuclear Waste Policy Amendments Act, As Ammended. With Appropriations Acts Appended* (DOE 1995), which reduced the number of potential repository sites to be characterized to one: Yucca Mountain. Prior to this event, work on the WP design for Yucca Mountain had followed the same rationale as that for salt and basalt repositories. In fact, the initial conceptual design of the WP developed in early 1983 was the same as that for the other two repositories. However, it was recognized that the expected conditions in Yucca Mountain were quite different from the other two in that the repository was

located in the unsaturated zone. The environment in this zone, although not firmly established, was expected to be oxidizing, but dry with low humidity most of the time. The design temperature for the WP surfaces was not expected to exceed 250°C. Liquid water was expected to be present only under transient conditions, and its composition was not expected to be very aggressive from a corrosion standpoint.

The limitations of 304L stainless steel, from the standpoint of SCC and LC had been recognized from early on. Consequently, alternative materials were being sought. In 1993 (CRWMS M&O 1994), the design was changed from thin-walled containers emplaced in bore holes to drift-emplaced robust multibarrier WP. The proposed materials were Alloy 825 as the inner barrier and a corrosion allowance material (CAM) "such as weathering steel" as an outer barrier. Degradation modeling of this WP design included only APC. It was assumed that no corrosion would occur above the temperature at which liquid-phase water could not exist on the WP surface.

Model enhancements were incorporated in 1995 (CRWMS M&O 1995) and were based upon the same double-wall WP design that was used in 1993. This model was an initial attempt to account for HAC and APC. The APC model had components that simulated pitting corrosion and galvanic coupling of the CAM and corrosion resistant materials (CRM). This model included estimates of the variability in WP corrosion, including package-to-package and patch-to-patch variability. Estimates of the uncertainty in the threshold RH for initiation of HAC and APC were also made. An empirical model for GC and LC of the CAMs was developed based upon published literature data. Rates of GC and LC of the CRM were based upon the collective opinion of a panel of experts (expert elicitation) (CRWMS M&O 1995). The model assumed that galvanic protection would delay LC (pitting) of the CRM until a specified percentage of the CAM thickness had been consumed by GC.

Exposure conditions included temperature, RH, presence of liquid-phase water (dripping), water chemistry, backfill, and rock fall (CRWMS M&O 1995).

Along with the improvements in the degradation modeling, the evaluation of materials selection for the WP barriers continued during the following several years. The corrosion resistant material, Alloy 825, was replaced with a more corrosion resistant nickel-based Alloy 625 during this period (CRWMS M&O 1996). The lifetime goals for the WP was increased further and resulted in the selection of Alloy 22 as the corrosion resistant barrier for the Viability Assessment design. The superiority of Alloy 22 is well known and generally accepted.

Additional improvements in the WP corrosion model were made for the Viability Assessment (VA) design (CRWMS M&O 1998a, Chapter 5). This model accounted for humid-air GC and LC of the CAM; aqueous-phase GC and LC of the CAM; and aqueous-phase GC and LC of the CRM. Degradation of the WP was modeled by dividing the surface into patches and populating the corrosion rates stochastically over the patches. The concept of a localization factor was used. Pitting of the CAM was assumed to occur under alkaline conditions ($pH \geq 10$).

Microbiologically influenced corrosion (MIC) and SCC were not accounted for in the TSPA models used for VA. The effects of salt deposition and evaporative concentration of dripping water on the WP surface were also neglected. These models were not based upon qualified

experimental data from materials testing in repository-relevant environments, but relied heavily on the opinion of experts and other published data. For this PMR, a broad range of laboratory data and associated process models have been developed to more realistically approximate the degradation processes of potential significance to repository performance. Changes to the degradation models have been necessitated by the changes in WP design and inclusion of the DS for Site Recommendation (SR).

2.3 TOTAL SYSTEM PERFORMANCE ASSESSMENT-SITE RECOMMENDATION APPROACH

The approach in the TSPA-SR WP degradation analysis is greatly enhanced version of that used in TSPA-VA. (For convenience of discussion in this section, the DS is modeled as an integral part of WP, and no separate discussion is given for DS.) The WAPDEG model, which is based on a stochastic approach, has been upgraded to include SCC and is used for the SR WP degradation analysis. The motivations for the stochastic approach used in the WAPDEG model are three-fold:

- To provide realistic representation of WP degradation processes in the repository.
- To capture the effects of variation and uncertainty both in exposure conditions and degradation processes over a geologic time scale.
- To perform analysis within a reasonable time and within computational resources.

Abstractions of the process-level models were developed for WAPDEG in a manner that allows important features of the process-level models to be captured as explicitly as possible, and in a manner that allows the degradation processes and their characteristics to be properly represented in the WP degradation analysis. More details of the TSPA-SR approach to WP and DS degradation analysis are given in the supporting AMR entitled *WAPDEG Analysis of Waste Package and Drip Shield Degradation* (CRWMS M&O 2000g).

As in the TSPA-VA analysis, effects of spatial and temporal variations in the exposure conditions over the repository were modeled by explicitly incorporating relevant histories of exposure condition into the WP degradation analysis. The parameters that represent exposure conditions were considered to be varying over the repository. These include RH and temperature at the WP surface, seepage into the emplacement drift, chemistry of seepage water, and rockfall. In addition, potentially variable corrosion processes within a single WP were represented by dividing the WP surface into unit areas called "patches" and stochastically populating the corrosion model parameter values and/or corrosion rates over each patch. The model parameter values and corrosion rates were sampled from their distribution over the range of the expected local exposure conditions.

In the nominal case analysis, the WPOB and DS were included in the WP degradation analysis. The stainless steel inner container, which is to provide structural support to WP, is not included in the degradation analysis. Although, this inner container would actually provide some performance for waste containment after the outer barrier breach, and would also provide a barrier to radionuclide transport after the WP is breached, the potential performance credit was

ignored in the nominal TSPA-SR analysis. This is a conservative approach. However, performance credit for the stainless steel is being evaluated for future consideration.

In summary, the TSPA-SR WP degradation analysis includes the following potentially important degradation processes:

- General corrosion (GC)
- Localized (pitting and crevice) corrosion (LC)
- Stress corrosion cracking (SCC) waste package outer barrier (WPOB only)
- Microbiologically influenced corrosion (MIC) (WPOB only)
- Long-term aging and phase instability of WPOB and their effect on corrosion, and
- Pre-existing manufacturing defects in the WP closure welds and its effect on SCC.

As previously discussed, significant improvements have been made to the GC and LC models, making them superior to those used in TSPA-VA. In the analysis, the DS was considered to be immune to SCC because it will be fully annealed before it is placed in the emplacement drift. Likewise, all the fabrication welds in the WP, except the welds for the closure lids, will be fully annealed and therefore not subject to SCC. Only the WP closure weld is considered in the SCC analysis. Two alternative SCC models were considered, the slip dissolution model and the threshold stress intensity factor model. The effect of radiolysis on corrosion is expected to be insignificant under the conditions expected in the repository (see Section 3.1.6.6), and was therefore not included in the nominal case analysis. The DS was assumed to be immune to the MIC. Since the bounding analyses have shown that the hydrogen uptake by the DS is much less than the threshold hydrogen concentration for HIC (CRWMS M&O 2000h, Sections 6.1.3 and 6.2.4), this mode of failure was not included in the DS degradation model.

WP failure requires through-wall penetration. The WAPDEG analysis tracks degradation of WP for three penetration modes: SCC (crack penetration), LC (rapid crevice penetration), and GC (slower uniform penetration). Here, localized attack is assumed to be crevice corrosion over an entire patch, which is conservative. The analysis provides, as output, the cumulative probability of WP failure by one of the three penetration modes as a function of time and also provides the number of penetrations for each of the penetration modes as a function of time. The WP failure time and number profiles for penetration are used as input to other TSPA analyses, such as the WF degradation and the radionuclide release rate from WPs.

The TSPA-SR analysis yields a more explicit representation (than previous TSPA analyses) of the uncertainty and variability in WP degradation (i.e., WP failure and penetration number profiles). For the corrosion models and parameters for which data and analyses are available, their uncertainty and variability were quantified and incorporated into the WAPDEG analysis. For other models and parameters for which the uncertainty and variability are not quantifiable, the variance in their value was assumed and used as uncertainty. In the TSPA-SR analysis, WP degradation was analyzed with multiple realizations of WAPDEG for the uncertainty analysis of the uncertain corrosion parameters—each WAPDEG realization corresponding to a complete WAPDEG run to account for the WP degradation variability for a given number of WPs. Accordingly, each of the WAPDEG analysis outputs (i.e., WP failure time, crack penetration number, pit penetration number, and patch penetration number) is reported as a group of curves that represents the potential range of the output values.

2.4 ISSUES RELATED TO WASTE PACKAGE DEGRADATION

This PMR also addresses related issues identified based on a review of the past two years Advisory Committee on Nuclear Waste (ACNW) and Nuclear Waste Technical Review Board (NWTRB) meeting summaries and correspondences, Viability Assessment (VA) Volume 3, Sections 6.5.2 and 6.5.3 and Volume 4 Section 4.3, TSPA peer review documentation, NRC comments on TSPA-VA, expert elicitation recommendations, and licensing correspondence files for the NRC, the State of Nevada, and the Nevada counties. Table 2-1 provides a summary of all identified issues and describes how each issue is addressed in this PMR. In addition, acceptance criteria from the *Issue Resolution Status Reports Key Technical Issue: Container Life and Source Term* (NRC 1999a), the *Issue Resolution Status Report Key Technical Issue: Total System Performance Assessment and Integration* (NRC 2000), and the *Repository Design and Thermal-Mechanical Effects Report* (NRC 1999b) are separately addressed in Table 4-1 in Chapter 4 of this document.

Table 2-1. Key External Issues for the Waste Package Degradation Process Model Report

Source	Issue	PMR Approach
TSPA-VA, Volume 3, Sec. 6.5.2 (DOE 1998)	Physical events and processes such as degradation of drift with time due to chemical and mechanical effects that have a potential for affecting the WP performance were not considered, or not sufficiently covered, within the TSPA-VA.	Degradation of the drift with time could result in rock fall, which can impact the DS and WP and increase potential for SCC. The incorporation of SCC as a failure mode initiated by rockfall (Section 3.1.7) may be useful in addressing early failures due to rockfall. This will have to be done in future analyses.
TSPA-VA, Volume 3, Sec. 6.5.2 (DOE 1998)	The panel believes that there is insufficient data to support the selection of the material for use in the final WP design.	Selection process for WP package materials has considered and evaluated all degradation processes. Several materials have been electrochemically tested, with a clear indication that Alloy 22 and Titanium Grade 7 are more corrosion resistant than other candidate materials. Section 3.1.1 provides an overview of the WP materials selected.
TSPA-VA, Volume 3, Sec. 6.5.2 (DOE 1998)	Uncertainties and limitations in WP degradation models (SCC, crevice corrosion, and WP surface chemistry) need to be verified.	In regard to crevice corrosion, experimental studies have been performed to define the crevice chemistry (pH, etc.). In regard to SCC, alternative models are employed. Stress mitigation techniques are being used as a means of eliminating SCC through elimination of the driving force (see Section 3.1.7). Details of these degradation modes are provided in the respective AMRs and PMR sections (Section 3.1.3, 3.1.6, and 3.1.7).
TSPA-VA, Volume 3, Sec. 6.5.2 (DOE 1998)	The issue states the need for additional research on water contact with the WP, critical crevice temperatures, Np solubility and technetium sorption on degraded WP.	Evaporative concentration experiments have been used to determine the concentrations of saturated electrolytes that may form on the surface of the hot WP (see Section 3.1.3). Critical crevice potentials and temperatures for the WP barrier materials have been determined and documented in the various AMRs and PMR Section 3.1.6. Np solubility and technetium sorption are not part of the scope of this PMR but are addressed in WF degradation PMR.
TSPA-VA, Volume 3, Sec. 6.5.3.2 (DOE 1998)	The rationale for including or excluding any potentially significant feature, event or process needs to be technically justified and clearly articulated.	Identification of FEP is discussed in Section 1.6.

Table 2-1. Key External Issues for the Waste Package Degradation Process Model Report (Continued)

Source	Issue	PMR Approach
TSPA-VA, Volume 3, Sec. 6.5.3.3 (DOE 1998)	Modeling assumptions should be consistent across different process models, unless there is a defensible technical rationale.	The AMRs that document assumptions for WP degradation are subject to thorough interdisciplinary reviews to help ensure consistency among assumptions made in more than one document about a given parameter. In addition, the PMR that summarize and integrate the results of the AMRs has been subjected to a review by a single review team, one of whose main objectives is to identify inconsistencies among the PMRs. Finally, assumptions used in the AMRs that feed WP degradation are documented in the WP PMR document. These measures provide confidence that consistent assumptions are used as appropriate among the various models that support the WP PMR.
TSPA-VA, Volume 3, Sec. 6.5.3.7 (DOE 1998)	Rockfall effects need to be considered in the design and performance of the Yucca Mountain repository system.	Analyses of seismically induced rockfall damage have been explicitly addressed in TSPA-SR.
NWTRB Letter to DOE (11-10-99) (Cohon 1999a)	The presentation on WP degradation indicated that valuable information is being collected on Alloy 22 at a rapid pace. However, concern still exists about the effects on corrosion of radiolytic species, including species formed in the vapor phase. Resolving that concern may necessitate additional experimental and theoretical work.	Experiments have been performed to determine the maximum increase in corrosion potential that can be caused by hydrogen peroxide, the primary product formed during gamma radiolysis of water. The maximum increase is approximately 200 mV, which is insufficient to cause initiation of LC with materials such as Alloy 22 (Section 3.1.6).

Table 2-1. Key External Issues for the Waste Package Degradation Process Model Report (Continued)

Source	Issue	PMR Approach
NWTRB Letter to DOE (8-3-99) (Cohon 1999b)	Regarding the engineered repository system, NWTRB highlights four areas: the need to vigorously pursue ongoing studies of degradation associated with stress-corrosion cracking and phase instability of proposed WP materials; the need to determine whether presently unrecognized corrosion mechanisms exist that would be important over the very long term; the need to complete experiments on the formation of radiolysis products in the near-field and to model the effects of such radiolysis products on near-field component degradation; and the need to intensify investigations into the performance of a titanium DS and the effect this DS and associated backfill would have on other elements of the engineered system.	Ongoing SCC studies are underway at the Corporate Research and Development Center of General Electric Corporation and at Lawrence Livermore National Laboratory (LLNL). All credible modes of corrosion such as phase stability and SCC are considered in the testing program and the WAPDEG code, so that the unexpected can be accounted for. Experiments have been performed to determine the maximum increase in corrosion potential that can be caused by hydrogen peroxide, the primary product formed during gamma radiolysis of water. The maximum increase is approximately 200 mV, which is insufficient to cause initiation of LC with materials such as Alloy 22. For example, a series of CP of Titanium Grade 7 have been performed in test solutions that are relevant to the repository (Sections 3.1.5 and 3.1.6).
NWTRB Letter to DOE (8-3-99) (Cohon 1999b)	Additional research is needed to determine the likelihood of new mechanisms (beyond typical LC processes) of deterioration that could affect the very-long-term stability of the passive layer for critical WP and other engineered barrier materials, such as Alloy 22 and titanium. This work could include, for example, examination of fundamental models of passive-regime stability and the factors that may cause deviation from passive-layer dissolution behavior assumed from short-term experiments, prediction of the behavior of the alloy surface under a thick layer of previous passive dissolution products, and a search for relevant natural and archeological analogs.	A variety of cutting edge techniques are now employed to study the long-term degradation of WP materials. For example, TEM is used to quantify the thermal aging of Alloy 22. Such quantification is in the form of TTT diagrams found in this PMR. Thermal aging is important in that it may result in the precipitation of undesirable intermetallic phases. These precipitates can lead to embrittlement and enhanced susceptibility to LC and SCC. Atomic force microscope (AFM) and X-ray photo electron spectroscopy are being employed to study passive film stability. SIMS is used to quantify the amount of hydrogen in the titanium-based materials that will be used for construction of the DS. All these modes of degradation are addressed in the PMR Sections 3.1.3 through 3.1.9. No appropriate natural or archeological analogs are available for Alloy 22 or titanium

Table 2-1. Key External Issues for the Waste Package Degradation Process Model Report (Continued)

Source	Issue	PMR Approach
NWTRB Letter to DOE (8-3-99) (Cohon 1999b)	The effects of the DS and backfill on the thermal and moisture regime between the DS and the WP and evaluating the corrosion behavior of titanium when it is in contact with backfill or rock fall. The vulnerability of the drip-shield connections to vibratory earthquake motion also needs to be addressed.	The testing of material samples have assumed same bounding chemistry for both the DS and the WP outer barrier (Section 3.1.3). The DS is designed to withstand expected earthquake motion and not separate.
TSPA Peer Review, Section II.C (Budnitz et al. 1999)	Experimental data are lacking throughout the treatment of the WP and EBS. In particular, the effect of realistic and extreme environments to come in contact with Alloy 22 and critical temperature for crevice corrosion of Alloy 22.	Electrochemical testing has been done in a wide variety of repository-relevant test solutions, including SDW, SCW, SAW, SCMW, SSW, and BSW. CP tests have been conducted in these media with artificial crevices. Long term exposure testing has been done in SDW, SCW, SAW, and SCMW at temperatures up to 90°C. To determine critical crevice temperatures, SCC testing is underway in similar solutions. Experiments have been performed to quantify the extent that pH can be lowered inside crevices, formed between the Alloy 22 WPOB and the 316NG SSSM (see Sections 3.1.6 and 3.1.7).
TSPA Peer Review, Section IV.D (Budnitz et al. 1999)	The TSPA-VA treatment of crevice corrosion was based on the adaptation of a pitting model. While similar chemical and electrochemical processes occur as part of both modes of corrosion, the TSPA peer review panel has concluded that a direct crevice corrosion model would be more realistic.	In the case of Alloy 22, pitting is not expected. If LC does occur, it is expected to be some form of crevice corrosion. Crevice chemistry determination has been conducted and documented in the supporting AMR and PMR Section 3.1.6.
TSPA Peer Review, Section IV.D (Budnitz et al. 1999)	There is a need both to improve the models and methods for analyzing water chemistries at the metal surfaces of the WPs under realistic conditions, and to collect experimental data to validate and verify these models and the associated analytical methods	From the evaporative concentration experiments, the saturated electrolytes that may form on the WP surface have been defined (Section 3.1.3).
TSPA Peer Review, Section IV.D (Budnitz et al. 1999)	As in the case of analyses of crevice corrosion, additional work will be necessary for SCC prior to the possible LA stage, especially in light of the tentative nature of the SCC model and the fact that failure mode is closely coupled to WP fabrication procedures.	The WAPDEG code now incorporates a wide variety of plausible failure modes, including SCC. The effects of residual weld stress in the final closure weld are now accounted for. The code has developed to a level of sophistication now able to account for stress mitigation techniques such as laser peening and induction annealing (Section 3.1.7).

Table 2-1. Key External Issues for the Waste Package Degradation Process Model Report (Continued)

Source	Issue	PMR Approach
TSPA Peer Review, Section IV.D (Budnitz et al. 1999)	At the present time, the corrosion behavior of WP with backfill or rock debris covering the WP is not well defined	Electrochemical testing has been done in a wide variety of repository-relevant test solutions, including SDW, SCW, SAW, SCMW, SSW, and BSW. BSW and SSW are determined to be bounding environments and cover the effects of backfill. CP tests are now being conducted in these media with artificial crevices. Experiments have been performed to quantify the extent that pH can be lowered inside crevices, formed between the Alloy 22 WPOB and the 316NG SSSM (Sections 3.1.3 and 3.1.6).
TSPA Peer Review, Section IV.D (Budnitz et al. 1999)	The treatment of Alloy 22 corrosion rates and the allocation of total variance to their variability and uncertainty need to be improved prior to the anticipated LA phase.	The large number of samples involved in testing in the LTCTF provide estimates of uncertainty for GC rates (for both HAC and APC). By performing large numbers of CP tests with at least three replicates at each condition, similar estimates of the uncertainty in electrochemical potential measurements are obtained. Separation of uncertainty and variability is difficult with these very corrosion resistant materials. In many cases, the corrosion rates are so low that the measurement limits are exceeded. The treatment of uncertainties and variability in the data is addressed in Section 3.1.9 of the PMR.
TSPA Peer Review, p. 8 (Budnitz et al. 1999)	The analyses (WAPDEG), however, were developed to a level of complexity that extended well beyond the data that were available. This complexity may be useful for the anticipated LA phase of sufficient data on key parameters become available. If not the panel believes that attempts to apply the WAPDEG model may compromise the transparency of the treatment. Necessary changes include an updating and/or revision of the model, including better integration of the multitude of process models used for analyzing various degradation modes or engineering enhancements and the development of a stronger case to confirm the linkage between the process models and their abstractions.	This comment is not longer applicable to the current WAPDEG model which is based on new data and new process models. As discussed in Section 3.2 of this PMR, several new models and correlations have been added replacing old models. The complexities of current models (general and localized corrosion, stress corrosion cracking etc.) are consistent with the available data.

Table 2-1. Key External Issues for the Waste Package Degradation Process Model Report (Continued)

Source		Issue	PMR Approach
AMR	Analysis and Model Report	SAW	simulated acidic concentrated water
APC	aqueous phase corrosion	SCC	stress corrosion cracking
BSW	basic saturated water	SCW	simulated concentrated water
CP	cyclic polarization	SCMW	simulated cement-modified water
DS	drip shield	SDW	simulated dilute water
EBS	engineered barrier system	SIMS	secondary ion mass spectrometry
GC	general corrosion	SSSM	stainless steel structural material
HAC	humid air corrosion	SSW	simulated saturated water
LA	License Application	TEM	transmission electron microscope
LC	localized corrosion	TSPA-VA	Total System Performance Assessment Viability Assessment
LTCTF	Long Term Corrosion Test Facility	TTT	time-temperature-transformation
Np	Neptunium	WPOB	waste package outer barrier
PMR	Process Model Report	WP	waste package

INTENTIONALLY LEFT BLANK

3. MODELS AND ABSTRACTED MODELS

The WP degradation process model consists of several different models: dry oxidation, humid air corrosion, aqueous phase corrosion, general corrosion, localized corrosion, microbiologically induced corrosion, stress corrosion cracking, and hydrogen-induced cracking. A generic integrated model containing the above component models is illustrated by Figure 1-4. This model can be applied to the DS and WP materials of interest.

3.1 MODEL DESCRIPTIONS

As stated above, the WP degradation process model includes a number of component models. These component models are discussed in the following sections. Model parameters and definitions for the individual models are provided in the respective AMRs.

3.1.1 Overview of Waste Package and Drip Shield Design

As described in the LADS report, the recommended WP design is EDA II (CRWMS M&O 1999a, Section 1.1.2). This design includes a double-wall WP underneath a protective DS. The DS is to be fabricated from Titanium Grade 7. The EDA II corrosion resistant WPOB is to be fabricated from nickel-based Alloy 22. Stainless steel 316NG is to be used for construction of the structural support container within the WPOB. The 316NG inner cylinder will increase the overall strength of the WP.

3.1.1.1 Titanium Drip Shield

Titanium alloys (1.5-cm thick) have been considered for construction of the DS. The current recommendation is to use Titanium Grade 7 [Unified Numbering System for Metals and Alloys (UNS) R52400]. The composition of this alloy is 0.03% N (max), 0.10% C (max), 0.015% H (max), 0.25% O (max), 0.30% iron (max), 0.12-0.25% Pd (max), and 0.4% Residuals (total), with the balance being Ti (approximately 98.7 to 98.8%). The nominal thickness of the DS is 15 mm. Properties and performance of these materials are reviewed elsewhere and cited in the respective AMRs. The unusual corrosion resistance of titanium alloys is due to the formation of a passive film of TiO_2, which is stable over a relatively wide range of electrochemical potential and pH. A similar material, Titanium Grade 16 with 0.04 to 0.08% Pd, is used as an analog for Titanium Grade 7 in some parts of the testing program. The rates of general corrosion and dry oxidation (or dry air oxidation) of this material have been shown to be very low. Corrosion testing of Titanium Grade 16 has been conducted in the Long Term Corrosion Test Facility (LTCTF) of the YMP (CRWMS M&O 2000d, Section 6.5).

3.1.1.2 Nickel-Based Waste Package Outer Barrier

Alloy 22 [UNS N06022] (2.0 cm thick) is now being considered for construction of the WPOB. This alloy consists of 20.0-22.5% chromium, 12.5-14.5% molybdenum, 2.0-6.0% iron, 2.5-3.5% W, and 2.5% Co (max), with the balance being nickel (approximately 50-60%). Other impurity elements include P, Si, S, Mn, Nb, and V. Alloy 22 is less susceptible to LC in environments that contain Cl^- than Alloys 825 and 625, materials of choice in earlier WP designs. Corrosion testing of Alloy 22 has been and continues to be conducted in the LTCTF of

the YMP (CRWMS M&O 2000c, Section 6). Nominal thickness of the Alloy 22 shell is 20 mm for the commercial spent fuel packages and 25 mm for the packages containing navy waste.

3.1.1.3 Stainless Steel Structural Material

316NG stainless steel (5-cm thick) is to be used for construction of the structural support inside the WPOB. This inner cylinder of 316NG stainless steel will increase the overall strength of the WP. 316L stainless steel is considered to be a good analog for 316NG stainless steel because the chemical composition of the two alloys is essentially the same, except that 316NG stainless steel has better mechanical properties than 316L. 316 stainless steel [UNS S31603] has a composition of 16-18% chromium, 10-14% nickel, 2-3% molybdenum, 2% Mn (max), 1% Si (max), 0.03% C (max), 0.045% P (max), 0.03% S (max), 0.10% N (max) and the balance being iron (65-69%). 316L stainless steel is less susceptible to LC in environments that contain Cl^- than stainless steel 304, but more susceptible than other corrosion resistant materials such as Alloys 22, 625 and 825 that have been considered in various WP designs. The superior LC resistance of 316L stainless steel in comparison to 304 stainless steel is apparently due to the addition of molybdenum, which helps to stabilize the passive film at low pH values. Molybdenum oxide is very insoluble at low pH. Consequently, 316L stainless steel exhibits relatively high thresholds for localized attack (CRWMS M&O 2000e, Section 1.2).

3.1.2 Manufacturing Defects (Early Failure AMR)

Manufacturing defects and failure modes that might lead to early failure of a WP are accounted for in an AMR (CRWMS M&O 2000m, Section 6) that supports this PMR. The AMR on early failure includes a literature review directed towards obtaining information on the rate of manufacturing defect-related failures in various types of welded metallic containers, the types of defects that produce these failures, and the mechanisms that cause defects to propagate to failure. Types of defects applicable to the current WP design are identified. For each applicable type of defect, the probability of its occurrence on a WP is estimated. Potential consequences to the long-term performance of the WP if the defect is present are discussed. Specific details on how the defect will affect WP materials are provided in separate AMR on SCC (CRWMS M&O 2000f, Section 6). Defects or flaws may serve as initiation sites for SCC.

3.1.2.1 Analysis Assumptions in AMR

The following assumptions support the development of probabilities for various size flaws in the welds of the WP shell and lids. Based on the similarity of the processes used for welding Alloy 22 and stainless steel, they are predicted to have the same frequency and size distributions for flaws. Information on the reliability of radiographic, ultrasonic, and dye-penetrant testing is assumed to be applicable to the materials and inspection methods that will be used for the WP. This information is based on older reliability studies of these non-destructive examination methods, and the assumption that future improvements in the inspection technology will result in increases in the probability of flaw detection. It was assumed that flaws detected by post-weld inspections will be repaired, whenever the flaw size is larger than the flaw size of concern for postclosure performance. Embedded weld flaws are not considered to be a concern for postclosure performance in the supporting AMR (CRWMS M&O 2000m, Section 6), since the WP is not a pressure vessel and will not be subjected to cyclic fatigue (the primary mechanism

for causing such flaws to grow through-wall in pressure vessels). However, as the weld undergoes GC, subsurface flaws may eventually be exposed.

The probabilities of human error have not been quantified for the specific actions associated with the fabrication of the WP, but the information used represents human error probabilities for similar types of actions.

In developing the probability of the use of improper material in the WP shell or lid welds, it is assumed that a field verification of the chemical composition of weld wire will be performed prior to its use in fabricating any weld and that material controls required in nuclear quality programs will be used. It is further assumed that such field verification will use state-of-the-art instrumentation. This assumption is based on the expected administrative requirements on the process qualification program.

Assumptions are used to support the development of the probability of having corrosion-enhancing surface contamination on the WP or improper heat treatment of the WP. These assumptions are based on the general descriptions of these activities. The assumptions support the development of event sequence trees for quantifying the probabilities of improper heat treatment or a failure in the cleaning process. The assumptions involve the number of operators involved in each process, the QA procedures and inspections governing the processes, and the reliability of the equipment used.

It is assumed that the probability of damaging a WP during transport or handling at the repository is equivalent to the probability of damaging spent nuclear fuel (SNF) assemblies during transport or handling. The basis for this assumption is that a WP will be subjected to about the same number of handling steps as a SNF assembly. It is assumed that both are handled with about the same amount of care. It is expected that the WP will be inspected for handling damage upon arrival at the repository and before final emplacement in the drift. It is further expected that the WP will be completely repaired or scrapped if such handling damage occurs.

3.1.2.2 Analysis Description in AMR

The AMR presents the results of a literature review performed to determine the rate of manufacturing defect-related failure for various types of welded metallic containers. In addition to providing examples of the rate at which defective containers occur, this information provides insight into the various types of defects that can occur and the mechanisms that cause defects to propagate to failure. In summary, eleven generic types of defects were identified. These are:

1. Weld flaws
2. Base metal flaws
3. Improper weld material
4. Improper heat treatment
5. Improper weld flux material
6. Poor weld joint design
7. Contaminants
8. Mislocated welds
9. Missing welds

10. Handling and installation damage
11. Administrative and operational error.

For dry storage casks, all of the defects were identified by post-weld inspection prior to commencement of the storage phase, and thus do not represent true instances of early failure as it is defined in the AMR. The eleven types of defects were reviewed for their applicability to the WP. From this review, the following generic defect types are considered *not applicable* to the WP: improper weld flux material, poor weld joint design, missing welds, and mislocated welds. This determination is based on the fact that the welding process for WP fabrication does not use flux as noted in the AMR. Poor joint design is unlikely because of extensive development and testing. Missing welds and mislocated welds are easily detected and controlled by process qualification. The probability of occurrence and the effect on postclosure performance of the WP are assessed for the remaining defects.

Using information on linear flaw density, flaw size distribution, inspection reliability, and information on various weld lengths, frequencies of weld flaws of various size that break the outer surface have been estimated in the supporting AMR (CRWMS M&O 2000m). The procedure is essentially the same for all cases. First, the total flaws per type of WP weld were calculated by multiplying the weld length by the linear flaw density and by an adjustment factor for the weld thickness. The base linear flaw density with credit for radiographic and dye-penetrant test inspections was used for the shell and bottom lid welds, and the uninspected flaw density was conservatively used for the top lid closure weld. Next, the flaw size distribution for that weld thickness was used to determine the probability that a flaw would have a size within a given range. A range size of 0.5% of the weld thickness was used. This was the largest size range that could be used without introducing any significant (within two significant figures) amount of numerical error associated with discretizing a continuous size distribution. The probability for each size range was then multiplied by the total number of flaws per weld to determine the expected number of flaws within that size range. For welds subjected to an ultrasonic (UT) inspection, the expected number of flaws within each size range was then reduced by multiplying by the probability of nondetection (PND) for the lower end of the size range. This is conservative because the PND is higher for smaller flaws and ultrasonic inspection identifies small flaws. Since the UT PND is based on a single angle UT examination and a multi-angle examination is planned for the lid welds (possibly four angles), the square of the PND was used for the lid welds. This effectively treats a multi-angle exam as two independent examinations. For all cases, each range was then multiplied by 0.34% to yield the expected number of outer surface breaking flaws within that range. Finally, the expected number of outer surface breaking flaws in each size range were summed to determine a new value for total flaws per weld which accounts for the UT inspections. A complementary cumulative distribution of outer surface breaking flaw size was also determined. These results are summarized in Figure 3-1 for the Alloy 22 barrier shell welds, and in Figure 3-2 for the Alloy 22 barrier lid welds.

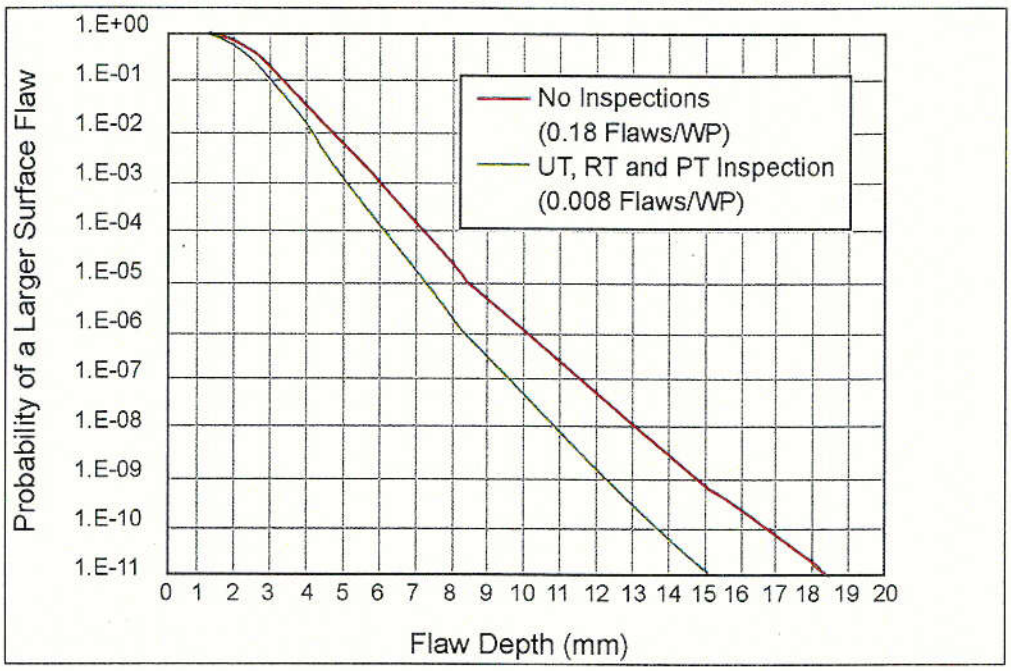

Source: CRWMS M&O 2000m

Figure 3-1. Size Distribution for Indicated Frequency of Occurrence for Outer Surface Breaking Flaws in Waste Package Alloy 22 Shell Welds

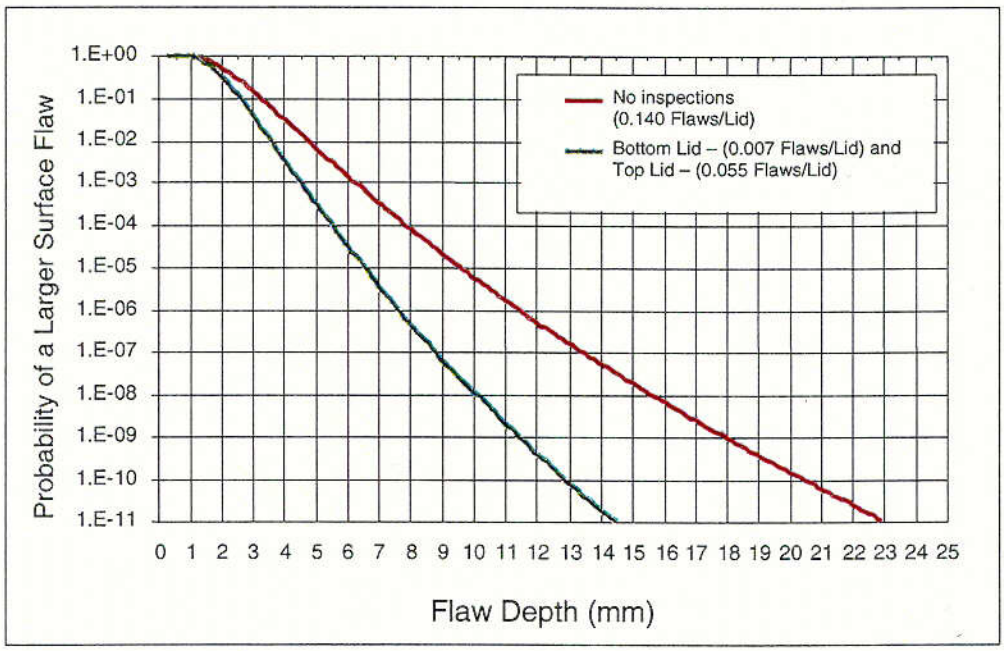

Source: CRWMS M&O 2000m

Figure 3-2. Size Distribution for Indicated Frequency of Occurrence of Outer Surface Breaking Flaws in Waste Package Alloy 22 Lid Welds

C-3

3.1.2.3 Uncertainties in AMR

The inputs used to estimate the probability of various defects that can potentially lead to early failure are open to interpretation and uncertainty. An uncertainty analysis was performed to develop an upper bound for an event sequence probability based on the uncertainty of modeled human actions. The analysis applies to those defects for which probabilities are estimated using event sequence trees, namely: DS emplacement error, WP handling error, WP surface contamination, thermal misload, and improper heat treatment. The method used to establish an upper bound value for event sequences combines the human error rates probabilistically. Uncertainties are considered only for human error probabilities related to failures. Probability components for success are treated at their nominal level (i.e., without uncertainty), which produces conservative results. No upper bounds were estimated for other failure probabilities related to mechanical failure or based on historical data. Accordingly, the upper bound for an event sequence probability is adjusted for human error probability uncertainties only (CRWMS M&O 2000m).

3.1.2.4 Analysis Conclusions in AMR

The AMR on early failure of the WP reviewed available literature on defect-related early failures of welded metallic components. Types of components examined include boilers and pressure vessels, nuclear fuel rods, underground storage tanks, radioactive cesium capsules, dry-storage casks for SNF, and tin-plate cans. The fraction of the total population that failed due to defect-related causes during the intended lifetime of the component is generally in the range of 10^{-3} to 10^{-6} per container. In most cases, defects that lead to failure of the component require an additional stimulus to cause failure (i.e., the component was not failed when it was placed into service). There were several examples that indicate that even commercial standards of quality control could reduce the rate of initially failed components well below 10^{-4} per container. The literature review identified eleven generic types of defects that could cause early failures in the components examined: weld flaws; base metal flaws; improper weld material; improper heat treatment; improper weld flux material; poor weld joint design; contaminants; mislocated welds; missing welds; handling and installation damage; and administrative error resulting in an unanticipated environment. The following defect types are considered "not applicable" to the WP: improper weld flux material, poor joint design, missing welds, and mislocated welds. The analysis estimates the probability that specific defect types will occur on a given WP, despite a set of quality controls designed to prevent their occurrence. Results of the analysis for the remaining seven types of defects are shown in Table 3-1.

Table 3-1. Summary of Estimated Probabilities and Performance Consequences for Various Types of Waste Package Defects

WP Defect Type		Probability per WP		Possible Consequences for Postclosure Performance				
		Alloy 22 Barrier	SS Structural Barrier	Minimal Effect	Degraded Mechanical Properties	Pitting or Crevice Corrosion	SCC	Early Water Contact
Weld Flaws (Outer Surface Breaking Only)		$< 10^{-4}$ for flaws > 4 mm deep	$< 10^{-4}$ for flaws > 10 mm deep			X	X	
Base Metal Flaws		Factor of 10^{-4} lower than uninspected weld flaw rate				X	X	
Improper Weld Material		1.5×10^{-5}	3.0×10^{-5}		X	X		
Improper Heat Treatment		2.2×10^{-5}			X	X	X	
Surface Contamination		7.3×10^{-5}	4.0×10^{-5}			X		
Handling Damage		5.1×10^{-6}	5.1×10^{-7}			X		
Administrative Error Leading to Unanticipated Environment	Thermal Misload of WP	1.0×10^{-3} to 1.0×10^{-6}			X			
	DS Emplacement Error	1.8×10^{-4}						X

NOTE: SS = stainless steel; WP = waste package

3.1.2.5 Accounting for Embedded Flaws

While the AMR based the determination of flaw density on surface-breaking flaws, a more conservative approach is to base such determinations on embedded flaws. The recent work by Khaleel et al. (1999) is cited. The TSPA analysis that will be discussed in subsequent sections uses estimates of flaw density based upon data given in Table V of this reference. Specifically, the values for embedded flaws at depths equivalent to the outer quarter of the wall thickness are used. In the dual-lid WP design, cumulative distribution functions are needed for the closure welds of both the inner and outer lids. The flaw density for the outer lid weld is 18 defects per WP at the 50^{th} percentile, and 40 defects per WP at the 100^{th} percentile. The flaw density for the inner lid weld is 15 defects per WP at the 50^{th} percentile, and 40 defects per WP at the 100^{th} percentile (same as outer lid at 100^{th} percentile). Note that each closure weld is represented by thirty two (32) WAPDEG patches.

3.1.2.6 Accounting for Flaw Orientation

In considering the potential effects of weld defects on SCC, the presence of planar defects in the region of the weld and heat-affected zone (HAZ), where weld-induced residual tensile stress exists, can lead to SCC initiation and growth. The two principal attributes of such weld defects that foster SCC are the stress concentration effect at the base of the defects, which can generate a stress intensity, and the occluded nature of such defects that may lead to the development of more aggressive crevice chemistry within the defect volume. However, as described in the SCC AMR, only defects oriented normal to the direction of the weld centerline (radially oriented defects) have sufficient calculated stress intensity to drive a stress corrosion crack through wall.

Weld defect types and expected defect orientation for the closure weld case are described briefly below.

The fabrication welds will be performed at the contractors' facilities. Currently, only two weld methods are being considered for the fabrication process, gas metal arc and tungsten inert gas methods. This automatically eliminates slag inclusions, the most commonly found defect when the autosubmerged arc welding process is used. The most common defects for gas metal arc and tungsten inert gas are lack of fusion. This occurs because of missed sidewall or lack of penetration in the sidewall. This generally produces large defects that are readily found by ultrasonic and radiographic inspection. The other defect types are tungsten inclusion, silicon, and porosity. Because both ultrasonic and radiographic methods will be used for post-weld inspections, there should be no undiscovered defects for these welds. Additionally, dye penetrant inspection will be performed on the surface of the weld to detect and repair any surface-breaking defects. The lack of fusion defect is, by definition, oriented in the direction of the weld bead. The silicon, porosity, and tungsten are rounded defects that have no direction.

The closure weld will be made in the hot cell facility using the narrow groove tungsten arc welding process. This, by definition, eliminates the lack of fusion defects between beads since this is a single-pass process. The other defects such as tungsten inclusion, caused by the flaking of the tungsten electrode, and porosity, caused by the loss of gas coverage, are easily detectable by monitoring systems that will be built into the welding system. This leaves only nonfusion

defects, which are detectable by ultrasonic testing (UT). All of the above defects are either rounded or in the direction of the weld seam; none is oriented in the radial direction.

The defect description discussed above is consistent with the brief comment on flaw orientation in the Early Failure AMR, "No information was found in the literature regarding angle of the flaw from a line parallel to the direction of the weld. However, most planar defects, such as lack of fusion and slag inclusions, would logically be expected to be oriented within a few degrees of the same direction in which the weld head is moving."

This flaw description is also consistent with the relevant literature paper (Shcherbinskii and Myakishev 1970) that describes a statistical treatment of weld-flaw orientations based on analysis of a significant data set of ultrasonic flaw orientation measurements. This paper concludes that planar-type weld defects detected ultrasonically tend to be predominately oriented in the direction of the weld centerline. It appears that more than 98% of the defects fall within ±16 degrees of the weld centerline in the case of steam-pipe welds. A similar conclusion is drawn from the data for sheet-structure welds. Statistical distribution of the defects with respect to the orientation angle yields a probability of 99% that the defects are located within about ±13 degrees. This suggests that much less than 1% of these flaws have a potential to undergo SCC.

Above discussions indicate that a correction factor for weld-flaw orientation for the embedded flaw density in the outer quarter of the thickness should be applied and used in waste package lifetime calculations. Based on the welding process and the inspection techniques to be employed for the closure welds, and the narrowness of the flaw orientation distributions presented in the subject paper, it is recommended that a conservative multiplication factor of 0.01 (1%) be used on total number of flaws of any given size for the subsurface flaws.

Ultrasonic examinations have now been performed on three actual WP welds on two mock-ups. These were unannealed closure welds, one on Alloy 625 and two on Alloy 22. The total length of weld was approximately 45 feet, and no defects were detected. Therefore, the probability of defects with actual welds is not inconsistent with low-defect densities that will result from this recommendation.

3.1.3 Environment on the Surface of the Waste Package and Drip Shield

The WP will experience a wide range of environments during its service life. Initially, it will be hot and dry due to the heat generated by radioactive decay. However, the temperature will eventually drop to levels where both HAC and APC will be possible. A companion AMR *Environment on the Surface of the Drip Shield and Waste Package Outer Barrier* (CRWMS M&O 2000a, Section 6) defines the detailed evolution of the environment on the WP surface. Input for this AMR includes bounding conditions for the local environment on the WP surface, which include temperature, RH, presence of liquid-phase water, liquid-phase electrolyte concentration (chloride, buffer, and pH), and oxidant level. This AMR has been used to define the threshold RH for HAC and APC, as well as a medium for testing WP materials under what is now believed to be a worst-case scenario. These test media are the neutral-pH SSW and the high-pH BSW, with nominal boiling points of 112 and 120°C, respectively.

Crevices will be formed between the WP and supports, beneath mineral precipitates, corrosion products, dust, rocks, cement, and biofilms. After the WP fails, the gap between the WPOB and the stainless steel structural support can form crevices where the environment may be more severe than the NFE. The hydrolysis of dissolved metal can lead to the accumulation of H^+ and a corresponding decrease in pH. Electromigration of Cl^- (and other anions) into the crevice must occur to balance cationic charge associated with H^+ ions. These conditions can exacerbate subsequent attack of the WPOB and stainless steel structural material by general and LC, SCC, and other mechanisms. Crevices might also form with the DS. These are addressed in the general and LC discussions in Sections 3.1.5 and 3.1.6.

3.1.3.1 Threshold Relative Humidity

As represented by Equation 3-1, HAC can occur at any RH above the threshold (CRWMS M&O 2000c, 2000d, 2000e):

$$RH \geq RH_{critical} \qquad \text{(Eq. 3-1)}$$

Rates of HAC and APC are represented by the same cumulative distribution function. HAC is assumed to occur uniformly over each patch used in the WAPDEG code. Each patch is comparable in size to that of a LTCTF test sample.

As discussed in the AMR *Environment on the Surface of the Drip Shield and Waste Package Outer Barrier* (CRWMS M&O 2000a, Section 6.4.2), hygroscopic salts may be deposited on the EBS components by aerosols and dust entrained in ventilation air, backfill, seepage water that enters the drifts, and the episodic water that flows through the drifts. Hygroscopic salts enable aqueous solutions to exist at relative humidities below 100%. The threshold RH ($RH_{critical}$) at which an aqueous solution will form for a particular salt is defined as the deliquescence point. This threshold RH defines the condition necessary for aqueous electrochemical corrosion of the metal to occur. The deliquescence point of NaCl is relatively constant with temperature, and is in the range 74-76% RH. In contrast, the deliquescence point of $NaNO_3$ has a strong dependence on temperature, ranging from an RH of 75.36% at 20°C to 65% at 90°C. The equilibrium RH is 50.1% at 120.6°C, which is the boiling point of the saturated solution at 101.32 kPa. The evaporative concentration of well J-13 water, which is assumed to be typical of waters contacting the EBS components, results in a solution of Cl^-, NO_3^-, CO_3^{2-} Na^+ , and K^+ ions. Other ions that could form salts with lower deliquescence points, such as Ca^{2+} and Mg^{2+}, are precipitated. It is therefore conservatively assumed that the deliquescence point of $NaNO_3$ determines the threshold RH. The equilibrium RH for a saturated solution of $NaNO_3$ as a function of temperature is shown in Figure 3-3. The experimental data fit the following polynomial in temperature:

$$RH_{critical} = -3.5932\times10^{-5}\times T(°C)^3 + 5.9649\times10^{-3}\times T(°C)^2 - 0.45377\times T(°C) + 81.701 \qquad \text{(Eq. 3-2)}$$

The goodness of fit is characterized by

$R^2 = 0.9854$

where R^2 is the coefficient of determination and where R is the coefficient of correlation. This correlation is shown in Figure 3-3 below. The uncertainty in $RH_{critical}$ is discussed in the AMRs on surface environment.

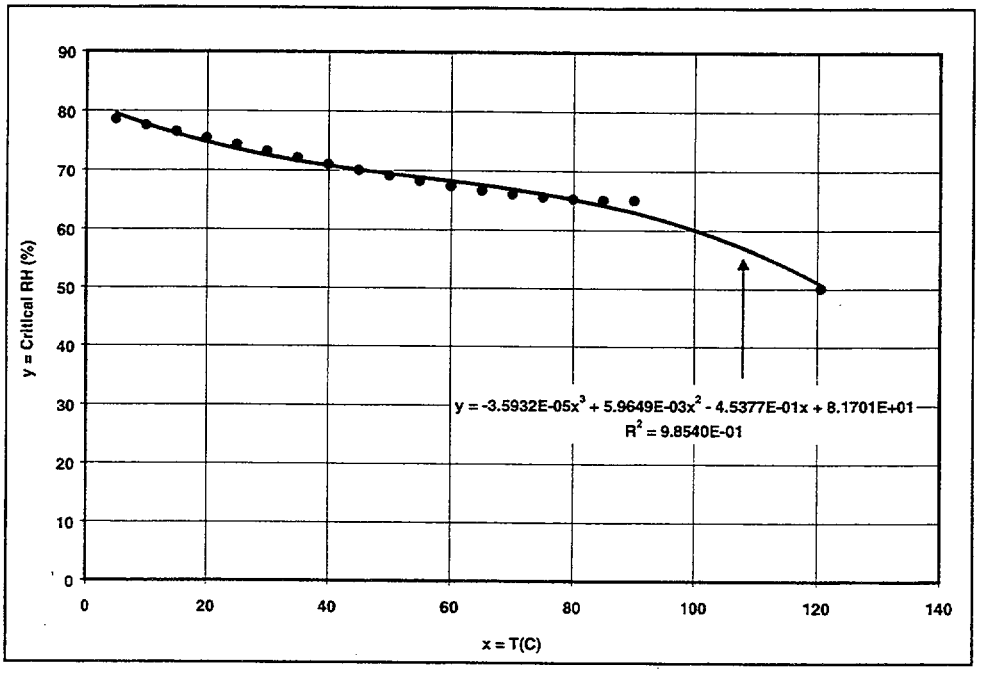

Source: CRWMS, M&O 2000a, Section 6.4.2

Figure 3-3. Deliquescence Point for Sodium Nitrate Solutions

The evaporation of J-13 water results in high concentrations of Na^+, K^+, Cl^-, NO_3^-, and CO_3^{2-}. The concentrations of F^- and SO_4^{2-} initially increase, but eventually fall due to precipitation. The SSW used for testing is an abstract embodiment of this observation (Section 1.5.4.3). This formulation is based upon the assumption that evaporation of J-13 water will eventually lead to a sodium-potassium-chloride-nitrate solution. The elimination of carbonate in this test medium is believed to be conservative, in that carbonate would help buffer pH in any occluded geometry such as a crevice.

3.1.3.2 Aqueous Phase Environments

At a given surface temperature, the existence of liquid-phase water on the WP depends upon the nature of the hygroscopic salt either present on the surface or contained in water dripping on the surface. Two conditions must exist for APC: dripping water, and RH above the deliquescence point of the hygroscopic salts in the dripping water. While dripping can occur without the latter condition being met, both conditions are necessary for APC. Without this level of RH, no aqueous phase could be sustained on the surface. However, this requires that the evaporation rate of water from the surface exceeds the rate of dripping so that equilibrium conditions exist (CRWMS M&O 2000a).

This model uses Equation 3-2 to conservatively estimate the threshold RH for APC ($RH_{critical}$). The composition of the electrolyte formed on the WP surface is assumed to be that of SCW below temperatures of 100°C, and that of SSW above temperatures of 100°C. These media are defined in Section 1.5.4.3. Their compositions are shown in Table 3-2 (CRWMS M&O 2000a, Section 6.12). General APC is assumed to occur uniformly over each WAPDEG patch, which is the same size as a standard LTCTF weight-loss sample. Effects of backfill are not considered on the APC threshold and rate.

Table 3-2. Composition of Standard Test Media Based upon J-13 Well Water

Ion	J-13 (mg liter^{-1})	SDW (mg liter^{-1})	SCW (mg liter^{-1})	SAW (mg liter^{-1})	SSW (mg liter^{-1})
K^{+1}	5.04	3.40E+01	3.40E+03	3.40E+03	1.416E+05
Na^{+1}	45.8	4.09E+02	4.09E+04	4.09E+04	4.870E+05
Mg^{+2}	2.01	1.00E+00	1.00E+00	1.00E+03	0.000E+00
Ca^{+2}	13.0	5.00E-01	1.00E+00	1.00E+03	0.000E+00
F^{-1}	2.18	1.40E+01	1.40E+03	0.00E+00	0.000E+00
Cl^{-1}	7.14	6.70E+01	6.70E+03	2.450+04	1.284E+05
NO_3^{-1}	8.78	6.40E+01	6.40E+03	2.300+04	1.310E+06
SO_4^{-2}	18.4	1.67E+02	1.67E+04	3.860+04	0.000E+00
HCO_3^{-1}	128.9	9.47E+02	7.00E+04	0.00E+00	0.000E+00
Si	28.5	27 (60°C), 49 (90°C)	27 (60°C), 49 (90°C)	27 (60°C), 49 (90°C)	0.000E+00
pH	7.41	8.1	8.1	2.7	7.0

3.1.3.3 Condensation Underneath Drip Shield

Moist air and liquid water flow into and within the drift over time. Although the RH underneath the DS increases with time, conditions for condensation on the DS can only occur if the DS is cooler than the top of the invert and the invert moisture content produces nearly 100% RH. This is unlikely since the surfaces of the WP and DS are at a higher temperature than the invert.

3.1.3.4 Composition of Water on Exposed Surfaces of Drip Shield and Waste Package

The YMP has used test media relevant to the environment expected in the repository. Relevant test solutions are assumed to include SDW, SCW, and SAW at 30, 60, and 90°C, as well as SSW at 100 and 120°C (Section 1.5.4.2). The compositions of all of the environments are given in Table 3-2. While most of the solutions have been used for several years, the SSW has been recently developed. In general, anions such as chloride promote LC, whereas other anions such as nitrate tend to act as corrosion inhibitors. Thus, there is a very complex synergism of corrosion effects in the test media.

BSW represents another plausible extreme in water chemistry. The BSW composition was established on the basis of results from a distillation experiment. Tables 3-3 and 3-4, show the corresponding water chemistry. The total concentration of dissolved salts in the starting liquid was approximately five-times (5×) more concentrated than that in the standard SCW solution. It was prepared by using five-times the amount of each chemical that is specified for the preparation of SCW. After evaporation of approximately ninety percent (~90%) of the water from the starting solution, the residual solution reaches a maximum chloride concentration and has a boiling point of ~112°C. The resultant BSW solution contains (sampled at 112°C) 9% chloride, 9% nitrate, 0.6% sulfate, 0.1% fluoride, 0.1% silicate, 1% (total inorganic carbon from carbonate and bicarbonate), 5% potassium, ion, and 11% sodium ion.

In order to add some soluble silica to the solution, the initial BSW solution recipe was later revised to contain ~1% metasilicate by adding sodium metasilicate ($Na_2SiO_3 \bullet 9H_2O$). This solution is designated as BSW-SC where SC indicates the presence of silicate and carbonate in the solution.

The pH of aqueous solutions is affected by the partial pressure of CO_2 in the gas phase. The implication of this is that unless an effort is made to control the pH of the BSW solution, the pH may vary with test conditions and time. In order to conduct long-term testing (months to years), the test environments should be stable. Stable test solutions require that carbonate and silicate not be added. Both of these species can affect pH. Furthermore, gaseous CO_2 must be removed from the air passing above the solution. With no gaseous CO_2 in contact with the solution, and with no carbonate-bicarbonate or silicates in solution, the test environments will be stable. Sodium hydroxide is used to maintain the higher pH of the solution.

Table 3-3. Initial Basic Saturated Water Solution Recipe

Chemical	Quantity (g)
Na_2CO_3 (anhydrous)	10.6
KCl	9.7
NaCl	8.8
NaF	0.2
$NaNO_3$	13.6
Na_2SO_4 (anhydrous)	1.4
H_2O	55.7

Source: CRWMS M&O 2000a, Section 6.12

Table 3-4. Modified Basic Saturated Water Solution Recipes

	BSW-13	BSW-12	BSW-11
Chemical	Quantity	Quantity (g)	Quantity (g)
KCl	8.7 g	8.7 g	8.7 g
NaCl	7.9 g	7.9 g	7.9 g
NaF	0.2 g	0.2 g	0.2 g
$NaNO_3$	13.0 g	13.0 g	13.0 g
Na_2SO_4 (anhydrous)	1.4 g	1.4 g	1.4 g
H_2O (deionized)	66 ml	66 ml	66 ml
10N NaOH	2 ml		
1N NaOH		2 ml	
0.1N NaOH			2 ml
CO_2 partial pressure	0	0	0
pH (measured at room temperature)	13.13	12.25	11. 11

Source: CRWMS M&O 2000a, Section 6.12

NOTE: The CO_2 partial pressure can be minimized by either scrubbing laboratory air or purchasing CO_2 free air.

In order to maintain constant pH conditions, the BSW solution was modified for corrosion tests, yielding BSW-11, BSW-12, and BSW-13. The three solutions have pH values of approximately 11, 12, and 13, respectively. The recipes of these solutions are given in Table 3-4.

3.1.4 Phase Stability and Aging

Exposure of materials like Alloy 22 to elevated temperatures can result in the formation of undesirable phases. The phases which form in Alloy 22 are often rich in molybdenum and chromium, the two elements that are responsible for the high degree of corrosion resistance of this material. The formation of precipitates depletes these alloying elements from the surrounding areas, therefore increasing susceptibility to general and LC, as well as SCC. Formation of brittle molybdenum- or chromium-rich intermetallics can also lead to embrittlement of the material and degradation of its mechanical properties. LRO in alloys similar to Alloy 22 has been linked to an increased susceptibility to SCC and hydrogen embrittlement.

The aging of Alloy 22 is dependent on both time and temperature. While the effects of aging have been observed for exposures to elevated temperatures (>600°C) for short time periods, it is important to know the kinetics of this process to enable prediction of aging effects for lower temperatures (200-300°C) and much longer times (10,000 years).

This section discusses the process-level model developed to account for aging and phase stability in Alloy 22. The development of this model is presented in detail in the corresponding AMR (CRWMS M&O 2000b). Only the highlights will be presented here.

3.1.4.1 Phase Identification in Alloy 22

The long-term aging of Alloy 22 at elevated temperature can cause the precipitation of undesirable intermetallic phases, if the temperature is sufficiently high. In order to provide a technical basis for the development of a model for aging effects in Alloy 22, samples were aged for a variety of times at different temperatures: for 40,000 hours at 260, 343, and 427°C; for 30,000 hours at 427°C; for 1000 hours at 482, 538, and 593°C; and for 16,000 hours at 593, 649, 704, and 760°C. Samples were then examined with transmission electron microscopy (TEM). A weld sample aged at 427°C for 40,000 hours was also examined in the weld metal, in the HAZ, and in the base metal removed from the weld. Several phases were observed to form in Alloy 22: P, μ, σ, carbide, and Ni_2 (Cr, Mo) LRO. At 593°C, P phase was observed only on the GB. At the higher aging temperatures (649, 704, and 760°C), both μ and P phases precipitated on grain boundaries. As the aging temperature increased, more μ and P phase precipitation occurred within the grains. GB carbide precipitation was observed in samples aged at 593 and 704°C. Because of the small amount of carbide present in these samples and the small volume examined in TEM, it is likely that carbides also form at 649°C. A σ phase was observed in the samples aged at 704 and 760°C. The amount of σ phase observed in these samples was small compared to the amount of μ and P phases. Long range order (LRO) was observed in the samples aged at 593°C for 16,000 hours and for 1,000 hours, in the sample aged at 538°C for 1,000 hours, and in the samples aged at 427°C for 40,000 hours and for 30,000 hours. These observations are summarized in Table 3-5.

3.1.4.2 Kinetics of Intermetallic Precipitation in Alloy 22 Base Metal

Table 3-6 shows the aging times for the various stages of intermetallic precipitation in Alloy 22 base metal as a function of temperature. These times were approximated from the examination of aged samples after approximately 1, 10, 100, 1000, and in some cases 16,000 hours. The errors noted are due to the uncertainty associated with the coarse time intervals of examination, and are not due to any measurement and test equipment uncertainties, which are much smaller. For example, if precipitation was observed on twin boundaries at 100 hours, it could have begun at any time between 10 and 100 hours. In that case, the time noted for the start of precipitation on the twin boundaries would be 55 hours (halfway between 10 and 100), with upper and lower error bars of 45 hours. Because of the coarse examination intervals, there is some judgment involved in choosing the times noted in Table 3-6. These measurements are only intended as an initial estimate of the precipitation kinetics. These measurements were also used to generate the isothermal time-temperature-transformation (TTT) diagram for Alloy 22 base metal shown in Figure 3-4. Some of the data presented in Table 3-5 are also shown in Figure 3-4. The curve associated with LRO came from TEM observations. Only a limited number of samples were examined in TEM; therefore, it is likely that ordering occurs at shorter times than indicated in Figure 3-4. The precipitation of intermetallic phases at grain boundaries in Alloy 22 is shown in Figure 3-5 as the white phase surrounding the grains.

Table 3-5. Intermetallic Phases Observed in Alloy 22 with Transmission Electron Microscopy

Aging Condition	Phases Observed to Form in Alloy 22
260°C for 40,000 hr	No LRO - No signs of GB precipitation in base metal
343°C for 40,000 hr	No LRO - No signs of GB precipitation in base metal
427°C for 30,000 hr	LRO - No signs of GB precipitation in base metal
427°C for 40,000 hr	LRO - No signs of GB precipitation in base metal
482°C for 1000 hr	No LRO - No signs of GB precipitation in base metal
538°C for 1000 hr	LRO - No signs of GB precipitation in base metal
593°C for 1000 hr	LRO - GB films of P phase
593°C for 16,000 hr	LRO - GB films of P phase – Carbide precipitates at GB
649°C for 16,000 hr	No LRO– Precipitation of P and μ phase mainly at GB
704°C for 16,000 hr	No LRO – Precipitation of P and μ phase at GB and within the grains - Carbide and σ precipitation at GB
760°C for 16,000 hr	No LRO– Precipitation of P and μ phase at GB and within the grains - σ precipitation at GB

Source: CRWMS M&O 2000b, Section 6.1

Table 3-6. Time Required for Precipitation of Intermetallic and Carbide Particles on the Grain Boundaries of Alloy 22 Base Metal

Temp (°C)	Time to Start on Grain Boundaries			Time to Cover Grain Boundaries		
	Lower Error	Time (hr)	Upper Error	Lower Error	Time (hr)	Upper Error
593	0	10	90	7500	8500	7500
649	1	1	9	450	550	450
704	0.5	0.5	0.5	90	100	900
760	0.5	0.5	0.5	9	10	109
800	0.5	0.5	0.5	9	10	90
Temp (°C)	**Time to Start on Twin Boundaries**			**Time to Start Within Grains**		
	Lower Error[a]	**Time (hr)**	**Upper Error[a]**	**Lower Error**	**Time (hr)**	**Upper Error**
593	N/A	None observed[b]	N/A	N/A	None observed[b]	N/A
649	450	550	450	7500	8500	7500
704	90	100	900	450	550	450
760	54.5	64.5	54.5	54.5	64.5	54.5
800	45	55	45	45	55	45

Source: CRWMS M&O 2000b, Section 6.2

[a] Lower and upper errors represent the lower and upper limits for the data

[b] None observed after 16,000 hrs.

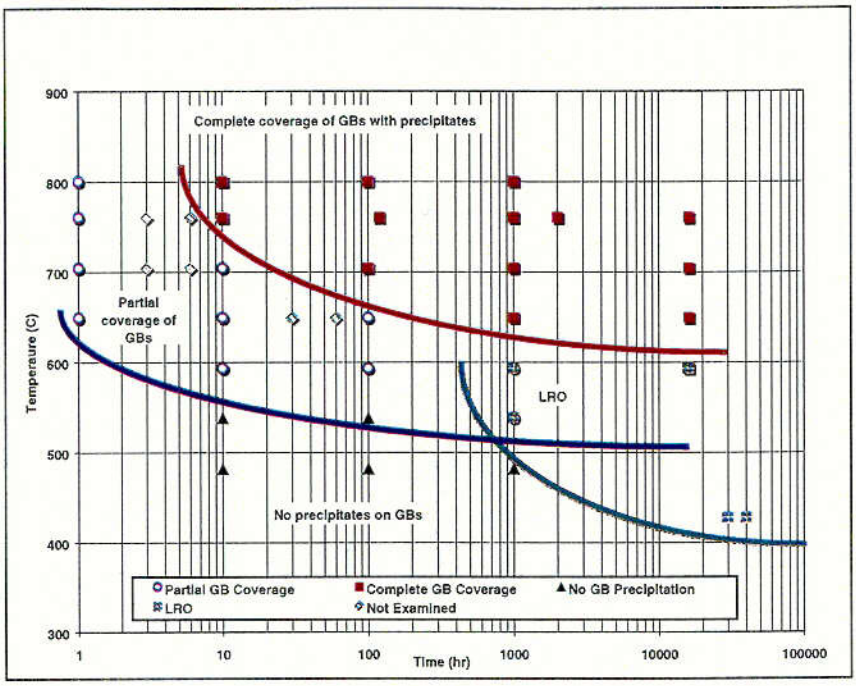

Source: CRWMS M&O 2000b, Section 6.2

Figure 3-4. Isothermal Time-Temperature-Transformation Diagram for Alloy 22 Base Metal

Nucleation and growth kinetics can be represented by an equation of the form:

$$f = 1 - \exp(-kt^n) \qquad \text{(Eq. 3-3)}$$

where f is the volume fraction of the precipitating phase, t is time and k and n are constants. The value of k depends on nucleation and growth rates, and, therefore, depends very strongly on temperature. This dependence is shown in Equation 3-4:

$$k = C_1 \exp(-C_2 / T) \qquad \text{(Eq. 3-4)}$$

where C_1 and C_2 are constants, and T is the absolute temperature in Kelvins. Combining Equation 3-3 and Equation 3-4 at constant volume fraction yields:

$$\ln(t_f) = \frac{C_2}{n} \cdot \frac{1}{T} + C_f \qquad \text{(Eq. 3-5)}$$

where t_f is the time to reach a given volume fraction of GB precipitation. Plots of logarithm of time versus reciprocal temperature for the various stages of precipitation in Alloy 22 base metal are shown in Figure 3-6. At the higher temperatures, GB precipitation is predicted to start after 1 hour, which is the shortest aging time investigated thus far.

C-4

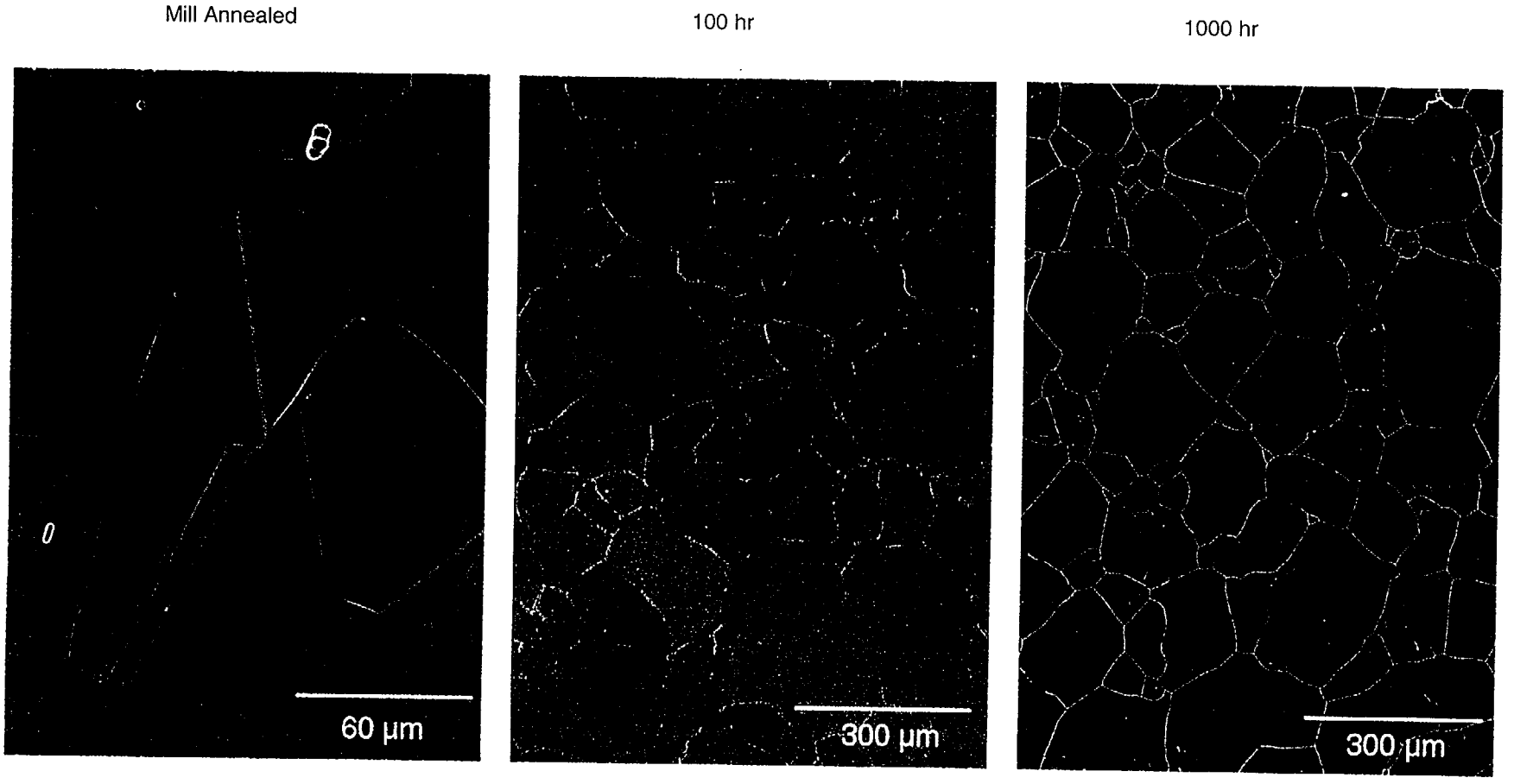

Source: CRWMS M&O 2000b, Section 4.1.2

NOTE: Increased precipitation in the GB after 1,000 hr of aging compared to 100 hr.

Figure 3-5. Effect of Thermal Aging at 649°C on the Precipitation of Intermetallic Phases at Grain Boundaries on Alloy 22

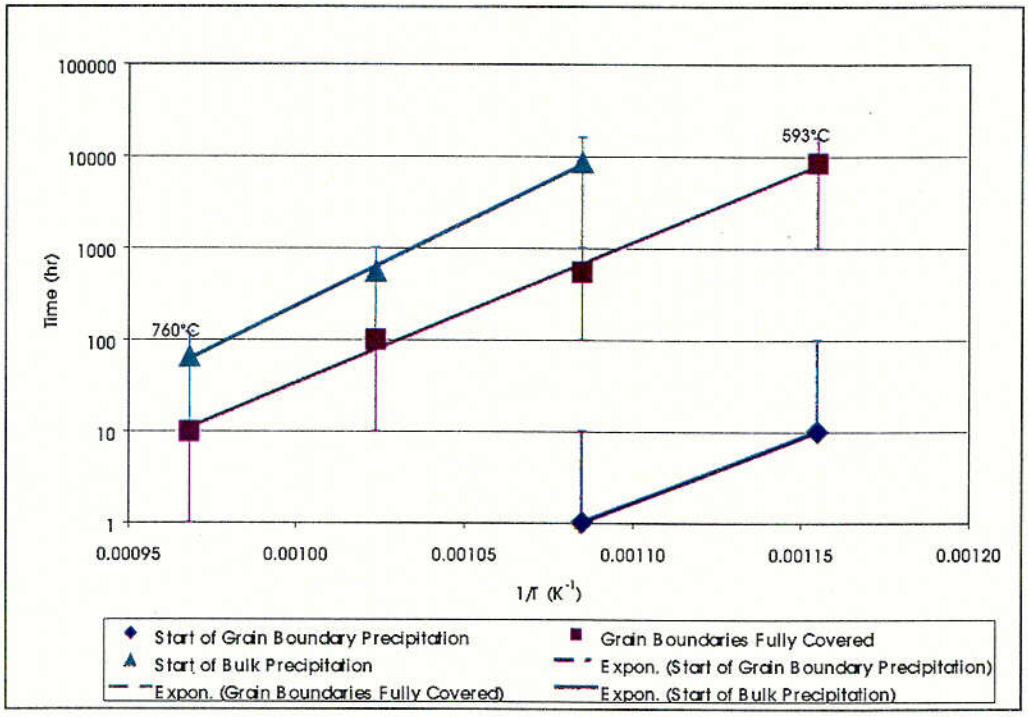

Source: CRWMS M&O 2000b Section 6.2

Figure 3-6. Time to Reach Various Stages of Precipitation in Aged Alloy 22 Base Metal Plotted on a Log Scale as a Function of Reciprocal Temperature (see Equation 3-5)

If it can be assumed that the precipitation mechanism does not change, the lines in Figure 3-6 can be extrapolated to give the times required for the various stages of precipitation at lower temperatures. The measured times are based on examination of micrographs of samples with widely spaced aging times. Extrapolation to lower temperature is difficult since the precipitation rate is very sensitive to temperature. A small change in slope can make a very large change in the time obtained from extrapolation to low temperature. In order to make a bounding argument, however, the curves associated with GB coverage and bulk precipitation in Figure 3-6 are graphically extrapolated to 10,000 years in Figure 3-7. The start of GB precipitation is not plotted because of the limited amount of available data. It must be noted that all data is regarded as preliminary at the present time. Additional work is needed.

c-4-1

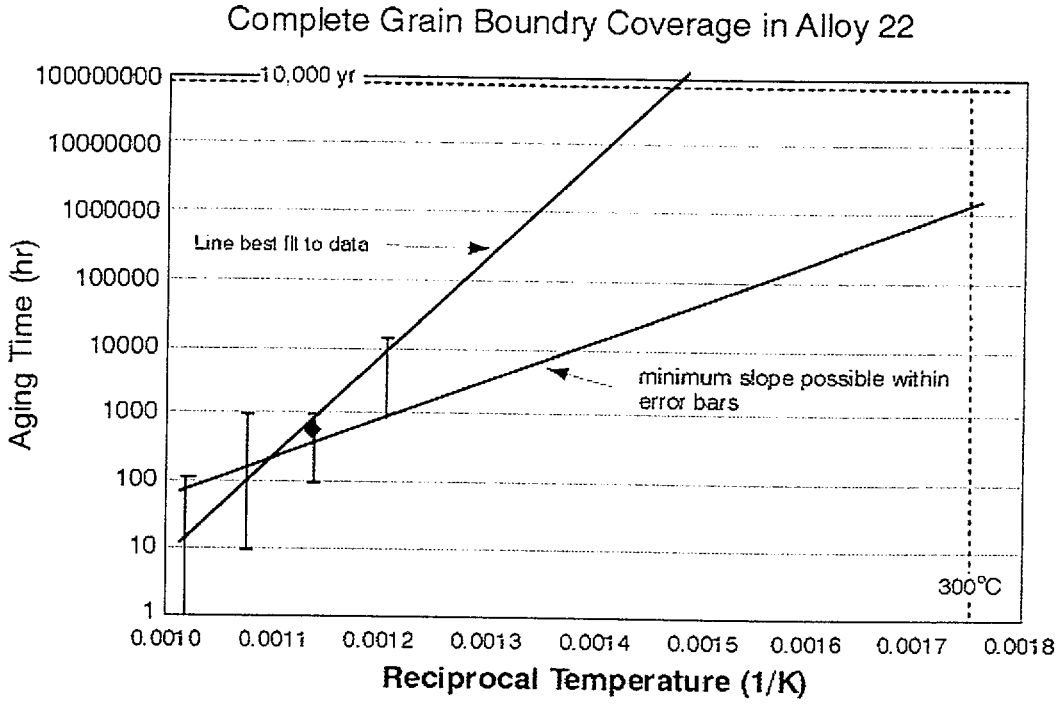

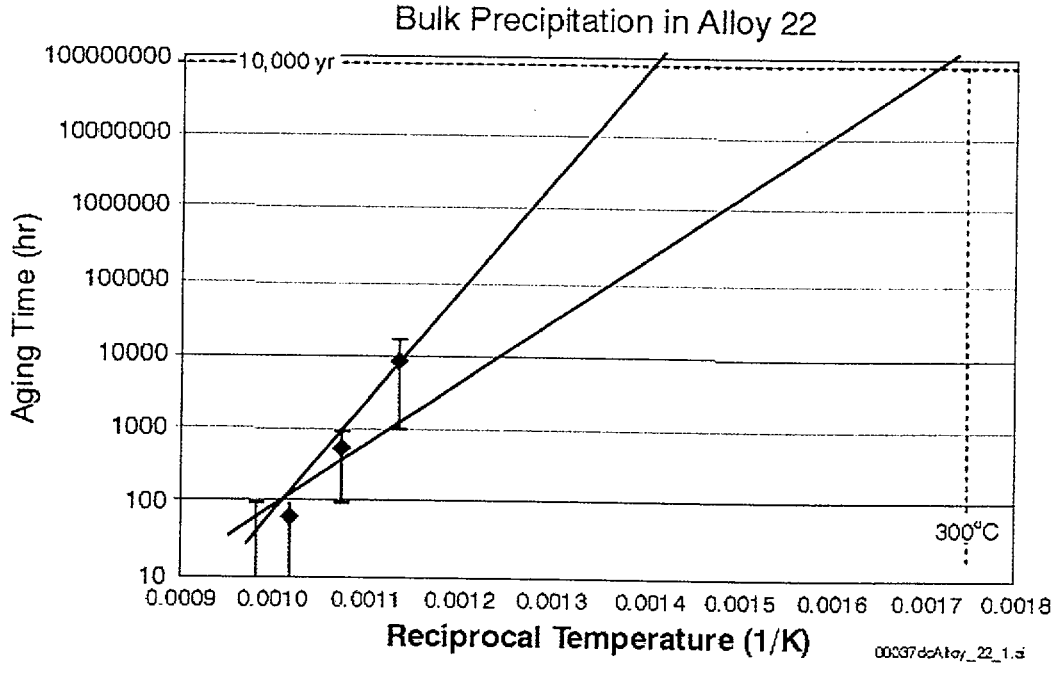

Source: CRWMS M&O 2000b, Section 6.2

Figure 3-7. Graphical Extrapolation of the Curves to Repository-Relevant Temperatures

The horizontal axes in Figure 3-7 are reciprocal temperature; temperature increases to the left. If an extrapolation of the data intersects the horizontal line corresponding to 10,000 years to the left of the vertical line corresponding to 300°C, then the temperature must be held higher than 300°C to get bulk precipitation in 10,000 years. In both cases, the data indicate that intermetallic precipitation will not occur in less than 10,000 years, even if the temperature is held at 300°C. Also plotted in Figure 3-7 are lines with the minimum possible slope allowed by the error bars on the data. Even accounting for the rather large uncertainty, bulk precipitation does not appear likely in 10,000 years at 300°C. However, GB precipitation might occur if the Alloy 22 stayed at 300°C for 10,000 years. Therefore, a good bounding argument would be to assume that precipitation covers the grain boundaries. As can be seen in the TTT diagram of Figure 3-4, samples aged in the laboratory for more than 100 hours at 700°C would produce a microstructure with precipitation covering the grain boundaries. Complete GB coverage is taken to represent a fully aged material (worst case). Corrosion data obtained from Alloy 22 base metal aged in such a way should represent a worst case condition in regard to phase stability. Corrosion data obtained with aged samples are presented in Section 3.1.4.5 and are presented in greater detail in the AMR on the WPOB (CRWMS M&O 2000c, Section 6.7).

Figure 3-7a shows calculated WP surface temperature as a function of repository storage time (CRWMS M&O 2000r). The curves shown are for the hottest (design basis) WP with and without backfill option. It can be seen that, for the case of "no backfill", WP temperatures are sufficiently low that phase stability of Alloy 22 should not be an issue.

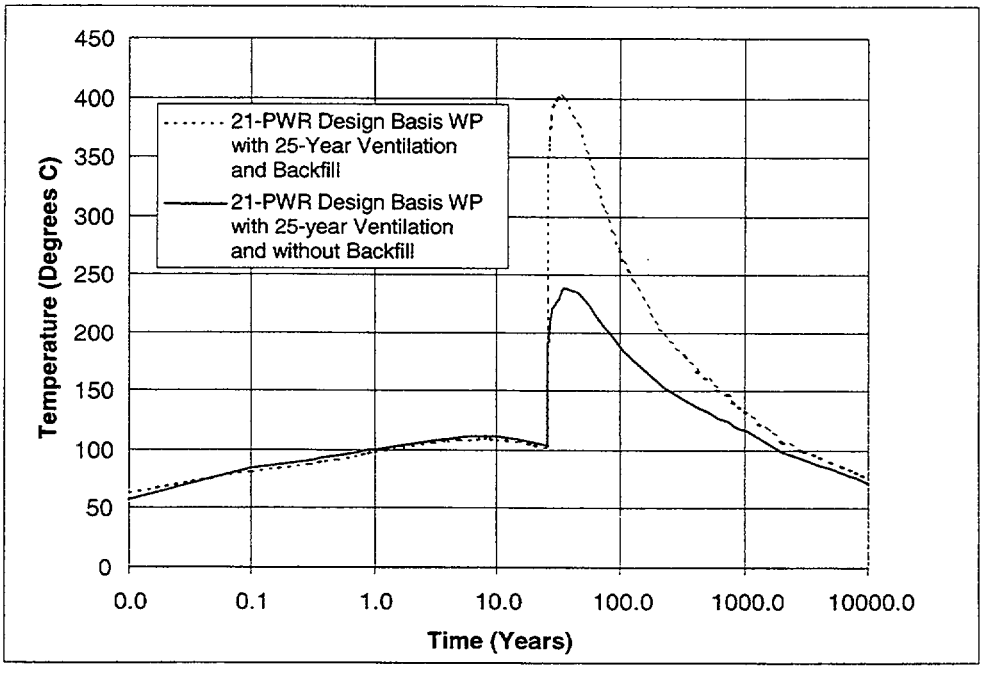

Source: CRWMS M&O 2000r

Figure 3-7a. Temperature of the WPOB Surface as a Function of Time for the Hottest Waste Package

As a measure of the reasonableness of the data plotted in Figure 3-7, the activation energy can be calculated. The slopes of the lines in Figure 3-7 (after accounting for the log(e) factor) are equal to C_2/n in Equation 3-5. If these slopes are averaged and n is assumed to be equal to one, then the activation energy is 280 kJ mol^{-1} (68 kcal mol^{-1} using a gas constant R=1.987 cal mol^{-1} K^{-1}). This is close to the value of 62 kcal mol^{-1} obtained for precipitation in Alloy C-276. This value is also typical for diffusion of relevant elements in nickel. For example, the activation energy for diffusion of chromium in nickel is 272.6 kJ mol^{-1}, that of iron is 253-270 kJ mol-1, and that of tungsten in nickel is 300-308 kJ mol^{-1}.

3.1.4.3 Kinetics of Intermetallic Precipitation in Alloy 22 Welds

The HAZ of a weld is the region of the base metal near the weld that is subjected to a significant thermal pulse during the welding process. Intermetallic precipitation processes in the HAZ are expected to be similar to that in the base metal, but actual rates of precipitation (kinetics) may be different. The high temperatures, approaching the melting point, seen in the HAZ of welds might trigger nucleation of intermetallic carbide precipitates. If nuclei are already present, precipitation will proceed much faster than in the base metal where they are not present.

Very few precipitates have been observed in the HAZ of weld samples thus far, but only two weld samples have been examined: one in the as-welded condition and one after aging at 427°C for 40,000 hours. These precipitates may simply be carbides that were present in the mill-annealed (as-received) condition. Carbides are known to be present in nickel-based alloys similar to Alloy 22, but they are usually within the grains. These are generally called primary carbides to distinguish them from other secondary phases that often form, on the GB after an aging treatment.

Welding causes melting of the alloy and the development of an as-cast structure upon cooling. As an Alloy 22 weld solidifies, molybdenum and chromium are rejected from the solid phase causing their concentration to increase in the liquid. Therefore, the interdendritic regions, which are the last solid to form in a weld, tend to have high concentrations of these elements relative to typical values for Alloy 22. Because formation of the intermetallic phases, which are also enriched in molybdenum and/or chromium, are favored by higher molybdenum and chromium concentrations, these phases are present in the interdendritic regions of Alloy 22 welds.

Because precipitates are present in Alloy 22 welds from the beginning, kinetics of precipitation in welds is not an issue. Corrosion data available from the LTCTF shows no measurable difference between welded and base metal samples.

3.1.4.4 Kinetics of Reactions in Alloy 22

The LRO is treated in a manner similar to that discussed for intermetallic and carbide precipitation. However, very little kinetic data exists for LRO in Alloy 22. Thus far, LRO has been observed in five samples. A very fine dispersion of ordered domains was seen in Alloy 22 base metal after aging for 30,000 and 40,000 hours at 427°C, and was also seen in a weld similarly aged. The ordering in these cases was so fine that it would have been very difficult to measure the volume fraction of the ordered domains. LRO was also observed in Alloy 22 base metal aged at 593°C for 16,000 hours, and at 538 and 593°C for 1,000 hours. The volume fraction of ordered domains has not been measured in these samples. No LRO was observed with TEM in Alloy 22 base-metal samples aged for 40,000 hours at 260 and 343°C, or for 1,000 hours at 482°C.

A bounding argument may be made by using two facts: LRO is just beginning after aging for 30,000 hours at 427°C together; LRO domains are small after aging for 1,000 hours at 538°C. The corresponding points are graphed as an Arhenius plot in Figure 3-8. Samples aged for shorter times at 427 and 538°C have not yet been examined in TEM. The curve in Figure 3-8 may shift to shorter times (down) after more data are collected. Because the LRO domains are very small after aging at 427°C for 30,000 hours, the point corresponding to this aging condition is not likely to change much (Figure 3-8). In other words, LRO is not likely to occur in Alloy 22 base metal at 427°C in times significantly less than 30,000 hours. After more data are collected, the data point corresponding to aging at 538°C for 1,000 hours will most likely shift down more than that corresponding to aging at 427°C for 30,000 hours. Since this shift will cause the slope to increase, the curve in Figure 3-8 represents a bounding case. This graph indicates that LRO may occur in less than 10,000 years at 300°C. Equation 3-6 was obtained by curve fitting and is shown in Figure 3-8:

$$\ln(t)=\ln\left(5x10^{-7}\right)+\frac{17395}{T} \qquad \text{(Eq. 3-6)}$$

Solving Equation 3-6 for temperature T yields:

$$T=\frac{17395}{\ln(t)-\ln(5x10^{-7})} \qquad \text{(Eq. 3-7)}$$

Based upon this analysis, it is concluded that no LRO will occur after 10,000 years (8.8×10^{7} hours), provided that the temperature remains below approximately 260°C (530 K). More samples are being tested to confirm this conclusion.

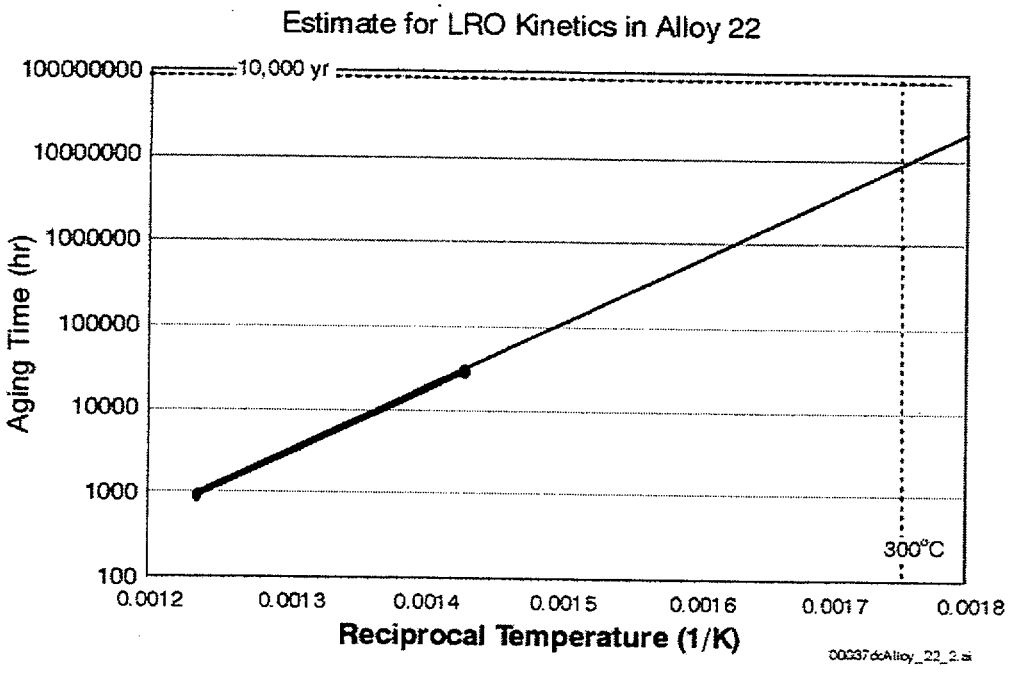

Figure 3-8. Graphical Extrapolation of the Limited Kinetic Data for Long Range Order in Alloy 22 Base Metal

3.1.4.5 Effects of Thermal Aging on Corrosion Potential and Rate

The long-term aging of Alloy 22 at elevated temperature can cause the precipitation of undesirable intermetallic phases. Based upon the analyses discussed in the preceding section, it is recommended that the WP surface temperature be limited to levels below 300°C. An extrapolation of the data shown in Figure 3-6 indicates that the phase stability of Alloy 22 base metal will not be a problem below this limit. The significance of the uncertainties in this data is discussed in Section 3.1.9. At temperatures above 350°C, there is unacceptable degradation of cladding on the SNF. With these two constraints, the impact of aging and phase instability on the corrosion of Alloy 22 should be minimal.

Samples of Alloy 22 were aged at 700°C for either 10 or 173 hours. The corrosion resistance of these aged samples is compared to that of base metal in several standardized test media. Figure 3-9 shows a comparison of CP curves for base metal and thermally aged material in SAW at 90°C. Both curves exhibit generic Type 1 behavior (see Section 3.1.6.3). Type 1 behavior is indicative of passive film stability between the corrosion potential and the thermodynamic limit of the electrolyte (oxygen evolution). In this case, aging shifts the corrosion potential to less noble values, from -176 to -239 mV (versus a standard Ag/AgCl reference electrode). The passive current density is increased slightly, which is interpreted as a slight increase in corrosion rate. The highest non-equilibrium passive current density observed for the base metal is approximately 4 $\mu A\ cm^{-2}$, compared to approximately 10 $\mu A\ cm^{-2}$ for fully aged material.

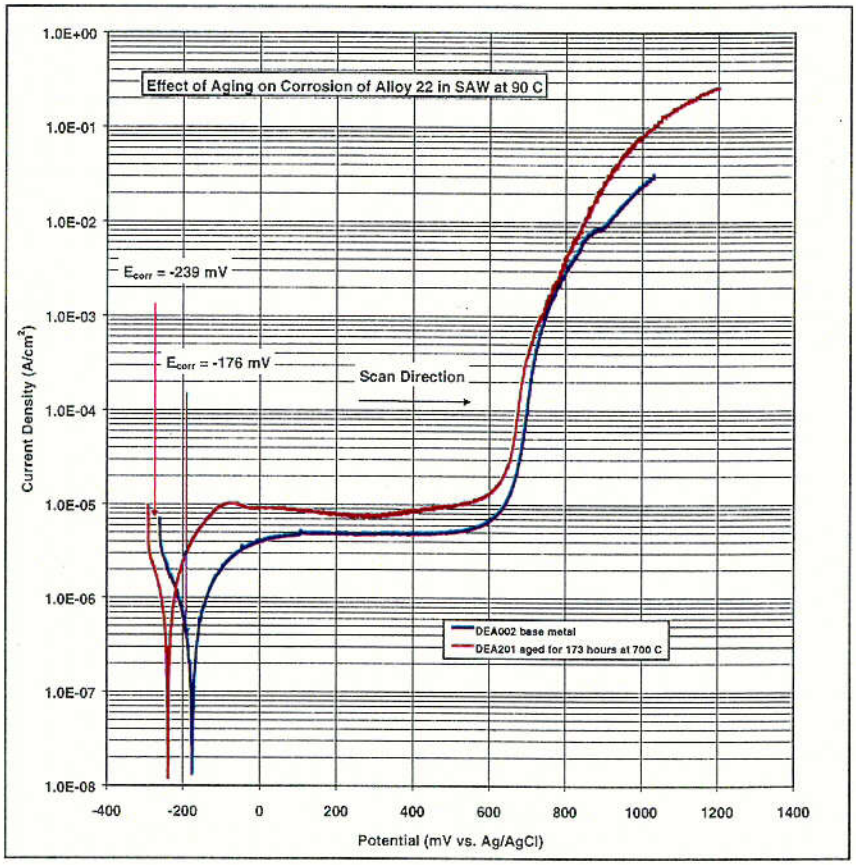

Source: CRWMS M&O 2000c, Section 6.7.1

Figure 3-9. Effect of Thermal Aging for 173 Hours at 700°C on the Corrosion Resistance of Alloy 22 in Simulated Acidic Concentrated Water at 90°C (DEA002 and DEA201)

Figure 3-10 shows a comparison of CP curves for base metal and thermally aged material in SCW at 90°C. In this case, aging also appears to shift the corrosion potential to less noble values, from -237 to somewhere between -328 and -346 mV versus a standard Ag/AgCl reference electrode. In all three cases, the anodic oxidation peak that is characteristic of generic Type 2 behavior is observed. See Section 3.1.6.3 for more detailed discussion. In tests with BSW-13, aging also appears to shift the corrosion potential to less noble values.

C-5

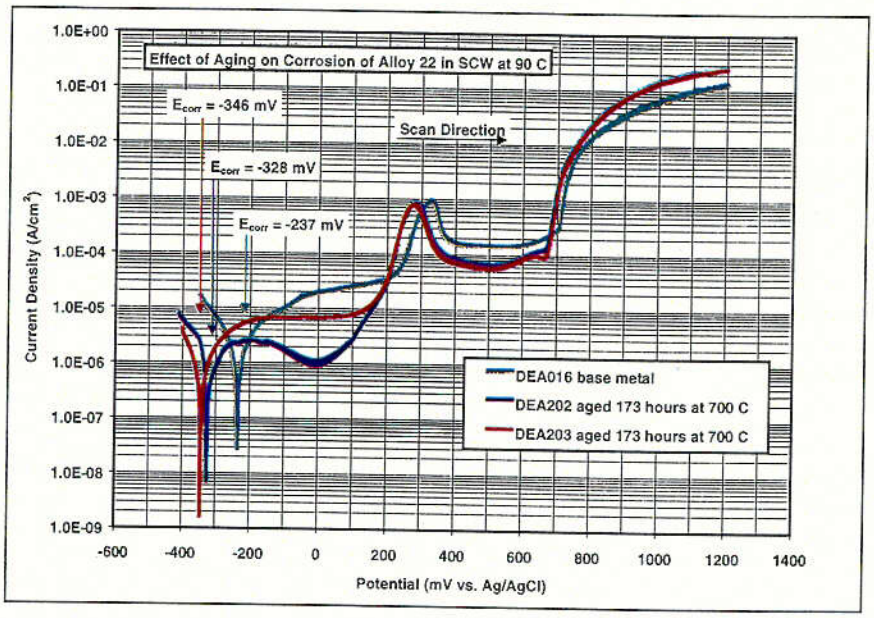

Source: CRWMS M&O 2000c, Section 6.7.1

Figure 3-10. Effect of Thermal Aging for 173 Hours at 700°C on the Corrosion Resistance of Alloy 22 in Simulated Concentrated Water at 90°C (DEA016, DEA202, and DEA203)

In summary, a fully aged sample of Alloy 22 appears to exhibit a less noble corrosion potential. Typically, the corrosion potential of such a sample is shifted approximately -63 mV in SAW at 90°C; -109 mV in SCW at 90°C; and more than -100 mV in BSW at 100°C. Based on this data, it appears that E_{corr} can be corrected to account for fully aged material by subtracting approximately 100 mV from values calculated for the base metal. The shift in $E_{critical}$ (Threshold Potential 1) also appears to be approximately 100 mV in most cases. Thus, the difference $E_{critical}$-E_{corr} is virtually unchanged. This implies that even though the corrosion potential is shifted, the susceptibility to LC remains unchanged.

The effect of thermal aging on the corrosion rate is accounted for in an enhancement factor, G_{aged}, and is based upon a ratio of the non-equilibrium passive current densities for base metal and aged material.

$$\left(\left.\frac{dp}{dt}\right|_{effective}\right)_{corrected} = G_{aged} \times \left(\left.\frac{dp}{dt}\right|_{effective}\right)_{original} \qquad \text{(Eq. 3-8)}$$

C-4

where *dp/dt* is the penetration rate for LC. The value of G_{aged} for Alloy 22 base metal is approximately one (G_{aged} ~ 1), whereas the value of G_{aged} for fully aged material is larger (G_{aged} ~ 2.5) (CRWMS M&O 2000c). Material with less precipitation than the fully aged material would have an intermediate value of G_{aged} ($1 \leq G_{aged} \leq 2.5$). Therefore, a value of 2.5 for G_{aged} is conservatively used to bound the potential aging effect. Corrosion is discussed in greater detail in the sections that follow.

3.1.5 General Corrosion

The integrated model for general corrosion of the materials of interest includes sub-models for dry oxidation, humid air and aqueous phase corrosion. Details of these sub-models are provided in supporting AMRs (CRWMS M&O 2000c, 2000d, and 2000e). A schematic representation of the integrated model for WP and DS materials, as well as an augmentation of this model, are shown in Figures 3-11 and 3-12. Only a brief summary of the integrated model and component sub-models is provided here.

3.1.5.1 Dry Oxidation

Dry oxidation (DOX) occurs at any RH below the threshold for HAC:

$$RH < RH_{critical} \qquad \text{(Eq. 3-9)}$$

This process results in the formation of an adherent, protective oxide film of uniform thickness. The rate of DOX may be limited by the rate of mass transport through the growing metal oxide film. In such cases, the oxide thickness is expected to obey a parabolic growth law (film thickness proportional to the square root of time). This scenario has been adopted for Alloy 22 and 316NG due to the availability of data at elevated temperature to support such a model. Reasonable values of the parabolic rate constant are discussed below. It must be noted that a logarithmic law may be more applicable at lower temperatures. However, there is insufficient data to support such a model for Alloy 22 and 316NG. There is sufficient data to support the application of a logarithmic law to the DOX of titanium. It is assumed that DOX occurs uniformly over each WAPDEG patch, which is comparable in size to that of a LTCTF sample with generic weight-loss geometry. Backfill effects are not included in the model for DOX threshold and rate.

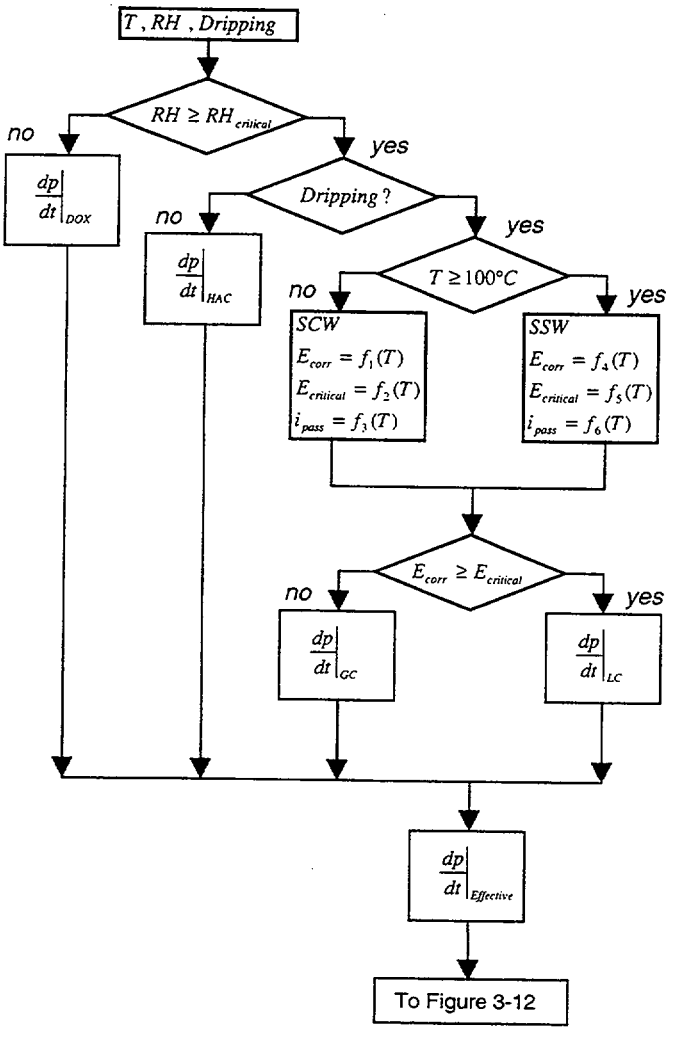

Source: CRWMS M&O 2000c, Section 6.10

Figure 3-11. Schematic Representation of Model for General Corrosion and Localized Corrosion of Drip Shield and Waste Package Materials

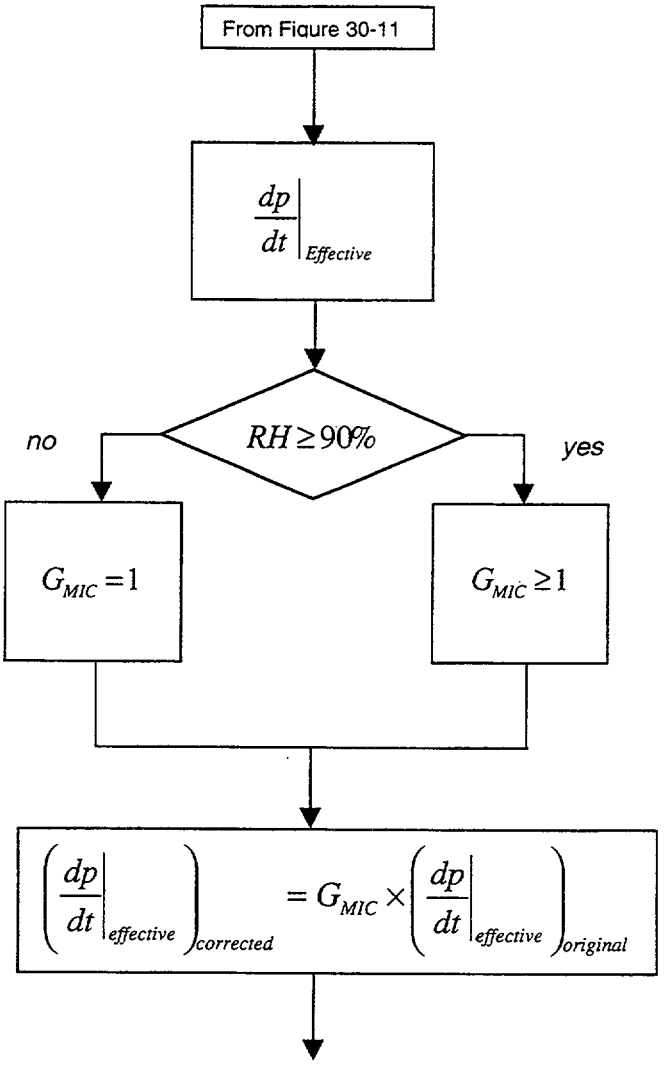

Source: CRWMS M&O 2000c, Section 6.10

NOTE: A similar strategy is used to account for aging.

Figure 3-12. Schematic Representation Showing Augmentation of Model for General Corrosion and Localized Corrosion to Account for Microbiologically Influenced Corrosion of Drip Shield and Waste Package Materials

3.1.5.1.1 Dry Oxidation of Alloy 22 and 316NG

DOX of Alloy 22 and 316NG stainless steel is expected to occur at any $RH < RH_{critical}$, thereby forming an adherent, protective oxide film of uniform thickness. It is assumed that the protective oxide film is primarily Cr_2O_3. The oxidation reaction is given as

$$4/3\ Cr + O_2 \longrightarrow 2/3\ Cr_2O_3 \qquad \text{(Eq. 3-10)}$$

The rate of DOX is limited by mass transport through this growing metal oxide film with the film thickness being proportional to the square root of time. This is represented by Equation 3-11:

$$x = \sqrt{x_0^2 + k \times t} \qquad \text{(Eq. 3-11)}$$

where x_0 is the initial oxide thickness, x is the oxide thickness at time t, and k is a temperature-dependent parabolic rate constant.

To facilitate an approximate calculation, published values of k can be used (CRWMS M&O 2000c, Sections 1.6 and 6.10). The highest WP temperature in the repository is expected to be approximately 350°C (623 K), which corresponds to the limit for the SNF cladding. Note that the cladding will be hotter than the WPOB. The value of k corresponding to this upper temperature limit is 2.73×10^{-24} m^2 s^{-1} (8.61×10^{-5} square μm per year). After one year, this corresponds to a growth of about 0.0093 μm. The estimated rate (9.3 nm y^{-1}) is comparable to that expected for APC at lower temperatures, based upon data presented in this PMR. The parabolic law is used to represent the DOX Alloy 22 and 316NG, and is relatively conservative.

3.1.5.1.2 Dry Oxidation of Titanium Grade 7

As discussed in the AMRs for general and LC of the DS (CRWMS M&O 2000d, Section 6.1), the logarithmic growth law may be more appropriate at low temperature than the parabolic law. However, such a logarithmic expression predicts that the oxide thickness (penetration) asymptotically approaches a small maximum value. In contrast, the parabolic law predicts continuous growth of the oxide, which is much more conservative. Figure 3-13 shows a regression analysis of DOX rate data for titanium, where X is the oxide thickness at time t and X_{max} is the maximum oxide thickness.

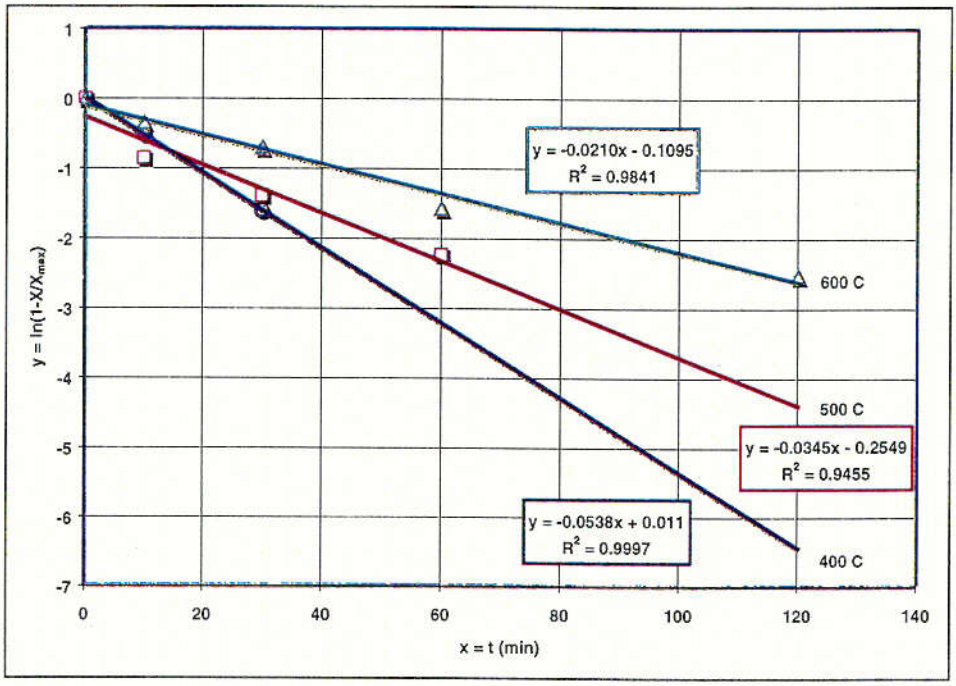

Source: CRWMS M&O 2000d, Section 6.1

Figure 3-13. Regression Analysis of Dry Oxidation Rate Data for Titanium

3.1.5.2 Humid Air Corrosion

HAC is assumed to occur above a threshold RH, provided that there are no impinging drips:

$$RH \geq RH_{critical} \qquad \text{(Eq. 3-12)}$$

The threshold RH for HAC ($RH_{critical}$) is assumed to obey Equation 3-2. Note that "threshold RH" and "critical RH" are synonymous terms. The existence of this threshold is due to the relationship between water adsorption and RH.

It can be conservatively assumed that the rate of HAC can be represented by the same corrosion rate distribution used for APC during the period where HAC is operable. It is further assumed that the corrosion rate is constant and does not decrease with time (at times greater than two years). Less conservative corrosion models assume that the rate decays with time. The rates for APC of stainless steel 316NG, Alloy 22, and Titanium Grade 16 (analog of Titanium Grade 7) are described in detail elsewhere in this section.

3.1.5.3 Aqueous Phase Corrosion

At a given temperature, the existence of liquid-phase water on the surface of the WP depends upon the presence of a salt deposit. In the presence of such a deposit, a thin-film liquid phase can be established at a higher temperature than otherwise possible. In the model discussed here, it is assumed that two conditions must be met for APC: RH above the deliquescence point of the

deposit at the temperature of the WP surface and drips impinging on the WP surface. The threshold RH for APC is identical to that for HAC:

$$RH \geq RH_{critical} \qquad \text{(Eq. 3-13)}$$

This threshold RH for APC ($RH_{critical}$) is also assumed to obey Equation 3-2, which is based upon the AMR entitled *Environment on the Surface of Drip Shield and Waste Package Outer Barrier* (CRWMS M&O 2000a, Section 6.4.2). For the time being, the composition of the electrolyte formed on the WP surface is assumed to be that of SCW below 100°C, and that of SSW above 100°C. The distributions of GC rates for APC of stainless steel 316NG, Alloy 22, and Titanium Grade 16 (analog of Titanium Grade 7) are described in detail in this PMR. It is conservatively assumed that the corrosion rate is constant and that it does not decrease with time (at times greater than two years).

3.1.5.4 Rates of General and Localized Corrosion

Penetration rates based upon GC are used in the model if the threshold potential ($E_{critical}$) is not exceeded. GC rates have been estimated based on the weight-loss data from the LTCTF. LC rates and failure mode characteristics (e.g., number of failure sites and opening size) must be estimated from other published data. Since pitting of Alloy 22 or Titanium Grade 16 has not been observed in the LTCTF, it is assumed that crevice corrosion is the primary mode of LC (if localized attack occurs at all). This accelerated mode of attack is assumed to occur uniformly over the entire affected WAPDEG patch. Uncertainty is accounted for in the WAPDEG stochastic simulation.

3.1.5.4.1 Rates for 316L Stainless Steel – Published Data

The samples involved in the YMP corrosion testing program do not include stainless steel specimens. Therefore, data published in the literature must be used to determine corrosion rates. Rates of LC are used if the threshold potential is exceeded. Otherwise, GC rates are used. The distribution of general and LC rates were estimated from the published data for Types 304 and 316 stainless steels presented in the AMR on degradation of the stainless steel structural material (CRWMS M&O 2000e, Section 6.5). These data are shown in Figures 3-14 through 3-17. Curves are shown for GC in atmospheric and aqueous-phase environments, as well as for LC in aqueous-phase environments. The corresponding distributions can be represented by the following general correlation:

$$y = b_0 + b_1 x \qquad \text{(Eq. 3-14)}$$

where y is the cumulative probability or percentile, and x is the logarithm of the corrosion rate, which is expressed in microns per year. Parameters are given in Figure 3-15. These cumulative distribution functions are truncated for any nonsensical calculated values above one-hundred percent (100%). These distributions do not reflect any environmental dependence, since such a correlation could not be established based upon published data. It is assumed that these distributions are primarily due to variability. In lieu of rigorous estimates of uncertainty, the uncertainty is assumed to be comparable to the variability.

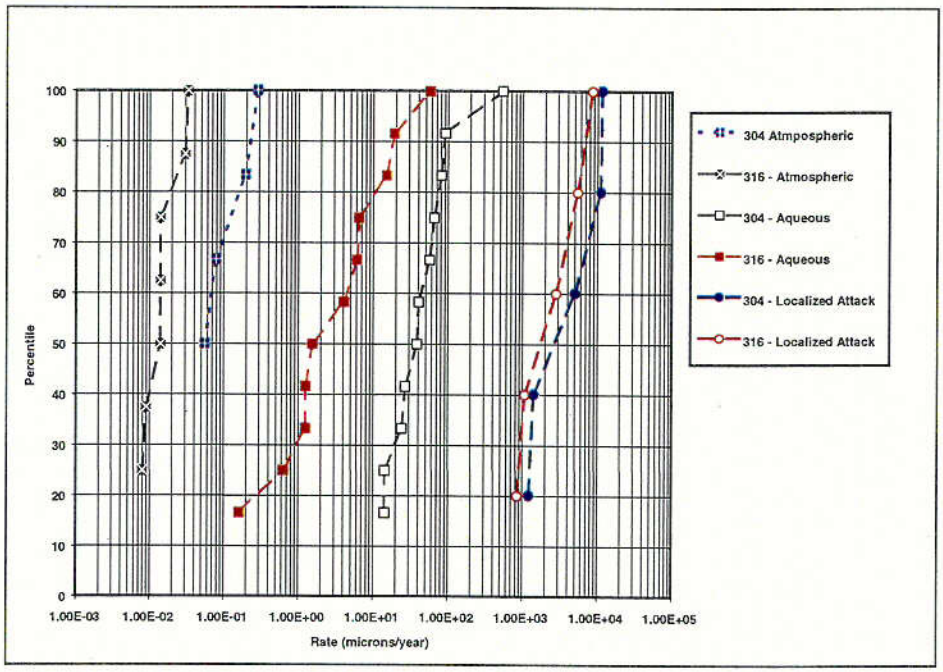

Source: CRWMS M&O 2000e, Section 6.5

Figure 3-14. Range of Observed Penetration Rates for Stainless Steels 304 and 316 Shown as Cumulative Probability Distributions

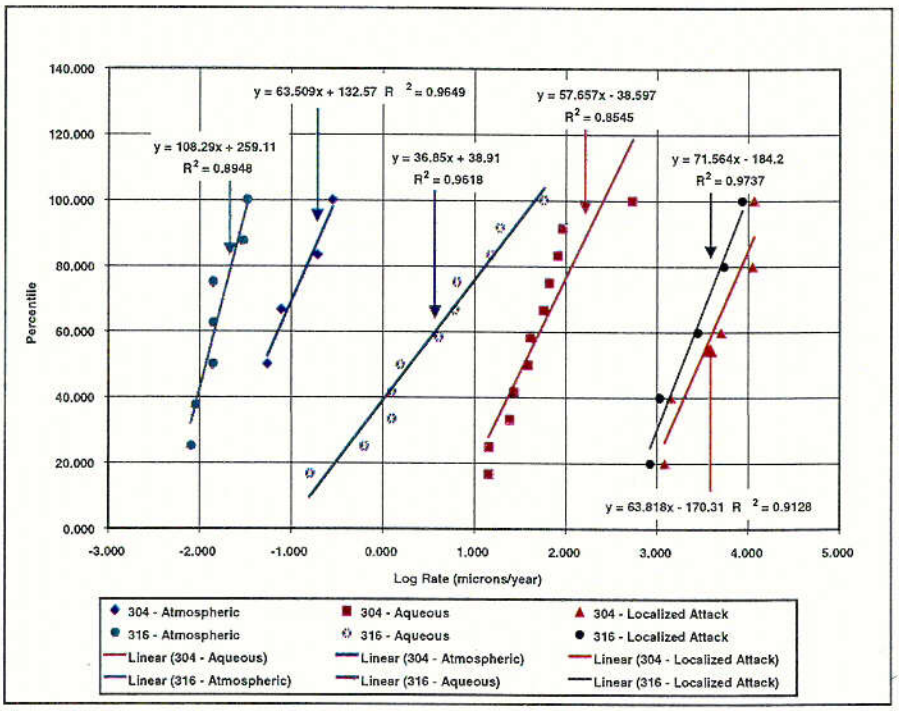

Source: CRWMS M&O 2000e, Section 6.5

Figure 3-15. Range of Observed Logarithms of Penetration Rates for Stainless Steels 304 and 316 Shown as Cumulative Probability Distributions

e-8

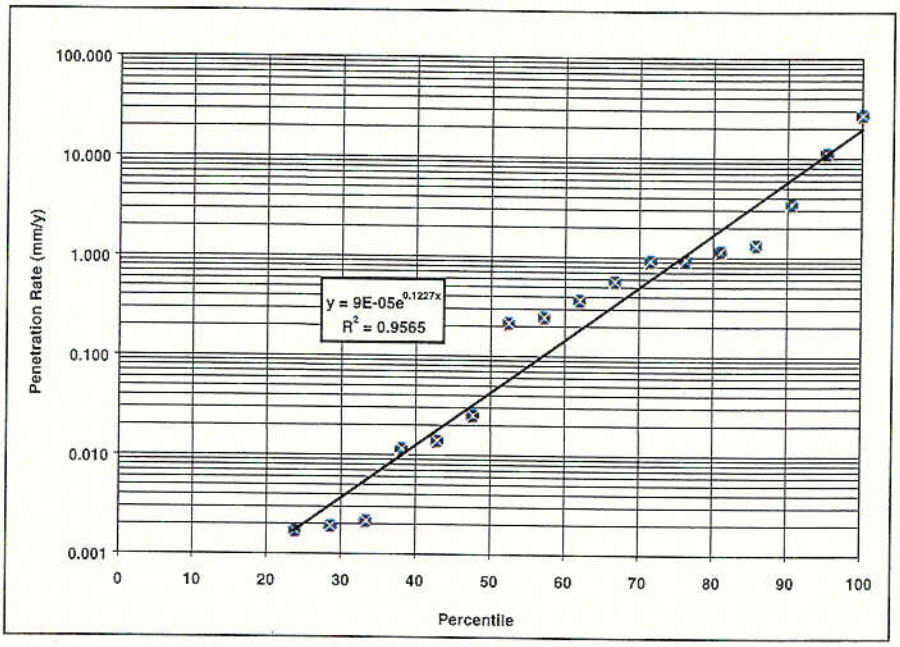

Source: CRWMS M&O 2000e, Section 6.5

Figure 3-16. Range of Localized Penetration Rates for Stainless Steels 304 and 316

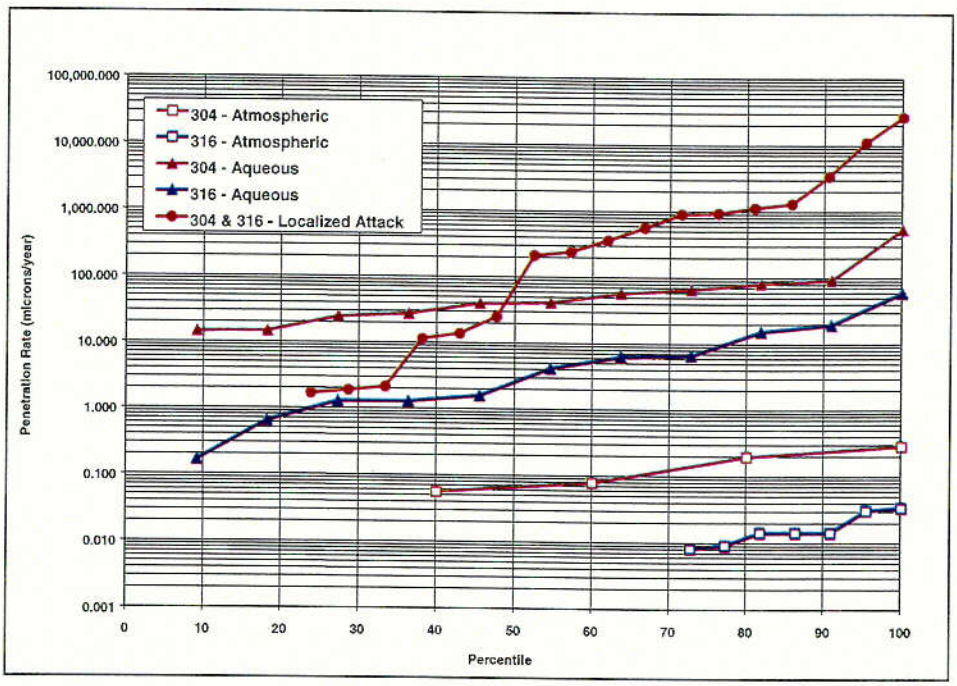

Source: CRWMS M&O 2000e, Section 6.5

Figure 3-17. Comparison of Observed Penetration Rates for Stainless Steels 304 and 316

C-9

From a comparison of the data for Types 304 and 316 stainless steels, the advantages of molybdenum additions are evident. Since Type 316 stainless steel contains more molybdenum than Type 304 stainless steel, the corrosion rates of Type 304 stainless steel are higher than comparable rates of Type 316 stainless steel. From Figure 3-14, the localized corrosion rates of Type 316 stainless steel appear to lie between 10^3 and 10^4 $\mu m\ y^{-1}$. The general corrosion rates for APC of Type 316 appear to lie between 10^{-1} and 10^2 $\mu m\ y^{-1}$. The general corrosion rates for HAC (atmospheric corrosion) of Type 316 stainless steel appear to lie between 10^{-3} and 10^{-1} $\mu m\ y^{-1}$. It is assumed that the published rates for Type 316 stainless steel are representative of those for Type 316NG stainless steel. The regression line shown in Figure 3-15 is assumed to represent the combined uncertainty and variability. Figures 3-16 and 3-17 show the probability distribution of the corrosion rates and comparison of the observed penetration rates for Types 304 and 316 stainless steels, respectively.

3.1.5.4.2 Rates for Nickel-Based Alloy 22 – Weight-Loss Measurements from Long Term Corrosion Test Facility

The Long-Term Corrosion Test Facility (LTCTF) provides a relatively complete source of corrosion data for Alloy 22 in environments relevant to the potential high-level radioactive waste (HLW) repository at Yucca Mountain. The results from that facility are described in detail in the AMR on GC of Alloy 22 (CRWMS M&O 2000c, Section 6.5.2). Testing is done in a wide range of plausible media, including SDW, SCW, SAW, and SCMW. SDW has ten times (10×) the ionic content of J-13 well water, while SCW has 1000× the ionic content. The measured pH levels of the 10× and 1000× J-13 waters are 9.5 to 10. SAW is acidified water that has 4000× the ionic content of J-13 water and a pH of approximately 2.7. These concentrated test solutions are intended to mimic the evaporative concentration of electrolytes on the hot WP surface. Due to solubility limitations, not all salts in the water concentrate to the same nominal levels. However, the more soluble anions such as chloride, sulfate, and nitrate (which have the biggest effects on corrosion) do reach nominal levels.

Specimens are tested at two temperatures (60 and 90°C) in each water chemistry. Half of the specimens are fully immersed, while the remaining half are exposed to the wet vapor above the water line. A few specimens are placed right at the water line. Half of the specimens contain welds, while the remaining half are unwelded.

Crevice specimens are mounted to support racks with Teflon-coated fasteners and washers. Teflon crevice-forming washers are spring loaded to ensure that contact is maintained between the washers and specimens (crevice effects are more severe in tight crevices).

At least 144 test specimens are measured during each exposure period (6-, 12-, and 24-month, thus far). The general corrosion rates are determined from weight-loss measurements made at the end of predetermined exposure periods. These measurements are based upon ASTM G 1-81 *Standard Practice for Preparing, Cleaning, and Evaluating Corrosion Test Specimens* or the more recent ASTM G 1-90, *Standard Practice for Preparing, Cleaning, and Evaluating Corrosion Test Specimens*. All specimens are cleaned in accordance with applicable American Society for Testing and Materials (ASTM) procedures prior to making weight and dimensional measurements. Uncertainty in the measured rates decreases with increasing exposure time. Details of the facility, sample configurations, and the procedure used for handling the samples

are provided in the AMR on general and localized corrosion of Alloy 22 (CRWMS M&O 2000c Section 6.5.2).

The general corrosion (penetration) rate of an alloy can be calculated from weight-loss data with the following general formula:

$$Corrosion\ Rate = \frac{(K \times W)}{(A \times T \times D)} \qquad \text{(Eq. 3-15)}$$

where K is a constant, T is the time of exposure in hours, A is the exposed area of the sample in square centimeters, W is the mass loss in grams, and D is the density of Alloy 22 in grams per cubic centimeter. The value of K used for the LTCTF data was $8.76 \times 10^7\ \mu m\ y^{-1} h\ cm^{-1}$. A sample calculation for Alloy 22 is shown below:

$K = 8.76 \times 10^7\ \mu m\, y^{-1} h cm^{-1}$

$W = 0.0001 g$

$A = 1.0 cm^2$

$T = 4320 h$

$D = 8.69 g\, cm^{-3}$

$$CorrosionRate = \frac{(8.76 \times 10^7\ \mu m\, y^{-1} h cm^{-1})(0.0001 g)}{(1.0\ cm^2)(4320\ h)(8.69 g\, cm^{-3})} = 0.23\ \mu m\, y^{-1}$$

General corrosion rates based on generic weight-loss samples are independent of temperature between 60 and 90°C. Furthermore, the composition of the test medium (SDW, SCW, or SAW) appears to have little effect. When all of the measured rates are ranked together, regardless of the test medium or temperature, the data appear to be normally distributed around a median value.

In regard to generic crevice samples, general corrosion rates are based on areas outside the crevice. In this case, the measurements are also independent of temperature and test medium. When all of the corrosion rates based on these samples are ranked together, most of the data points appear to be normally distributed around a median value. There are four samples (outliers) that have abnormally high weight losses, which yield rates up to 731 nanometers per year. No crevice attack of these four samples is evident with microscopic examination. The high weight-loss values for these samples may be due to the accidental removal of material during mechanical assembly of the crevice. These outlier rates will not lead to failure of the WPOB by general corrosion during the first 10,000 years of service.

The average corrosion rate based upon all weight-loss samples with 6- and 12-month exposure is 20 nm y^{-1}, with a standard deviation of 40 nm y^{-1}. The average corrosion rate based upon all crevice samples with comparable exposure is 71 nm y^{-1}, with a standard deviation of 89 nm y^{-1}. If the four abnormally high rates are omitted, the average rate is then calculated to be 57 nm y^{-1}, with a standard deviation of 40 nm y^{-1}. At temperatures less than 90°C, it does not appear that the life of the WPOB will be determined by GC.

It should be noted that the measured corrosion rates include some negative values. These negative rates correspond to cases where the samples actually appear to have gained weight during exposure, due to oxide growth or the formation of silicate deposits. To substantiate these interpretations, atomic force microscopy (AFM) and X-ray diffraction (XRD) have been used to inspect a number of samples removed from the LTCTF. Results of this study are discussed in detail in Attachment I of the AMR on the general and LC of Alloy 22 (CRWMS M&O 2000c, Section 6.5.5) and summarized later in this subsection.

Based upon these data and the associated error analysis, one conservative and defensible overall representation of the observed corrosion rates with 6- and 12-month exposure has been proposed. This approach involves combining the distributions of rates calculated from weight loss and crevice samples. These data are for samples having the generic weight-loss and crevice geometry, respectively. It is conservatively assumed that no scale formation occurs, so all negative rates are eliminated and the entire distribution is assumed to be due to uncertainty. The rate at the 50^{th} percentile is approximately 50 nm y^{-1}, the rate at the 90^{th} percentile is approximately 100 nm y^{-1}, and the maximum rate is 731 nm y^{-1}. Approximately 10% of the values fall between 100 and 731 nm y^{-1}.

Data representing 24 months of exposure has recently become available. Various cumulative distribution functions (CDFs) generated with 24-month data alone are shown in Figures 3-18 through 3-21. The mean corrosion rate in Figure 3-21 is 10 nm y^{-1}. The rates of GC do not appear to depend strongly on temperature and chemical composition of the water. Negative corrosion rates may indicate a weight gain by the specimen, even after thorough cleaning to remove corrosion products and oxides from the surface.

CDFs generated with a combined data set representing 6-, 12-, and 24-month data are shown in Figures 3-22 and 3-23. The curve shown in Figure 3-22 includes apparent negative rates, while those negative values have been eliminated from the curve shown in Figure 3-23. The curve shown in Figure 3-23 is summarized in Table 3-7. The distributions based upon the 24-month data are more narrow than comparable distributions based upon 6- and 12-month data. Since rates are calculated by dividing exposure time into the weight loss, a doubling of exposure time reduces the estimated error by a factor of two (2X). While outliers were observed in the 6-month data, as previously discussed, none were observed in the 12- and 24-month (one- and two-year) data.

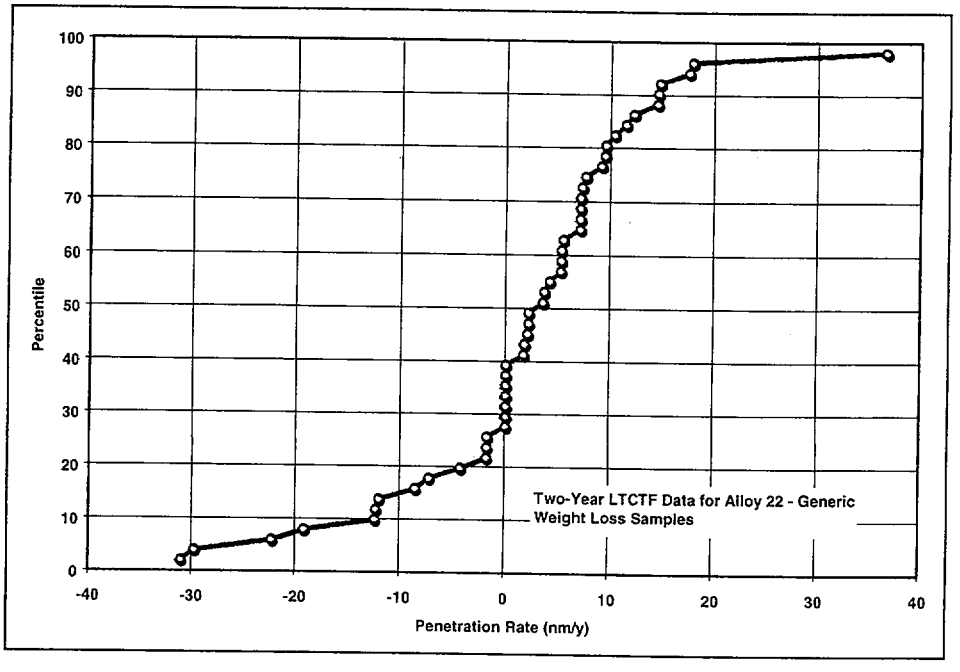

Source: CRWMS M&O 2000c, Section 6.9

Figure 3-18. Two-Year General Corrosion Rate Data from Long Term Corrosion Test Facility Based Upon Generic Weight-Loss Samples

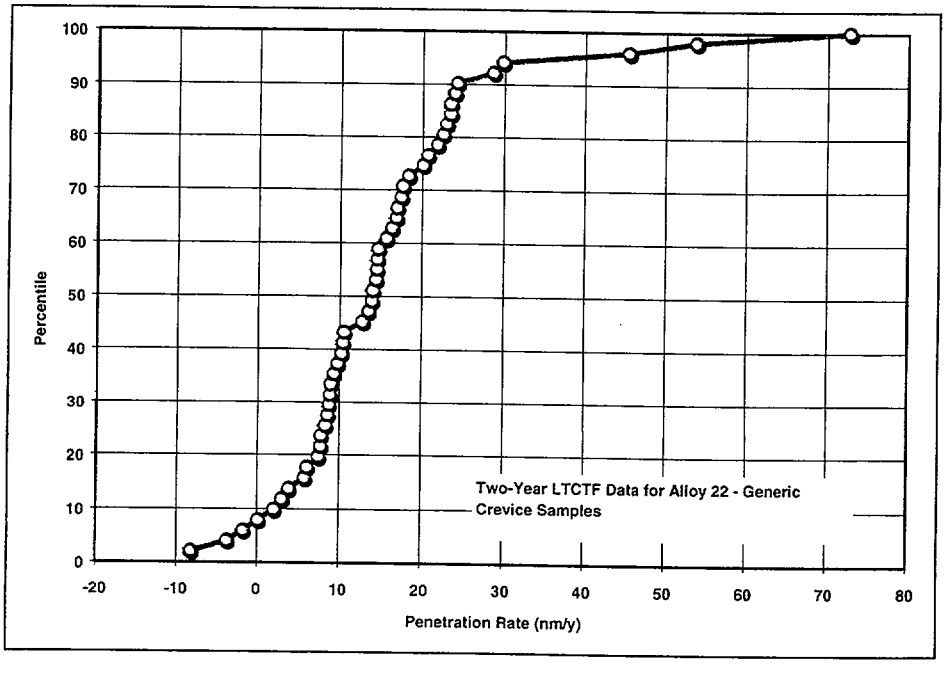

Source: CRWMS M&O 2000c, Section 6.9

Figure 3-19. Two-Year General Corrosion Rate Data from Long Term Corrosion Test Facility Based Upon Generic Crevice Samples

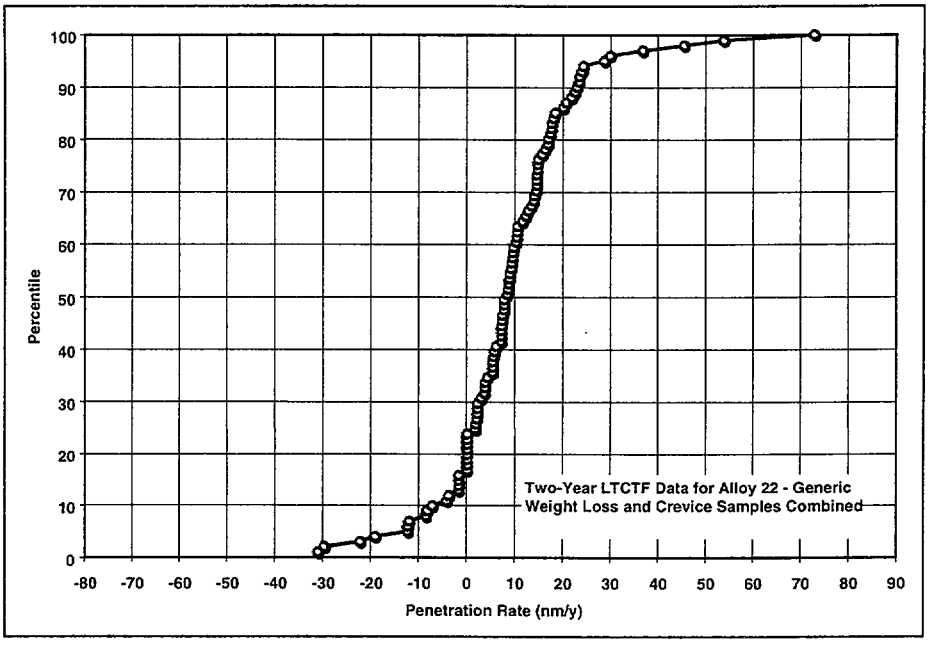

Source: CRWMS M&O 2000c, Section 6.9

Figure 3-20. Two-Year General Corrosion Rate Data From Long Term Corrosion Test Facility Based Upon Both Generic Weight-Loss and Crevice Samples, Including Those with Apparent Negative Rates

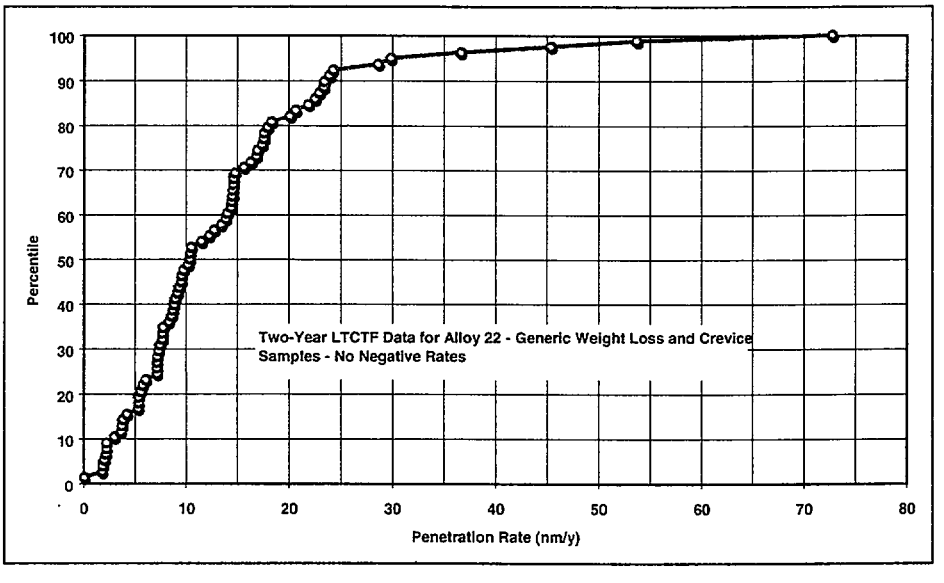

Source: CRWMS M&O 2000c, Section 6.9

Figure 3-21. Two-Year General Corrosion Rate Data From Long Term Corrosion Test Facility Based Upon Both Generic Weight-Loss and Crevice Samples, Excluding Those with Apparent Negative Rates

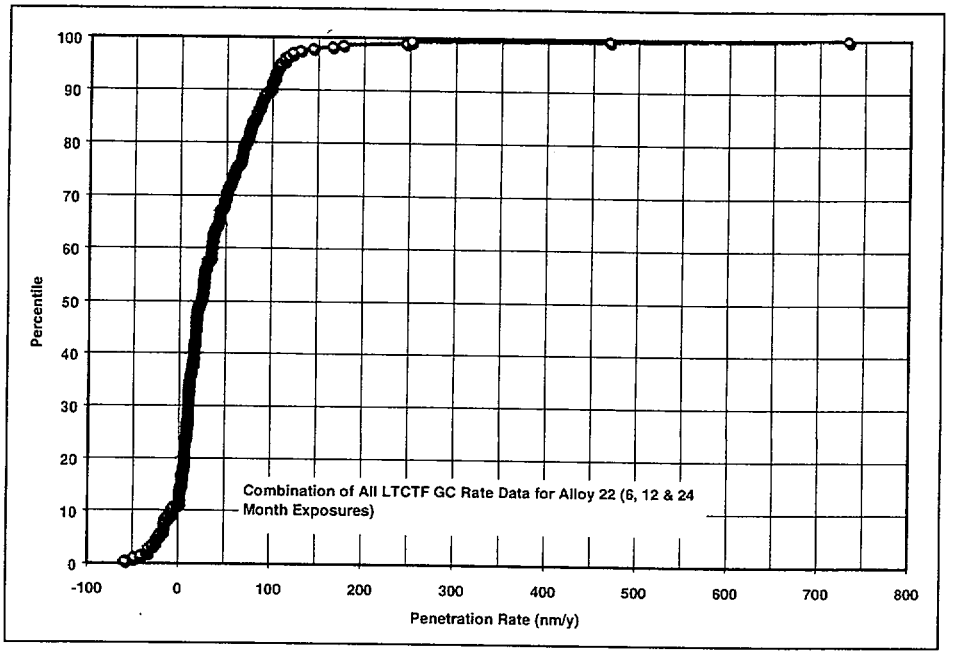

Source: CRWMS M&O 2000c, Section 6.9

Figure 3-22. Combination of All General Corrosion Rate Data for Alloy 22 from Long Term Corrosion Test Facility, Including 6-, 12-, and 24-Month Exposures

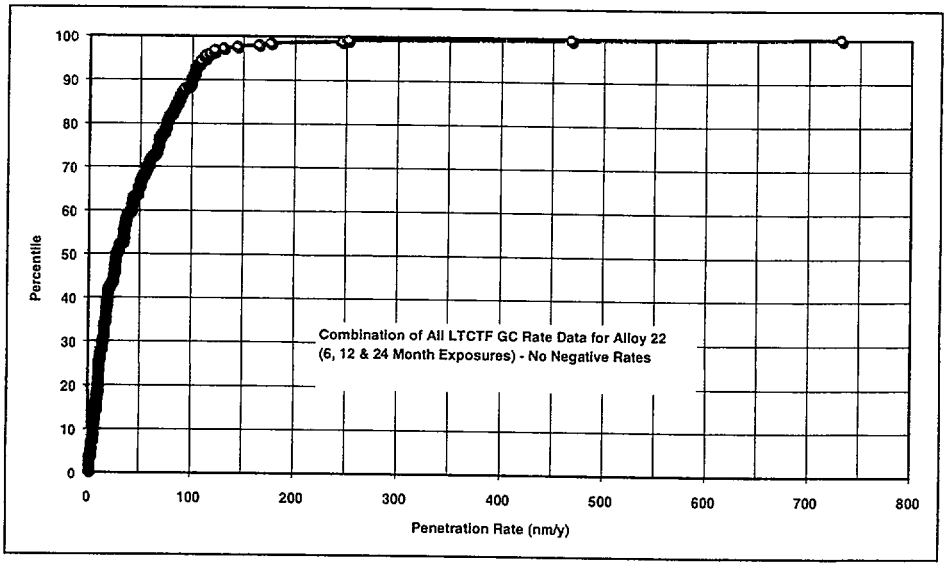

Source: CRWMS M&O 2000c, Section 6.9

Figure 3-23. Combination of All General Corrosion Rate Data for Alloy 22 from Long Term Corrosion Test Facility, Including 6-, 12-, and 24-Month Exposures with Negative Rates Excluded

In summary, the ranges of general corrosion rates measured at three time intervals (6, 12, and 24 months of exposure) are:

6-month exposure:	range –0.06 to +0.73 μm y^{-1}; mean 0.05 μm y^{-1}
12-month exposure:	range –0.04 to +0.10 μm y^{-1}; mean 0.03 μm y^{-1}
24-month exposure:	range –0.03 to +0.07 μm y^{-1}; mean 0.01 μm y^{-1}

The AFM has been used to characterize the surface topographies of five weight-loss coupons of Alloy 22, which had been exposed to various environments in the LTCTF for one year (CRWMS M&O 2000c, Section 6.5.5). Having sub-nanometer vertical resolution, the AFM is an ideal tool for detecting extremely small penetrations in corrosion-resistant materials such as Alloy 22. These samples include an unexposed control sample, a sample exposed to aqueous-phase SAW, a sample exposed to vapor-phase SAW, a sample exposed to aqueous-phase SCW, and a sample exposed to vapor-phase SCW. After the samples were removed from the LTCTF, they were ultrasonically agitated in deionized water, acetone, and methanol for ten minutes each. The Digital Instruments DM3100 AFM was then used for imaging. Each set of data consists of a large-area scan (25 μm × 25 μm), followed by smaller-area details of the region displayed in the large-area scan.

The gross surface topography is dominated by the machining grooves, with typical heights of several hundred nanometers and typical lateral periodicities of several microns, features plainly visible on images of the control sample. Samples removed from the LTCTF exhibit varying degrees of coverage by a deposit on top of this gross topography. The AFM images show that the most extensive deposit formation occurred on the sample exposed to aqueous-phase SAW (CRWMS M&O 2000c, Attachment 1). The next most extensive deposit formation occurred on the sample exposed to vapor-phase SAW. X-ray diffraction (XRD) of all five coupons show that the deposit is predominantly a silicate (SiO_2), with some NaCl appearing on the two samples which were in the SAW tank (CRWMS M&O 2000c, Attachment 1). Based upon both AFM and XRD data, the two samples exposed to SCW showed lesser degrees of coverage by the silicate deposit. In some cases, depressions can be seen in the silicate deposit. However, it is not believed that any of these penetrate to the underlying metal.

At the present time, there is insufficient data to determine the amount of silicate removed from exposed Alloy 22 samples by the standard cleaning method (CRWMS M&O 2000c). Accordingly, a worst-case estimate of the impact of SiO_2 on measured GC rates can be used.

The formation of SiO_2 deposits on the surface of the Alloy 22 could bias the distributions of GC rate shown in earlier sections of this PMR. From various AFM images of Alloy 22 samples removed from the LTCTF, it appears that a typical deposit can have a thickness as great as 0.25 microns after 12 months of exposure. It is assumed that the deposit has the density of lechatelierite (amorphous SiO_2), which is approximately 2.19 g cm^{-3}. It is further assumed that the surface is completely and uniformly covered by this deposit. The estimated surface areas of the weight-loss and crevice samples are 30.65 and 57.08 cm^2, respectively (4.75 and 8.85 in^2, respectively). Consequently, the deposit thickness (0.25 microns) translates into a mass change of 1.678 and 3.125 mg for weight-loss and crevice samples, respectively, after 12 months of exposure. The formula used to calculate the corrosion rate from weight-loss and dimensional change is then applied to determine the impact of such a positive mass change on the calculated rate. The estimated maximum bias is 0.063 μm per year (63 nm y^{-1}) for all weight-loss samples.

The distributions of GC rate shown in previous sections can be corrected for the maximum bias due to SiO_2 deposit formation by adding a constant value of 63 nm y^{-1} to each estimated value of the GC rate. This is equivalent to shifting the curves shown in figures to the right by 63 nm y^{-1}. Similar corrections could be applied to the Titanium Grade 7 data. Since the entire surface may not be covered by SiO_2, it may be preferable to distribute the correction between 0 and 63 nm y^{-1}.

The AFM has been used to examine areas inside and outside of Alloy 22 crevices exposed to SCW at 90°C for 12 months. Though the images were obtained with a welded sample, the unwelded area was imaged with the AFM. There appears to be no significant difference between the roughness of the four areas that were examined. Since it has been observed that corrosion tends to roughen the surface, it is concluded that there is no more attack inside the crevice than outside.

The observed decrease in the mean corrosion rate and in the range of data scatter with increasing exposure time from 6 months to 24 months is fully consistent with the expected corrosion behavior of passive alloys such as Alloy 22 under repository type aqueous conditions. For example, examination of very long term monitored corrosion results on passive type alloys are shown plotted in the Metals Handbook, (ASM International 1987, Vol 13, p. 911, Figure 42). As can be seen in this figure for aluminum alloys exposed to various marine environments for times up to 30 years, there is an initial higher corrosion rate at short times (< ~ 1 year), and the rate drops off in a parabolic manner with increasing time. This is expected behavior for alloys where the passive film grows by a parabolic or logarithmic diffusion controlled process. For this type behavior, the expected scatter at very short times where the rate is varying rapidly will be greater that at longer times where the rate is much lower. This type of behavior can also be seen for Alloy 22 where the extensive general corrosion test results now available from the LTCTF show a significantly larger 6-month mean rate of 0.05 μm y^{-1} as compared to a mean value of 0.01 μm y^{-1} at 24 months. Further, the observed 6-month data scatter is much greater (-.06 to +0.73 μm y^{-1}) than at 24 months (-0.03 to +0.07 μm y^{-1}) as expected and indicates that it is conservative to use the 24 month results to represent the much longer term general corrosion behavior of Alloy 22 under expected repository conditions

The maximum observed rate, which is much less than 1 micron per year, clearly indicates that the life of the WPOB will not be limited by general corrosion. No evidence of localized corrosion has been observed, even after two years of exposure. Examination of plastically strained U-bend specimens, again for all three time periods, indicates no initiation of SCC in both the base material and in the welded material. Half the number of these U-bend specimens contained welds.

Table 3-7. Summary of the Distribution of Rates for General Corrosion of Alloy 22 Samples

Percentile	Penetration Rate (nm y^{-1})
0.00	0
5.20	2.07
10.00	4.21
50.40	26.64
90.00	97.99
95.20	112.54
97.60	143.08
99.20	250.56
99.60	467.28
100.00	730.77

Source: CRWMS M&O 2000c, Section 6.9

3.1.5.4.3 Rates for Titanium Grade 16 – Weight-Loss Measurements from Long Term Corrosion Test Facility

All GC rates for Titanium Grade 16 are based on LTCTF weight-loss samples and are shown in Figure 3-24. It appears that these measurements are independent of temperature between 60 and 90°C. Furthermore, the composition of the test medium (SDW, SCW, or SAW) appears to have little impact on the measurements. With the exception of four outliers with negative values, most of the rates plotted in Figure 3-24 are between -200 and +200 nanometers per year. The median is at approximately zero. The outliers with large negative rates are believed to represent samples where there was significant oxide growth or scale formation (CRWMS M&O 2000c).

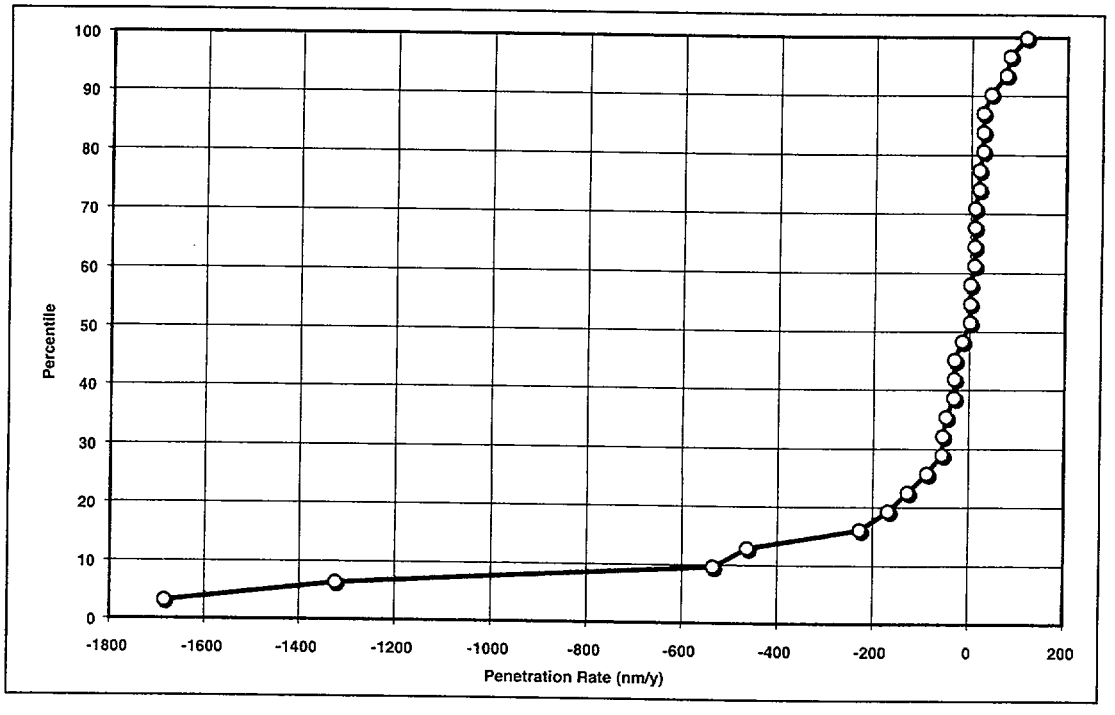

Source: CRWMS M&O 2000d, Section 6.5.2

Figure 3-24. General Corrosion of Titanium Grade 16: 12-Month Weight-Loss Samples from Long Term Corrosion Test Facility

This analysis only includes Titanium Grade 16 samples exposed for 12 months in the LTCTF. As discussed in the supporting AMR (CRWMS M&O 2000d, Section 6.5.2), the cleaning method employed with the 6-month titanium samples caused significant metal loss, thereby yielding unusually high corrosion rates that proved to be artifacts. Very little cleaning was used for the 12-month samples, which may account for the large negative values in Figure 3-24 (scale formation).

All GC rates for Titanium Grade 16 based on LTCTF crevice samples are shown in Figure 3-25 (rates based on areas outside of crevice). In this case, it also appears that the measurements are independent of temperature and test medium. Most of the rates plotted in Figure 3-25 are between -350 and +350 nanometers per year. The median is at approximately zero. The largest measured rate shown in Figure 3-25, which is less than +350 microns per year, will not lead to failure of the DS during the first 10,000 years of its service life. Based upon these data, it does not appear that the life of the DS will be limited by the general corrosion of Titanium Grade 16 (analog of Titanium Grade 7) at temperatures less than those involved in the test (90°C).

The crevice samples were configured in such a way as to reveal crevice corrosion if it occurred. Since no obvious crevice attack was observed with the samples represented by these figures, it is assumed that all weight loss in the crevice samples was due to GC outside of the crevice region (area underneath washer). However, higher scatter may indicate more variability of corrosion inside the crevice. Corrosion inside may be influenced by differential aeration, and pH changes.

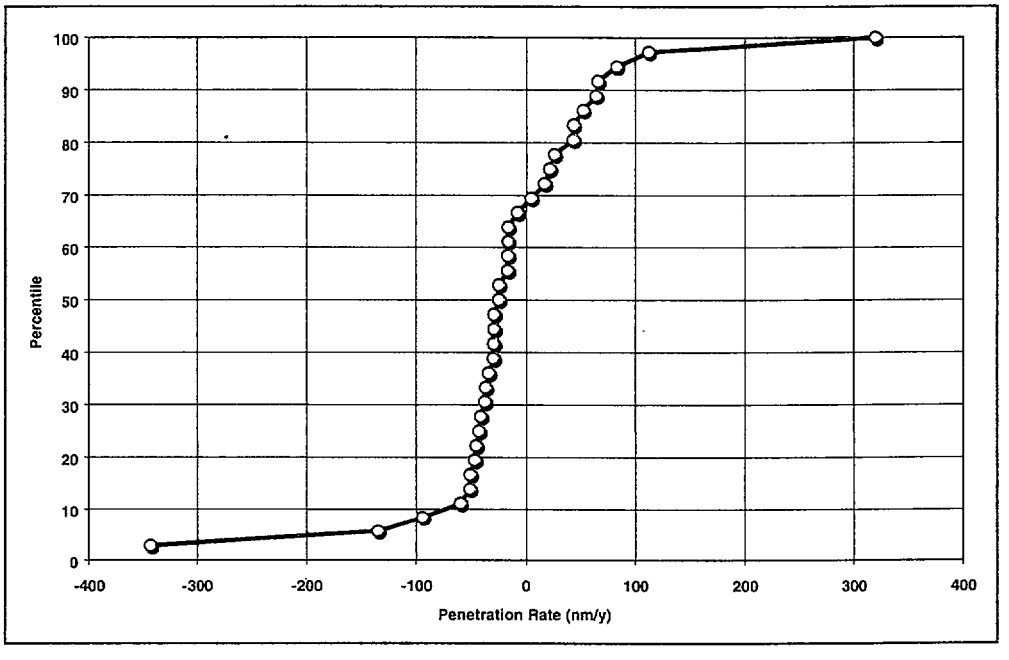

Source: CRWMS M&O 2000d, Section 6.5.2

Figure 3-25. General Corrosion of Titanium Grade 16: 12-Month Crevice Samples From Long Term Corrosion Test Facility

One simple and defensible representation of these GC rates has been proposed. The distribution of GC rates determined from weight-loss samples (Figure 3-24) and the distribution of GC rates determined from crevice samples (Figure 3-25) are combined into a single distribution. All negative rates are eliminated and the entire distribution is assumed to be due to uncertainty. From Figure 3-26, it can be seen that the rate at the 50th percentile is approximately 25 nanometers per year, the rate at the 90th percentile is approximately 100 nanometers per year, and the maximum rate is less than 350 nanometers per year. About 10% percent of the values fall between 100 and 350 nanometers per year. Figure 3-27 shows that the cumulative probability is a linear function of the logarithm of the observed GC rates (log-uniform distribution).

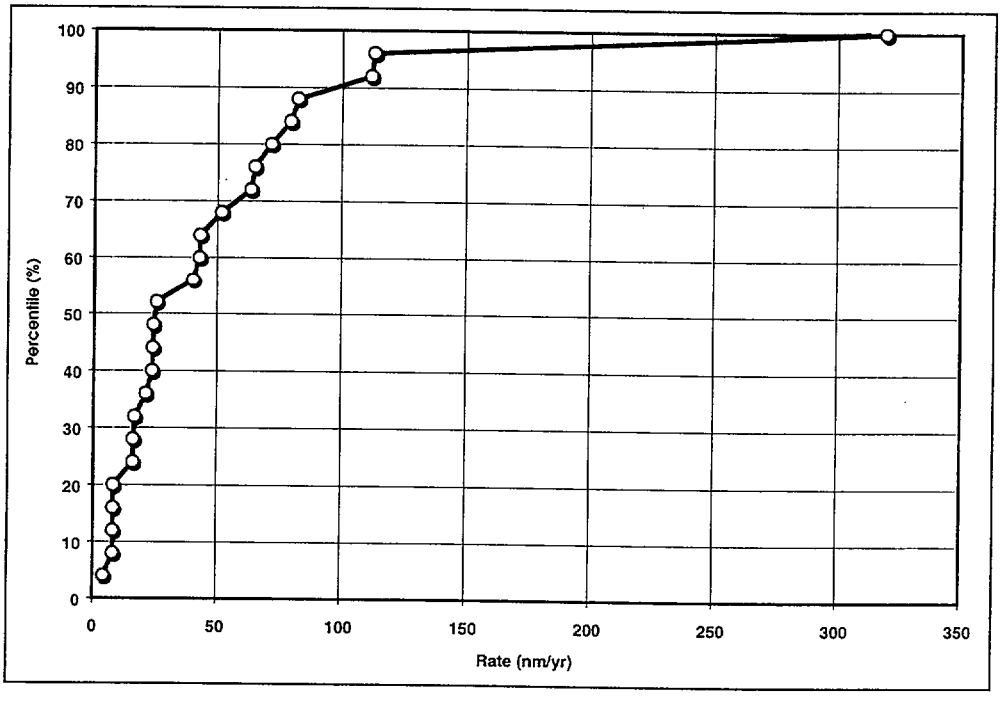

Source: CRWMS M&O 2000d, Section 6.5.4

Figure 3-26. Distribution of Positive General Corrosion Rates Based Upon Weight-Loss and Crevice Samples

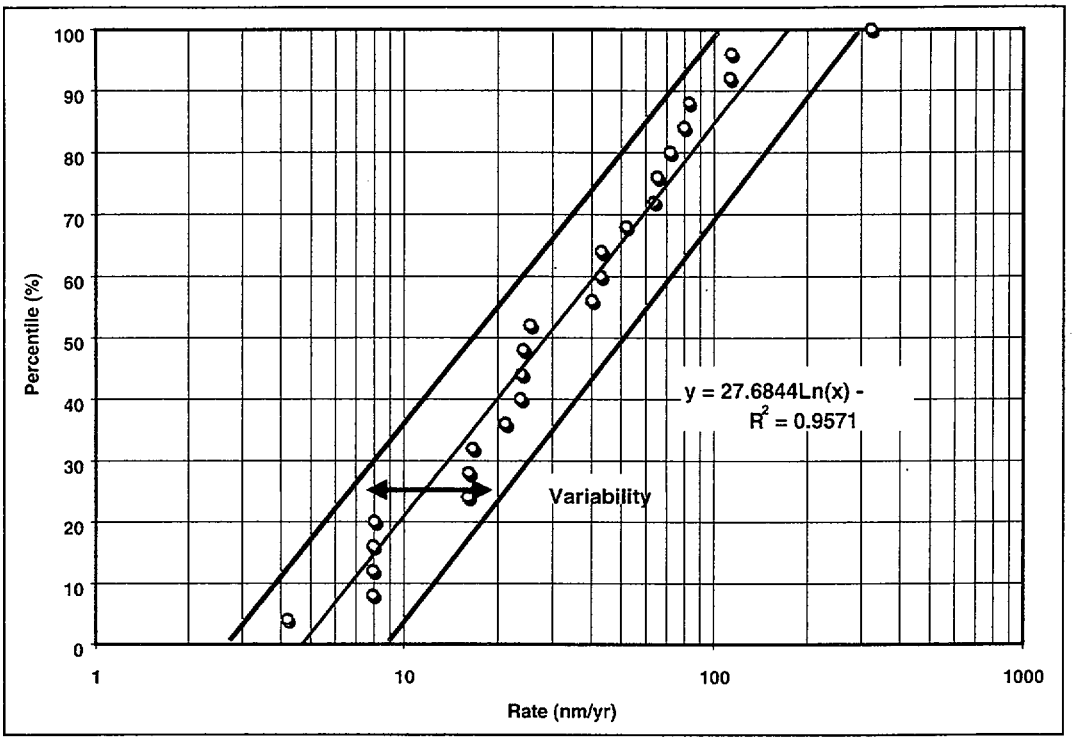

Source: CRWMS M&O 2000d, Section 6.5.4

Figure 3-27. Distribution of Positive General Corrosion Rates with Variability Based Upon Weight-Loss and Crevice Samples

3.1.5.5 Error Analysis for Corrosion Rates – Weight-Loss Measurements from Long Term Corrosion Test Facility

The general method used in the formal error analysis is presented in the AMR on general and LC of the WPOB (CRWMS M&O 2000c, Section 6.5.3). The methodology is important since it enables correct interpretation of the data. Only the results of that analysis are presented here. In the case of Alloy 22, the estimated error is shown in Table 3-8. The corresponding error for Titanium Grade 16 (Titanium Grade 7 analog) is shown in Table 3-9.

Table 3-8. Summary of Error Analysis for Corrosion Rates Based Upon Weight Loss of Alloy 22

	Assumed Weight Loss		0.0001 g	0.0010 g	0.0100 g
Case	Sample Configuration	Exposure Time	Δy nm y^{-1}	Δy nm y^{-1}	Δy nm y^{-1}
1	Crevice	6 month	12	13	20
2	Weight Loss	6 month	23	25	38
3	Crevice	12 month	6	6	9
4	Weight Loss	12 month	11	12	18

Source: CRWMS M&O 2000c, Section 6.5.3

NOTE: Δy = error in GC rate

Table 3-9. Summary of Error Analysis for Corrosion Rates Based Upon Weight Loss of Titanium Grade 16

	Assumed Wt. Loss		0.0001 g	0.0010 g	0.0100 g
Case	Sample Configuration	Exposure Time	Δy nm y^{-1}	Δy nm y^{-1}	Δy nm y^{-1}
1	Crevice	6 month	24	26	47
2	Weight Loss	6 month	45	49	89
3	Crevice	12 month	12	13	22
4	Weight Loss	12 month	22	24	42

Source: CRWMS M&O 2000d, Section 6.5.3

NOTE: Δy = error in GC rate

It is concluded that the typical uncertainty observed in weight-loss and dimensional measurements prevents determination of corrosion rates for Alloy 22 that are less than approximately 38 nm y^{-1}. The maximum uncertainty is estimated to be between 6 and 20 nm y^{-1} in the case of crevice samples, and between 11 and 38 nm y^{-1} in the case of weight-loss samples. These estimates of probable error are believed to correspond to about one standard deviation (1σ). Any measured corrosion rate greater than 160 nm y^{-1} (4σ) should be easily distinguishable from measurement error. Any rate less than 160 nm y^{-1} will be difficult to distinguish from measurement error. The maximum error in the corrosion rate for Titanium Grade 16 is estimated to be approximately 89 nm y^{-1}, significantly larger than a comparable estimate for Alloy 22. The difference between estimated errors for Alloy 22 and Titanium Grade 16 is attributable to the differences in density.

3.1.6 Localized Corrosion

The difference between E_{corr} and $E_{critical}$ is used to determine whether or not LC will occur. If $E_{critical}$ is less than or equal to E_{corr}, LC is likely. These potentials are measured experimentally in electrolyte compositions believed to representative of the repository environment (Section 1.5.4.3) (Tables 3-2, 3-3, and 3-4). Such electrolytes are described in a supporting AMR (CRWMS M&O 2000c, Section 6.4).

Junction potentials for the reference electrode in all test solutions of interest have been calculated and are discussed in the supporting AMR on GC and LC of the WPOB (CRWMS M&O 2000c, Section 6.4). Since these calculated junction potentials are not very large, it is concluded that no significant error in any measurement of potential results by neglecting to correct for the junction potential.

3.1.6.1 Threshold Potentials

The generic LC model for WP materials assumes that localized attack occurs if the open circuit corrosion potential (E_{corr}) exceeds the threshold potential for breakdown of the passive film ($E_{critical}$):

$$E_{corr} \geq E_{critical} \qquad \text{(Eq. 3-16)}$$

This model of LC initiation is referred to as Method A. In some cases, the threshold potential is assumed to be the repassivation potential. The repassivation potential is the level at which a failed passive film repassivates, or heals, thereby protecting the surface. In other cases, the threshold potential is assumed to be the pit or crevice initiation potential.

3.1.6.2 Published Threshold Potentials for Alloy 22

Compared to materials proposed for use in earlier WP designs, Alloy 22 has superior resistance to LC. The AMR on general and LC of the WPOB includes published repassivation potentials found in the literature (CRWMS M&O 2000c, Section 6.4). These data show that the threshold potential for LC of Alloy 22 is far greater than that of Alloy 625, thereby substantiating the claim that Alloy 22 is superior to the corrosion resistant materials used in earlier WP designs.

3.1.6.3 Cyclic Polarization in Synthetic Concentrated J-13 Waters

Pitting and crevice corrosion are usually associated with the breakdown of passivity. Tests for evaluating the susceptibility of a material to pitting and crevice corrosion include CP. These tests can be used to detect pit and crevice initiation potentials (where they exist), and repassivation potentials if losses in passivity are observed. Most recently, the procedure described in ASTM G 61-86, *Standard Test Method for Conducting Cyclic Potentiodynamic Polarization Measurements for Localized Corrosion Susceptibility of Iron-, Nickel-, or Cobalt Based Alloys* has been developed for conducting CP measurements of iron- or nickel-base alloys in chloride environments.

Cyclic polarization measurements are based on a procedure similar to ASTM G 5-94, *Standard Reference Test Method for Making Potentiostatic and Potentiodynamic Anodic Polarization Measurements* with appropriate and necessary deviations. For example, ASTM G 5-94 calls for an electrolyte of 1N H_2SO_4, whereas SDW, SCW, SAW, and SSW are used here. Furthermore, aerated solutions are used, unlike the procedure that calls for de-aerated solutions. A baseline curve with Pt in SCW is shown in Figure 3-28. Representative CP curves are shown in Figures 3-29 through 3-37. The shapes of these CP curves are categorized as Type 1, 2, 3, or 4, as explained in the following paragraphs.

A generic Type 1 curve exhibits complete passivity (no passive film breakdown) between the corrosion potential and the point defined as Threshold Potential 1. This interpretation was verified by visual inspection of samples after potential scans. Photographic documentation is maintained for some of the samples (all samples are held in the archives at LLNL). Threshold Potential 1 is in the range where the onset of oxygen evolution is expected and is defined by a large excursion in anodic current. This particular definition of Threshold Potential 1 is specific to Type 1 curves. Type 1 behavior has only been observed with Alloy 22 and is illustrated by Figure 3-29. The interpretation of Type 1 curves as exhibiting no passive film breakdown is consistent with Chapter 7 of ASTM G 61-86.

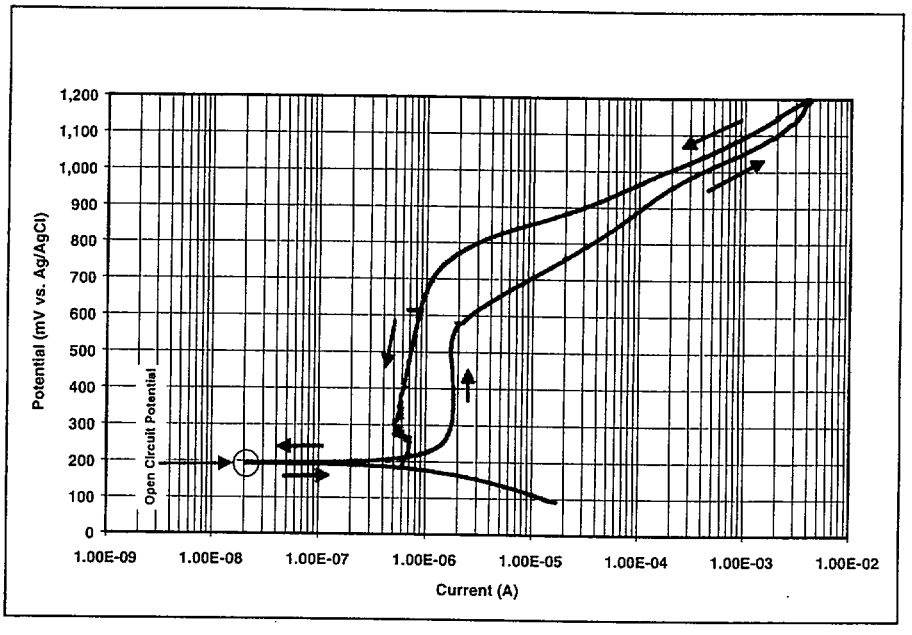

Source: CRWMS M&O 2000c, Section 6.4

Figure 3-28. Baseline – Platinum in Simulated Concentrated Water at 90°C (PT001)

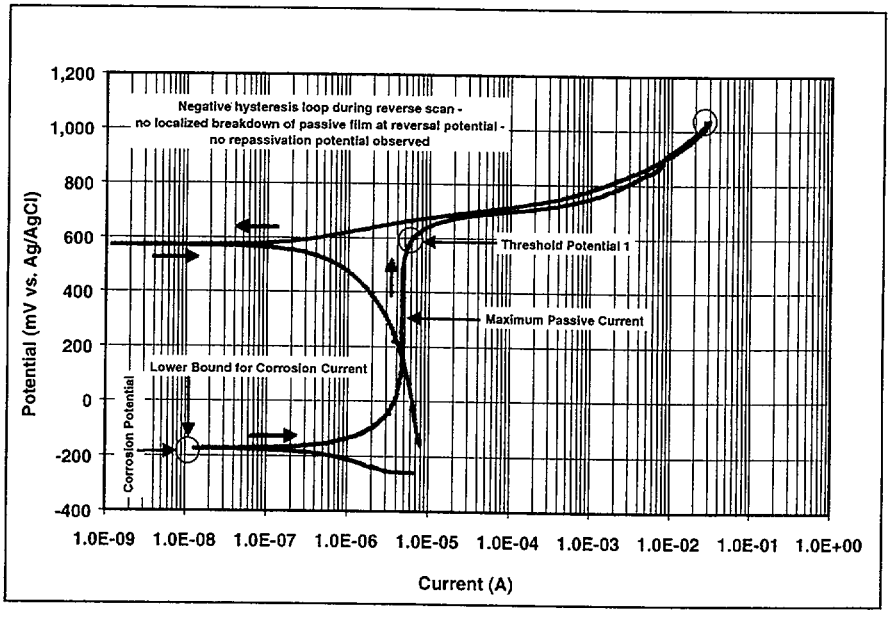

Source: CRWMS M&O 2000c, Section 6.4

Figure 3-29. Type 1–Alloy 22 in Simulated Acidic Concentrated Water at 90°C (DEA002)

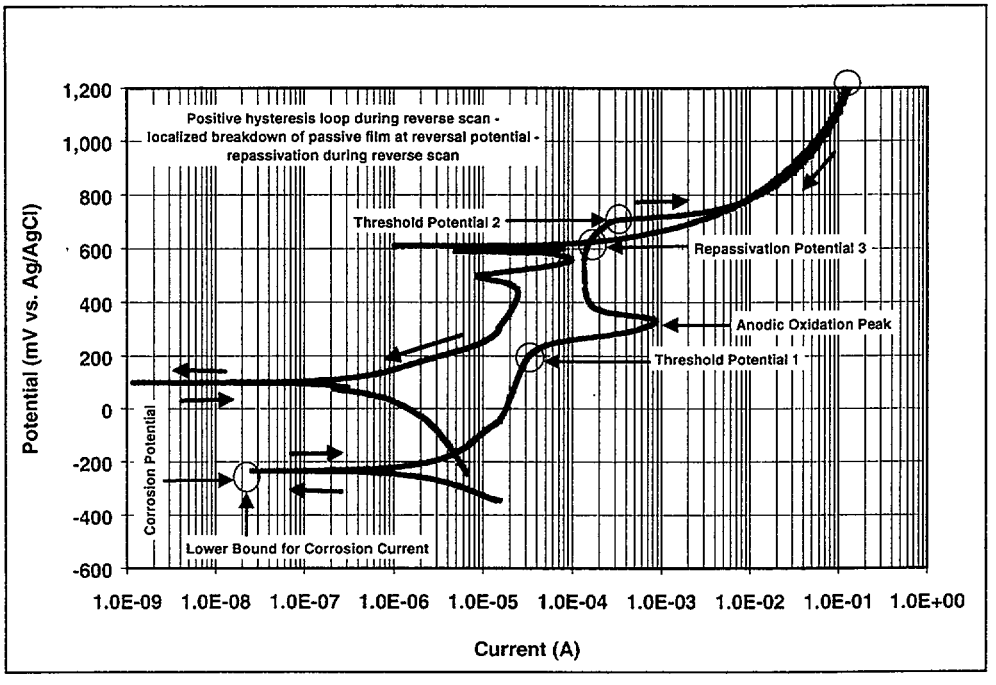

Source: CRWMS M&O 2000c, Section 6.4

Figure 3-30. Type 2–Alloy 22 in Simulated Concentrated Water at 90°C (DEA016)

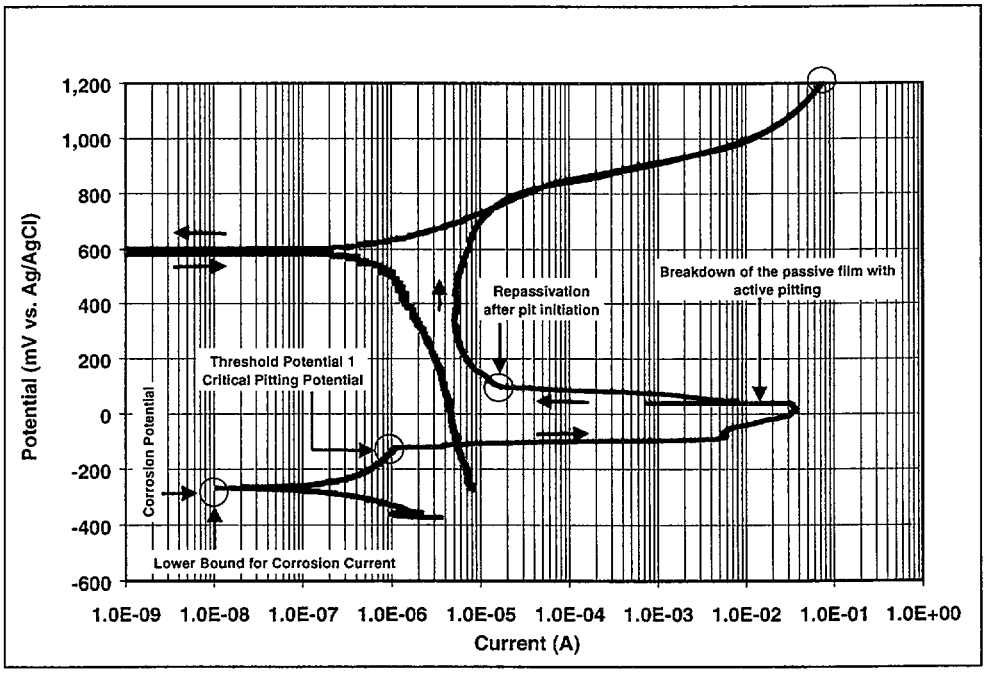

Source: CRWMS M&O 2000c, Section 6.4

Figure 3-31. Type 3–316L in Simulated Saturated Water at 100°C (PEA016)

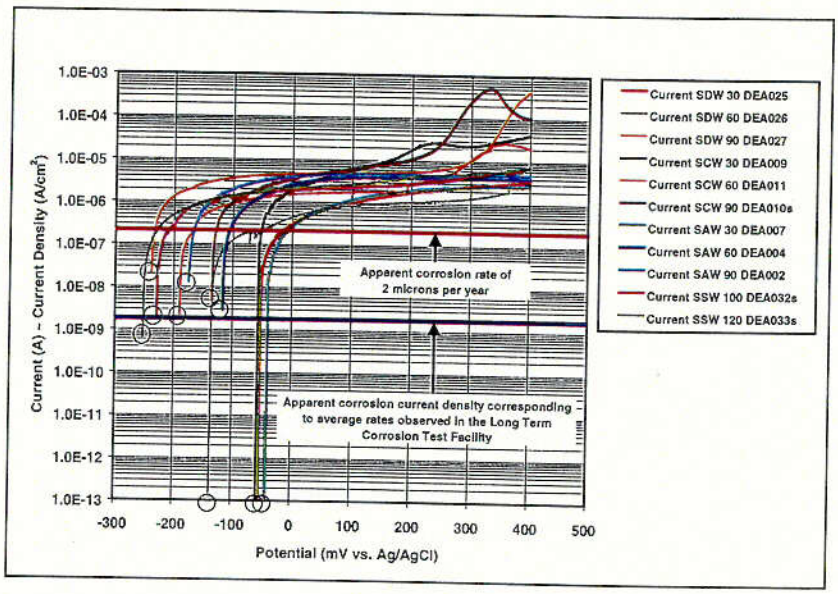

Source: CRWMS M&O 2000c, Section 6.4.2

Figure 3-32. Alloy 22 in Various Repository Media – Comparison of Cyclic Polarization Data

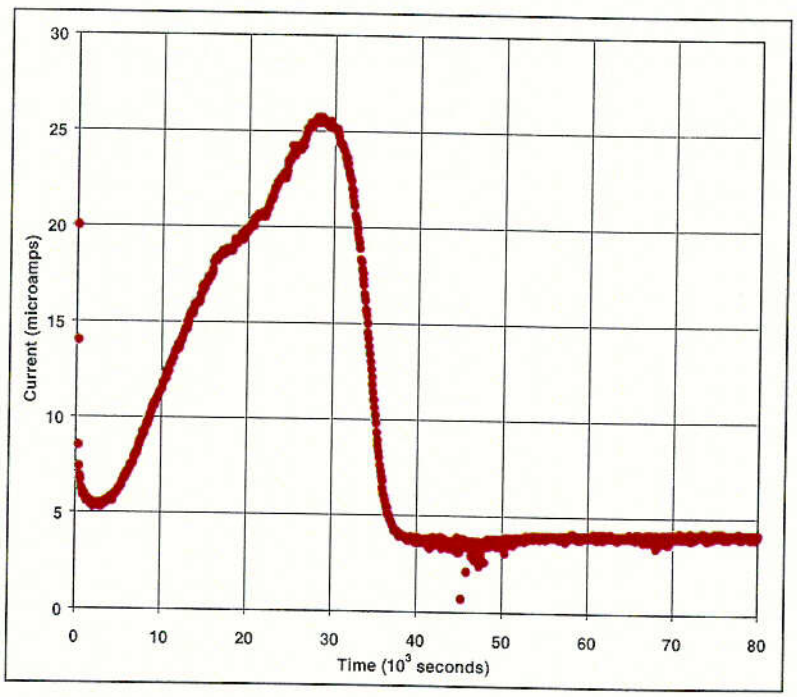

Source: CRWMS M&O 2000c, Section 6.4.2

Figure 3-33. Potentiostatic Polarization of Alloy 22 in Simulated Concentrated Water at 90°C and 200 mV Versus Ag/AgCl

C-10

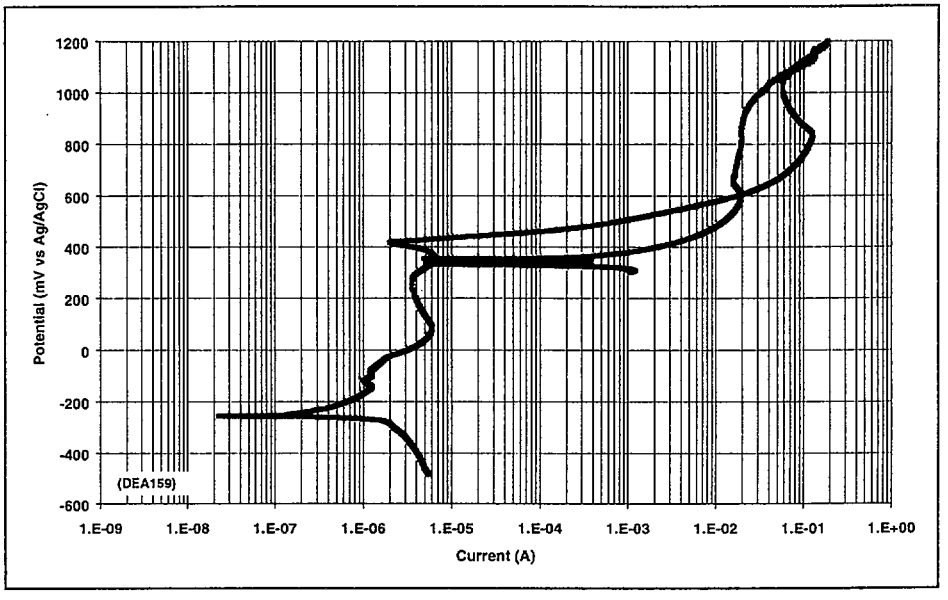

Figure 3-34. Cyclic Polarization Curve for Alloy 22 in 110°C Basic Saturated Water – Thermally Aged at 700°C for 10 Hours (DEA159)

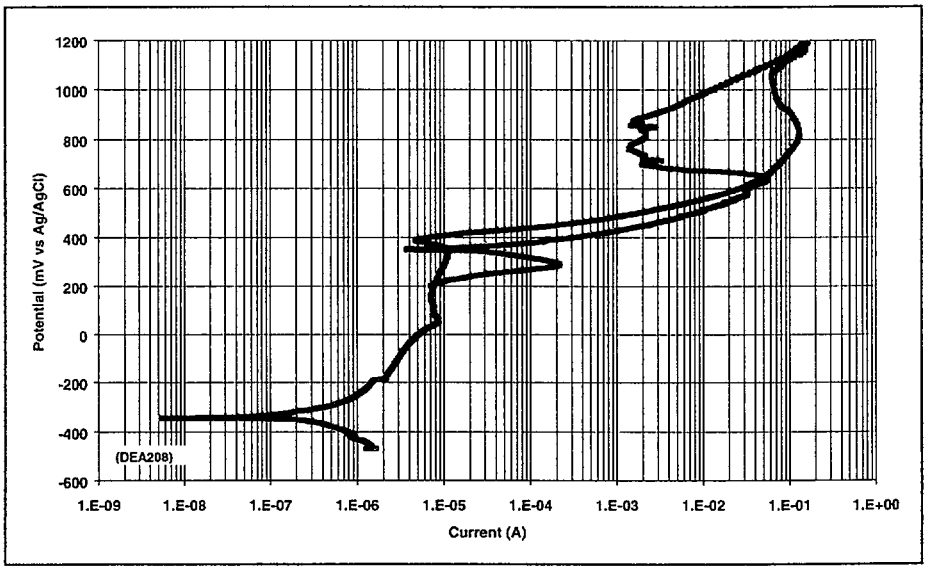

Source: CRWMS M&O 2000c, Section 6.9.2

Figure 3-35. Cyclic Polarization Curve for Alloy 22 in 110°C Basic Saturated Water – Thermally Aged at 700°C for 173 Hours (DEA208)

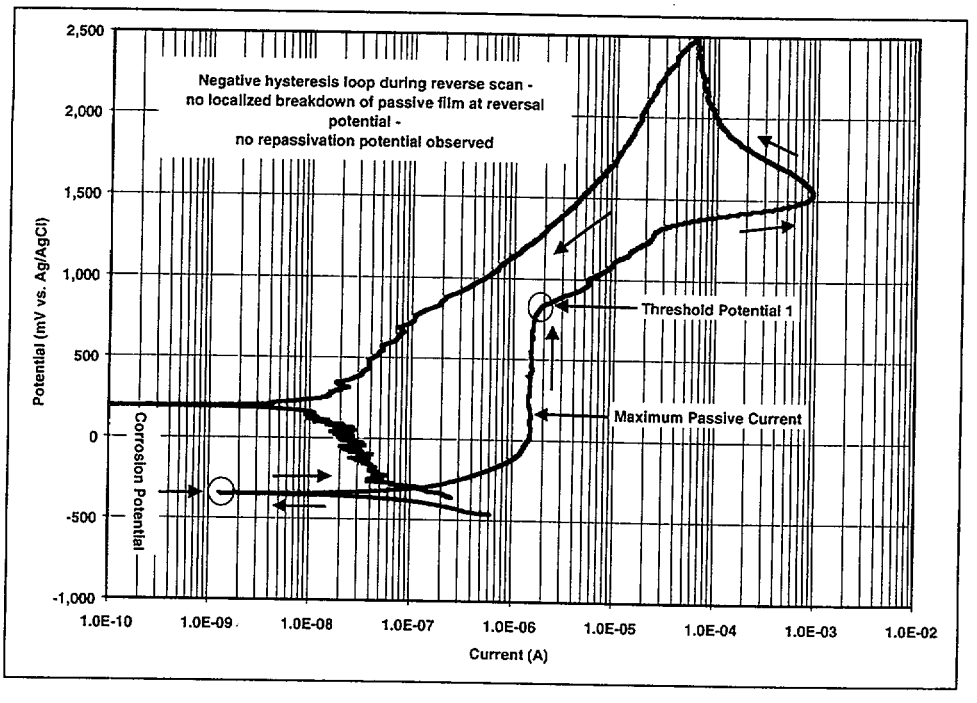

Figure 3-36. Titanium Grade 7 in Simulated Saturated Water at 120°C (NEA031s)

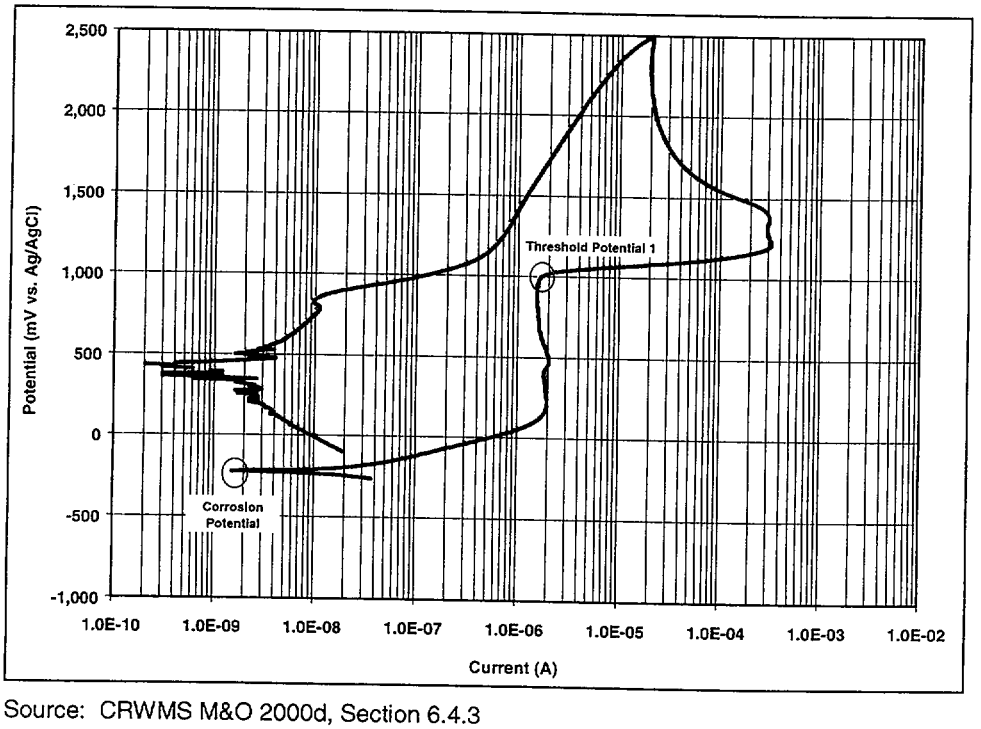

Source: CRWMS M&O 2000d, Section 6.4.3

Figure 3-37. Titanium Grade 7 in Simulated Concentrated Water at 90°C (NEA003)

A generic Type 2 curve exhibits a well defined oxidation peak at the point defined as Threshold Potential 1. Threshold Potential 2 is in the range where the onset of oxygen evolution is expected, and is defined by a large increase in anodic current. These particular definitions of the threshold potentials are specific to Type 2. Repassivation Potentials 1 and 2 are defined as the points where the hysteresis loop passes through a current levels of 4.27×10^{-6} and 10^{-5} amps, respectively (not shown). Repassivation Potential 3 is determined from the first intersection of the hysteresis loop (reverse scan) with the forward scan. Type 2 is observed with both Alloy 22 and Type 316L stainless steel. In the case of Alloy 22, this behavior is illustrated by Figure 3-30. Definitions of the threshold and repassivation potentials are somewhat subjective, and may vary from investigator to investigator. The threshold potential for initiation of crevice corrosion on Alloy 22 is defined as the point during the potential scan in the forward direction where the current density increases to a level of 10^{-6} to 10^{-5} A cm^{-2}. The repassivation potential is defined as the point during the potential scan in the backward direction where the current density drops to 10^{-6} to 10^{-7} A cm^{-2}. This definition is comparable to that of Repassivation Potential 3. The basis for these current densities is discussed in detail in the AMR on general and LC of the WPOB (CRWMS M&O 2000c, Section 6.4).

As previously discussed, a representative curve for platinum in SCW at 90°C is shown in Figure 3-28. The CP measurements of Pt were made to serve as a basis of comparison for similar measurements with Alloy 22 and other materials of interest. From such comparisons, it is concluded that the anodic oxidation peak observed in Type 2 curves (between 200 and 600 mV) for Alloy 22 is due to an anodic reaction of the passive film. No anodic oxidation peak is observed in the curve for platinum. X-ray photoelectron spectroscopy measurements of the passive film polarized at potentials above and below the anodic oxidation peak have shown that the anodic reaction increases the oxidation state of metal cations in the film, which remains intact.

A generic Type 3 curve exhibits a complete breakdown of the passive film and active pitting at potentials relatively close to the corrosion potential (E_{corr}). In this case, Threshold Potential 1 corresponds to the critical pitting potential. Type 3 behavior has only been observed with stainless steel 316L in SSW and is illustrated by Figure 3-31. SSW is a saturated sodium-potassium-chloride-nitrate electrolyte, formulated to represent the type of concentrated electrolyte that might evolve on a hot WP surface. This formulation has a boiling point of approximately 120°C at ambient pressure. In contrast to the Type 3 behavior exhibited by stainless steel 316L in SSW, Alloy 22 maintains passivity at potentials up to the reversal potential (1,200 mV versus Ag/AgCl).

A composite of the CP data for Alloy 22 is shown in Figure 3-32. It should be noted that the axes of this figure are changed in comparison to previous figures. The initial portions of these curves show that passivity is maintained at potentials at least as high as 400 mV versus Ag/AgCl in all cases. The lowest potential at which any electrochemical reactivity of the passive film is observed is approximately 200 mV versus Ag/AgCl. Based upon data presented here, it is concluded that pitting attack of Alloy 22 should not occur under conditions expected in the repository. To further substantiate this conclusion, it is noted that no pitting of Alloy 22 has yet been observed in samples removed from the LTCTF after two years of exposure to SDW, SCW, and SAW at 60 and 90°C.

In regard to Type 2 polarization curves for Alloy 22 in SCW, the electrochemical process leading to the anodic oxidation peak (leading edge at approximately 200 mV versus Ag/AgCl) cannot be determined from the CP data alone. As previously discussed, this peak is due to some change in oxidation state of the passive film and probably has very little to do with any loss of passivity. To augment these potentiodynamic measurements, potentiostatic polarization tests have been performed. Figure 3-33 shows the observed transient current when an Alloy 22 sample is polarized at 200 mV versus Ag/AgCl in SCW at 90°C, close to the potential where the leading edge of the anodic oxidation peak is located. The current density initially increases to a maximum of approximately 25 $\mu A\ cm^{-2}$ (the sample size is approximately 0.96 cm^2) at 9 hours. This corresponds to a typical non-equilibrium passive current density measured for Alloy 22 at this potential and in the absence of the anodic oxidation peak. For example, see a Type 1 polarization curve for Alloy 22 in SAW. It is therefore concluded that the anodic oxidation peak observed in Type 2 polarization curves does not define any LC or loss in passivity. Threshold Potential 1 (leading edge of the anodic oxidation peak at approximately 200 mV versus Ag/AgCl) should not be used as the basis for switching on LC of Alloy 22. In such cases, it should be assumed that Threshold Potential 2 (oxygen evolution) represents the lower bound for breakdown of the passive film.

Several CP measurements have now been made with BSW electrolytes and are summarized in Table 3-10 and Figures 3-34 and 3-35. As previously discussed in Section 3.1.4.5, extreme aging of Alloy 22 can shift the corrosion potential in a less noble (cathodic) direction by approximately 100 mV. This is accompanied by a slight increase in non-equilibrium passive current density. There is some evidence of an anodic oxidation peak, characteristic of Type 2 curves. For the present time, we will classify these CP curves as intermediate Type 1-2.

Examples of CP data for Titanium Grade 7 in SSW and SCW are shown in Figures 3-36 and 3-37, respectively. Both CP curves are Type 4, showing little evidence of passive film breakdown over a very wide range of potential.

Table 3-10. Electrochemical Potentials Determined from Cyclic Polarization of Alloy 22 in Basic Saturated Water

Sample ID	Aging Time	Aging Temp.	Medium	Temp.	Reversal Potential	Corrosion Potential	Threshold Potential 1	CP Curve Type
	hours	°C		°C	mV	mV	mV	
DEA158	10	700	BSW	110°C	1200	-233	418	Type 1-2
DEA159	10	700	BSW	110°C	1200	-257	419	Type 1-2
DEA208	173	700	BSW	110°C	1200	-345	394	Type 1-2
DEA209	173	700	BSW	110°C	1200	-372	361	Type 1-2

Source: CRWMS M&O 2000c, Section 6.9.2

The University of Virginia (Uva) has recently generated some CP data with very tight crevices and concentrated electrolytes consisting of 5 M LiCl, 0.24 to 0.024 M $NaNO_3$, 0.026 to 0.26 M Na_2SO_4, and HCl. Testing was conducted at two temperature levels, 80 and 95°C. The crevices were formed with a multiple crevice former, and an applied torque of 70 inch pounds. Under these circumstances, some electrochemical activity indicative of crevice corrosion was

observed at potentials ranging from 71 to 397 mV versus Ag/AgCl, depending upon the composition of the electrolyte. Using a current density criterion for repassivation of 10^{-5} A cm^{-2}, repassivation potentials were determined to be slightly above, but relatively close to the open-circuit corrosion potential.

The concentrated lithium-chloride based electrolytes used in the UVa tests are not relevant to those conditions anticipated in the repository. Unlike compositions based upon J-13 well water, these electrolytes have no buffer ions *per se*. Continued testing is underway with samples configured like those used by UVa and test media relevant to the repository (BSW). In these tests, it has been found that simulated repository waters with buffer inhibit the type of crevice corrosion observed in tests with electrolytes based upon lithium chloride, even at the boiling point of saturated solutions. As more data become available, correlation equations for the corrosion and threshold potentials should be updated, expressing these quantities in terms of temperature, pH, and the concentrations of various ions. The UVa approach appears ideally suited for determining repassivation potentials when they exist.

Conclusions from tests with UVa-type samples and BSW are corroborated by other measurements. Relatively wide crevices (110 to 540 microns) formed from passive Alloy 22 and filled with SCW do not appear to undergo significant increases in hydrogen ion concentration (pH suppression) at reasonable electrochemical potentials. These potentials are generally below the thresholds determined by CP. Finally, Alloy 22 and Titanium Grade 16 crevices exposed in the LTCTF do not indicate significant crevice corrosion. Recall that Titanium Grade 16 is considered to be an analog of Titanium Grade 7.

In the case of 316 stainless steel data shown in Figure 3-31 and Figures 3-14 and 3-15 suggest that localized corrosion may be likely under certain conditions. However, even if the material fails by localized corrosion (pitting) the structural shell will retard the ingress of water into the waste package as the pits are narrow and deep. Nevertheless, the stainless steel structural material is not used as a containment barrier at this time to provide for a conservative approach.

3.1.6.4 Correlation of Potential Versus Temperature Data for Various Test Media

Values of corrosion and threshold potentials for the three WP materials of interest have been correlated as a function of temperature for repository-relevant test media. In general, it has been found that these potential versus temperature data can be represented by the following simple regression equation:

$$y = b_0 + b_1 x + b_2 x^2 \qquad \text{(Eq. 3-17)}$$

where y is either the corrosion or threshold potential (mV vs. Ag/AgCl) and x is the temperature (°C). Parameters for Equation 3-21 are found in Figures 3-38 through 3-48. These parameters were used to calculate values of E_{corr} and $E_{critical}$ for WP materials in SDW, SCW, SAW, and SSW at 10°C intervals. These calculations and tabulations of the parameters are found in the supporting AMR documents (CRWMS M&O 2000c, Section 6.4.3, 2000d, Section 6.4.3, 2000e Section 6.4.3,).

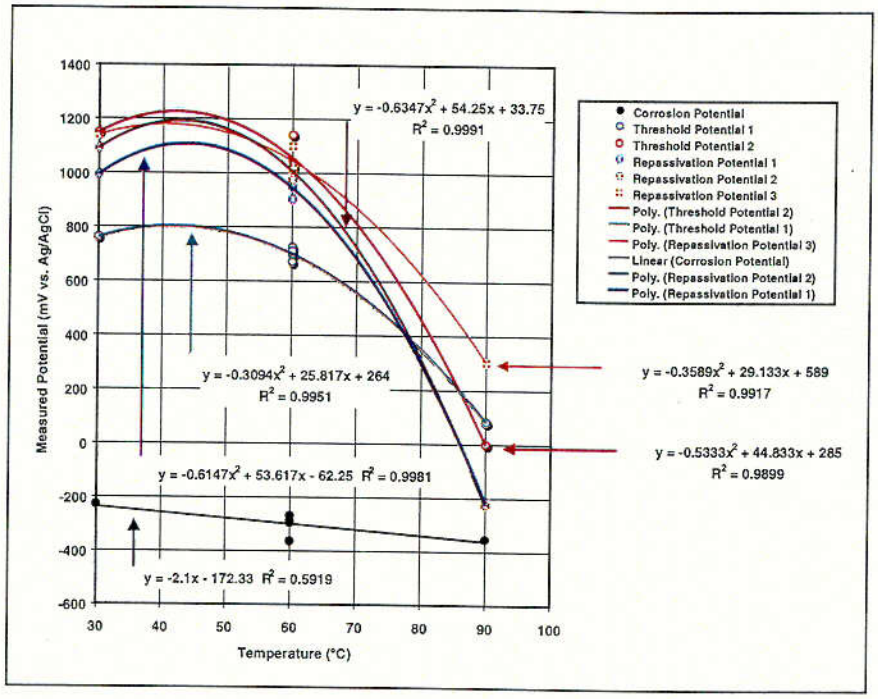

Source: CRWMS M&O 2000e, Section 6.4.3

Figure 3-38. Potentials versus Temperature – Stainless Steel 316L in Simulated Acidic Concentrated Water

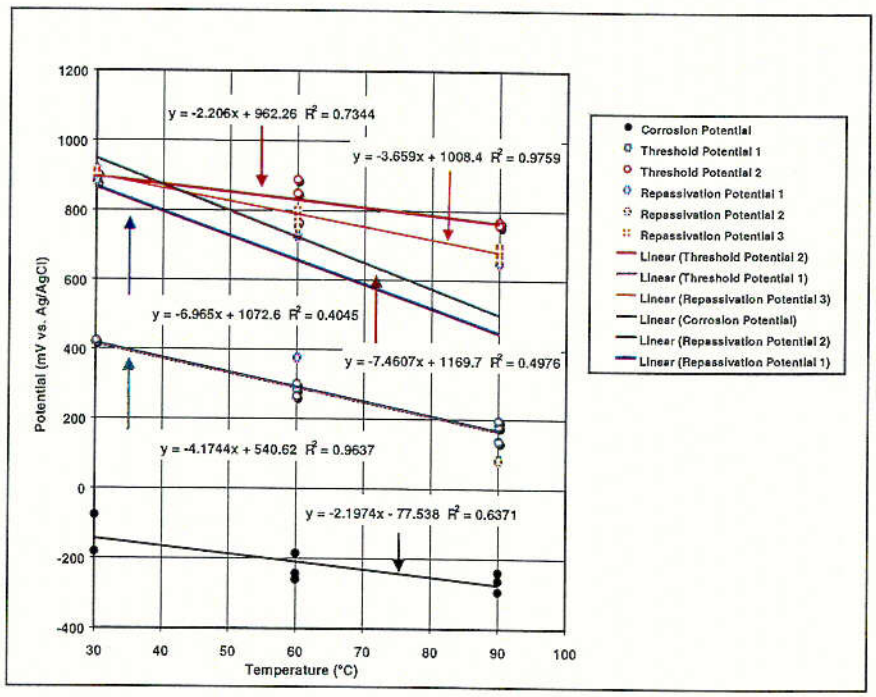

Source: CRWMS M&O 2000e, Section 6.4.3

Figure 3-39. Potentials versus Temperature – Stainless Steel 316L in Simulated Concentrated Water

C-11

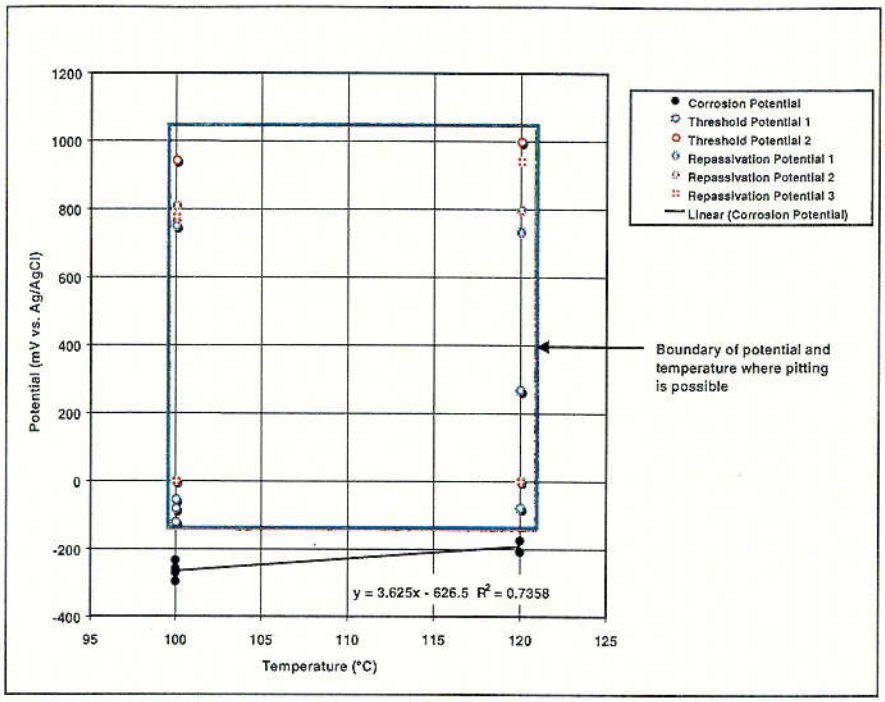

Source: CRWMS M&O 2000e, Section 6.4.3

Figure 3-40. Potentials versus Temperature – Stainless Steel 316L in Simulated Saturated Water

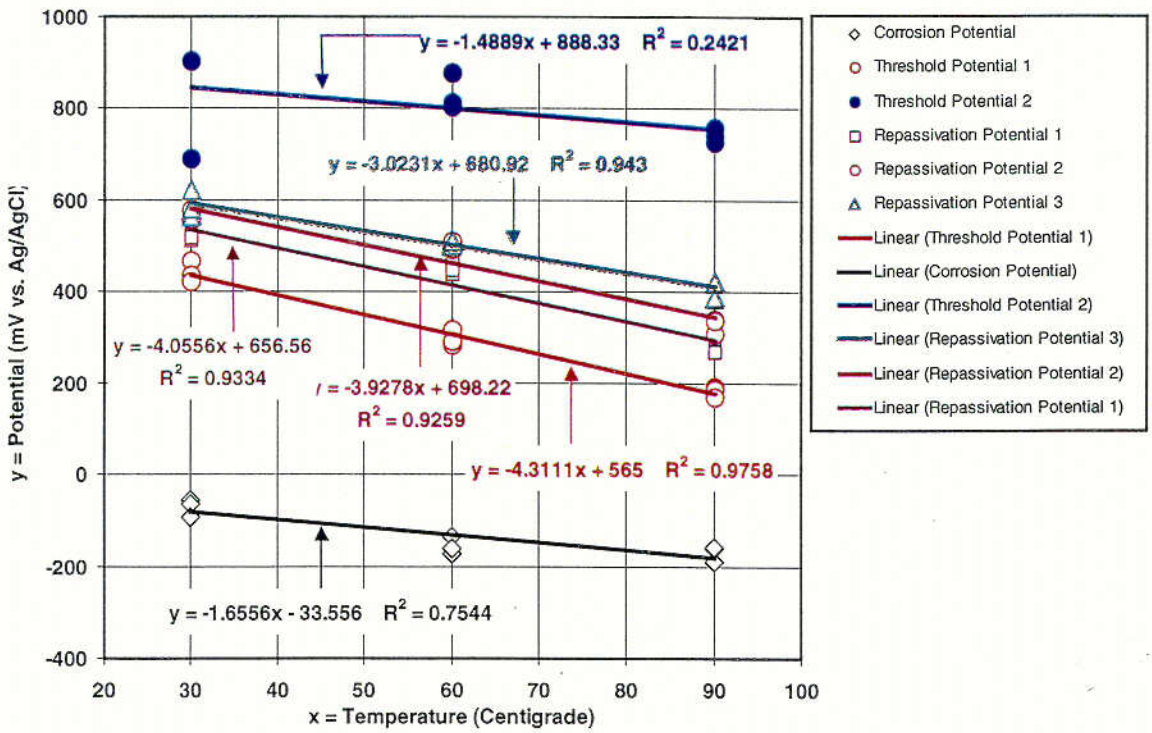

Source: CRWMS M&O 2000c, Section 6.4.3

C-12

Figure 3-41. Potentials versus Temperature – Alloy 22 in Simulated Dilute Water

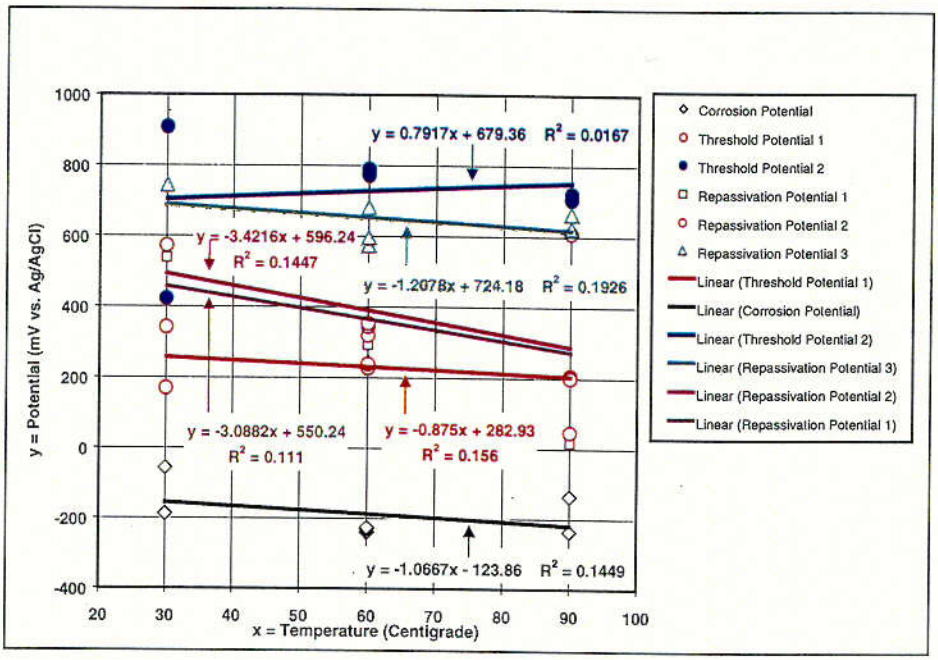

Source: CRWMS M&O 2000c, Section 6.4.3

Figure 3-42. Potentials versus Temperature – Alloy 22 in Simulated Concentrated Water

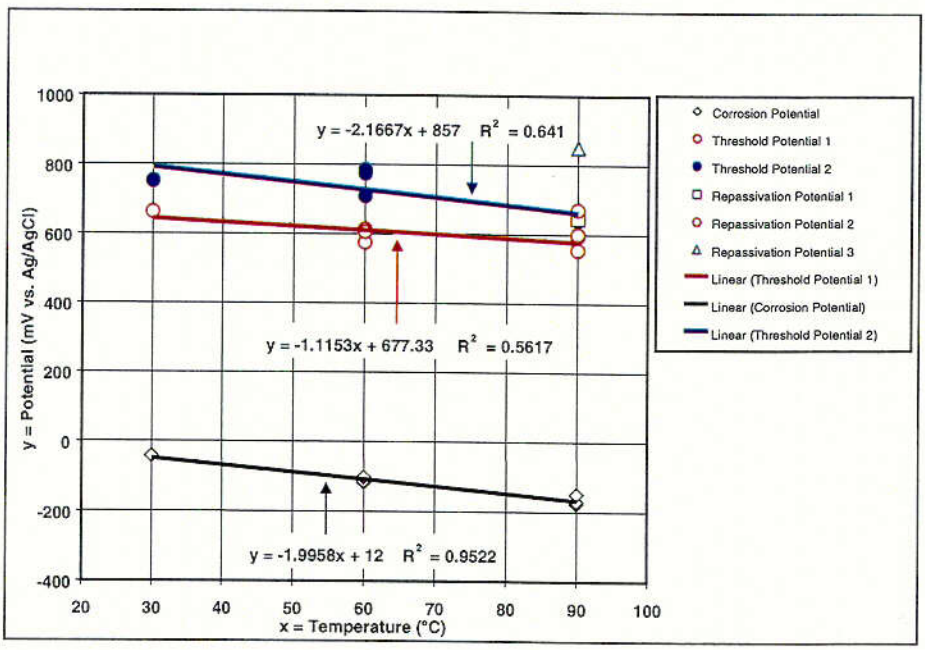

Source: CRWMS M&O 2000c, Section 6.4.3

Figure 3-43. Potentials versus Temperature – Alloy 22 in Simulated Acidic Concentrated Water

C-13

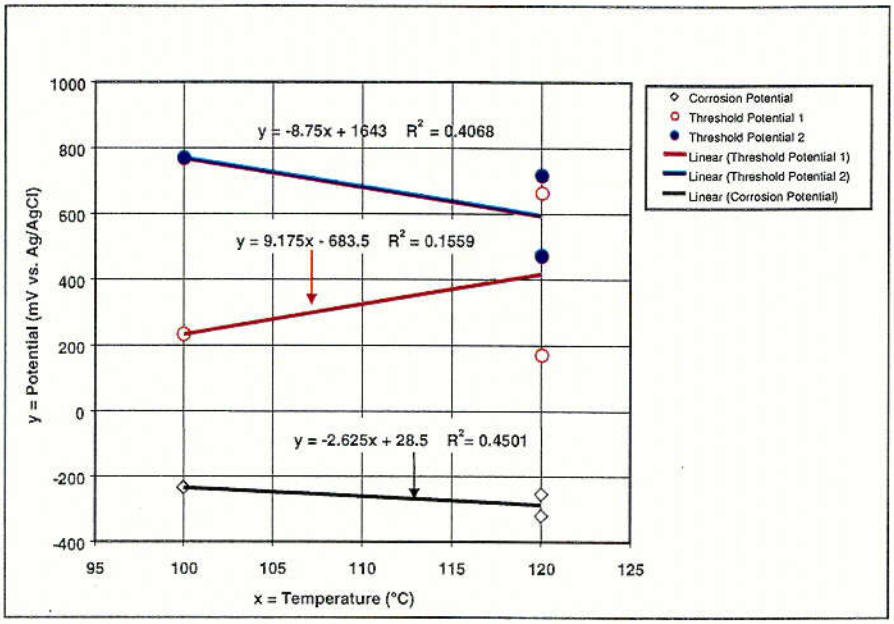

Source: CRWMS M&O 2000c, Section 6.4.3

Figure 3-44. Potentials versus Temperature – Alloy 22 in Simulated Saturated Water

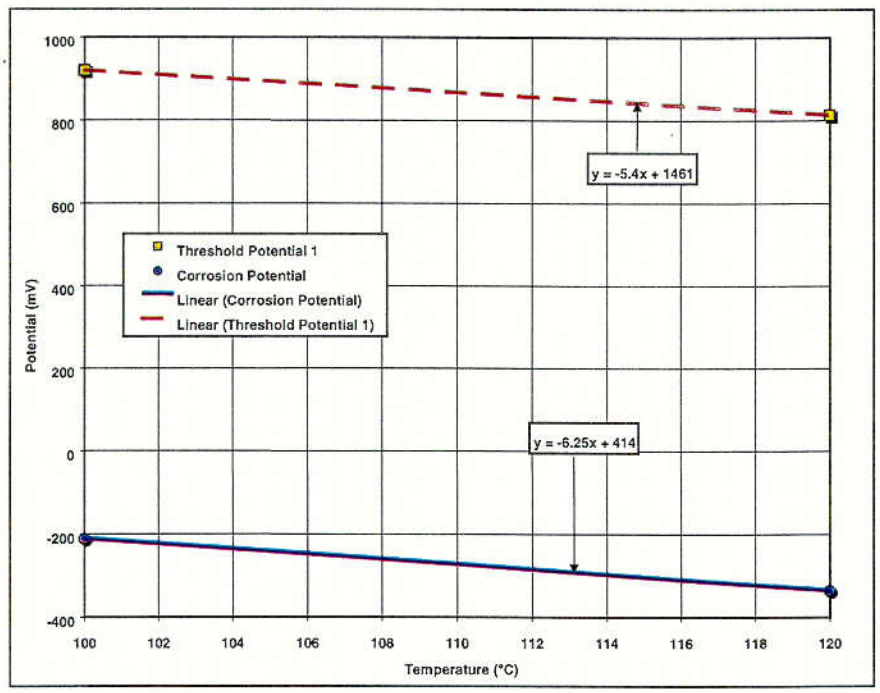

Source: CRWMS M&O 2000d, Section 6.4.3

Figure 3-45. Corrosion and Threshold Potentials of Titanium Grade 7 in Simulated Saturated Water (NEA031s)

C-14

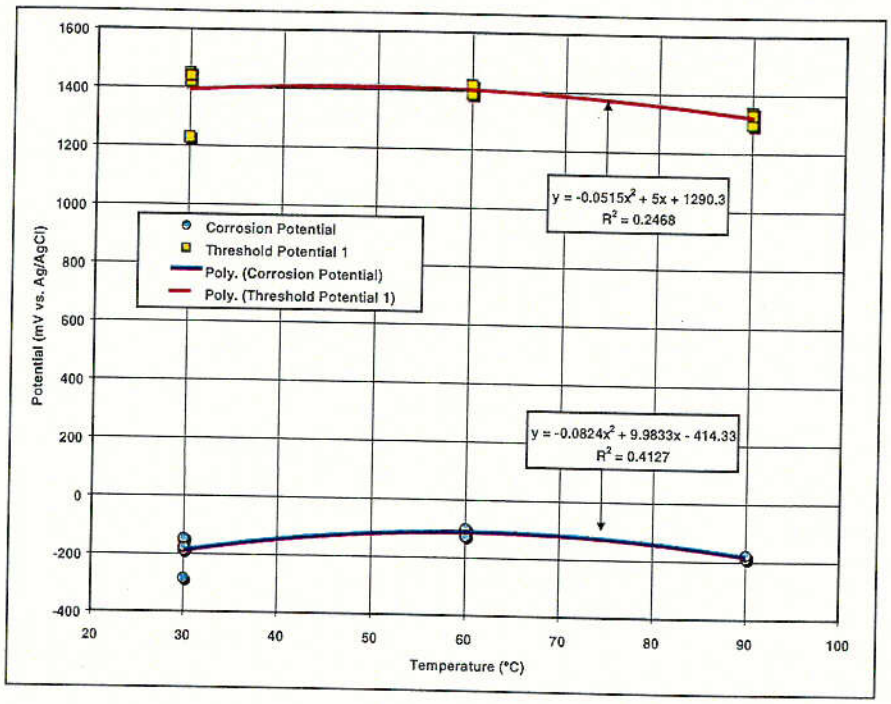

Source: CRWMS M&O 2000d, Section 6.4.3

Figure 3-46. Corrosion and Threshold Potentials for Titanium Grade 7 in Simulated Acidic Concentrated Water

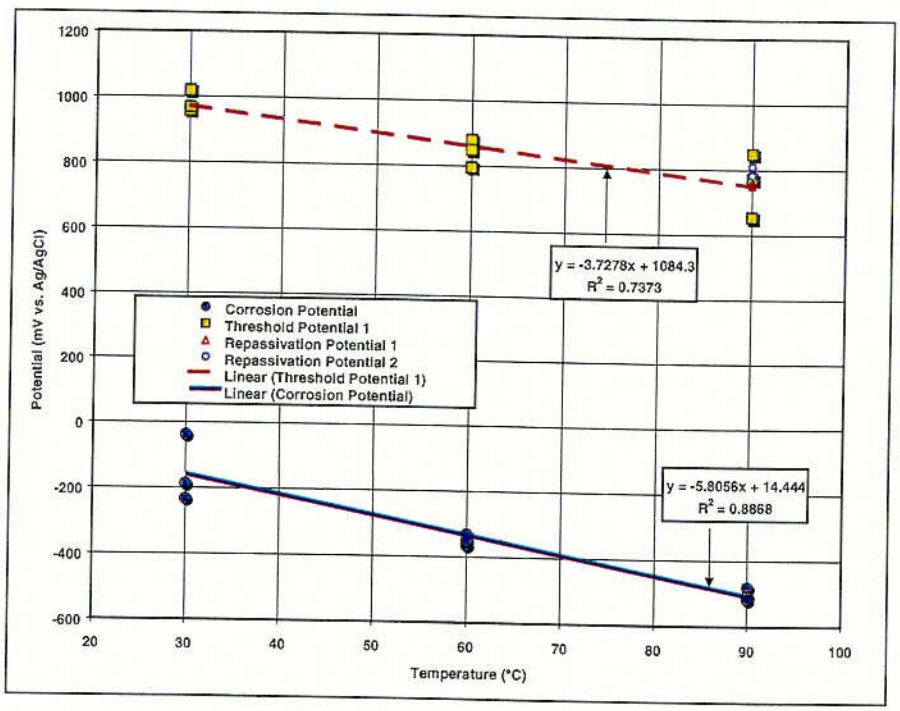

Source: CRWMS M&O 2000d, Section 6.4.3

Figure 3-47. Corrosion and Threshold Potentials for Titanium Grade 7 in Simulated Concentrated Water

C-15

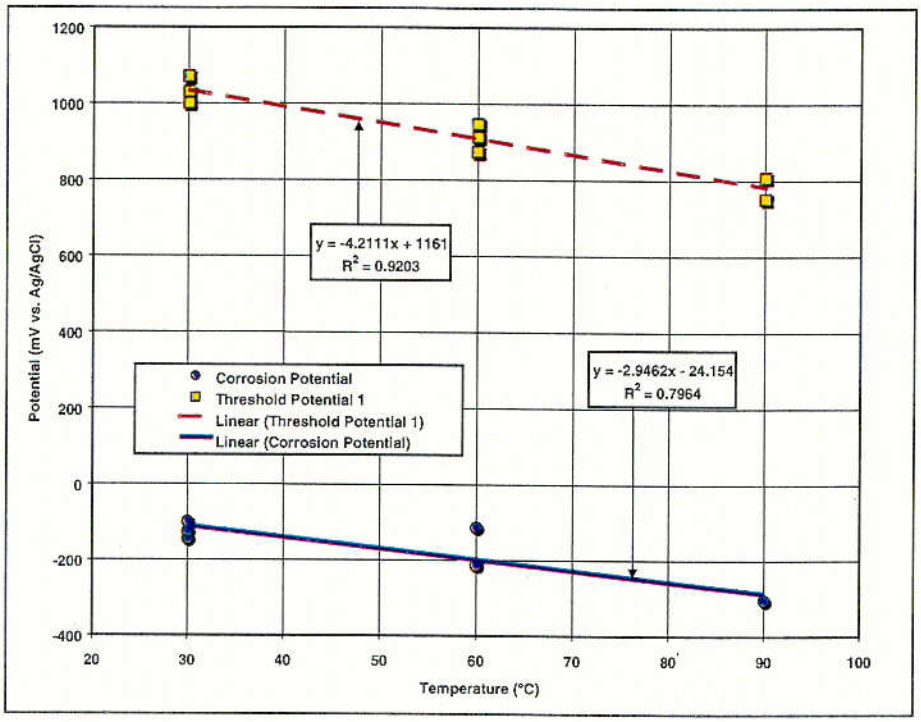

Source: CRWMS M&O 2000d, Section 6.4.3

Figure 3-48. Corrosion and Threshold Potentials for Titanium Grade 7 in Simulated Dilute Water

All correlation equations for stainless steel 316NG are found in Figures 3-38 through 3-40. The correlation for E_{corr} and the most conservative correlation for the threshold potential, $E_{critical}$, are labeled. In the case of Type 2 CP curves, the selected threshold potential is determined by the position of the observed anodic oxidation peak, and may not result in any actual loss of passivity. In the case of Type 3 CP curves, the measured threshold potentials are scattered. The transparent square in Figure 3-40 therefore represents the range of potential and temperature where pitting attack is believed to be possible. The lower boundary of the square appears to be very close to the line representing the corrosion potential. Note that these very low threshold potentials are entirely consistent with the published temperature-dependent pitting potentials. These data are represented by Equation 3-17 where $b_0 = 547.76$, $b_1 = -6.617$ and $b_2 = 0$. As this correlation is extrapolated to 100°C, the pitting potential approaches the lower boundary of the transparent box used to bound the threshold potentials.

C-1 Le

All correlation equations for Alloy 22 are found in Figures 3-41 through 3-44. The correlation for the corrosion potential (E_{corr}) and the conservative correlation for the threshold potential ($E_{critical}$) are labeled. While calculated values of y are believed to have only three significant figures, coefficients in that regression equation are given with more figures. The correlation equations for Titanium Grade 7 are found in Figures 3-45 through 3-48. The data presented in these figures clearly show that the threshold potentials for localized corrosion of Titanium Grade 7 and Alloy 22 are not exceeded under conservatively assumed media.

In an ideal case, the crevice corrosion temperature can be estimated from the intersection of the lines representing the corrosion and threshold potentials at elevated temperature. Such intersection is evident in Figure 3-38. Better correlations of E_{corr} and $E_{critical}$ with material history, water chemistry, and temperature may ultimately allow precise prediction of the crevice corrosion temperature. Improved correlations would provide rigorous statistical estimates of uncertainty and variability in E_{corr} and $E_{critical}$. The precise determination of uncertainty and variability in E_{corr} and $E_{critical}$ would enable designers to determine the impact of accepting 100% of the supplied WP material on repository performance. In the meantime, crevice corrosion can be forced to occur in the model by equating E_{corr} and $E_{critical}$ over temperature ranges of uncertainty (90-120°C). This assumption would provide a conservative estimate of the crevice corrosion temperature. Improved LC models with accurate temperature dependence will allow a precise sensitivity study, assessing the impact of various WP design changes on the radiological dose at the site boundary.

There are precedents for using electrochemical measurements as the basis of water chemistry and materials specifications in the nuclear industry. For example, measurements of corrosion potential are indicative of dissolved oxygen and can be used to assure adequate deaeration in various regions of the steam cycle. The role of electrochemical potential on SCC has been well documented (CRWMS M&O 2000c).

3.1.6.5 Prediction of Critical Temperatures for Pitting and Crevice Corrosion

As previously discussed, a threshold temperature (critical temperature) can be used as an alternative to a threshold potential for the initiation of LC. This initiation model for LC is referred to as Method B. In an ideal case, the critical temperatures for pitting and crevice corrosion can be estimated from the intersection of the lines representing the corrosion and threshold potentials as functions of temperature. This intersection occurs at elevated temperature, as illustrated by Figure 3-38. The critical temperature for pitting of stainless steel 316L is illustrated by Figures 3-49 and 3-50. To force crevice corrosion to occur in the model, E_{corr} and $E_{critical}$ can simply be equated above the critical temperature.

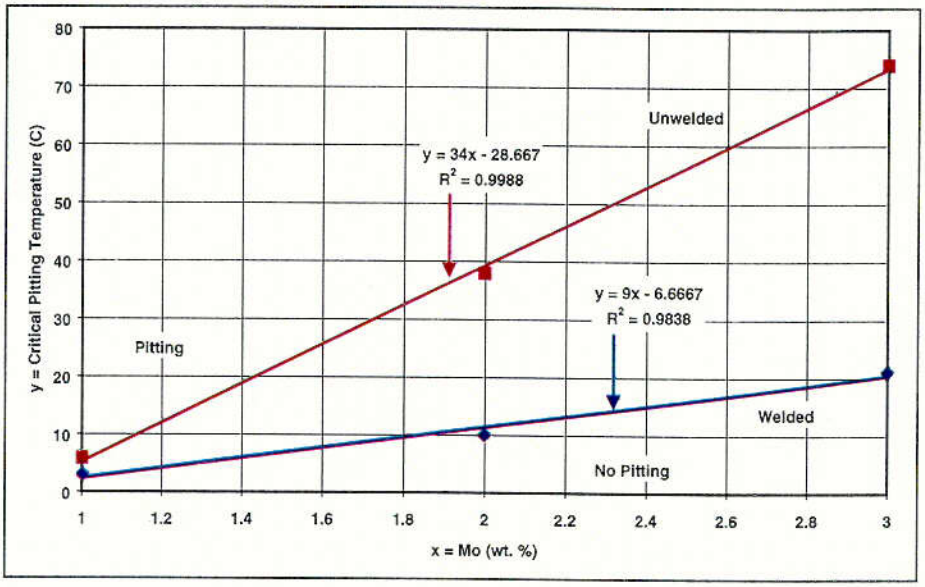

Source: CRWMS M&O 2000e, Section 6.4.5

Figure 3-49. Effect of Molybdenum on the Critical Pitting Temperature of Stainless Steels in Ferric Chloride Solution

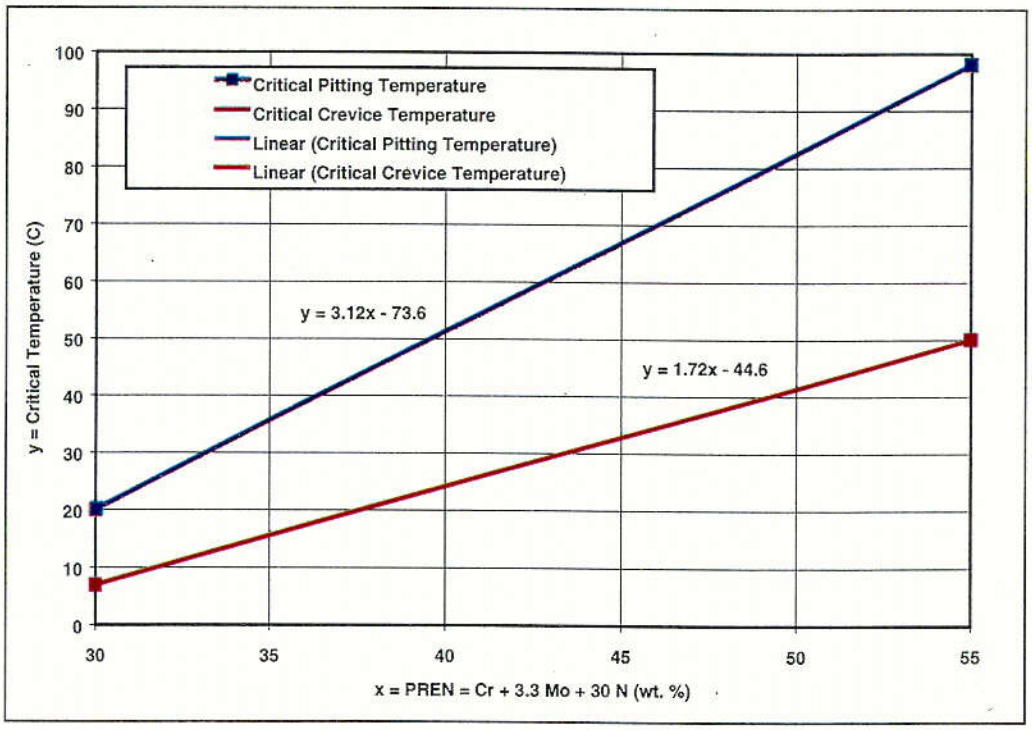

Source: CRWMS M&O 2000e, Section 6.4.5

Figure 3-50. Effect of Pit Resistance Equivalence Number on the Critical Pitting and Crevice Corrosion Temperature of Stainless Steels in Ferric Chloride Solution

C-17

3.1.6.6 Effect of Gamma Radiolysis on Corrosion Potential

Anodic shifts in the open circuit corrosion potential of stainless steel in irradiated aqueous environments have been experimentally observed (CRWMS M&O 2000c, Section 6.4.4). It is now accepted as fact by much of the engineering community that this observation is due to the generation of hydrogen peroxide by the radiation. The CP experiments performed at ambient temperature with 316L samples in 0.018-M NaCl solution during exposure to 3.5-Mrad hr^{-1} gamma radiation have shown that the corrosion potential shifts in the anodic direction by approximately 200 mV. It was concluded that there is very little increase in the corresponding corrosion current density. However, the separation between the corrosion potential and the threshold for localized attack decreased slightly. This shift in corrosion potential was shown to be due to the formation of hydrogen peroxide. This finding was subsequently confirmed by another independent CP experiment with 316 stainless steel at ambient temperature in acidic 1.5-M NaCl solution (pH~2) during exposure to 0.15-Mrad hr^{-1} gamma radiation. A 100-mV anodic shift in the corrosion potential was observed in this case, with very little effect on the corrosion current density. Note that these experiments were performed on stainless steels, not Alloy 22.

To determine the maximum impact that gamma radiolysis could have on the corrosion potential of Alloy 22, hydrogen peroxide was added to electrolytes used for testing WP materials. Experiments at 25°C are illustrated by Figures 3-51 and 3-52. As the concentration of hydrogen peroxide in SCW approaches 72 ppm (calculated from number of added drops of H_2O_2), the corrosion potential asymptotically approaches 150 mV versus Ag/AgCl, well below any threshold where localized attack would be expected in SAW. Similarly, as the concentration of hydrogen peroxide in SCW approaches 72 ppm, the corrosion potential asymptotically approaches –25 mV versus Ag/AgCl, well below any threshold where localized attach would be expected in SCW. This change in corrosion potential is also below any level where a change in oxidation state of metal cations in the passive film would be expected (anodic oxidation peak in Type 2 polarization curves). Gamma radiolysis is not expected to exacerbate the LC of Alloy 22 since the maximum shift in corrosion potential induced by hydrogen peroxide additions is less than that required for breakdown of the passive film.

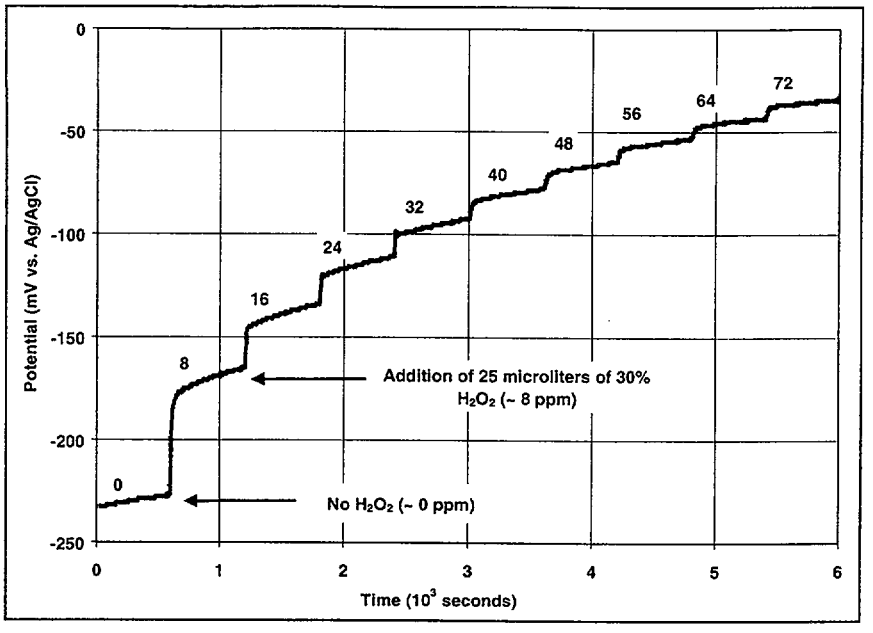

Source: CRWMS M&O 2000c, Section 6.4.4

NOTE: The numbers above the curve correspond to parts per million (ppm) H_2O_2

Figure 3-51. Effect of Hydrogen Peroxide on Corrosion Potential of Alloy 22 in Simulated Acidic Concentrated Water at 25°C

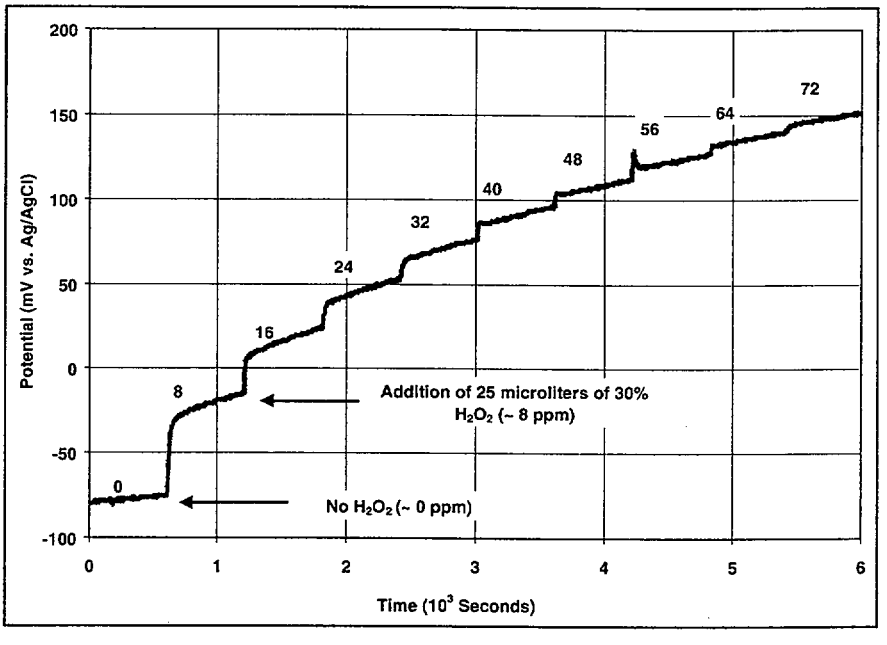

Source: CRWMS M&O 2000c, Section 6.4.4

NOTE: The numbers above the curve correspond to ppm H_2O_2

Figure 3-52. Effect of Hydrogen Peroxide on Corrosion Potential of Alloy 22 in Simulated Concentrated Water at 25°C

3.1.6.7 Crevice Corrosion

3.1.6.7.1 Deterministic Models of Crevice Chemistry

Crevices can form at points of contact between the WP and other solid objects. These occluded geometries can lead to differential aeration of the crevice solution (electrolyte). Dissolved oxygen can become depleted deep within the crevice, while the concentration near the crevice mouth remains relatively high. Cathodic reduction of dissolved oxygen at the crevice mouth may create a sufficiently high electrochemical potential to drive anodic processes inside the crevice, thereby causing an anodic current to flow along the crevice towards the crevice mouth. Anodic processes inside the crevice are therefore expected to occur at a rate that corresponds to the local passive current density. Given this scenario, two primary electrochemical processes can lead to acidification of the solution in a crevice: (1) the preferential transport of anions into the crevice from the mouth, driven by the electric field that accompanies the crevice current, and (2) hydrolysis reactions of dissolved metal cations.

Chloride anion will be driven into the crevice by the potential gradient, as discussed in the literature and summarized in the AMR. The concentration in the crevice is governed by Equation 3-18:

$$[Cl^-] = [Cl^-]_0 \exp\left[-\frac{F}{RT}\Phi(x)\right] \qquad \text{(Eq. 3-18)}$$

where $[Cl^-]_0$ is the concentration at the crevice mouth, $\Phi(x)$ is the potential in the crevice relative to that at the mouth, and (x) is the distance from the crevice mouth. Field-driven electromigration of Cl^- (and other anions) into the crevice must occur to balance cationic charge associated with H^+ ions, as well as the charge associated with Fe^{2+}, Ni^{2+}, Cr^{3+}, and other cations. If such conditions do develop inside Alloy 22 crevices, accelerated attack of this material by LC or SCC may be possible.

A detailed deterministic model has been developed to calculate the spatial distributions of electrochemical potential and current density in WP crevices, as well as transient concentration profiles of dissolved metals and ions (CRWMS M&O 2000c, Section 6.6.4). These quantities are calculated with the transport equations, which govern electromigration, diffusion, and convective transport. First, the axial current density along the length of the crevice is calculated by integrating the wall current density. The electrode potential along the length of the crevice can then be calculated from the axial current density. The partial differential equations that define transient concentrations in the crevice require determination of the potential gradient, as well as the local generation rates for dissolved species. The concentrations of dissolved metals at the crevice mouth are assumed to be zero. Computations are facilitated by assuming that the crevices are symmetric about a mirror plane where the flux is zero. This model has been used to estimate the extent of pH depression in WP crevices due to the simultaneous hydrolysis and transport of dissolved iron, nickel, chromium, molybdenum, and tungsten. The experimental measurements discussed below were used for validation.

3.1.6.7.2 Experimental Determinations of Crevice pH and Current

In crevices made of steels containing more than 20 weight percent chromium, very acidic pH levels have been observed (pH < 2). The effect of chromium content on the ultimate crevice pH in a number of commercial and binary iron-chromium alloys is illustrated by Figure 3-53, while the increase in concentration of dissolved metals in such crevices is illustrated by Figure 3-54 (CRWMS M&O 2000e, Section 6.7). Based upon experimental work with passive crevices without buffer, it is believed that the applied potentials required for significant acidification (pH < 5) are not plausible (CRWMS M&O 2000c). Therefore, a minimum crevice pH of about 5 should be assumed in the absence of buffer and inhibitor ions.

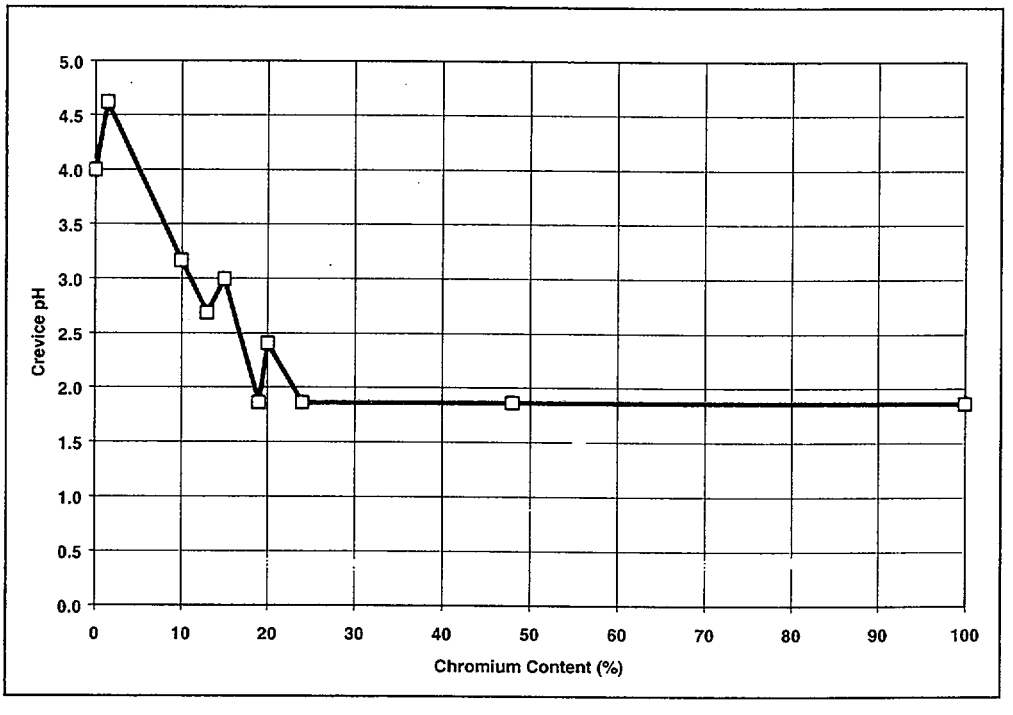

Source: CRWMS M&O 2000e, Section 6.7.1

Figure 3-53. Effect of Chromium Content in Nickel-Chromium Alloys on Ultimate Crevice pH

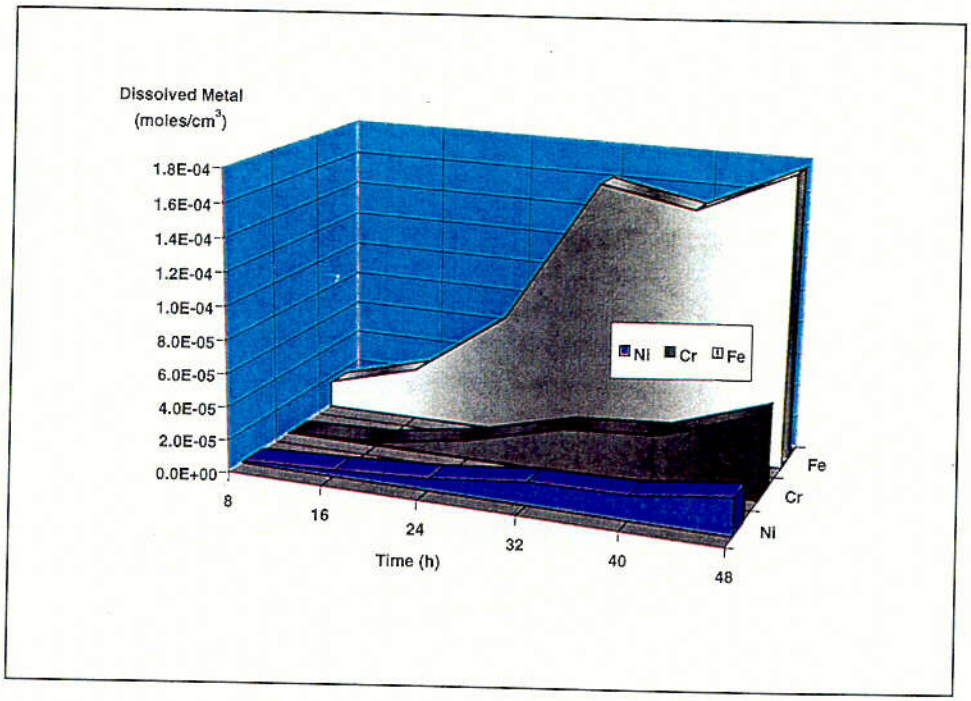

Source: CRWMS M&O 2000e, Section 6.7.1

Figure 3-54. Concentrations of Dissolved Metals in Stainless Steel 304 Crevice Exposed to 0.1 N NaCl

The local crevice environments for Alloy 22 and other relevant materials have been determined experimentally (CRWMS M&O 2000c, Section 6.6.5). Crevices were constructed from square metallic samples, 2 inches on each side and 1/8 inch thick (same size as crevice samples used in the LTCTF). The samples were masked with plastic tape, thereby forming an exposed square area, 1.7 inches on each side. The exposed area was placed underneath a clear plastic window with an access port for a pH sensor in the center. In this case, the sensor was a miniature reference electrode separated from the crevice solution with a thin glass membrane. A second pH sensor was located at the mouth of the crevice, in close proximity to a Saturated Calomel Electrode (SCE). In parallel experiments, paper strips with a pH-sensitive dye (pH paper) were sandwiched between the clear plastic window and photographed with a digital electronic camera in a time-lapse mode to add confidence to the measurements made with pH sensors. Spectroscopic-grade graphite counter electrodes were also placed in the electrolyte lying outside the mouth of the crevice. A potentiostat was then used to control the electrochemical potential at the mouth of the crevice. Temperature, potential, current, and pH were then recorded electronically during the course of the experiment.

An example of the pH measurements inside a crevice formed from Type 316L stainless steel is shown in Figure 3-55. The electrolyte was 4M NaCl and was maintained at ambient temperature. Since this electrolyte contained no buffer ions, it was considered to be a far more severe medium than media representative of various concentrations of J-13 well water. The electrochemical potential at the mouth was maintained at 200 mV vs. Ag/AgCl. Crevice corrosion could be seen initiating near the crevice mouth and propagating towards the pH sensor, which was located about 0.5 cm inside the crevice mouth. When the corrosion front reached the

pH sensor, the pH dropped from the initial value (pH~7) to a very low value (pH~1). The fixed one-liter volume of electrolyte outside of the crevice became slightly alkaline. In similar experiments with 316L exposed to SCW, no significant lowering of the pH was observed. In crevices formed between the WPOB and the stainless steel structural material, a low pH is expected only if buffer and inhibitor ions are removed from the electrolyte.

Measurements of pH inside crevices formed with Alloy 22 surfaces are shown in Figure 3-56 for a 4M NaCl electrolyte. The data illustrate the effect of incrementally increasing the applied potential, eventually exceeding the threshold required for localized breakdown of the passive film. The corresponding measurements of crevice current can be found in the supporting AMR (CRWMS M&O 2000c, Section 6.6.5). At an applied potential of 400 mV, the steady-state crevice pH remained close to neutrality (pH~6.1). As the potential was stepped to 1000 mV, the crevice current increased dramatically and the pH dropped below one. At an applied potential of 1100 mV, extreme localized attack of the Alloy 22 was observed at the crevice mouth, with a crevice pH measurement near zero. In similar experiments with Alloy 22 in SCW, no crevice attack and no significant lowering of the pH was observed. Elevations of the eletrochemical potential due to gamma radiolysis (~700 mV) are insufficient to drive the crevice pH to low levels, even in the absence of buffer and inhibitor.

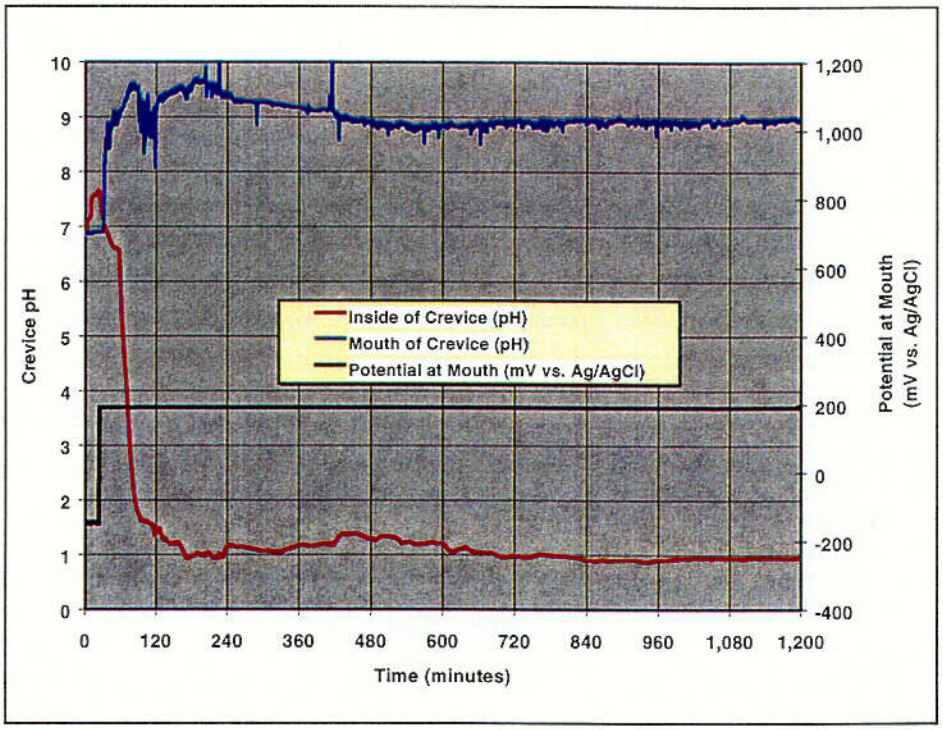

Source: CRWMS M&O 2000e, Section 6.7.5

Figure 3-55. Stainless Steel 316L, 4M NaCl, 200 mV and 23°C – Crevice pH versus Time

C-19

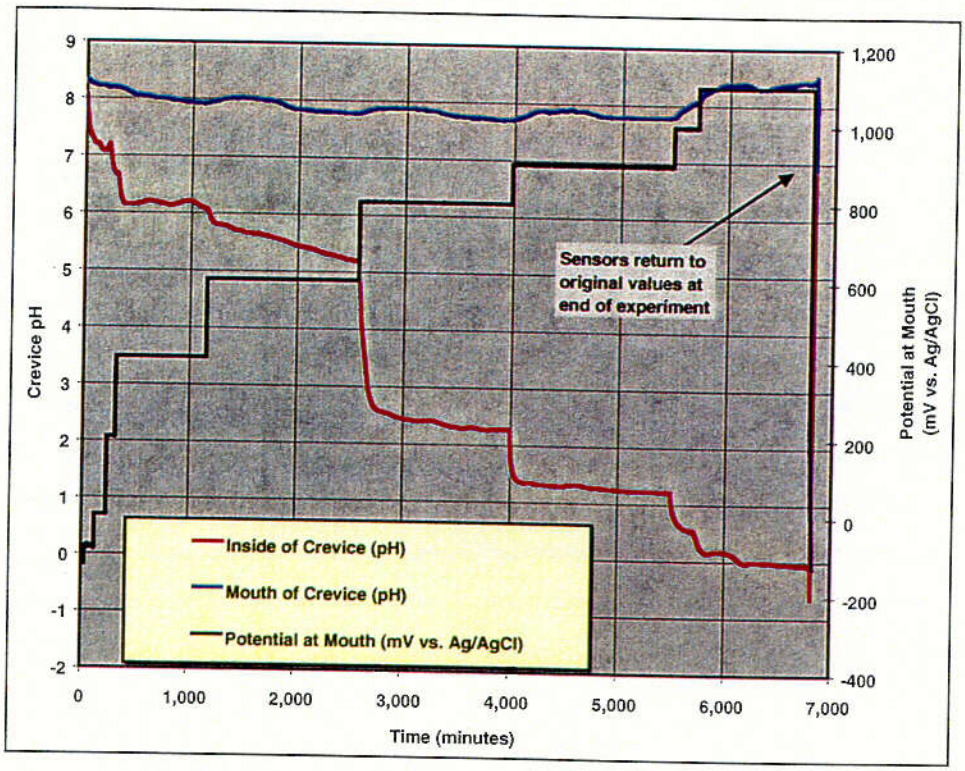

Source: CRWMS M&O 2000c, Section 6.6.5

Figure 3-56. Alloy 22, 4M NaCl at 23°C – Crevice pH versus Time

Figure 3-57 is a summary of several experiments where crevice pH was determined in situ as a function of applied potential. These data are represented by the following polynomial:

$$y = b_0 + b_1 x + b_2 x^2 \qquad \text{(Eq. 3-19)}$$

where x is the potential applied at the crevice mouth (mV versus Ag/AgCl) and y is the steady-state pH inside the crevice. Coefficients for the above equation are shown in the figure for both Alloy 22 and 316L, under a broad range of conditions. The correlations for 4M NaCl and SCW could be used to bound the crevice pH, using interpolation based upon the concentration of buffer ion between the two limits. Similar behavior is expected in titanium alloys. Additional testing with titanium-based materials is planned to confirm this.

C-20

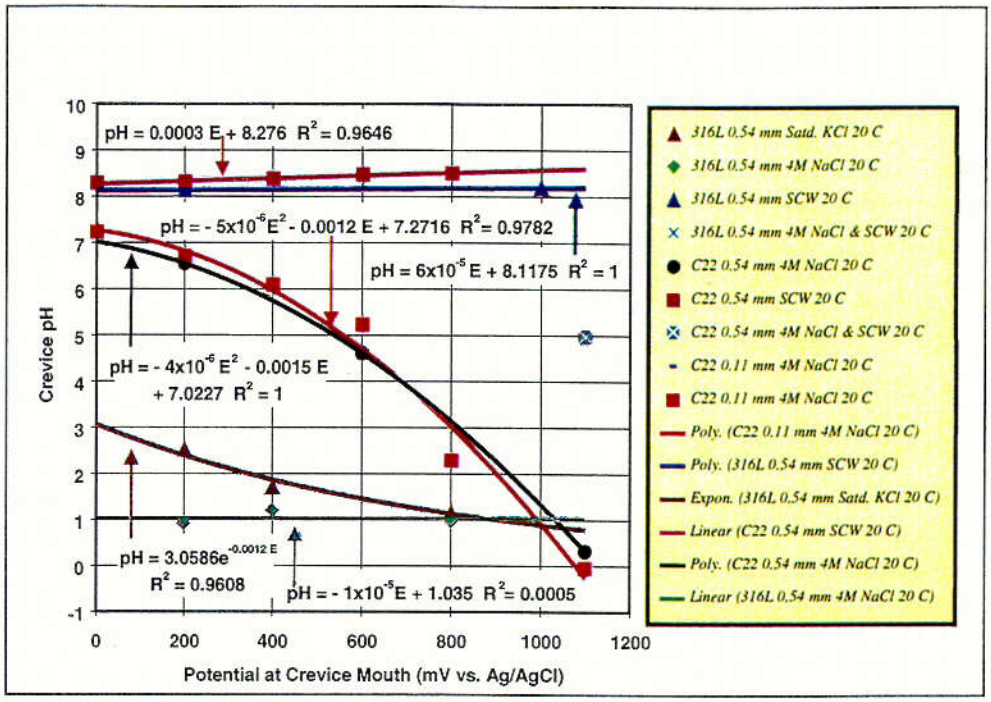

Source: CRWMS M&O 2000c, Section 6.6.5

Figure 3-57. Determination of Crevice pH for Waste Package Materials

In conclusion, there was no visible evidence of localized corrosion inside crevices at applied potentials less than the threshold. However, even though crevices remained passive at potentials below the threshold, the passive current density and imposed electric field within the crevice were sufficient to cause significant acidification of 4M NaCl at higher applied potential. The buffer and inhibitor ions found in simulated concentrated J-13 waters prevent acidification of crevices, even at high applied potential. In many of the experiments described here, both the applied potential and the test medium are more severe than those expected in the repository. It is concluded from these results, that the conditions required for initiation of localized corrosion will be present in the repository and, therefore, degradation of these materials by localized corrosion is not a credible machanism.

L-21

3.1.6.7.3 Estimated Localized Corrosion Rate of Alloy 22 and Titanium Grade 7

If the threshold potential or temperature for localized attack is exceeded, a corrosion rate representative of LC must be assumed. Due to the outstanding corrosion resistance of Alloy 22, very little data exists for such LC under plausible conditions. Work summarized in the AMR indicates that the corrosion rate of Alloy 22 in 10 wt. % $FeCl_3$ at 75°C might be as high as 12.7 µm per year. This rate is significantly higher than those measured in the LTCTF, and may be representative of the rates expected for LC in the absence of inhibitor and buffer ions, including crevice corrosion. In a solution composed of 7 vol. % H_2SO_4, 3 vol. % HCl, 1 wt. % $FeCl_3$, and 1 wt. % $CuCl_2$, a penetration rate of 610 µm per year was observed at 102°C. Alloy C-276 has a composition similar to that of Alloy 22, and is therefore considered to be an appropriate analog. In other work, the corrosion rate of Alloy C-276 in dilute HCl at the boiling point is somewhere between 5 and 50 mils per year (127 and 1270 µm per year). Comparable rates would be expected for Alloy 22. The highest passive current density found for Alloy 22 is approximately 10 µA cm^{-2}, which corresponds to a corrosion rate of approximately 100 µm per year. It is expected that the logarithm of the LC rate of Alloy 22 can be based on the aforementioned data and is normally distributed, as shown in Table 3-11. This distribution reasonably bounds those extreme penetration rates found in the literature, and is centered about the rate corresponding to the passive current density.

Like Alloy 22, Titanium Grade 7 has outstanding corrosion resistance. Therefore, relatively little data exists for LC under plausible conditions. The published literature cited in the AMR (CRWMS M&O 2000d, Section 6.7) discusses a crevice corrosion depth of 250 microns, which was observed in a crevice formed from Ti-0.2%Pd and Teflon after a 582-day exposure in deaerated brine at 90°C (157 µm per year). In a metal-metal crevice, a crevice corrosion depth of 70 µm was observed in a crevice formed from Ti-0.2%Pd after 489 days (52 µm per year). Other more severe values are shown in Table 3-12 below. A rectangular distribution based on this table is assumed for the LC of Titanium Grade 7.

Table 3-11. Distribution of Localized Corrosion Rates for Alloy 22

Percentile	LC Rate (µm per year)
0^{th}	12.7
50^{th}	127
100^{th}	1270

Source: CRWMS M&O 2000c, Section 6.6.6

Table 3-12. Distribution of Localized Corrosion Rates for Titanium Grade 7

Percentile	LC Rate (µm per year)	Conditions
0^{th}	490	19% HCl + 4% $FeCl_3$ + 4% $MgCl_2$ at 82°C
100^{th}	1120	Boiling 3:1 Aqua Regia

Source: CRWMS M&O 2000d, Section 6.7

3.1.6.8 Microbial Corrosion

It has been observed that nickel-based materials such as Alloy 22 are relatively resistant to MIC (CRWMS M&O 2000c, Section 6.8). Furthermore, it is believed that microbial growth in the repository will be limited by the availability of nutrients. For example, H^+ is known to be generated by bacterial isolates from Yucca Mountain. Furthermore, thiobacillus ferrooxidans oxidize Fe^{2+}, while geobacter metallireducens reduce Fe^{3+}. Other microbes can reduce SO_4^{2-} and produce S^{2-}. Ultimately, the impact of MIC should be accounted for by adjusting E_{corr}, $E_{critical}$, pH and the sulfide concentration. The possible acceleration of abiotic corrosion processes by microbial growth is accounted for here. Horn et al. (CRWMS M&O 2000c) have shown that MIC can enhance corrosion rates of Alloy 22 by a factor of two (2×). Figure 3-11 is a schematic representation of the corrosion model for the Alloy 22 outer barrier. The augmentation of corrosion rates due to MIC is accounted for in the model as shown in Figure 3-12. The enhancement factor, G_{MIC}, is defined by Equation 3-20.

$$\left(\left.\frac{dp}{dt}\right|_{effective}\right)_{corrected} = G_{MIC} \times \left(\left.\frac{dp}{dt}\right|_{effective}\right)_{original} \qquad \text{(Eq. 3-20)}$$

This factor is calculated as the ratio of corrosion rates (microbes to sterile). Horn et al. (CRWMS M&O 2000e, Section 6.9) have shown that MIC can enhance corrosion rates of 304 stainless steel by a factor of about ten (×10). The value of G_{MIC} for 304 stainless steel in sterile media is about one ($G_{MIC} \sim 1$), whereas the value of G_{MIC} for 304 stainless steel in inoculated media is larger ($G_{MIC} \sim 10$). It is assumed that MIC will have the same effect on 316NG stainless steel. The value of G_{MIC} for Alloy 22 in sterile media is about one ($G_{MIC} \sim 1$), whereas the value of G_{MIC} for Alloy 22 in inoculated media is larger ($G_{MIC} \sim 2$).

The principal nutrient-limiting factor to microbial growth in situ at Yucca Mountain, has been determined to be low levels of phosphate. There is virtually no phosphate contained in J-13 groundwater. Yucca Mountain bacteria grown in the presence of Yucca Mountain tuff are apparently able to dissolve phosphate contained in the tuff to support growth to levels of 10^6 cells ml^{-1} of groundwater. When exogenous phosphate is added (10 mM), the levels of bacterial growth increase to 10^7 to 10^8 cells ml^{-1}. The difference of one to two orders-of-magnitude in bacterial growth with and without the presence of exogenous phosphate is not considered to be significant with respect to effects on corrosion rates. Therefore, nutrient limitation was not factored into the overall MIC model. It may be noted, however, that the 2-fold correction for MIC ($G_{MIC} \sim 2$) included in the model was in the presence of sufficient phosphate to sustain higher levels of bacterial growth (in an effort to achieve accelerated Alloy 22 attack).

Other environmental factors that could effect levels of bacterial growth include temperature and radiation. However, these factors are closely coupled to RH. As temperature and radiation decrease in the repository, RH is predicted to increase. There are some types of micro-organisms that can survive elevated temperatures (≤ 120°C) and high radiation doses. However, if there is no available water, bacterial activity is completely prevented. Thus, water availability is the primary limiting factor for MIC. Water availability is as expressed by RH and is used as the primary gauge of microbial activity. This factor is coupled to other less critical limiting factors.

A conservative approach is to assume that a critical mass of bacteria exists for MIC. Bacterial densities in Yucca Mountain rock have been determined to be on the order of 10^4 to 10^5 cells g^{-1} of rock. In absolute terms, this is almost certainly above the threshold required to cause MIC. Further, bacterial densities have been shown to increase one to two (1 to 2) orders-of-magnitude when water is available. More germane concerns are the types of bacteria present, their abundance, and how their relative numbers are affected when water is available for growth. Corrosion rates will be affected on some WP materials if organic acid producers compete more aggressively than sulfate reducers or inorganic acid producers for available nutrients, provided that water is sufficient to support growth. No data is currently available regarding the composition of the bacterial community over the changing environmental conditions anticipated during repository evolution. Instead, this issue has been addressed in the current model by determining overall corrosion rates under a standardized set of conditions, in the presence and absence of a defined set of characterized Yucca Mountain bacteria.

3.1.7 Stress Corrosion Cracking

3.1.7.1 Background

One of the potential failure modes of the drip shield (DS), the waste package outer barrier (WPOB), and the stainless steel structural material is the initiation and propagation of SCC. Such environmental cracking may be induced by appropriate combination of metallurgical susceptibility, corrosive environment, and sustained tensile stress. The DS and the stainless steel structural material are excluded from this SCC evaluation. The DS is excluded because the stress that is relevant to SCC is considered to be insignificant. The major sources of stresses in the DS are loadings due to backfill and earthquakes. These stresses will not induce SCC because the stress caused by backfill is generally compressive stress and the stress caused by earthquakes is temporary in nature. The stainless steel structural support is excluded from this SCC evaluation since no corrosion performance is claimed for the 316NG. The purpose of this section of the PMR is to provide a detailed description of the process-level models that can be used to predict the performance of the WPOB in repository-relevant environments that may be capable of causing SCC.

The three driving forces for SCC are metallurgical susceptibility, a corrosive environment, and static (or sustained) tensile stresses. Environments that cause SCC are usually aqueous and can be either condensed layers of moisture or bulk solutions. The SCC of a particular alloy is usually caused by the presence of a specific chemical species in the environment. For example, the SCC of copper alloys is almost always due to the presence of ammonia in the environment. Chloride ions cause SCC in stainless steels and aluminum-based alloys. Sulfides are known to cause SCC in nickel-based alloys such as Alloy 22. Changes in the environmental conditions, which include temperature, dissolved oxygen, and ionic concentrations, will normally influence the SCC process.

The effects of stress on the propagation of SCC can be characterized by the stress intensity factor (K_I). The definition and detailed calculations of the stress intensity factor are described in the AMR on SCC (CRWMS M&O 2000f, Section 6.2).

The SCC evaluation is focused on the WPOB closure weld because this weld cannot be stress relieved at the same time as other container welds. This region of the WP is potentially susceptible to SCC since welding will produce high-tensile residual stress in close proximity to the weld and since pre-existing flaws due to fabrication and welding have much higher distribution in the weld than in the base metal. An effective approach to eliminate the threat of SCC and resultant through-wall cracking in the closure weld is to implement a post-weld stress mitigation process to either remove residual tensile stresses in the weld region, or reduce them below threshold values for SCC initiation and growth. The initial process selected to mitigate SCC in the WPOB closure weld was single-pass laser peening. The laser peening process utilizes a rapidly pulsed, high energy density laser beam rastered across the surface region of the closure weld to induce a compressive surface layer with a thickness (depth) of 2-3 mm, thus removing the potential for SCC. However, the rate of removal of this beneficial layer by GC indicated that it would be eliminated in an unacceptably short time leading to possible SCC initiation and through-wall growth. The closure design was therefore modified to include two lids (inner and outer lid) with two separate post-weld stress mitigation processes; laser peening of the inner lid and induction annealing stress relief of the outer lid weld. During the induction annealing process, the weld region is very rapidly heated to the solution annealing temperature to remove weld residual stresses and rapidly cooled to avoid precipitation of potentially deleterious intermetallic phases (CRWMS M&O 2000f, Section 6.2).

Two alternative process-level models that deal with SCC and the effect of stress on cracking propensity are described and evaluated in the supporting AMR. The first model, Method A, is based on the theory that there exists a threshold value of the stress intensity factor (K_{ISCC}) such that no growth occurs in a crack having a stress intensity factor (K_I) less than the threshold value. This model is described in a subsequent section.

The second model, Method B, relates crack advance to the metal oxidation that occurs when the protective film at the crack tip is ruptured. This slip dissolution or film rupture model is described in a subsequent section. In this case, the existence of a nominal threshold stress for SCC initiation on a smooth surface ($\sigma_{threshold}$) is assumed.

Leakage can occur if SCC propagates to the point where a crack penetrates the container wall. Since the model predictions indicate that SCC can lead to WPOB breach, it is necessary to mitigate stress as described to lower the probability of cracking.

3.1.7.2 Overview of Two Alternative Models for Stress Corrosion Cracking

3.1.7.2.1 Model A – Stress Corrosion Cracking Threshold Model

The concept of a threshold stress intensity factor (K_{ISCC}) has been commonly used to assess the susceptibility of material to SCC, as described in the SCC AMR (CRWMS M&O 2000f, Section 6.3). The applicability of this model to Alloy 22 (the material to be used for the WPOB) has been studied experimentally at Lawrence Livermore National Laboratory (LLNL).

3.1.7.2.2 Model B – Stress Corrosion Cracking Slip Dissolution or Film Rupture Model

The theory of slip dissolution or film rupture has been successfully applied to assess the SCC crack propagation for light water reactors at high temperature (approximately 288°C). The detailed description of the SCC model based on the theory of slip dissolution or film rupture can be found in the AMR devoted to SCC (CRWMS M&O 2000f, Section 6.4). This model has been adopted to

assess the SCC capability of the material to be used for the WPOB. In this case, the existence of a nominal threshold stress for SCC initiation on a smooth surface is assumed.

3.1.7.3 Stress Analysis

No software codes were used directly in the development of this PMR. However, this report does include the results from software codes used in the supporting AMRs.

ANSYS, Version 5.3, which is a finite element analysis code used for thermal and stress analyses, was used to develop data cited in SCC AMR (CRWMS M&O 2000f).

pcCRACK, Version 3.1, is a fracture mechanics code used for stress intensity and crack growth simulation analyses. This code was also used to develop data cited in the SCC AMR (CRWMS M&O 2000f).

3.1.7.4 Parameters and Inputs for Stress Corrosion Cracking Models

3.1.7.4.1 Material Properties

The specific properties of the WP materials are important in the determination of the residual stress in the closure weld. The properties used in this evaluation are documented in the AMR supporting the SCC model (CRWMS M&O 2000f, Section 4.1.1).

3.1.7.4.2 Welding Parameters

In evaluating weld-induced stress, the effect of each weld pass was determined by simulating the heat being deposited by the welding process over a prescribed time interval. Key parameters needed for this evaluation include the rate of electrical energy input, weld speed, and heat transfer. This information presented in the AMR supporting the SCC process-level model was used to determine the heat generation rate for the elements that represent each weld pass (bead).

3.1.7.4.3 Threshold Stress Intensity Factor

K_{ISCC} values for Alloy 22 were evaluated by using precracked wedge-loaded double cantilever beam (DCB) specimens in deaerated acidic brine (pH 2.7) at 90°C. Duplicate samples of each material were loaded at four initial levels of the stress intensity factor (K_I) with values ranging from 20 to 39 ksi $in^{1/2}$ (or 22 to 43 MPa $m^{1/2}$). Both metallography and compliance methods were used to determine the final crack length. The final stress intensity factor for SCC (K_f) was computed from the measured final wedge load on the DCB specimens and the average crack length. The final stress intensity factor K_f was taken to be the SCC threshold value, K_{ISCC}. Studies are now underway to determine K_{ISCC} using reversing direct current potential drop (DCPD) technique, by which the value of K_I is determined at zero crack velocity.

3.1.7.4.4 Input for Slip Dissolution Model

As discussed in Section 3.1.7.8.2, the slip dissolution model has four parameters: $\bar{A}$, $\bar{n}$, K_I, and $\sigma_{threshold}$. The stress intensity factor K_I has already been discussed. The parameter n in the crack growth equation for the slip dissolution model was obtained from reverse DCPD tests of Alloy 22 at 110°C, and at a stress intensity factor of 30 MPa $m^{1/2}$ (CRWMS M&O 2000f, Section 4.1.4). These measurements indicate that the value of n is 0.84, which is considered an upper bound value. A

lower bound value of 0.75 was derived from engineering judgement based on comparison of available data for Alloy 22 and more SCC resistant stainless steels (CRWMS M&O 2000f, Section 3.2.2).

3.1.7.4.5 Stress Mitigation

Residual stress in WPOB can be mitigated by the multiple-pass laser peening technique. Preliminary measurements indicate that single-pass laser peening of an Alloy 22 plate (1-inch thick) is capable of producing a compressive surface layer that is about 1.5-mm deep, with compressive stress in the range of 20 to 60 ksi. Compression can be achieved at greater depths with multiple-pass laser peening, or localized induction annealing. If this stress mitigation approach is used, the life of the WP will be limited by the time required to remove the compressive layer by GC.

3.1.7.5 Assumptions in Stress Corrosion Cracking Models

In regard to SCC of the WPOB, the only stress that is significant is the residual stress in the closure weld. Dead-load stress is insignificant. Seismic stress is temporary in nature.

Only the WPOB will be subjected to SCC susceptibility. The DS and the stainless steel structural support will be excluded from the evaluation for reasons discussed in Section 3.1.7.1. For the WPOB, only the closure welds will be considered for performance assessment. Unlike seam welds, the closure weld will not be stress-relieved at the time of fabrication. Welding procedures can produce ery high tensile stress in the weld region, and pre-existing flaws due to fabrication and welding may have much higher distribution in the weld. Without post-weld stress mitigation, this region of the WP will be susceptible to SCC.

The SCC models have been applied to the single-lid WPOB design with and without laser peening. This initial application demonstrated the methodology. The model has more recently been applied to the dual-lid WPOB design. To remove deleterious residual tensile stresses, the closure weld in the outer lid will be treated by localized induction annealing, while the closure weld in the inner lid will be treated by multiple-pass laser peening. The dual-lid concept has been adopted for the WPOB to prolong the design life based on experience learned from previous unmitigated closure-weld designs, where both calculated and measured residual weld stress were found to be high.

For the WP closure welds, the flaw orientation most likely susceptible to crack propagation is assumed to be that of either a circumferential flaw (parallel to weld) or a radially oriented flaw (perpendicular to weld). A radially oriented flaw would be driven by hoop stress, whereas a circumferentially oriented flaw would be driven by the radial stress. The distribution of flaw orientation is discussed in Section 3.1.2.6.

In the Performance Assessment (PA), only radial cracks will be considered because the driving force (stress intensity factor) for a radial crack is much higher than the driving force for a circumferential crack. About one radial crack per closure weld patch was considered (CRWMS M&O 2000f, Section 5)). The patch size used in the WAPDEG analysis will be twice the lid thickness (~ 2 inches) (CRWMS M&O 2000f, Section 5). More careful review of published data has shown that this estimate is too conservative. See Sections 3.1.2.5 and 3.1.2.6.

The slip dissolution mechanism (Section 3.1.7.8.2, Equation 3-28) relies on the crack-tip strain rate (which encompasses the effects of mechanics parameters), as well as the repassivation rate, (which

encompasses the effects of material characteristics and water chemistry). Because of the expected similarity in SCC behavior and mechanical response of face centered cubic alloys, the same crack-tip strain rate formulations that were employed for quantitative prediction of SCC in austenitic 304 or 316 stainless steels in 288°C high-purity boiling water reactor (BWR) water can be used for this analysis.

The rate of repassivation is captured by the parameter n, the repassivation slope. A characteristic of the slip dissolution or film rupture model is that SCC susceptibility decreases with increasing values of n (CRWMS M&O 2000f, Section 5). For stainless steels more susceptible to SCC than Alloy 22, test data indicates that $n = 0.54$. Recent test results for SCC crack growth in Alloy 22 indicate that $n = 0.84$ (CRWMS M&O 2000f, Section 5). Conservatively the upper bound for n is set at a value of 0.84 (CRWMS M&O 2000f, Section 5). Based on published literature values for SCC-resistant stainless steels, the lower bound for n is set at a value of 0.75. For highly SCC-resistant Alloy 22, this is judged to be appropriate (Section 3.1.7.4.4) (CRWMS M&O 2000f, Section 5).

Although the slip dissolution model assumes crack growth can initiate at any surface defect that can generate a stress intensity (K_I), regardless of defect size and tensile stress, examination of the relevant SCC literature indicates that there is a threshold stress ($\sigma_{threshold}$) below which SCC will not initiate on a "smooth" surface. In the case of the WP closure weld, a "smooth" surface is defined as an as-machined surface with a maximum roughness of 250 rms. This threshold stress is conservatively estimated to be between 10 and 40% of the yield stress (YS), based on published SCC initiation data for susceptible stainless steels. This range of threshold values is supported by data for drop evaporation tests at 200°C found in Uhlig's Corrosion Handbook (Erbing Falkland 2000). Types 304 and 316 stainless steels have thresholds of 10% of the YS, whereas the other more SCC-resistant materials have thresholds ranging from 40 to 90% of the YS. While the highly SCC-resistant Alloy 22 would be expected to have a threshold in the 40 to 90% YS range, a very conservative distribution of 10 to 40% YS is assumed for the TSPA expected case. If the stress is less than 10% YS, SCC does not initiate and the crack velocity (V_t) is set to zero. Below the threshold stress, the film rupture model is not invoked.

The supporting AMR on SCC (CRWMS M&O 2000f, Section 6.3) discusses published threshold stress values for susceptible stainless steels in boiling solutions of magnesium chloride (~155°C). These values tend to indicate a less conservative range of 20 to 30% YS. This range has also been used in some TSPA cases.

3.1.7.6 Stress Analysis and Stress Intensity Factor Calculations

During the evaluation of the process-level model for SCC, two WP closure designs were considered: a single-lid design for WPOB, and a double-lid design for WPOB. Due to the relative simplicity of the single-lid design, it is used in the initial discussion to illustrate the approach used to model SCC. Insight gained from evaluations of the single-lid WPOB lead to a more robust double-lid design, which is addressed in PA calculations shown in Section 3.2.4.

3.1.7.6.1 Calculation of Stress Intensity from Weld Residual Stress

Determining the residual stress in the closure weld is a problem that can best be solved using finite element methods. The ANSYS Version 5.3 finite element model was used for developing data in support of the SCC model. As mentioned previously, the methodology and approach used to calculate the weld residual stresses and stress intensities will be demonstrated initially for the unmitigated and mitigated (laser peened) single-lid design. Then, calculated values specific to the dual-lid longer life design are reviewed. The mesh used to represent the unmitigated single-lid WPOB closure weld is shown in Figure 3-58. Results of the analysis are shown in Figures 3-59 and 3-60 for the radial and hoop stresses, respectively (CRWMS M&O 2000f, Section 6.2.2.2).

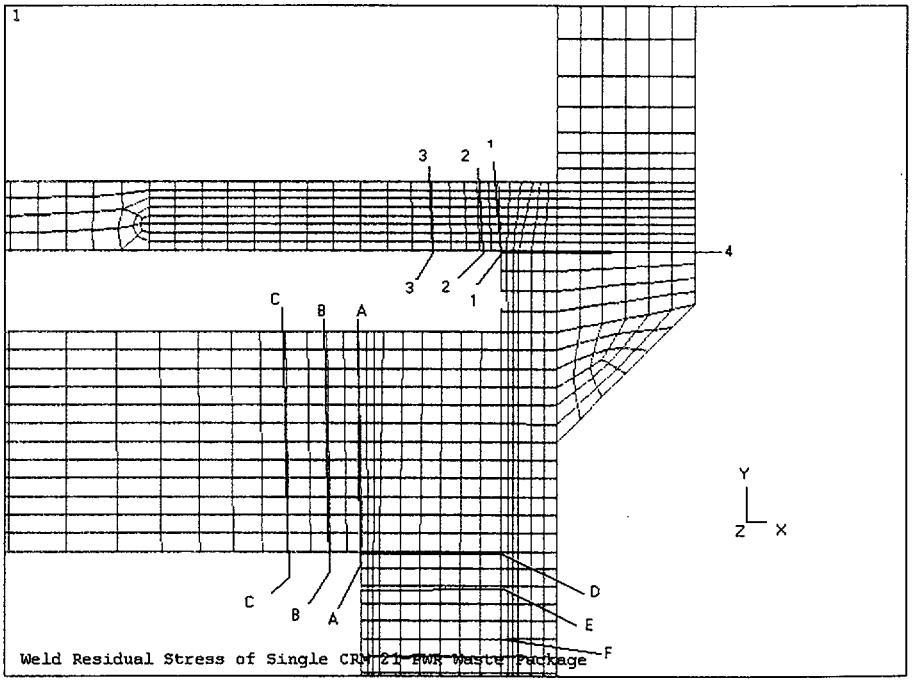

Source: CRWMS M&O 2000f, Section 6.2.2.2

Figure 3-58. Finite Element Model for the Initial WPOB Design and Selected Cross Sections for Stress Plots (single-lid design)

As previously discussed, the flaw orientations in the closure welds of the WPOB most susceptible to crack propagation are circumferential (parallel to weld) and radial (perpendicular to weld). Figure 3-61 shows these flaw orientations in relationship to the closure weld. A radially oriented flaw is driven by the hoop stress, whereas a circumferentially oriented flaw is driven by the radial stress.

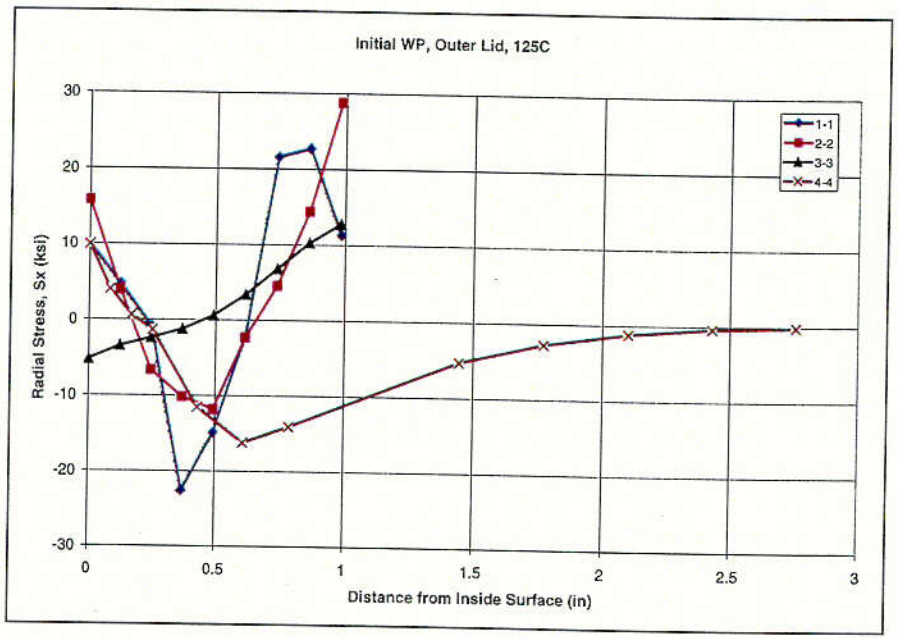

Source: CRWMS M&O 2000f, Section 6.2.2.2

Figure 3-59. Radial Stress - Initial WPOB Outer Lid at 125°C Plots (single-lid design)

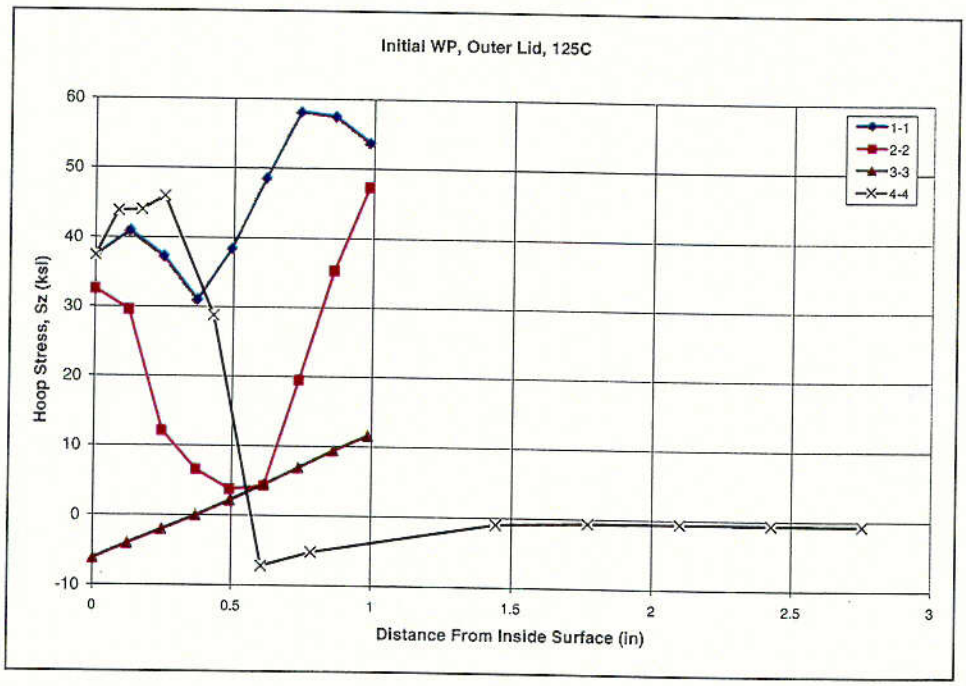

Source: CRWMS M&O 2000f, Section 6.2.2.2

Figure 3-60. Hoop Stress - Initial WPOB Outer Lid at 125°C Plots (single-lid design)

C-22

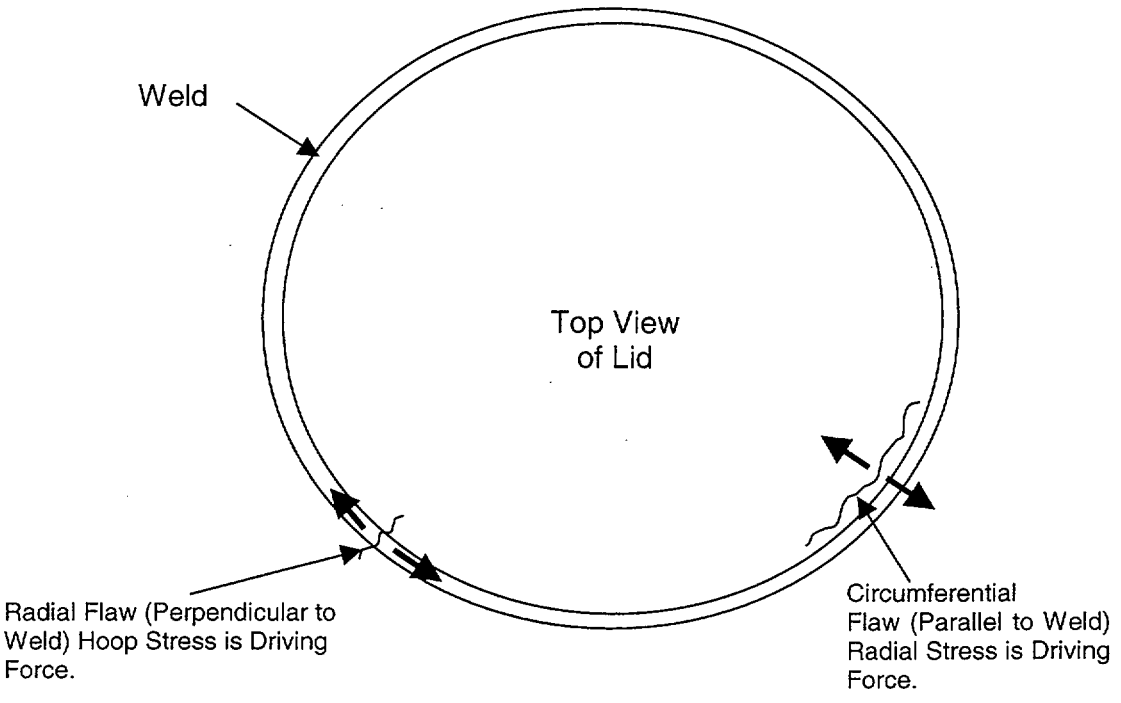

Source: CRWMS M&O 2000f, Section 6.2.2.2

Figure 3-61. Flaw Orientations for Lid Welds

3.1.7.6.2 Impact of Corrosion on Stress and Stress Intensity Factor

The initial results presented in the AMR on SCC of the WPOB (CRWMS M&O 2000f, Section 6) are for the as-built condition. This analysis assumes the full thickness for all WP components. In order to simulate the effect of wall thinning caused by GC, a layer of elements from the outside surface of the outer lid is removed. The thickness of this layer is 0.125 inches, which is equivalent to 12.7% of the thickness of the outer lid. The maximum corrosion rate of Alloy 22 is very small, and is approximately 0.07 μm per year after two years of exposure. At this rate, more than 4,500 years would be required to remove the outer layer of mesh elements.

Figure 3-62 shows the stress intensity factor distributions for the circumferential crack. This figure shows the stress intensity factor as a function of absolute distance from the outside surface. This figure demonstrates that the overall effect of GC is small, but can make the stress intensity factor slightly higher.

3.1.7.6.3 Mitigation of Weld Residual Stress

Examination of the predicted stress distribution at the closure weld of the initial WPOB design (Figures 3-59 to 3-60) reveals, as expected, that tensile stresses may exceed 20% of the yield stress (~ 10 ksi) in both the radial and circumferential directions. This indicates that SCC initiation in unacceptably short times cannot be precluded with the as-welded design. Furthermore, examination of Figure 3-62 indicates that, at least for radially-oriented cracks, through-wall propagation is possible once a crack initiates. Since high residual tensile stresses are generated in the as-welded closure, it is necessary, as discussed previously, to implement a post-weld process to mitigate these potentially deliterious driving forces. This process can be implemented after the closure weld is made, thereby extending WP lifetime.

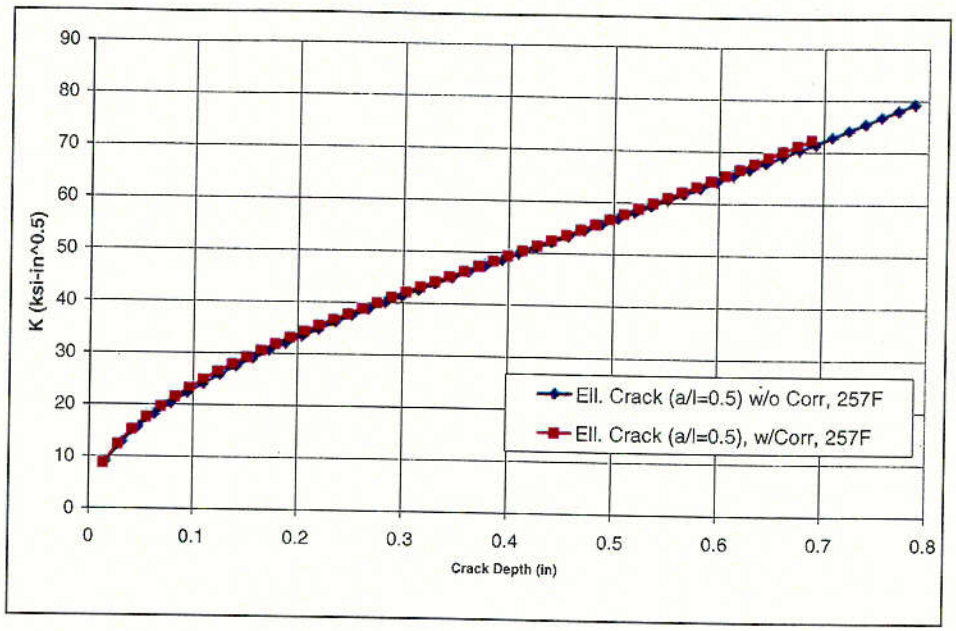

Source: CRWMS M&O 2000f, Section 6.2.2.4

Figure 3-62. Stress Intensity Factor for Radial Crack in Initial WPOB Outer Lid (single-lid design)

To reduce residual weld stresses below the SCC initiation threshold, Waste Package Department has been evaluating improved designs of the WPOB (such as the dual-lid concept shown in Figure 3-63), welding techniques that generate low residual stress, and post-weld stress mitigation techniques such as localized induction annealing and laser peening. The specific selections of laser peening and localized induction annealing are based upon preliminary tests, published data, and the analyses presented here. Experimental measurements were made to quantify the stress-reduction benefit derived from laser peening. Figure 3-64 shows the effect of laser peening on the hoop stress profile in the single-lid closure weld. The corresponding stress intensity factor profile is shown in Figure 3-65. Evaluation of the time required to initiate SCC with a single-lid design led to the conclusion that a dual-lid design was needed, with both laser peening and localized induction annealing. This new design promises adequate performance (first breach beyond 10,000 years), with enough margin to allow for the unexpected. The thermal cycle used for localized induction annealing involves increasing the temperature of the weld region to 1120°C in 35 seconds, while maintaining a gradual temperature gradient between the induction heated weld region and the remainder of the WPOB. The imposed temperature distribution is held constant for 10 seconds. The surface temperature is then lowered to room temperature in 30 seconds, thereby simulating the effect of quenching. The heat is dissipated by conduction within the WP. Simulation indicates that steady state is approached after five minutes.

As can be seen by examination of the predicted stress distributions, both processes are capable of reducing the residual stress to below 10% of the yield stress (SCC initiation threshold) at depths down to 2 to 3 mm for laser peening, and at least 6.5 mm for post-weld induction annealing. Figure 3-64 illustrates the effect of laser peening. However, as discussed previously, since GC of the WPOB may eventually corrode away the beneficial surface layer with mitigated weld stress, it was deemed prudent to further modify the closure-weld design, incorporating two separate Alloy 22 lids with the weld in the outer lid being induction annealed, and the weld in the inner lid laser peened (Figure 3-63).

C22-1

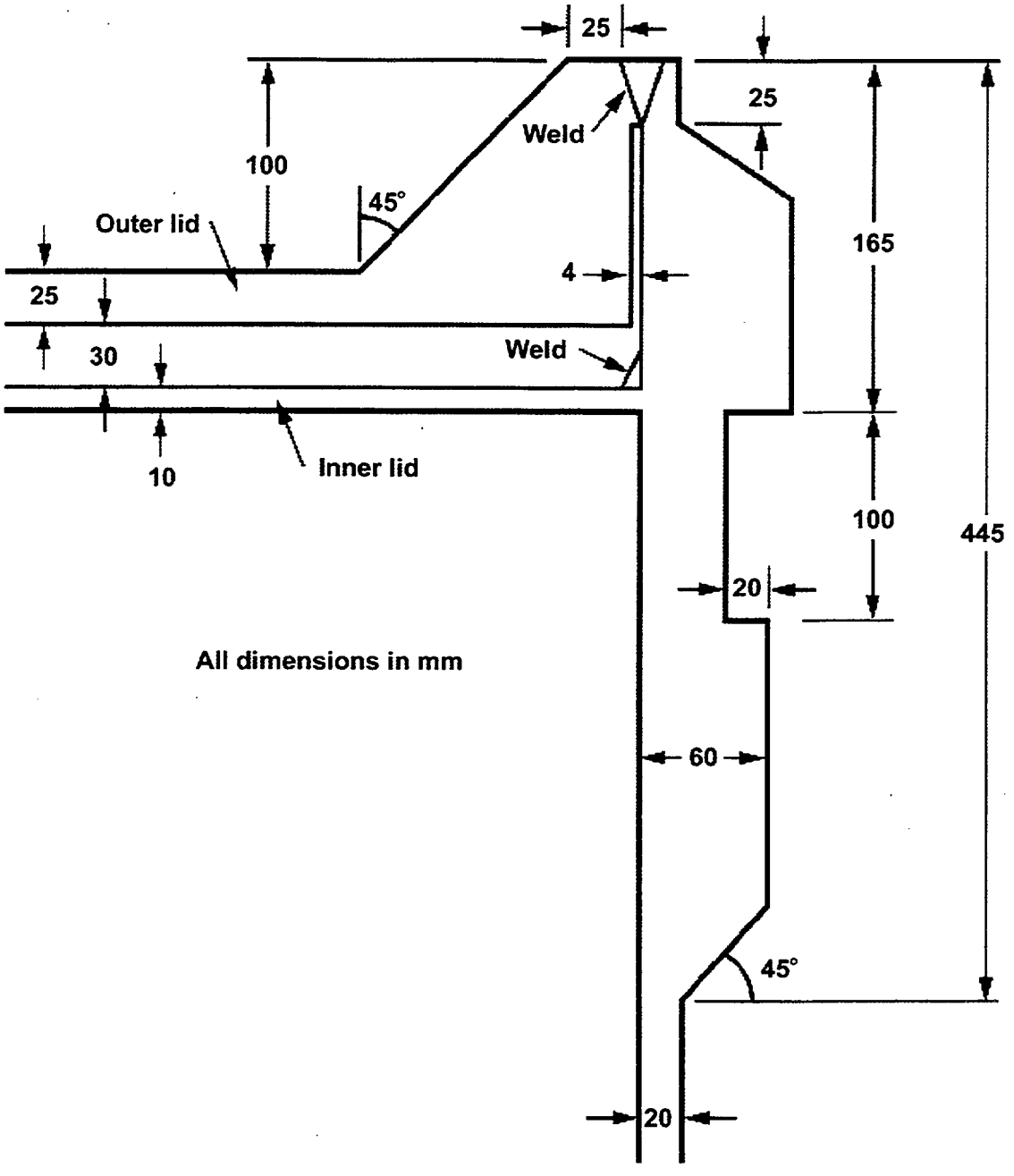

Source: CRWMS M&O 2000f, Section 6.2.2

Figure 3-63. Schematic and Dimensions for Dual-Lid WPOB Design

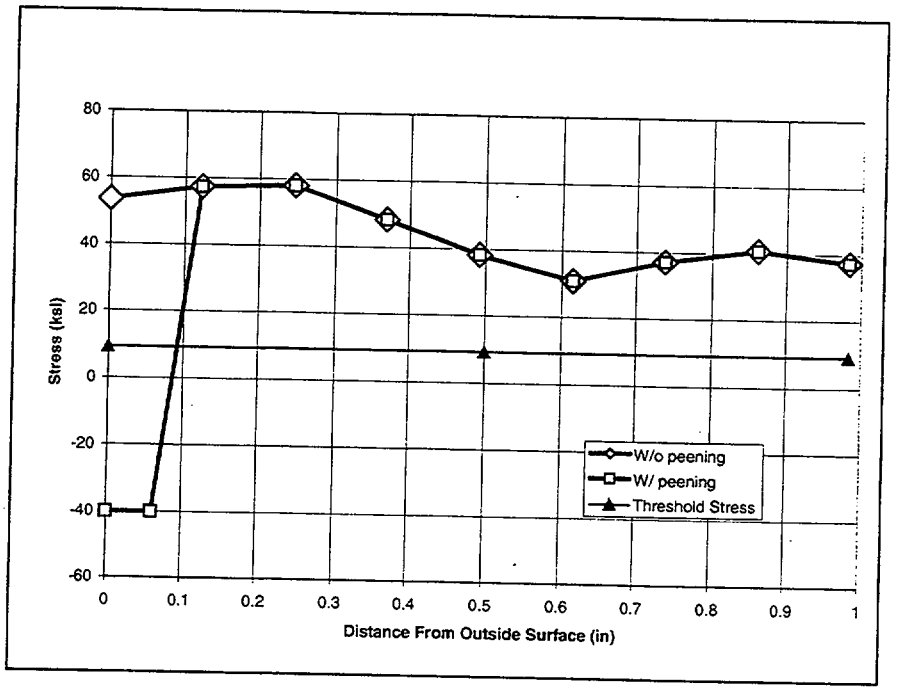

Source: CRWMS M&O 2000f, Section 6.2.2.4

NOTE: Figure modified from that in the AMR (Single-Lid Design)

Figure 3-64. Measured Hoop Stress with and without Single-Pass Laser Peening Compared to Threshold Stress for SCC

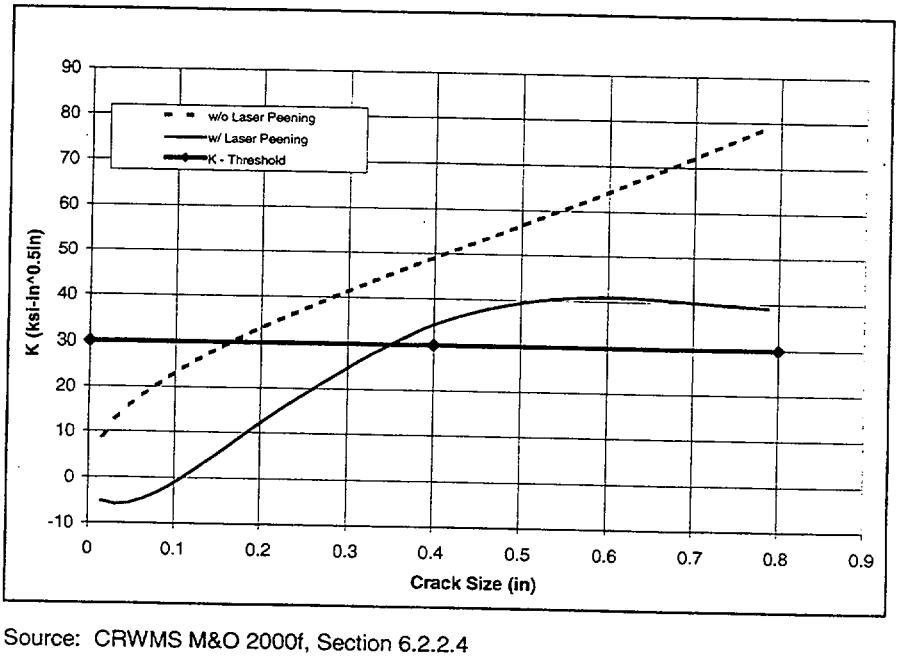

Source: CRWMS M&O 2000f, Section 6.2.2.4

NOTE: Figure modified from that in the AMR (Single-Lid Design).
Threshold stress intensity factor for SCC is also shown.

Figure 3-65. Calculated Stress Intensity Factor for Hoop Stress with and without Laser Peening

3.1.7.7 SCC Method A – The Threshold Stress Intensity Factor Model

For SCC to occur three factors have to exist: tensile stress; a susceptible microstructure; and a material-specific corrosive environment. Flaws can exacerbate SCC by concentrating the tensile stress. Such flaws (surface defects) can be formed during manufacture, localized corrosion, or other in situ processes. Once a crack is initiated, the crack will grow by SCC when the applied stress intensity factor, K_I, is equal to or larger than SCC resistance parameter, K_{ISCC}.

$$K_I \geq K_{ISCC} \qquad \text{(Eq. 3-21)}$$

K_{ISCC} is a material- and environment-dependent property which can be obtained through fracture mechanics testing of the material in the specified environment.

The stress intensity factor K_I is usually defined as a function of stress (σ) and crack depth (a):

$$K_I(a,\sigma) = \beta\sigma\sqrt{\pi a} \qquad \text{(Eq. 3-22)}$$

where β is a geometry factor dependent on the shape of the crack and the configuration of the structural component, and σ is the stress in a given direction.

According to the current design, the material to be used for the WPOB is Alloy 22. Currently, the only existing source of K_{ISCC} values for Alloy 22 and Titanium Grade 7 is the experimental work performed at LLNL as described in the AMR on SCC (CRWMS M&O 2000f, Section 6.3).

The final stress intensity factor (K_f) obtained by examining DCB samples at the end of the test period is interpreted as K_{ISCC}, although it may represent only an upper bound of this threshold and may therefore not be conservative. The K_f values for the eight Alloy 22 specimens are 27.96, 28.73, 28.78, 29.58, 29.66, 30.94, 31.98, and 32.39 ksi $in^{1/2}$ (CRWMS M&O 2000f, Section 6.3.2). If a normal distribution is assumed, the mean value ($K_{ISCC}|_{MEAN}$) and the standard deviation can be calculated:

$$(K_{ISCC}|_{MEAN}) = 30 \pm 1.6\ ksi\ in^{1/2}\ or\ 33 \pm 1.8\ MPa\ m^{1/2} \qquad \text{(Eq. 3-23)}$$

The K_{ISCC} value can vary in accordance with different environmental conditions. In the absence of more data needed for the assessment of the variability of K_{ISCC}, the values given here are used. These values are considered conservative in regard to test environment since acidic NaCl solutions were used.

The mean value of K_{ISCC} is 33 MPa $m^{1/2}$ for an Alloy 22 lid. The maximum values of K_I calculated for circumferential flaws in the closure welds are 22 MPa $m^{1/2}$ for the outer lid and 13 MPa $m^{1/2}$ for the inner lid. Since the mean value of K_{ISCC} is less than the values of K_I associated with circumferential flaws, SCC initiation at these flaws is not a significant concern. However, the maximum value of K_I for the hoop stress in either lid may exceed the threshold value. This is illustrated for the outer lid in Figure 3-62 where K_I for the hoop stress can exceed 80 MPa $m^{1/2}$.

3.1.7.8 SCC Method B–The Slip Dissolution or Film Rupture Model

3.1.7.8.1 Background on Slip Dissolution or Film Rupture Model

As stated previously, environmental cracking has historically been separated into "initiation" and "propagation" phases. This distinction is almost always arbitrary, for initiation is invariably defined as the time at which a crack is detected, or when the load has relaxed a specific amount (in a strain-controlled test): Initiation, therefore, corresponds to a crack depth of significant metallurgical dimensions (> 2 mm).

A lifetime prediction model should be based on a fundamental understanding of the cracking mechanism. The formulation of such a crack propagation model requires a working hypothesis for the cracking mechanism and the evaluation of the parameters of importance in the mechanism. For the systems of interest, the slip dissolution or film rupture mechanism has been chosen. This cracking mechanism has been successfully applied to model the SCC for stainless steel, low-alloy steel, and nickel-based alloys in light water reactor environments as described in the SCC AMR (CRWMS M&O 2000f). The model is described in detail in the AMR on SCC.

3.1.7.8.2 Application to Stainless Steel in Boiling Water Reactor

The slip dissolution mechanism is represented by Equation 3-28, which shows the dependence of crack propagation rate (V_t) on the crack tip strain rate ($\dot{\varepsilon}_{ct}$) (CRWMS M&O 2000f, Section 6.4.2):

$$V_t = A\left(\dot{\varepsilon}_{ct}\right)^n \qquad \text{(Eq. 3-24)}$$

The parameters A and n depend upon the material and environment at the crack tip. These two parameters can be determined from the measured rate of repassivation. Such measurements are made by rapidly straining wires that are fabricated from the material of interest.

The initial application of the slip dissolution model was the quantitative prediction of crack extension in Type 304 or 316 stainless steel in 288°C high-purity water, representative of that used in a BWR. These extensive investigations led to a quantification of the model parameters:

$$A = 7.8\times10^{-3}(n)^{3.6} \qquad \text{(Eq. 3-25)}$$

Equations 3-28 and 3-29 have been combined to yield Equation 3-26:

$$V_t = 7.8\times10^{-3}(n)^{3.6}\left(\dot{\varepsilon}_{ct}\right)^n \qquad \text{(Eq. 3-26)}$$

where V_t has the unit of cm s^{-1} and $\dot{\varepsilon}_{ct}$ has the units of s^{-1}. The crack tip strain rate in Equation 3-26 is related to the engineering stress (or stress intensity) parameters via the formulations in the given in the SCC AMR (CRWMS M&O 2000f, Section 6.4.2). The relationship for constant load is:

$$\dot{\varepsilon}_{ct} = 4.1\times10^{-14}\, K_I^4 \qquad \text{(Eq. 3-27)}$$

where K_I is the stress intensity factor in the units of MPa $m^{1/2}$. Since the stress in the WP closure weld (load) is essentially constant with time, substitution of Equation 3-27 for constant load into Equation 3-26 yields the following alternative expression:

$$V_t = \overline{A}\left(K_I\right)^{\overline{n}} \qquad \text{(Eq. 3-28)}$$

where

$$\overline{A} = A\left(4.1\times10^{-14}\right)^n \qquad \text{(Eq. 3-29)}$$

and

$$\overline{n} = 4n \qquad \text{(Eq. 3-30)}$$

3.1.7.8.3 Application To Waste Package Outer Barrier Material

There is ample reason to hypothesize that SCC of nickel-based Alloy 22 occurs by the same fundamental mechanism characterized by the slip dissolution model described in Section 3.1.7.8.2, (i.e., Equations 3-24 through 3-30). The only question that remains is that associated with the quantification of the repassivation rate, which is represented by the parameter n (repassivation slope).

A characteristic of the slip dissolution model is that SCC susceptibility decreases as the repassivation slope increases. For stainless steels, test data indicate that n = 0.54 (CRWMS M&O 2000f, Section 6.4.3). Recent SCC tests of Alloy 22 indicate that n = 0.84 for the WPOB (CRWMS M&O 2000f, Section 6.4.4). To be conservative, n = 0.84 is considered to be the upper bound for n. A lower bound of n = 0.75 is judged to be appropriate for a highly SCC-resistant material such as Alloy 22 (CRWMS M&O 2000f, Section 6.4.4).

In the smooth metal components dealt with in this PMR, the size of an incipient crack is expected to be exponentially distributed with a maximum possible size of 50 μm and a median size of 20 μm . The orientation of this crack will be either circumferential or radial, as shown in Figure 3-61. Only one crack per weld patch (WAPDEG element) will be considered. Based on the relatively high stress intensity factors for radial cracking in the outer lid of the initial WP design, it is evident that the slip dissolution model predicts eventual through-wall radial cracking. A modified WP design with dual-lids and stress mitigation in the closure welds has been developed to provide greatly enhanced service life.

It is generally assumed that crack initiation will not occur if the stress is below a threshold value. Available data suggested that the threshold stress lies between 10 and 40% of the yield stress.

3.1.7.9 Estimate of Crack Opening

Leaking through cracks can occur if the cracks grow into through-thickness cracks. A comprehensive, finite-element analysis may be used in the future to estimate the crack opening. However, a simplified approach is described here. The following assumptions are made for this simplified approach:

1. A given crack in the WPOB closure weld is either circumferential (perpendicular to the radial stress) or radial (perpendicular to the hoop stress). A circumferential crack has a semi elliptical shape with depth a and length $2c$. A radial crack has a semi-circular shape ($a = c$).

2. The crack length $2c$ of a circumferential crack remains unchanged, but the final length of a through-wall crack is at least twice the wall thickness. Under this assumption, most cracks will grow in both directions of the minor (depth a) and major (length $2c$) axes and assume the semi-circular shape (i.e., $a = c$) when they become through-wall cracks. According to fracture mechanics, a tends to grow faster than c because the stress intensity factor tends to have a maximum value at the end of the minor axis and a minimum value at the end of the major axis. Eventually, a semi-elliptical crack will become a semi-circular crack. The crack length $2c$ will remain unchanged only for very long cracks, with initial crack length greater than twice the wall thickness. For such long cracks, the occurrence rate is usually very low. The length of a semi-circular crack will always be equal to twice the crack depth.

3. The crack opening has an elliptical shape with length $2c$ and a gap δ.

The AMR on SCC (CRWMS M&O 2000f, Section 6.5.4) shows that the opening of a crack in an infinite sheet is given for plane stress condition as:

$$\delta = \frac{(4c)\sigma}{E} \qquad \text{(Eq. 3-31)}$$

where δ is the crack opening, $2c$ is the crack length, σ is the stress and E is Young's modulus. The opening area for an elliptical crack, A_{cr}, can then be estimated with Equation 3-36:

$$A_{cr} = \tfrac{\pi}{4}\delta(2c) = \frac{(2\pi c^2)\sigma}{E} \qquad \text{(Eq. 3-32)}$$

When Equations 3-35 and 3-36 are used to estimate the crack opening(δ) and opening area (A_{cr}), the stress (σ) is either the radial stress (for a circumferential crack) or the hoop stress (for a radial crack).

3.1.7.10 Summary of Stress Corrosion Cracking Model

Two alternative models that deal with SCC have been developed for the PA of the materials to be used for the WPOB. The first model (Method A) is based upon the concept of a threshold stress intensity factor at a pre-existing surface flaw, whereas the second model (Method B) is based upon the concept of a threshold stress at a "smooth" surface. Method B assumes crack propagation via the slip dissolution model, provided that the threshold stress is exceeded.

The first model (threshold stress intensity factor concept) is based on the theory that there exists a threshold value (K_{ISCC}) for the stress intensity factor such that there is no growth of a crack having a stress intensity factor less than the threshold value (CRWMS M&O 2000f). The concept of threshold stress intensity factor (K_{ISCC}) has been commonly used to assess the susceptibility of materials to SCC. The applicability of this model to Alloy 22 (the material to be used for the outer shell of the WP) has been studied experimentally.

Preliminary results based on Method A show that the initial WP design is able to arrest circumferential SCC, but not radial SCC. For circumferential flaws in the closure welds, the maximum values of K_I are less than the mean values of K_{ISCC}. Therefore, SCC should not initiate (CRWMS M&O 2000f, Section 6.3.2). The mean values of K_{ISCC} are 33.00 MPa $m^{1/2}$ for the outer lid and 20.54 MPa $m^{1/2}$ for the inner lid. The maximum values of K_I estimated for a circumferential flaw initiated at the outer surface are 22 MPa $m^{1/2}$ for the outer lid. However, based on the threshold value, through-wall, radial cracking can occur.

Method B (slip dissolution or film rupture concept) relates crack advance to the metal oxidation that occurs when the protective film at the crack tip is ruptured. In this case, the theory of slip dissolution was successfully applied to predict the SCC propagation rate in light water reactors at high temperature. This model was adopted to assess the SCC susceptibility of the materials to be used for the WPOB (Alloy 22). Method B also predicts eventual through-wall radial cracking, based on the high radial K_I value calculated for the outer weld in the initial design.

3.1.7.11 Mitigation or Elimination of Stress Corrosion Cracking

Since the crack growth analyses produced by either SCC model indicate that through-wall radial cracking is a potential threat to the WP, it is necessary to implement post-weld stress mitigation processes to eliminate the driving force for SCC.

As mentioned previously, two methods have been identified for localized treatment of the closure weld region. One of these involves use of induction heating coils to affect a localized annealing of the weld region. This process has been used successfully in the annealing of weld stresses in large components such as girth welds in large-diameter casings of solid-fuel rockets. This process is expected to neutralize the residual tensile stress initially present in the closure weld at substantial depths. This post-weld process may be able to mitigate stress to greater depths than laser peening. However, there are several concerns associated with this approach. Calculations indicate that temperature gradients experienced during cool down tend to shift the location of the tensile stresses to another adjacent region of the WP, making that region potentially vulnerable to SCC. A second concern is that the process may heat the waste to unacceptably high temperatures. As discussed earlier, both possibilities were analyzed using the finite element code ANSYS. The results of this analysis show that localized annealing by induction heating is a viable approach for producing low tensile stresses (less than 20% YS at depths greater that 7 mm).

The second method involves the use of laser peening, where a high-powered laser beam is used to cause shock waves in the surface of the material. These pulses produce compressive stresses in the surface. Multiple-pass laser peening can be used to increase the depth of the compressive stress layer. This process has been successfully demonstrated at LLNL on sample weldments (Figure 3-64). It has been shown that compressive stress can be produced at depths of 2 to 3 mm with multiple-pass laser peening. Additional depth may be possible, but has not been demonstrated. As discussed, a shortcoming of this approach is that this process only delays the potential initiation of

SCC. Below the layer of compressive stress, the weld region is still under tensile stresses. When the compressive layer of material is lost due to corrosion, the remaining material is still vulnerable to SCC. This applies to both mitigation techniques laser peening and induction annealing.

An optimized closure weld design was developed based on ANSYS stress analysis. Through-wall residual stresses have been calculated for two post-weld stress mitigation processes with the ANSYS computer program (CRWMS M&O 2000f, Section 6). Based on these analyses, a dual-lid WP design employing both stress mitigation processes was developed to maximize the expected WP lifetime, which appears to be limited by SCC at the closure welds.

3.1.7.12 Uncertainty in Stress Distributions for Closure Welds

In this PMR, weld stress uncertainty limits of ± 10% of yield are recommended for use in the calculations to estimate time to first SCC through-wall cracking. This uncertainty range is based on the close degree of control anticipated for the Alloy 22 material, the welding process for the closure, and the post-weld stress mitigation processes. In contrast, weld stress uncertainty limits for axially oriented stresses as high as ± 35% of yield around the mean yield value are described in the literature (Mohr 1996). This high degree of uncertainty was empirically developed by bounding the measured scatter in residual stress developed for a large number of welded carbon-steel pipes covering a range of thicknesses, welding processes, weld joint configurations, weld heat inputs, yield strengths, etc. In the case of the final closure weld, the various parameters contributing to residual stress variation will be closely controlled. This includes close, automated control of the welding process parameters, the allowable material and the weld wire yield strength range, the weld joint configuration and spacing, etc.

In contrast to the high degree of scatter noted in the carbon-steel paper (Mohr 1996), data available for shot-peened Incoloy 908, a high-performance nickel-based alloy, indicate a relatively narrow scatter (Pasupathi 2000). Data are for as-welded and as-welded plus shot-peened material with 1-sigma values of ± 3% of the measured stress value. This corresponds to an uncertainty range of about ± 9% at the 3-sigma level. In comparison, the residual stresses measured in a peened surface with X-ray diffraction (XRD) showed a measurement uncertainty of about ± 15 MPa, which is about 5% of the Alloy 22 yield strength (Lu 1996). The data given by (Pasupathi 2000) are for both welded and non-welded samples (peened and unpeened), many of which also contain some cold work due to tube reduction drawing. Thus, they represent a good sampling of the entire range of material conditions that may be encountered. Since shot peening is analogous to laser peening in its effect on metals, the peened data are also relevant to the peened case for the inner lid. A stress variation similar to the peened case would be expected for material processed by localized induction annealing. During the induction annealing process cycle, all the residual weld stress in the heated weld region is fully relieved at ~1120°C, and the remaining post-process stresses are produced during the cool-down portion of the thermal cycle. Since it is planned to control this cool-down process in a reproducible manner, we expect to see residual stress variations similar to those for laser and shot peening.

In the case of the WP closure weld, XRD measurements of residual stress will be made of the final Alloy 22 material with post-weld stress mitigation. These measurements will be made in the near-surface region of the weld and HAZ. If stresses are found to deviate from the specified range, the weld will either be reprocessed, repaired, or scrapped. Thus, a defensible range of uncertainty in the stress distribution of ± 10% of the yield stress is more conservative than the observed 3-sigma scatter band. This range of uncertainty is believed to be appropriate for WAPDEG SCC calculations.

3.1.8 Hydrogen-Induced Cracking

As discussed in Sections 3.1.5 and 3.1.6, the DS is to be fabricated from a titanium-based alloy and is highly resistant to general and LC. Other degradation mechanisms do not appear to be life-limiting. The material has been shown to be susceptible to SCC under certain conditions. As discussed in Section 3.1.7, mitigation of residual weld stress makes this an unlikely mechanism when backfill is present to preclude rockfall-generated stresses. Another possible failure mechanism for titanium and its alloys under waste disposal conditions is via hydrogen absorption, which can lead to HIC. HIC is also called hydrogen embrittlement and, can cause a decrease of the fracture toughness or ductility of a metal due to the presence of atomic hydrogen. The usual failure mode for a ductile material is the ductile tearing observed during slow crack growth. The decrease of fracture toughness can also cause fast crack growth (brittle fracture) of a normally ductile material under sustained load. During slow crack growth, material will fail as the stress intensity factor K_I reaches a value K_S. During fast crack growth, the same material will fail as the stress intensity factor K_I reach a value K_H, which is less than K_S.

It has been observed that the passive oxide film on titanium acts as an excellent barrier to the absorption of hydrogen under open-circuit conditions. However, hydrogen absorption may be too slow to observe analytically during practical tests (up to tens of years). This absorption could lead to a significant accumulation of hydrogen and the danger of HIC during exposures of 10^3 to 10^5 years.

Under Canadian waste repository conditions, a very simple approach was adopted to predict when HIC might become a potential failure process in a waste container. In essence, this model is a susceptibility model or the equivalent of an initiation model for LC processes such as pitting and crevice corrosion. The basic premise of the model is that failure will occur when the concentration of hydrogen in the titanium exceeds a critical value (H_c). Combinations of stress intensity factor and hydrogen concentration that lead to brittle fracture or ductile rupture are discussed in AMR on HIC (CRWMS M&O 2000h, Section 6.1.3). The stress intensity factors for brittle fracture and ductile rupture are K_H and K_S, respectively.

This model is presented in the AMR and is very conservative because it assumes that, when the environmental and material conditions can support cathodic hydrogen-charging processes, failure will be effectively instantaneous.

Clearly, the propagation of a corrosion pit, a crevice, a stress corrosion crack, or a hydrogen-induced crack does not proceed instantaneously to failure. However, if the rate of propagation is fast on the geologic time scales being considered, then the process can be thought of as instantaneous. Another factor ignored in this analysis is the impact of propagation-limiting processes. For example, repassivation may occur with a pit or crevice; or crack blunting could occur with a stress corrosion crack. In the HIC model described below, no crack initiation or crack blunting processes are considered.

3.1.8.1 Model Description

The model can best be summarized as follows:

1. The passive oxide is assumed to be permeable to atomic hydrogen.

2. Atomic hydrogen is generated at the surface of the Ti alloy. This is described by a hydrogen generation rate, which is taken to be proportional to the general corrosion rate of the passive material.

3. A fraction of the hydrogen is absorbed into the oxide and assumed to directly enter the alloy. The remainder combines to yield hydrogen gas, which is lost to the surroundings. The rate of absorption is taken to be directly proportional to the hydrogen generation rate multiplied by an absorption efficiency coefficient.

4. Once in the alloy, the hydrogen is transported throughout the entire thickness of the material to yield a uniform distribution of hydrogen. In other words, transport processes within the alloy are rapid compared to the rate of absorption.

5. The hydrogen content of the alloy is allowed to increase until a critical level is reached. The material then fails immediately. The model allows for the calculation of hydrogen content and for comparison with the critical concentration.

3.1.8.2 Elements of the Model Assumptions

3.1.8.2.1 The Oxide is Assumed to be Permeable to Hydrogen

The potential repository at Yucca Mountain will not achieve anoxic conditions. During the early stages of repository operation, the temperature will be high, but the oxygen and water content will be low. Since water is the only significant source of hydrogen (due to reaction with the titanium), hydrogen absorption rates should be lower during the initial stage of repository operation than during subsequent periods. Oxidizing conditions and an open-circuit corrosion potential too positive to allow the redox transformations in the oxide will eventually be established. Under oxidizing conditions, any exposed intermetallic or noble-metal particles (Ti_2Ni in Titanium Grade 12; Ti and Pd in Titanium Grades 16 and 7) will be passivated by a surface oxide film. Consequently, their catalytic properties for hydrogen production and absorption may be lost.

The oxide film remains impermeable to hydrogen until the electrical potential becomes sufficiently negative that the oxide becomes chemically unstable. When this occurs, Ti (IV) within the TiO_2 oxide is reduced to Ti (III) and hydrogen can be incorporated as a doping defect. When this process becomes possible, it is conservatively assumed that the oxide becomes permeable to hydrogen. Absorbed hydrogen then has free access to the alloy; in other words, any hydrogen entering the oxide can be rapidly transported to the metal (CRWMS M&O 2000h, Section 6.1.5).

Several mitigating factors indicate that this is a very conservative scenario. First, experimental evidence suggests that total permeability is not established as soon as this oxide transformation begins. Second, in the absence of specific unexpected reducing reagents, it is unlikely that such redox transformations could be induced in the passive film.

Assuming that the maximum temperature at which an aqueous condition can be sustained on the titanium is 125°C, a pH > 13 would be required for significant hydrogen absorption (CRWMS M&O 2000g). Therefore, it would be judicious to assume that hydrogen absorption is possible within the temperature range of approximately 100 to 125°C. This range effectively defines a window of susceptibility for hydrogen absorption.

The probability of hydrogen absorption by titanium alloys at Yucca Mountain is low but cannot be ruled out entirely.

3.1.8.2.2 Hydrogen is Generated at the Surface of the Titanium Alloy

The only feasible source of absorbable hydrogen appears to be the reaction of Ti with water. The direct absorption of radiolytically produced hydrogen requires a combination of high dose rate (> 10^4 R h^{-1}) and high temperature (> 200°C) and a steam or aqueous environment. This combination of conditions seems extremely unlikely at Yucca Mountain. Under open-circuit conditions, the rate of hydrogen production will be directly related to the GC rate. In the presence of dissolved oxygen, this rate has been shown to be extremely low and effectively immeasurable by standard procedures such as weight change measurements. Consequently, the rate of hydrogen production (the essential model boundary condition) will also be extremely low.

Further, oxidizing conditions expected in the repository will not lead to a significant enhancement of GC; the process will be blocked by the excellent protective properties of the passive TiO_2 film. Under these oxidizing conditions, the intermetallic precipitates should be covered by a passive oxide film and their catalytic properties severely degraded.

Thus under Yucca Mountain repository conditions, the corrosion rate of titanium alloys (with the possible exception of Titanium Grade 12), and, hence, the rate of hydrogen production, will most likely be slow and transitory. Evidence suggests that even when corrosion, in the form of film growth, is initially accelerated under oxidizing conditions, the accumulation of mineral precipitates leads to the eventual blocking of corrosion processes.

3.1.8.2.3 A Fraction of the Hydrogen is Absorbed into the Metal

Even if the oxide film present on the titanium surface provides just a semi-impermeable barrier to hydrogen absorption into the metal, only a fraction of the hydrogen produced will actually be absorbed into the metal, and hence, contribute to the eventual embrittlement of the alloy. This critical fraction must be known. A consistent single value may not represent the real absorption efficiency of the alloy because this efficiency would be expected to change as the condition of the surface changed. The initial surface could be relatively free of absorbed hydrogen, and the initial absorption efficiency could be high. Subsequently, it would be expected to decrease as the number of available surface sites for absorption become saturated. These absorption sites could be the usual defects and dislocations known to trap hydrogen and, in addition, noble metal intermetallic particles, which would have a high solubility for hydrogen. Alternatively, the formation of surface hydrides could lead to a change in the mechanism of proton reduction and a decrease in the rate of hydrogen absorption into the alloy.

The concern remains that in the temperature range extending from 100°C to 125°C and in the presence of an aggressive saline solution, the passive oxide film may be degraded and the hydrogen absorption efficiency increased. The rate of passive film growth (rate of hydrogen production), as well as the hydrogen absorption rate for Titanium Grade 12 in extremely saline solutions at 25 and 100°C, are discussed in the AMR on HIC (CRWMS M&O 2000h, Section 6). These values for passive film growth rate and hydrogen absorption efficiency of 0.03 μmy^{-1} and 10%, respectively, would be conservatively appropriate for Titanium Grade 7 in a degraded passive condition.

3.1.8.2.4 Hydrogen is Uniformly Distributed in Titanium Alloy

Once hydrogen is in the metal, its fate becomes dependent on the diffusion rate. The diffusivity is affected by the microstructure of the material, as well as the strength and distribution of stresses within the material.

It was assumed that, because the rate of absorption of hydrogen into the metal would be very slow, its transport throughout the bulk would be comparatively rapid. Hence, absorbed hydrogen would be uniformly distributed throughout the alloy. At the high absorption rates experienced during electrochemical experiments, absorbed hydrogen can lead to the formation of a surface hydride layer. Since the presence of such a layer appears to impede the further absorption of hydrogen, its presence may actually reduce the absorption efficiency of the material (CRWMS M&O 2000h).

However, hydrogen accumulates at the titanium surface. A conservative assumption is that it remains available for transport into the alloy. When the temperature is low enough so that the transport rate can be assumed to exceed the absorption rate (below 100°C), the thickness of the hydride layer will decrease as the hydride is redissolved in the alloy. The layer of hydride on the surface serves as a source of hydrogen for infusion into the bulk material. The hydride continues to redissolve until the surface layer is depleted.

3.1.8.2.5 Hydrogen Concentration Increases to Critical Level where Failure Occurs

The slow strain rate tests (CRWMS M&O 2000h, Section 6.2.3) show that titanium can tolerate substantial amounts of hydrogen before it becomes susceptible to cracking. This critical hydrogen concentration is not related to the solubility of hydrogen in the alpha matrix of the alloy but to the number density of precipitates, which must be capable of supporting a crack propagation process through the material. Values for critical hydrogen concentration (H_c) were obtained from published literature for Titanium Grades 2, 12 and 16 (CRWMS M&O 2000h, Section 6). The high value for Titanium Grade 16 (greater than 1,000 µg per gram) appears to be due to the ability of the intermetallics to soak up hydrogen, thereby preventing them from forming hydride precipitates in the alloy.

Whichever process is assumed for the dispersion of hydrogen throughout the titanium alloy, failure is assumed to occur once this critical value is achieved. However, this remains a very conservative approach because slow strain rate tests have determined the point at which the necessary stress level will inevitably be achieved. Also, the critical value is a threshold value, representing the lowest concentration at which influence of hydrogen is observed. It is feasible that much higher concentrations of hydrogen could be tolerated before failure actually occurs.

3.1.8.3 Determination of the Critical Hydrogen Concentration

Using the slow strain rate technique on precracked compact tension specimens precharged with known amounts of hydrogen, it has been shown that fracture toughness of Titanium Grade 2 and that of Titanium Grade 12 is not significantly affected until their hydrogen content exceeds a critical value, H_c. The as-received materials, containing 20 to 50 µg per gram of hydrogen, are very tough and fail by ductile overload under high stress. This ductile tearing is also observed during slow-crack growth for both materials. The hydrogen concentration above which slow-crack growth is no longer observed and only fast-crack growth occurs is defined as H_c.

Critical hydrogen concentrations (H_c) of 400 to 2,000 μg per gram were reported for Titanium Grade 2, 400 to 1,000 μg per gram for Titanium Grade 12, and 1,000 to 2,000 μg per gram for Titanium Grade 16 (CRWMS M&O 2000h, Section 6.2.2). Critical hydrogen concentrations are not available for Titanium Grade 7. The value of H_c for Titanium Grade 7 is conservatively assumed to be at least 400 μg per gram, which is the lower bound value observed for Titanium Grades 2, 12, and 16, as indicated previously.

3.1.8.4 Determination of Hydrogen Concentration

Analytical formulas can be derived to represent the hydrogen concentration in the metal as a function of time of emplacement of the container. There are two processes by which hydrogen could be produced, and possibly absorbed, under passive conditions: (1) direct absorption of hydrogen produced by water radiolysis and (2) absorption of atomic hydrogen produced by the corrosion process to produce oxide. The direct absorption of radiolytically produced hydrogen does not appear to be significant except at high dose rate (>102 Gy/h) and high temperature (>150°C). This condition is clearly unattainable under Yucca Mountain conditions, and will not be considered, leaving the corrosion process as the only feasible source of hydrogen for absorption.

The rate of hydrogen absorption will be controlled by the rate of the corrosion reaction, which dictates the rate of production of absorbable hydrogen. Since titanium oxide, TiO_2, is extremely stable and protective in the repository environment, the corrosion reaction will be effectively limited to an oxide film growth reaction.

While the rate of hydrogen production and absorption is directly proportional to the rate of film growth, the fraction of hydrogen absorption needs to be determined. Available test data suggest 0.1 and 0.02 for fractional efficiency for absorption values, f_h to represent high and low hydrogen absorption efficiencies for titanium alloys. The low value would appear most appropriate for Titanium Grade 2 since the passive film is a good transport barrier to hydrogen absorption. For Titanium Grades 7 and 16 in which intermetallic formation is very limited or avoided, the lower value is appropriate.

Based on a constant film growth rate, and hence the corrosion rate, the concentration of hydrogen in the metal, H_A, can be calculated as a function of time of emplacement (t in years) from the expression,

$$H_A = 4(\rho_{Ti}/10^3) f_h R_{uc} t \, [M_{Ti}(d_o - R_{uc}t)]^{-1} \qquad \text{(Eq. 3-33)}$$

where

H_A = hydrogen content (g mm^{-3})
ρ_{Ti} = density of Ti (g cm^{-3})
f_h = fractional efficiency for absorption
R_{uc} = rate of general passive corrosion (mm y^{-1})
t = time of emplacement in years (y)
M_{Ti} = atomic mass of Ti = 47.9
d_o = original corrosion allowance (mm) = container wall thickness (mm)

The units of atomic mass are grams per gram-atom, which for hydrogen is 1.0 grams per gram-atom and for titanium is 47.9 grams per gram-atom. Since there is 1 gram of hydrogen per gram-atom, the values of H_A in (g mm^{-3}) and in (g-atoms mm^{-3}) are equal (to within less than 1 percent).

Considering a Titanium Grade 7 plate with 1 mm^2 surface area, it is noted in Equation 3-33 that hydrogen in grams produced by the GC after t years of emplacement is based on the reaction:

$$Ti + 2H_2O \rightarrow TiO_2 + 2H_2$$

The derivation of Equation 3-37 is based on a constant GC rate. It was noted that the assumption of constant corrosion rate is conservative and less conservative corrosion models assume that the rate decays with time. (CRWMS M&O 2000d, Section 6.5.4)

The rate of general passive corrosion, R_{uc}, can be calculated from the rate of oxide film thickness, R_{ox}, by the following formula:

$$R_{uc} = R_{ox} (\rho_{ox}/M_{ox})(\rho_{Ti}/M_{ti})^{-1} \qquad \text{(Eq. 3-34)}$$

where

ρ_{ox} = density of the oxide in g cm^{-3}
M_{ox} = molecular mass of the oxide

Since the value of $(\rho_{ox}/M_{ox})(\rho_{Ti}/M_{Ti})^{-1}$ is always greater than unity, it is conservative to assume that $R_{uc} = R_{ox}$.

The GC rates reported for Titanium Grade 7, at the 50th percentile is approximately 25 mm y^{-1}, the rate at the 90th percentile is approximately 100 mm y^{-1}, and the maximum rate is less than 350 mm y^{-1} (CRWMS M&O 2000d, Section 6.5.4).

3.1.8.5 Critical Hydrogen Concentration

The H_C value for Titanium Grade 7 is assumed to be at least 400 µg/g, which is the lower bound value observed for Titanium Grades 2 and 12 as indicated previously (CRWMS M&O 2000h, Section 6.2). This assumption appears to be extremely conservative based on data reported for Titanium Grade 16. As noted, Titanium Grades 7 and 16 are similar alloys because of their similar chemical compositions.

The fractional efficiency for absorption, based on previous discussion, is f_h = 0.02 for Titanium Grade 7. The rate of general passive corrosion is R_{uc} = 100x10^{-6} mm y^{-1} (90th percentile value) or 25x10^{-6} mm y^{-1} (50th percentile value). The time of employment is t = 10,000 years. A minimum wall thickness of 15 mm is assumed for d_o.

Case 1: Conservative Estimate

R_{ox}=100x10^{-6} mm y^{-1} (90th percentile value)
f_h=0.02
d_o=15 mm
t=10000 y
H_A=119 µg g^{-1} < Hc = 400 µg g^{-1}

Case 2: Best Estimate

R_{ox}=25x10^{-6} mm y^{-1} (50th percentile value)
f_h=0.02
d_o=15 mm
t=10000 y
H_A=28 µg g^{-1} < Hc = 400 µg g^{-1}

The hydrogen concentration in the DS at 10,000 years after emplacement is 119 $\mu g\ g^{-1}$ resulting from a conservative estimate and 28 $\mu g\ g^{-1}$ from a best estimate. The estimated hydrogen concentration in either case is significantly less than the conservatively selected critical hydrogen concentration of 400 $\mu g\ g^{-1}$ for Titanium Grade 7. These results indicate that there exists a big margin of safety for the DS against the effects of HIC and this degradation mechanism is not credible under repository conditions.

3.1.8.6 Results for HIC Model

In the description of the HIC model presented in the corresponding AMR (CRWMS M&O 2000h, Section 6), extensive evidence has been provided to support a qualitative assessment of Titanium Grade 7 as an excellent choice of material for the DS with regard to degradation caused by hydrogen-induced cracking. Quantitative evaluation based on this model indicates that the DS material (Titanium Grade 7) is able to sustain the effects of hydrogen-induced cracking. Available corrosion test data show that the hydrogen concentration is below 120 μg per gram, which is less than the critical hydrogen concentration of 400 μg per gram for Titanium Grade 7.

The current model is based on the use of backfill, which protects the DS from coming into contact with ground support materials such as carbon steel, rock bolts, wire mesh, etc. However, in the absence of backfill, the DS will likely come in contact with these materials and, therefore, may be subject to hydrogen pickup and embrittlement. This issue is being addressed in the revision of the AMR and is beyond the scope of this PMR.

3.1.9 Model Uncertainties

Uncertainties in each of the process models were identified in the discussion of the models in the previous sections and in the individual AMRs. The approach used in dealing with these uncertainties is to be conservative and bound the uncertainties. A review of the uncertainties in the various models is presented below.

3.1.9.1 Thermal Aging

A graphical approach to bounding the uncertainty in the aging model is illustrated in Figure 3-7. The line representing a "best fit" to the data for "complete GB coverage" predicts that more than 10,000 years at 300°C will be required to completely cover the grain boundaries of Alloy 22 with intermetallic precipitates. However, the line with the "minimum slope possible within the error bars" shows that complete GB coverage might occur in as little as 100 years (very unlikely bounding case). The "best fit" line is the most likely scenario. In the case of bulk precipitation, none is predicted with the line representing the minimum possible slope. Thus, we conclude with reasonable certainty that no bulk precipitation will occur after 10,000 years at 300°C.

From Figures 3-9 and 3-10, it appears that a fully aged sample of Alloy 22 could change the observed corrosion potential. For example, corrosion potential was shifted in a less noble (negative) direction by 63 mV in SAW at 90°C. This potential was shifted in a less noble (negative) direction by 99 mV in SCW at 90°C. Full aging of Alloy 22 (complete coverage of the grain boundaries) does not appear to significantly alter passive film stability.

Thermal aging of Titanium Grade 7 at 300°C is expected to have little impact on the corrosion resistance of this material. Since no credit is claimed for the corrosion resistance of 316NG, the TSPA calculation is insensitive to the uncertainty associated with the corrosion of 316NG.

3.1.9.2 Dry Oxidation

In the case of Alloy 22, the rates of DOX are very small (CRWMS M&O 2000c, Section 6.1). Therefore, uncertainty in the DOX rate is not expected to have any significant impact on the performance of these materials. The current model is based upon published data, and does not include estimates of uncertainty (CRWMS M&O 2000c, Section 6.1).

3.1.9.3 Humid Air and Aqueous Phase Corrosion

The threshold RH is represented by Equation 3-2. This correlation represents the deliquescence point of $NaNO_3$ and has an excellent fit of the data (correlation coefficient of 0.9854). Uncertainty in this threshold is primarily due to the composition of the salt film. The WP and DS would always experience some combination of HAC and APC. The uncertainty in this parameter is discussed in more detail in the associated AMRs. The correlation used for the threshold RH in a consecutive bonding case as the deliquescence point for Na NO_3 is assumed to determine the threshold RH for the formation of aqueous film. As the temperature is increased, the lowest RH under which an aqueous film can be sustained is represented by the data for Na NO_3.

The distribution of GC rates for either HAC or APC represented by the curves given in Section 3.1.5.4. Distributions for 316NG are represented by Figure 3-15, which shows distributions formed from published data. Figure 3-23 shows the distribution of rates for Alloy 22, based upon data taken from the LTCTF. Figures 3-26 and 3-27 shows the distribution for Titanium Grade 7 rates, also based upon data from the LTCTF. The dispersion in these curves is assumed to be entirely due to uncertainty.

The variability is assumed to be comparable in magnitude and is represented by a triangular distribution.

A detailed analysis of the error in GC rate is given in each supporting AMR, with the results summarized in Tables 3-8 and 3-9.

Determinations of corrosion and threshold potential are based upon three replicate CP measurements at each combination of environment and temperature. The results are tabulated in the supporting AMR, as summarized in Figures 3-38 through 3-48. The uncertainty in the corrosion potential due to gamma radiolysis is addressed by Figures 3-51 and 3-52 (maximum positive shift in error of about 250 mV). Some uncertainty in the selection of corrosion and threshold potential is shown in the figures as Threshold Potential 1 through 3. The bounds of the threshold potential are shown graphically in the figures. Numerical representations of this uncertainty have been made and are embedded in WAPDEG.

The rates of LC have been bounded with the range of values found in the published literature, and are summarized in Tables 3-11 and 3-12.

3.1.9.4 Stress Corrosion Cracking

For the first time, SCC has been included in the performance assessment calculation done with WAPDEG. Two alternative SCC models have been considered, one based upon a threshold stress intensity factor (Method A), and another based upon a threshold stress for a smooth surface (Method B). In the second approach, cracks are assumed to propagate by the slip-dissolution mechanism after initiation. Method B is used as the basis of the PA. The slip-dissolution model (Method B) predicts that crack propagation is a function of the local stress intensity at the crack tip. Thus, the uncertainty in this driving force must be estimated.

The local stress intensity is calculated from the local stress and the crack penetration. The uncertainties in the stress distribution (stress vs. depth) are based upon analyses of measured residual stresses in welds, before and after mitigation, as well as finite element modeling with the ANSYS code. These uncertainties are abstracted for WAPDEG and shown quantitatively for the initial PA in Figures 3-73 through 3-80.

Aside from the stress intensity, K_I, the parameters in the slip-dissolution model for SCC propagation are based upon measurements for stainless steel from the BWR industry. Since stainless steels are much more prone to SCC than Alloy 22, these parameter estimates are projected to be conservative.

The threshold stress for initiation of SCC on a smooth surface is conservatively estimated to be approximately 10 to 40% of the yield stress, based upon the determination of such thresholds for related but more susceptible alloy systems exposed to very aggressive environments. The uncertainty is assumed to be within ± 10% of the median value.

3.1.10 Model Validation

According to ASTM C1174-97 *Standard Practice for Prediction of the Long-Term Behavior of Materials, Including Waste Forms, Used in Engineering Barrier Systems (EBS) for Geological Disposal of High-Level Radioactive Waste,* model validation is the process through which independent measurements are used to ensure that a model accurately predicts an alteration behavior of WP materials under a given set of environmental conditions (e.g., under repository environment over the time periods required). Obviously, no model can be validated over the 10,000-year service life (time period) of the repository. The only means of validating models must involve accelerated testing. According to the same ASTM procedure, an accelerated test is a test that results in an increase in the rate of an alteration mode, when compared with the rates for service condition. Changes in alteration mechanism, if any, must be accounted for in the use of the accelerated test data.

Model validation of specific process models is addressed in each of the AMRs as required by the procedures used to develop these models. Key elements are presented here.

The thermal aging model is represented by equations 3-5 and 3-6, both of which assume Arhenius-type kinetics. Precipitation and LRO can be accelerated by increasing the temperature above those levels expected in the repository. If the model can accurately predict the kinetics of these phenomena at combinations of time and elevated temperature, it will be considered valid for making predictions at lower temperature and longer time.

Since all available data has been used to establish these correlations the correlations are considered valid for their intended use. Additional data that are being collected will help to reduce uncertainties and improve the level of confidence in the model.

The effects of precipitation and LRO on corrosion are determined by electrochemical techniques. Through application of electrochemical potentials more anodic than the open circuit corrosion potential, corrosion phenomena can be accelerated. Variations in corrosion and threshold potential can be correlated with the extent of thermal aging. Similarly, variations in rates of dissolution through the stable passive film can also be correlated with the extent of thermal aging. These rates of dissolution are accelerated by application of a potential between the corrosion and threshold potentials, and are proportional to the passive current density. The corrosion rate enhancement factor is determined by calculating the ratio of measured passive current densities for aged and unaged samples. Since all available electrochemical data have been used to establish the corrosion model for thermally-aged samples, this model is considered valid for its intended use.

The models for DOX of Alloy 22, Titanium Grade 7, and 316NG stainless steel are based upon published data found in the scientific literature. More specifically the model for DOX of Alloy 22 is based upon the parabolic growth of the oxide film at elevated temperature. However, in the absence of any such low-temperature data, the parabolic rate constant for high temperature is applied at low temperature. Given the extremely small magnitudes of these rates, DOX is expected to have no significant impact on WP performance.

The threshold RH for HAC is based on the deliquescence point of sodium nitrate. The threshold for salt films deposited in the repository may be slightly different. However, salt deposits produced by evaporating simulated J-13 water to dryness, support this basis.

Rates of HAC are expected to follow distributions of GC rates based upon weight-loss data from the LTCTF. The distributions for Alloy 22 data for 6, 12, and 24 months of exposure to a variety of test media. Corroborative measurements made with the atomic force microscope (AFM) and other surface analytical techniques have also been used as further means of model validation. The test program will continue; ultimately providing data for 60-months of exposure. Future data will be considered independent and corroborative, and will be used to reduce uncertainties and conservatism in the model.

The threshold RH for APC is the same as that used for HAC. The same approach has been used for validation. Rates of GC in the aqueous phase also obey the general distributions based upon weight-loss data from the LTCTF. The same approach described for validation of the rate model for HAC has been employed for validation of the rate model for GC in the aqueous phase.

Comparisons of corrosion and threshold potentials are used to determine whether rates for GC or LC are applicable. The initial correlations given in this PMR are based upon standard CP measurements in SDW, SCW, SAW, and SSW, covering a broad range of temperature.

The SCC model is primarily based on published data. Very limited data have been obtained under repository relevant conditions. The data obtained under the YMP include pre-cracked specimens tested under very aggressive environments. Thus the model uses a very conservative approach. Future data obtained by the Project will serve to reduce the level of conservatism and improve the confidence in the model.

3.1.11 Alternative Approaches or Models

Alternative models have been considered for rates of DOX, LC thresholds, stress corrosion thresholds, stress corrosion cracking, stress mitigation, & HIC. These alternatives are summarized below.

3.1.11.1 Dry Oxidation

Method A – Parabolic Growth Law
Method B – Logarithmic Growth Law

In the case of DOX, Method A is used for Alloy 22 (CRWMS M&O 2000c), while Method B is used for Titanium Grade 7 (CRWMS M&O 2000d). These model selections were based upon the availability of published data to support the corresponding models.

3.1.11.2 Localized Corrosion Threshold

Method A – Threshold Electrochemical Potential
Method B – Threshold Temperature

In the case of LC, Method A is used because the threshold potential model is more solidly rooted in the theoretical concepts underlying passive film stability (CRWMS M&O 2000c, 2000d). Furthermore, it is expected that good correlations of threshold and corrosion potential can be used to deduce a threshold temperature. The threshold temperature would be the temperature at which the corrosion and threshold potentials are equivalent.

3.1.11.3 Stress Corrosion Cracking

Method A – Threshold Stress Intensity Factor at Pre-Existing Flaw
Method B – Initiation at Threshold Stress on Smooth Surface/Propagation by Slip-Dissolution Mechanism

Method B is preferred for SCC since it is believed to be the more conservative model, and since it has been used for predicting the performance of BWRs, and since a wealth of data exists for stainless steel, a material more prone to SCC than Alloy 22. In prediction based upon a correlation for stainless steel would yield a conservative prediction for Alloy 22 (CRWMS M&O 2000f, Section 6.4.4).

Weld Stress Mitigation

Method A – Induction Annealing
Method B – Laser Peening

In regard to stress mitigation, Method A is preferred for any external lid on the Alloy 22 WPOB. This selection is based upon the ability of the induction annealing process to place compressive stress deeper into the weld. Method B, laser peening will be used on any internal lid weld, due to the occluded nature of such a weld.

3.1.11.4 Hydrogen-Induced Cracking – Titanium

Method A – Threshold Electrochemical Potential
Method B – Threshold Hydrogen Concentration

HIC evaluation is based upon a threshold hydrogen concentration. Since such concentrations are possible to measure with secondary ion mass spectrometry (SIMS), Method B is therefore preferred. The DS design avoids any galvanic couple that would lead to the possibility of HIC via Method A, the threshold electrochemical potential method.

A simple and conservative model has been developed to evaluate the effects HIC on the DS. The basic premise of the model is that failure will occur once the hydrogen content exceeds a certain limit or critical value (H_c). This model is very conservative because it assumes that, once the environmental and material conditions can support that particular corrosion process, failure will be effectively instantaneous. Extensive evidence has been provided to support a qualitative assessment of Titanium Grade 7 as an excellent choice of material for the DS with regard to degradation caused by HIC (CRWMS M&O 2000h, Section 6.1.3).

Quantitative evaluation based on the HIC model described in the corresponding AMR indicates that the DS material (Titanium Grade 7) is able to sustain the effects of HIC. Available test data show, that the hydrogen concentration is below 180 μg per gram, which is less than the critical hydrogen concentration of 400 μg per gram for Titanium Grade 7.

3.2 INTEGRATED MODEL

The WAPDEG software was used to develop and implement an integrated model for WP and DS degradation analysis, and to perform the degradation simulations. WAPDEG (Version 4.0) is an appropriate tool for this application, because it was specifically designed to analyze DS and WP degradation profiles in a manner consistent with the information requirements for implementation in the TSPA model. WAPDEG (Version 4.0) was used within the range of values for which it is being validated (CRWMS M&O 2000g).

3.2.1 Concept for the Integrated Model

This section discusses the concept for the integrated model for WP and DS degradation analysis in TSPA-SR. More detailed descriptions of the conceptual model are given in the companion AMR, *WAPDEG Analysis of Waste Package and Drip Shield Degradation* (CRWMS M&O 2000g). In the TSPA-SR analysis, WAPDEG models various types of corrosion mechanisms that may occur on a WP and DS as a function of the exposure time and conditions. (For convenience of discussion in this section, DS is considered as an integral part of WP. Except where it is necessary, no separate discussion is given for DS.) In the nominal case analysis of TSPA-SR, the WPOB and DS were included in the WP degradation analysis. Because the stainless steel inner container, which is to provide structural support to the WP, is not expected to provide any substantial time-period for the waste-containment performance after an initial breach of the WPOB. Once exposed to corrosive condition, the stainless steel inner container is expected to fail by localized corrosion and SCC in a relatively short time period (see CRWMS M&O 2000e for the details of the inner container degradation). Because of this, performance credit of the inner container is not taken in the waste degradation analyses discussed in Section 3.2.7. This is based on the penetration rates shown in Figures 3-14 and 3-15 which suggest that the material may fail by localized corrosion under certain

conditions. However, in reality it would provide "some" performance for waste containment after breach of the WPOB, and would also serve as a barrier to radionuclide transport after the WP failure. Such potential performance credit of the inner container is ignored in the nominal TSPA-SR analysis. This is a conservative approach.

As discussed in detail in Section 3.1.7, a dual closure-lid design has been proposed for the closure-end of waste package outer barrier—one Alloy 22 lid on one end of the outer barrier and two Alloy 22 lids on the closure end of the outer barrier. This dual-lid design is to mitigate potential premature failure of waste packages by stress corrosion cracking (SCC). A schematic shown in Figure 3-66 illustrates the dual closure-lid design. The dual closure-lids are referred to as the outer-lid and inner-lid, respectively, in this section. The outer lid is 25-mm thick and the inner lid is 10-mm thick. There is a physical "gap" between the two lids. Thus, any SCC cracks penetrating the outer closure-lid stop at the gap between the closure lids. Then the inner closure-lid welds are subject to the SCC crack initiation and growth. This design feature is captured in the waste package degradation analysis as described below in this section.

Abstracted models of the process models for implementation in the WAPDEG model were developed in such a manner that important features of the process models are captured as explicitly as possible and that the degradation processes and their characteristics are properly represented in the waste package degradation analysis. More details of the TSPA-SR approach to waste package and drip shield degradation analysis are given in the supporting AMR (CRWMS M&O 2000g – *WAPDEG Analysis of Waste Package and Drip Shield Degradation*). As was done in the TSPA-VA analysis, effects of spatial and temporal variations in the exposure conditions over the repository were modeled by incorporating explicitly relevant exposure condition histories into the waste package degradation analysis. The exposure condition parameters that were considered to be varying over the repository are relative humidity and temperature at the waste package surface, seepage into the emplacement drift, chemistry of seepage water, and rockfall. In the waste package degradation analysis the humid-air corrosion condition is defined as an exposure condition that there is no dripping water and that the RH at the waste package surface is equal to or greater than the no-drip threshold RH (i.e., threshold RH in the absence of drips). The aqueous corrosion condition requires the presence of drips and the RH at the waste package surface equal to or greater than the drip threshold RH (i.e., threshold RH in the presence of drips).

In the WAPDEG analysis the waste package (or drip shield) surface is discretized into many subareas referred to as "patches", and relevant corrosion model parameter values and/or corrosion rates are populated over the patches. A schematic showing the conceptual model approach is shown in Figure 3-67. This approach is to represent potentially "variable" corrosion processes and other degradation processes on a single waste package. For example, patches wetted by dripping water (those marked with "s") could be subject to localized corrosion depending on the exposure conditions (especially chemistry of contacting water) that those patches experience. Patches with closure welds (those marked with "y") could be subject to SCC depending on the stress state and exposure conditions. In addition, general corrosion rate may vary over the waste package surface, and the potential variability is represented by populating the general corrosion rate over the patches.

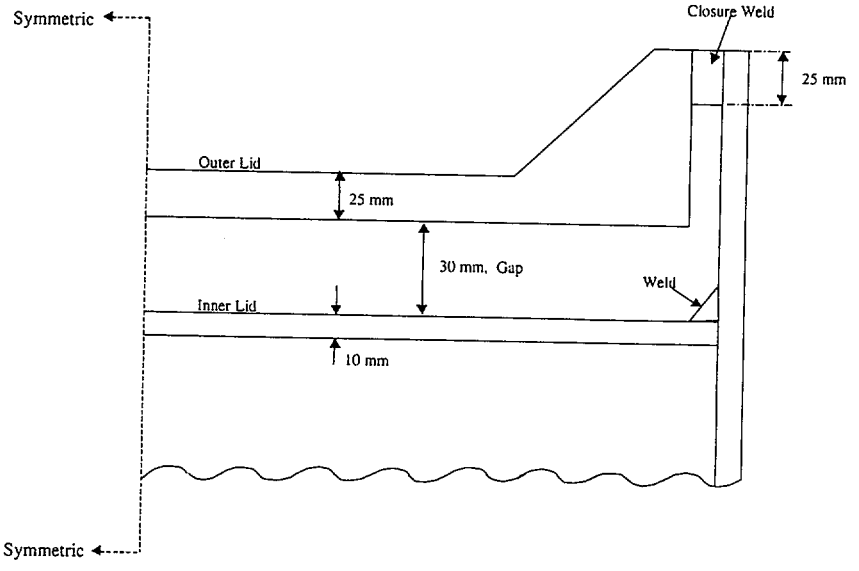

Figure 3-66. Schematic of the Dual-Closure-Lid Design for Waste Package Outer Barrier

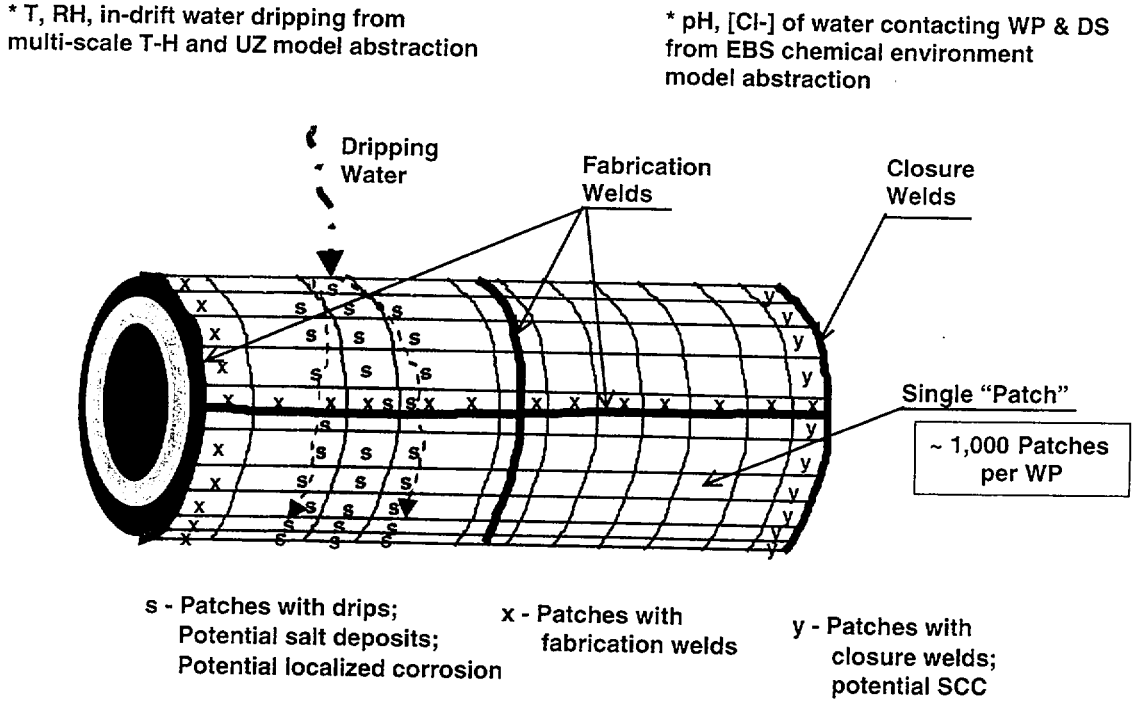

Figure 3-67. Schematic of the Conceptual Model of Stochastic Waste Package Degradation Model (WAPDEG) for TSPA-SR

Figure 3-68 shows a logic flow in the WAPDEG model for waste package (or drip shield) degradation analysis for TSPA-SR. In the figure each of the yellow boxes represents a model abstraction or model abstractions. The logic flow repeats for a drip shield, if included in the analysis, and each container layer of waste package. Exposure conditions that are included in the TSPA-SR waste-package degradation analyses are temperature and relative humidity at the waste package (and drip shield) surface, in-drift water dripping, and pH of the water contacting waste package (and drip shield). The temperature and relative humidity histories at the waste package and drip shield surface are provided from the multi-scale thermal-hydrologic model abstraction. The evolution of pH of solution contacting waste package is provided from the EBS chemical environment abstraction.

In the analysis, the waste package surface RH is tested against the threshold RH (RH_{th}) for corrosion initiation of the waste package. The RH_{th} is based on the deliquescence point of $NaNO_3$ salt as discussed in Section 3.1.3. If the surface RH becomes greater than or equal to the threshold RH, the waste package (or drip shield) undergoes corrosion. Depending on whether it is dripped on or not, it could undergo different corrosion degradation modes. In the current analysis, the same threshold RH is used for both the dripping and no-drip conditions. Both the upper and under sides of drip shield are assumed subject to corrosion if the initiation threshold is met, that is, the RH on the drip shield being equal to or greater than the threshold RH. This is because the both sides are exposed to the exposure conditions in the emplacement drift.

For waste packages that are not dripped on, they undergo humid-air corrosion all the time during the simulation. Under humid-air conditions, the waste packages undergo general corrosion all the time and fail eventually by gradual thinning of the container wall. No localized corrosion occurs in the absence of drips. The general corrosion rates of the waste package outer barrier (and drip shield) are very low (see Section 3.2.2). For the waste package outer barrier and drip shield, the current model assumes the same general corrosion rate distribution for both humid-air general corrosion and aqueous general corrosion (i.e., regardless of whether it is dripped on or not). The WAPDEG model assumes that microbiologically influenced corrosion (MIC) is possible if RH at the surface is greater than or equal to the MIC threshold RH (90% RH) (Section 3.1.5). The MIC effect is modeled with a corrosion enhancement factor, which is applied to the general corrosion rate of the barrier. The enhancement factor has uniform distribution between 1 and 2 (Section 3.1.5). The MIC enhancement factor is applied to the entire surface as long as the RH is above the MIC threshold RH. The drip shield is assumed not subject to microbiologically influenced corrosion (MIC) under the repository exposure condition (CRWMS M&O 2000d; also see Section 3.1.5).

The current model assumes that the Alloy 22 outer barrier is subject to aging and phase instability under the expected repository condition. The effect is modeled with a corrosion enhancement factor that is applied to the general corrosion rate (Section 3.1.4). The aging enhancement factor has uniform distribution between 1 and 2.5 (Section 3.1.4), and is applied to the entire surface of the outer barrier. The drip shield is assumed not subject to aging and phase instability (see Section 3.1.4).

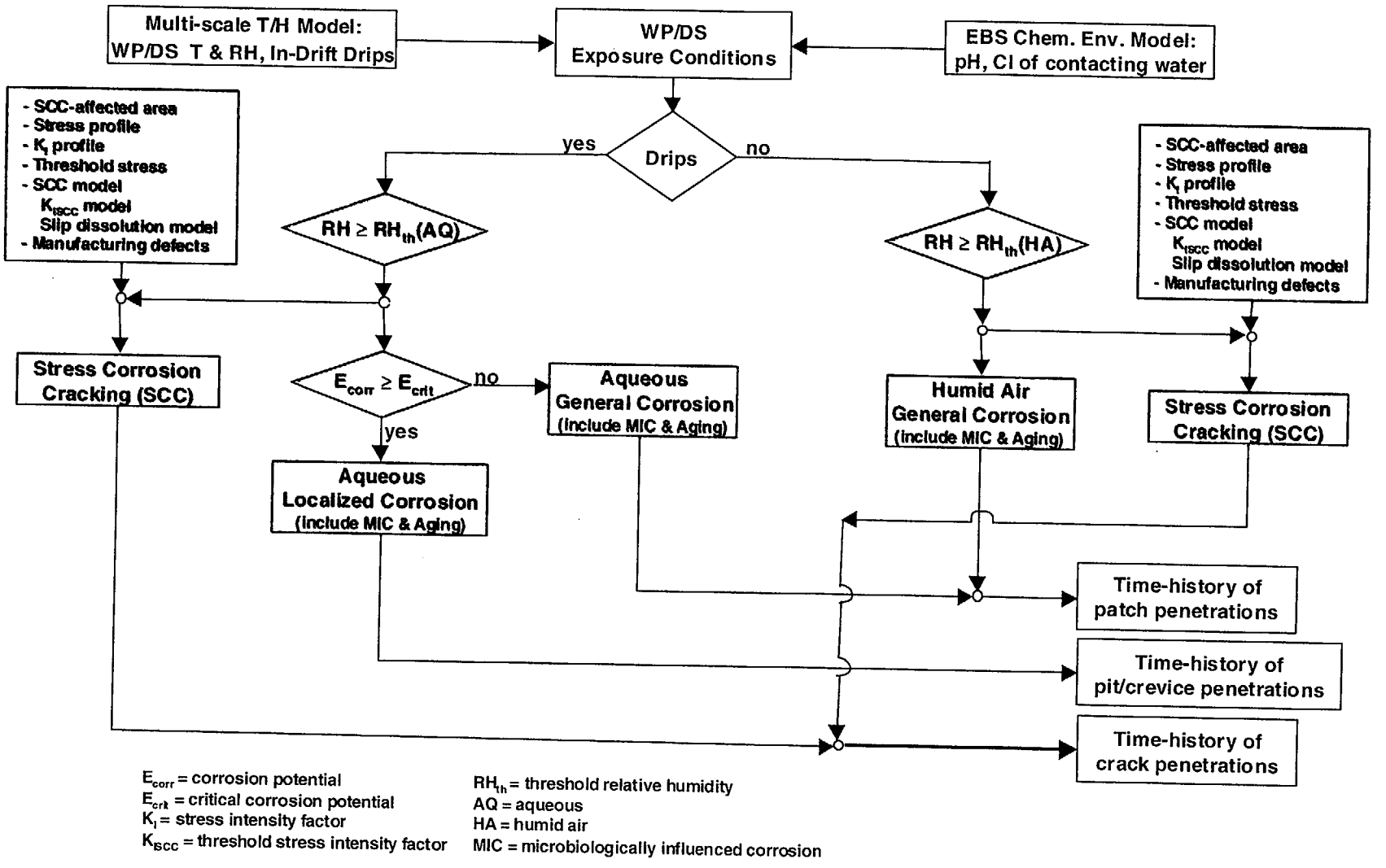

Figure 3-68. Logic Flow for Nominal-Case Model for Waste Package and Drip Shield Degradation Model for TSPA-SR

In the current model SCC is possible if the RH at the waste package surface is greater than or equal to the threshold RH for corrosion initiation (RH_{th}) (i.e., no dripping or highly corrosive water chemistry is not required). As indicated in the logic flow, the input components to the SCC analysis are: (1) the area subject to SCC such as closure-lid welds in the current analysis; (2) stress and stress intensity factor (K_I) versus depth of the affected area; (3) SCC crack propagation model (slip dissolution model or threshold stress intensity factor (K_{ISCC}) model); (4) threshold stress for crack propagation; and (5) manufacturing defect occurrence and size in the affected area.

Both the slip dissolution model and the threshold stress intensity factor model have been incorporated in the WAPDEG model, and a selection between the two models is made with a flag for the model selection. For the SCC analysis with the slip dissolution model, the following should be met before initiating a SCC crack propagation in a patch: (1) the stress intensity factor (K_I) should be positive, and (2) the stress state must be greater than or equal to the threshold stress. In the WAPDEG analysis, for those patches with a compressive stress zone (or layer) in the outer surface, the compressive stress zone is removed by general corrosion, and this delays the application of the slip dissolution model for the crack propagation rate. The delay time depends on the compressive zone thickness and the general corrosion rate sampled for the patch.

The drip shield is assumed not subject to SCC because it will be fully annealed before it is placed in the emplacement drift. Likewise, all the fabrication welds in the waste container, except the welds for the closure lids, are assumed fully annealed and thus not subject to SCC. Therefore, only the closure-lid welds were considered in the SCC analysis.

In addition, pre-existing manufacturing defects in a patch are assumed all surface-breaking, and the defects grow at the general corrosion rate sampled for the patch. This is based on the modeling assumption that the same exposure condition that a patch experiences during a given time step is also applicable to the interior of the defects in the patch. Growth of the defects at the general corrosion rate of the patch is a conservative assumption. Patches with pre-exisiting defects would be subject to SCC earlier than other patches without defect.

For waste package (or drip shield) that is dripped on, the wetted area (or patches) of the waste package by dripping water is assumed to undergo aqueous corrosion if the RH at the surface is greater than the threshold RH. As indicated above, the same threshold RH is used for both the dripping and no-drip conditions. It is assumed that the entire surface of waste package (or drip shield) is wetted by the drips if it is dripped on. While the drip shield is operative (i.e., not failed), the waste package underneath the drip shield is assumed to undergo humid-air corrosion as described above. General corrosion occurs all the time under aqueous corrosion condition. As indicated above, for the waste package outer barrier and drip shield, the current model assumes the same general corrosion rate distribution for both humid-air general corrosion and aqueous general corrosion (i.e., regardless of whether it is dripped on or not). The same MIC and aging and phase instability enhancement factors as under humid-air condition are also applied to general corrosion under aqueous corrosion condition. Also, the same SCC model and inputs are applied for both humid-air and aqueous conditions.

Initiation of localized (pitting and crevice corrosion) corrosion is dependent on the local exposure environment on the wetted patches. In the current analysis, it is assumed that localized

corrosion of the drip shield and waste package outer barrier can initiate only under dripping conditions. This is because of the necessary presence of aggressive ions (such as chloride) in order to initiate and sustain pit and crevice growth and because the only mechanism for these species to gain ingress to the drift is through drips. Localized corrosion of a patch is assumed to initiate if the corrosion potential (E_{corr}) of the patch is greater than or equal to the "threshold" critical corrosion potential (E_{crit}) sampled for the patch. After initiated, localized corrosion continues while $E_{corr} \geq E_{crit}$. If E_{corr} becomes less than E_{crit},, or dripping ceases, localized corrosion stops. Potential for MIC and aging and phase instability effects on localized corrosion is represented with the same corrosion rate enhancement factors as used for general corrosion, that is, the MIC enhancement factor with uniform distribution between 1 and 2, and the aging and phase instability enhancement factor with uniform distribution between 1 and 2.5. These enhancement factors are applied to the localized corrosion rate.

After failure of the drip shield, it is assumed that the dripping water finds the opening(s) in the drip shield regardless of the opening location in the drip shield (i.e., top or side of the drip shield), and the waste package underneath the failed drip shield is assumed to be subject to dripping. Although, in realty, the area of the waste package surface wetted by drips underneath the failed drip shield would depend on the drip rate, and the penetration opening location, size and number in the drip shield, the current model assumes that the entire surface of the waste package is wetted by the dripping water through the drip shield opening (or openings). The waste package is subject to the aqueous corrosion degradation processes (general corrosion, localized corrosion, and SCC) described above.

When waste package fails, the WAPDEG model also considers corrosion degradation of the waste package from the inside-out corrosion. The inside-out corrosion analysis includes general corrosion and localized corrosion of the waste package outer barrier. The inside-out corrosion would cause penetrations by general and localized corrosion in addition to those by the outside-in corrosion only. The inside-out general corrosion is assumed to initiate at the time of the waste package failure. Like the outside-in localized corrosion, initiation of the inside-out localized corrosion is based on the corrosion potential and critical corrosion potential, which are a function of the pH of water inside the failed waste package. The in-package water chemistry results from degradation of the waste form and other internal structural materials (such as basket materials).

The current model does not include the radiolysis enhanced corrosion of waste package outer barrier and drip shield because the materials are not subject to radiolysis enhanced corrosion under the repository conditions (Section 3.1.6). Also the curret model does not consider the rockfall induced mechanical damage to drip shield and its effect on the corrosion because the rockfall effect is assumed insignificant because of the presence of backfill over the drip shield. The bounding analyses have shown that the hydrogen uptake by the drip shield is much less than the threshold hydrogen concentration to cause hydrogen induced cracking (HIC) under the repository exposure condition (CRWMS M&O 2000h), and thus the HIC is not included in the drip shield degradation analysis.

The WAPDEG analysis tracks down corrosion degradation of waste packages for three types of penetration modes: crack penetration by SCC, pit and crevice penetration by localized corrosion, and patch penetration by general corrosion. The analysis provides, as output, the cumulative probability of waste package failure by one of the three penetration modes as a function of time,

and the number of penetrations for each of the penetration modes as a function of time. The waste package failure time and penetration number profiles are used as input to other TSPA analyses such as waste form degradation and radionuclide release rate from waste packages.

In the analysis the HAC condition is defined as an exposure condition for which the RH at the WP surface is equal to or greater than the threshold RH in the absence of drips. APC requires the presence of drips.

3.2.2 Abstraction of General Corrosion Models for Waste Package Outer Barrier and Drip Shield

This section discusses the approaches and assumptions used in the abstraction of GC models for WPOB and DS, and the abstraction results. Details of the abstraction approaches are described in CRWMS M&O (2000i).

3.2.2.1 Approaches and Assumptions

The model abstractions are to develop two cumulative distribution functions (CDFs) each one representing the GC rate distribution for the WPOB (Alloy 22) (CRWMS M&O 2000c, Sections 5.3 and 6.5) and the other for the DS (Titanium Grade 7) (CRWMS M&O 2000d, Sections 5.3 and 6.3). For each alloy, the weight loss and crevice sample penetration rate data were combined to yield one GC rate data set for each alloy. For the WPOB the general corrosion rate data with 6-month, 1-year and 2-year exposure were considered. As shown in Figure 3-69, the variance in the corrosion rate data is reduced with the exposure time, and the median rate decreases also with the exposure time (see Section 3.1.5.4.2). It was concluded that the 2 year data are sufficiently conservative to represent long-term general corrosion rate of the WPOB. Therefore only the 2-year data were used in the model abstraction (i.e., the 6-month and 12-month data were not included). For the drip shield the 12-month data were used in the model abstraction. The cleaning method employed with the 6-month titanium samples caused significant metal loss, thereby yielding unusually high corrosion rates that proved to be artifacts (CRWMS M&O 2000d, Section 6.5.2). Therefore the 6-month data were not included in the abstraction development.

The GC rate data were then sorted in ascending order. Any negative GC rates were then deleted from the data set as suggested in Section 3.1.5. Cumulative probabilities were assigned to each GC data point based on its rank (position) in the sorted data set yielding a CDF. The units of the GC rates were converted from nm per year (reported in Section 3.1.5) to mm per year. An upper bound (corresponding to the 100^{th} percentile cumulative probability) was also applied to the resulting GC rate CDFs. The upper bound was 7.30E-5 mm/year for Alloy 22 (see the assumption below) and 3.25E-4 mm/year for Titanium Grade 7 (see the assumption below). Details of the abstraction approaches are described in CRWMS M&O (2000i).

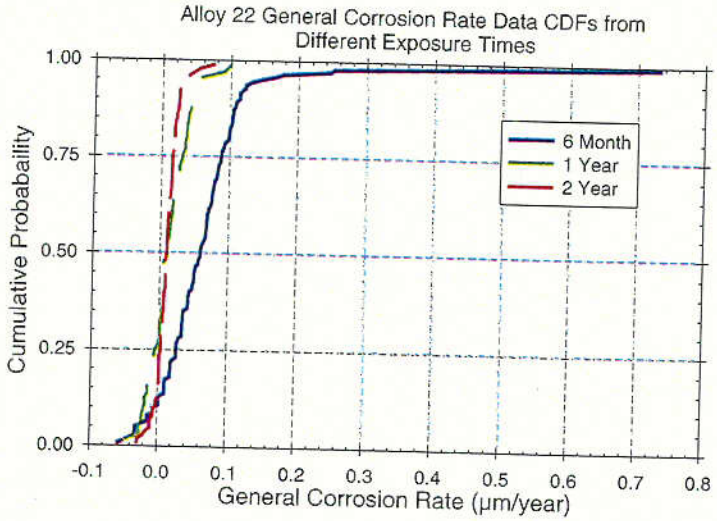

Figure 3-69. Cumulative Distribution Functions for the General Corrosion Rate of Alloy 22 Derived from 6-month, One-Year, and Two-Year Exposure Data

A set of assumptions were employed in the model abstraction. Key assumptions are described below.

- For both alloys considered (Alloy 22 and Titanium Grade 7), corrosion penetration rate data from the weight loss of both plain and creviced geometry test coupons were considered to represent GC penetration rate.

- The maximum GC rate for Alloy 22 was set to 7.30E-5 mm/year. This assumed upper bound is greater than the maximum penetration rate of 7.25E-5 mm/year observed in the LTCTF (Section 3.1.5).

- The maximum GC rate of Titanium Grade 7 was set to 3.25E-4 mm/year. This assumed upper bound is greater than the maximum penetration rate of 3.19E-4 mm/year observed in the LTCTF (Section 3.1.5).

- The Gaussian Variance Partitioning (CRWMS M&O 1998b, Section 5.7.2.2) is an adequate method to separate uncertainty and variability from a distribution that represents the combination of the both. Details of the Gaussian Variance Partitioning technique is described in Section 3.2.2.2 below.

Detailed discussion of the assumptions employed in the model abstraction is given in CRWMS M&O (2000i).

C-23

3.2.2.2 Gaussian Variance Partitioning Technique for Uncertainty and Variability Representation

The Gaussian Variance Partitioning is a technique that decomposes a Cumulative Distribution Function (CDF) containing both uncertainty and variability into two distributions that characterize each element separately. This provides a better conceptual understanding of TSPA model sensitivity to the elements of uncertainty and variability. Gaussian variance partitioning starts with a distribution that involves both uncertainty and variability and then works backward to obtain two separate distributions, one that characterizes variability and another that characterizes uncertainty. This is accomplished by assuming that uncertainty and variability are independent. If the mixed distribution is normally distributed, i.e. $N(\mu,\sigma_\mu^2+\sigma_v^2)$, then it can be represented as a random variable γ having the form

$$\gamma = m + v \qquad \text{(Eq. 3-35)}$$

where m is a normal random variable with mean μ and variance σ_μ^2, and v is a normal random variable with mean zero and variance σ_v^2. Thus, γ is a random variable distributed around the mean μ with a total variance given by the sum of the variances due to uncertainty and variability. If uncertainty is defined as the uncertainty in the mean value and variability as the variance about that mean, then γ can be alternatively parameterized as

$$\gamma \sim N(m,\sigma_v^2), \text{ where } m \sim N(\mu,\sigma_\mu^2) \qquad \text{(Eq. 3-36)}$$

The uncertain mean is represented by the random variable, m, which is normally distributed with mean, μ and variance, σ_μ^2. The random variable, γ, is then the convolution of the distributions of the random variable given by m and a random variable, v, which can be represented by the addition of two normal random variables as given above where

$$m \sim N(\mu,\sigma_\mu^2) \text{ and } v \sim N(0,\sigma_v^2) \qquad \text{(Eq. 3-37)}$$

Thus, given the distributions for m and v, a variability distribution is realized by sampling a value from the parameter uncertainty distribution and adding it to the mean zero variability distribution.

This partitioning method can be extended to non-normal distributions by means of a score transform (Deutsch and Journel 1992, p.138) mapping the percentiles of the non-normal CDF to those of the standard normal by a lookup table. The normal score transforms works best if the non-normal CDF is as symmetric as possible. This may sometimes be accomplished by using the natural logarithms of CDF values. The natural logarithms of the CDF values are used to perform the normal score transformation and the transformed distribution is used to partition the total variance of the transformed distribution between uncertainty and variability. Finally the normal score transformation is applied in reverse to the resultant distributions to obtain a final distribution for variability.

3.2.2.3 General Corrosion Model for Waste Package Outer Barrier

The original cumulative distribution function (CDF) for the GC rate for the Alloy 22 WPOB is shown in Figure 3-70. The CDF is considered a mix of uncertainty and variability of the GC rate. However, quantification of uncertainty and variability in the corrosion rate measurements is limited because the corrosion rates are extremely low and considered to be within the measurement noise. Because of this, it is difficult to separate what the fraction of the total variance in the parent CDF represents the uncertainty and what fraction represents the variability. In the WP degradation (WAPDEG) analysis the fraction for the split of the uncertainty and variability from the parent CDF is treated as an uncertain parameter (CRWMS M&O 2000g). Figure 3-70 also shows, along with the original CDF, the resulting variability CDFs for GC rates using 25%-75%, 50%-50%, and 75%-25% uncertainty and variability partitioning ratios, and 50th uncertainty percentile. Figures 3-71 and 3–72 show the resulting variability CDFs using 25th and 75th uncertainty percentile, respectively.

3.2.2.4 General Corrosion Model for Drip Shield

The resulting original CDF for the GC rate for the Ti-7 DS is shown in Figure 3-73. As with the CDF for the WPOB GC rate, the DS general corrosion CDF is considered a mix of uncertainty and variability of the GC rate. However, quantification of uncertainty and variability in the corrosion rate measurements is also limited because the corrosion rates are extremely low and considered within the measurement noise. Because of those it is difficult to separate what the fraction of the total variance in the parent CDF represents the uncertainty and what fraction represents the variability. In the WP degradation analysis the fraction for the split of the uncertainty and variability from the parent CDF is treated as an uncertain parameter (CRWMS M&O 2000g). Figure 3-73 also shows, along with the original CDF, the resulting variability CDFs for GC rate using 25%-75%, 50%-50%, and 75%-25% uncertainty and variability partitioning ratios, and the 50th uncertainty percentile. Figures 3-74 and 3-75 show the resulting variability CDFs using 25th and 75th uncertainty percentile respectively.

3.2.2.5 Alternative Conservative Model for Waste Package and Drip Shield General Corrosion

As discussed in Section 6.5.5 of CRWMS M&O (2000c), the formation of silica scale deposit on the surface of the Alloy 22 sample coupons could bias the distributions of the original estimated general corrosion rate (shown as "Original Distribution" in Figures 3-70 to 3-72). The potential measurement bias for the weight loss sample coupons was estimated to be 0.063 μm/year (CRWMS M&O 2000c, Section 6.5.5). It was recommended that the distributions of Alloy 22 general corrosion rate be corrected for the maximum bias due to silica scale deposit formation by adding a constant value of 0.063 μm/year to each estimated value of the general corrosion rate (CRWMS M&O 2000c, Section 6.5.5).

In the model abstraction it was assumed that the range of the corrosion rate increase from the scale deposit is represented with uniform distribution between zero (i.e., no scale deposit) and the maximum bias (0.063 μm/year). Then the corrosion rate increment was sampled from the assumed distribution and added to each original estimated value of the general corrosion rate (the CDF shown as "Original Distribution" in Figures 3-70 to 3-72). The resulting general corrosion rate data were sorted in ascending order. Cumulative probabilities were assigned to each GC data point based on its rank (position) in the sorted data set yielding a new CDF. The same data treatment was conducted for the correction of the Ti-7 drip shield general corrosion rate data.

The resulting general corrosion rate CDF for the Alloy 22 WPOB and Ti-7 drip shield is shown in Figures 3-76 and 3-77 respectively, along with their respective original CDF. As shown from comparing the CDFs, the corrosion rate correction causes the median rate (50th percentile value) increased by about 50 percent. Effect of this rate increase on waste package and drip shield degradation is discussed in the WAPDEG analysis results in Section 3.2.7.

Figure 3-78 also shows, along with the original CDF, the resulting variability CDFs for the GC rate abstraction results of the Alloy 22 WPOB using 25%-75%, 50%-50% and 75%-25% uncertainty and variability partitioning ratios, and 50th uncertainty percentile. Figures 3-79 and 3–80 show the resulting variability CDFs using 25th and 75th uncertainty percentile, respectively. The uncertainty and variability partitioning was accomplished using the Gaussian Variance Partitioning technique described in Section 3.2.2.2. A set of new CDFs for the Ti-7 DS general corrosion rate abstraction using 25%-75%, 50%-50% and 75%-25% uncertainty and variability partitioning ratios at 50th, 25th and 75th uncertainty percentile are shown in Figures 3-81 to 3-83 respectively.

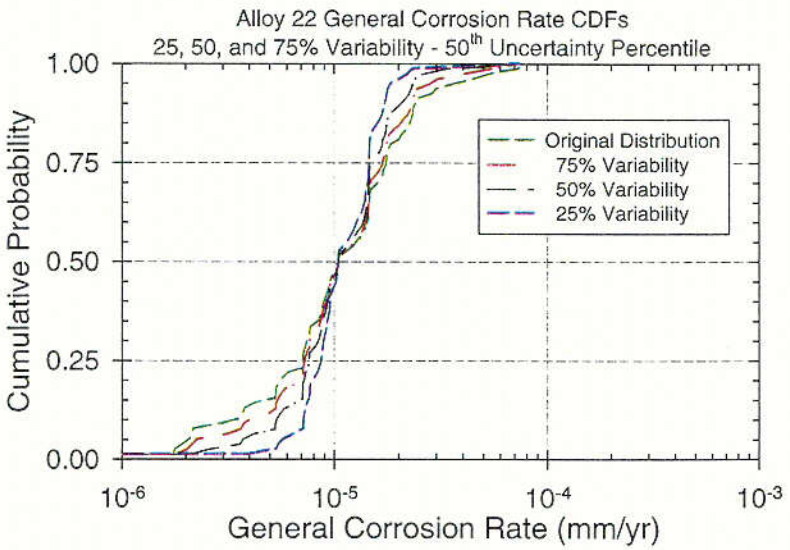

Figure 3-70. The Variability Cumulative Distribution Functions for the General Corrosion Rate of the Alloy 22 Waste Package Outer Barrier Using 25%-75%, 50%-50%, and 75%-25% Uncertainty and Variability Partitioning Ratios and 50th Uncertainty Percentile

C-24

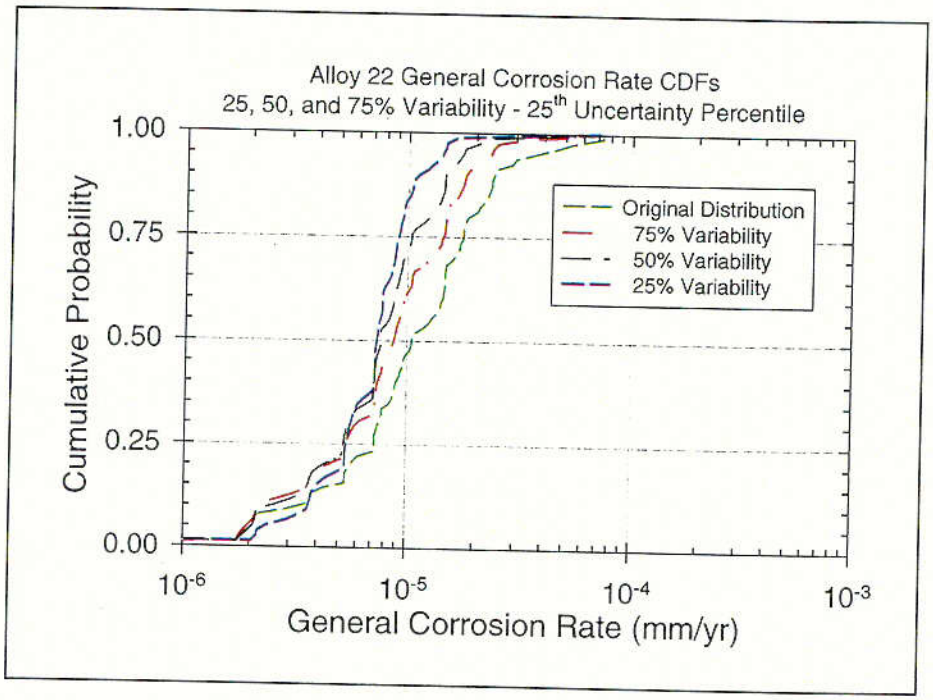

Figure 3-71. The Variability Cumulative Distribution Functions for the General Corrosion Rate of the Alloy 22 Waste Package Outer Barrier Using 25%-75%, 50%-50%, and 75%-25% Uncertainty and Variability Partitioning Ratios and 25th Uncertainty Percentile

C-25

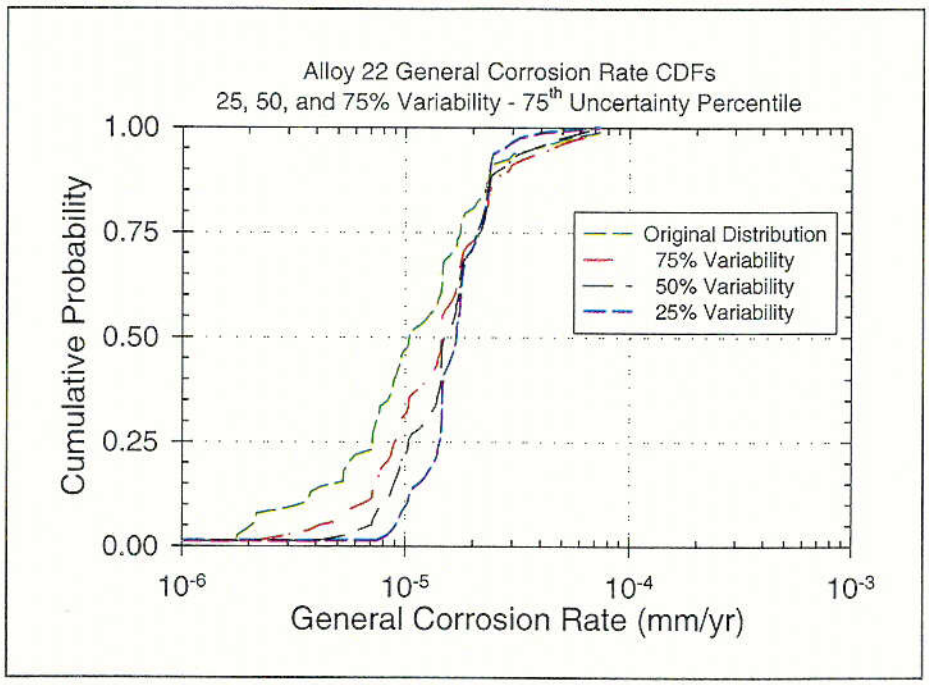

Figure 3-72. The Variability Cumulative Distribution Functions for the General Corrosion Rate of the Alloy 22 Waste Package Outer Barrier Using 25%-75%, 50%-50%, and 75%-25% Uncertainty and Variability Partitioning Ratios and 75th Uncertainty Percentile

C·26

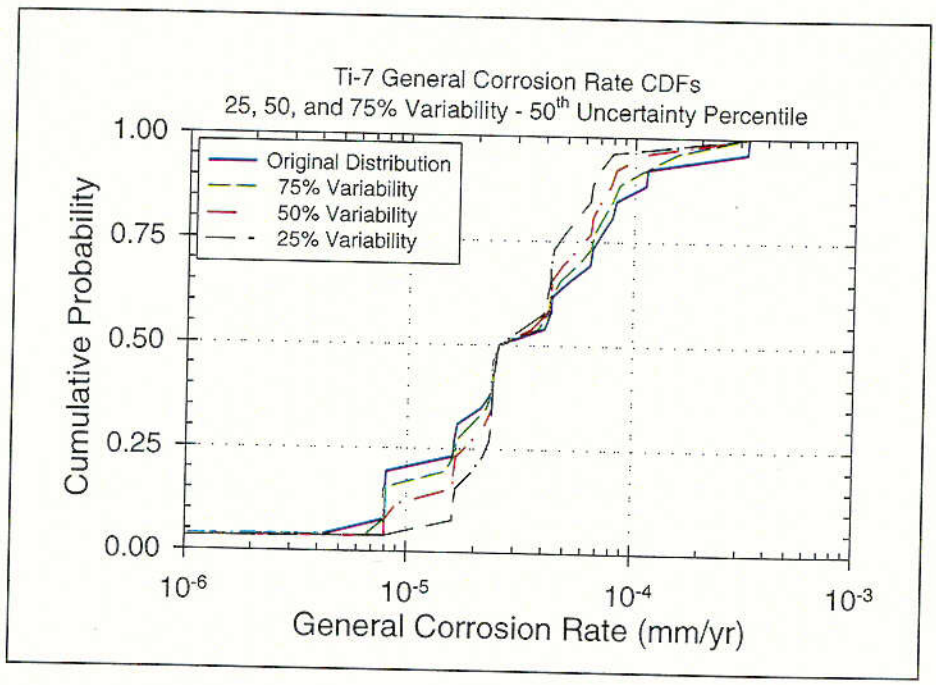

Figure 3-73. The Variability Cumulative Distribution Functions for the General Corrosion Rate of the Ti-7 Drip Shield Using 25%-75%, 50%-50%, and 75%-25% Uncertainty and Variability Partitioning Ratios and 50th Uncertainty Percentile

C-27

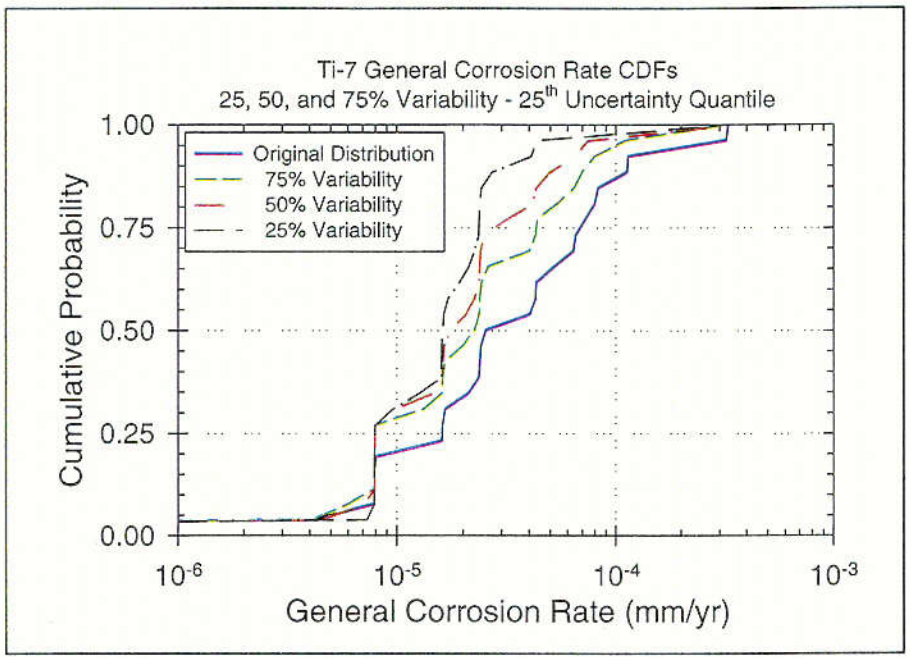

Figure 3-74. The Variability Cumulative Distribution Functions for the General Corrosion Rate of the Ti-7 Drip Shield Using 25%-75%, 50%-50%, and 75%-25% Uncertainty and Variability Partitioning Ratios and 25th Uncertainty Percentile

C-29

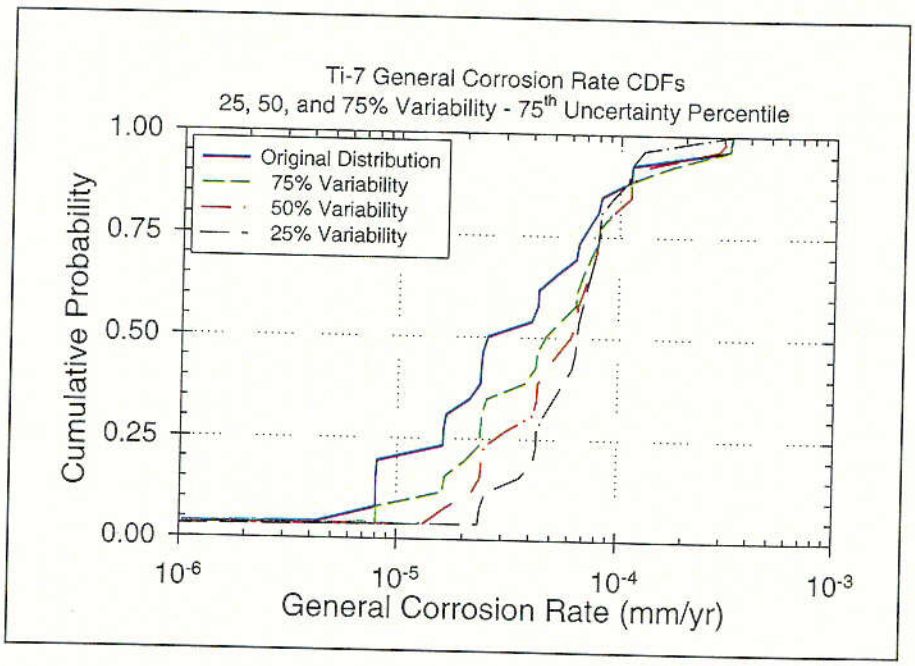

Figure 3-75. The Variability Cumulative Probability Distribution Functions for the General Corrosion Rate of the Ti-7 Drip Shield Using 25%-75%, 50%-50%, and 75%-25% Uncertainty and Variability Partitioning Ratios and 75th Uncertainty Percentile

C-30

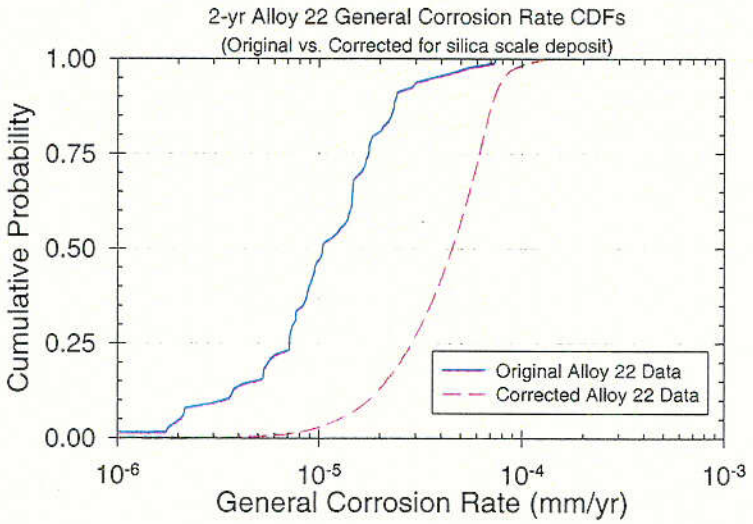

Figure 3-76. Cumulative Probability Distribution Functions for the General Corrosion Rate of Alloy 22 Waste Package Outer Barrier Before (Original) and After (Corrected) Accounting for Bias Due to Possible Silica Scale Deposits

C30-1

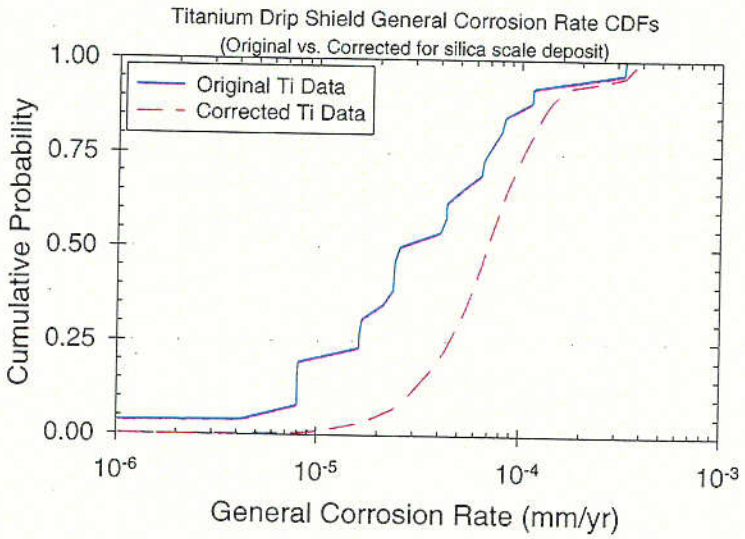

Figure 3-77. Cumulative Probability Distribution Functions for the General Corrosion Rate of the Ti-7 Drip Shield Before (Original) and After (Corrected) Accounting for Bias Due to Possible Silica Scale Deposits

C30-2

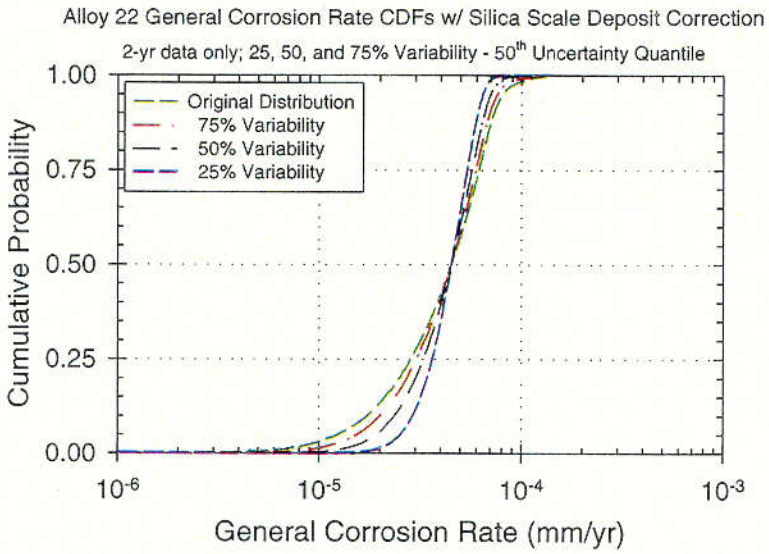

Figure 3-78. The Variability Cumulative Distribution Functions for the General Corrosion Rate of the Alloy 22 Waste Package Outer Barrier with the Silica-Scale Deposit Correction Using 25%-75%, 50%-50%, and 75%-25% Uncertainty and Variability Partitioning Ratios and 50th Uncertainty Percentile

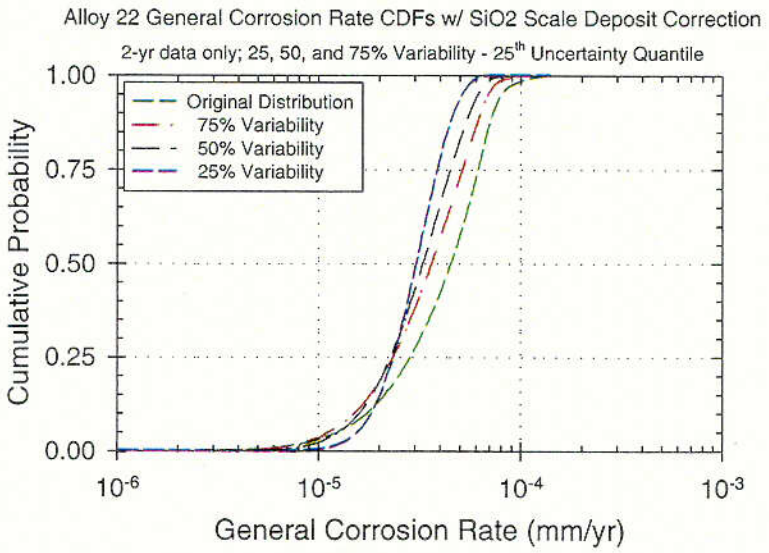

Figure 3-79. The Variability Cumulative Distribution Functions for the General Corrosion Rate of the Alloy 22 Waste Package Outer Barrier with the Silica-Scale Deposit Correction Using 25%-75%, 50%-50%, and 75%-25% Uncertainty and Variability Partitioning Ratios and 25th Uncertainty Percentile

C-31

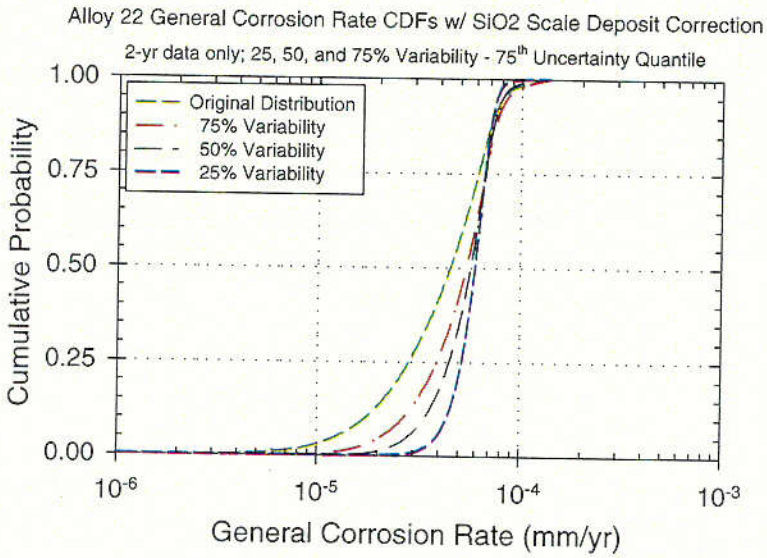

Figure 3-80. The Variability Cumulative Distribution Functions for the General Corrosion Rate of the Alloy 22 Waste Package Outer Barrier with the Silica-Scale Deposit Correction Using 25%-75%, 50%-50%, and 75%-25% Uncertainty and Variability Partitioning Ratios and 75th Uncertainty Percentile

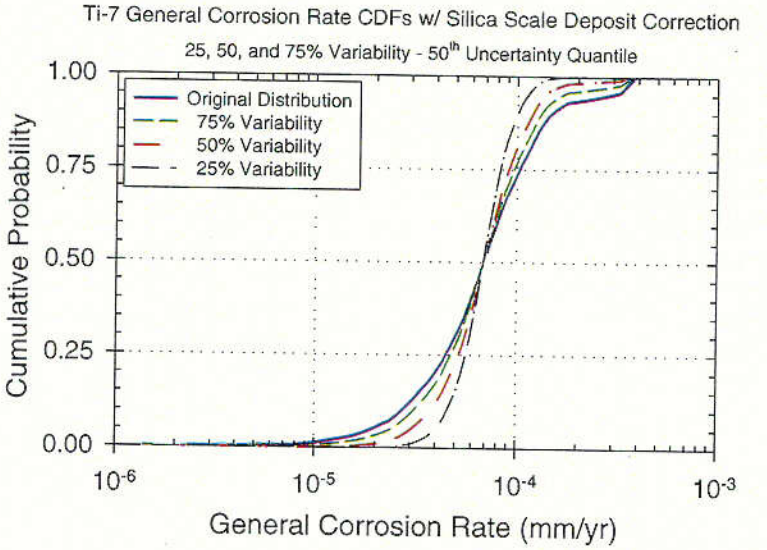

Figure 3-81. The Variability Cumulative Distribution Functions for the General Corrosion Rate of the Ti-7 Drip Shield with the Silica-Scale Deposit Correction Using 25%-75%, 50%-50%, and 75%-25% Uncertainty and Variability Partitioning Ratios and 50th Uncertainty Percentile

C-32

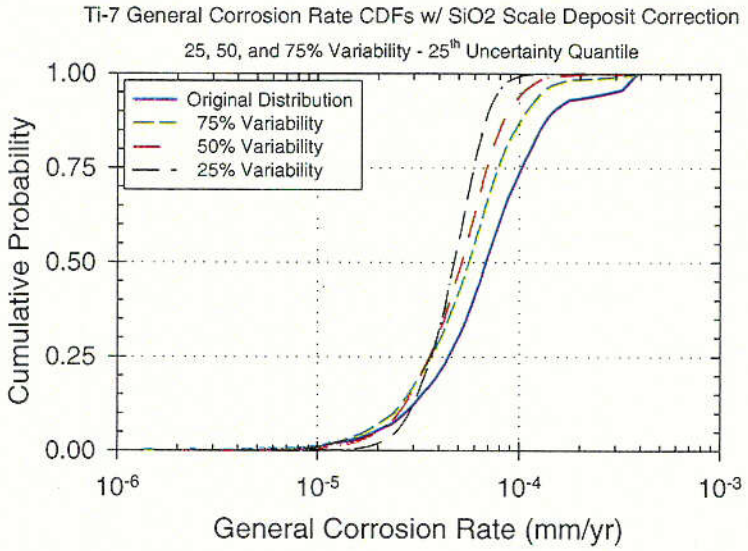

Figure 3-82. The Variability Cumulative Distribution Functions for the General Corrosion Rate of the Ti-7 Drip Shield with the Silica-Scale Deposit Correction Using 25%-75%, 50%-50%, and 75%-25% Uncertainty and Variability Partitioning Ratios and 25th Uncertainty Percentile

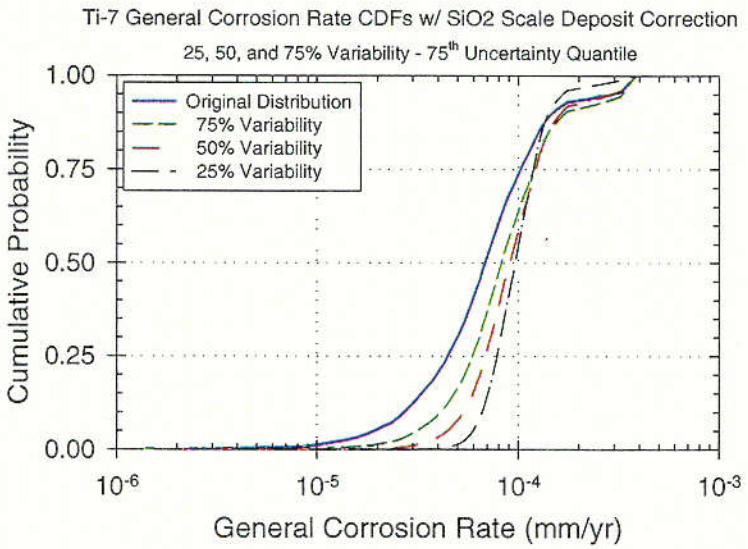

Figure 3-83. The Variability Cumulative Distribution Functions for the General Corrosion Rate of the Ti-7 Drip Shield with the Silica-Scale Deposit Correction Using 25%-75%, 50%-50%, and 75%-25% Uncertainty and Variability Partitioning Ratios and 75th Uncertainty Percentile

C-33

3.2.3 Abstraction of Localized Corrosion Models for Waste Package Outer Barrier and Drip Shield

This section discusses the approaches and assumptions used in the abstraction of localized corrosion (LC) models for waste package outer barrier (WPOB) and drip shield (DS), and the abstraction results.

3.2.3.1 Approaches and Assumptions

The model abstractions are to develop two localized corrosion initiation criteria; one representing the LC initiation criterion for the WPOB (Alloy 22) and the other for the LC initiation criterion for the DS (Titanium Grade 7). As discussed in Section 3.1.6.3, cyclic polarization (CP) measurements were made in several synthetic concentrated J-13 waters. For each CP curve obtained, the critical potential for localized corrosion initiation, E_{crit}, and the corrosion potential, E_{corr}, were determined. The potential difference between E_{crit} and E_{corr} (i.e., $\Delta E = E_{crit} - E_{corr}$) was then fit to a function of relevant exposure parameters. Consistent with the discussion in Section 3.6.1.3, localized corrosion should initiate if $\Delta E < 0$ (i.e., $E_{crit} < E_{corr}$). Details of the abstraction approaches are described in CRWMS M&O (2000n).

A set of assumptions were employed in the model abstraction. Key assumptions are described below.

- "Threshold Potential 1" (see Figures 3-40 through 3-48) was used as the critical potential above which localized corrosion can initiate. This is the lowest (most conservative) of the various critical thresholds discussed in Section 3.1.6.3.
- For both the WPOB (Alloy 22) and the DS (Titanium Grade 7), it was assumed that ΔE varied linearly with relevant exposure parameters.

Detailed discussion of the assumptions employed in the model abstraction is given in CRWMS M&O (2000n).

3.2.3.2 Localized Corrosion Model for Waste Package Outer Barrier

The CP data for the WPOB (Alloy 22) was first used to fit ΔE to a function of absolute temperature, T, the base 10 logarithm of the chloride ion concentration (mol/L), solution pH, and solution pH^2, i.e.,

$$\Delta E = b_0 + b_1 \cdot T + b_2 \cdot log(Cl^-) + b_3 \cdot pH + b_4 \cdot pH^2 + \gamma \qquad \text{(Eq. 3-38)}$$

however, it was found that ΔE exhibited little dependence on absolute temperature or the base 10 logarithm of the chloride ion concentration. Therefore, the CP data for the WPOB (Alloy 22) was used to fit ΔE to a function of solution pH and pH^2 only i.e.,

$$\Delta E = c_0 + c_1 \cdot pH + c_2 \cdot pH^2 + \varepsilon \qquad \text{(Eq. 3-39)}$$

Linear regression gave the following estimates for the parameters in Equation (3-39): $c_o = 1160$, $c_1 = -193$ and $c_2 = 12.0$. The covariance matrix (s) and correlation matrix (C) resulting from the fitting procedure were determined to be:

$$s = \begin{bmatrix} 3530 & -1040 & 64.4 \\ -1040 & 364 & -24.4 \\ 64.4 & -24.4 & 1.69 \end{bmatrix} \quad C = \begin{bmatrix} 1 & -0.915 & 0.835 \\ -0.915 & 1 & -0.982 \\ 0.835 & -0.982 & 1 \end{bmatrix} \qquad \text{(Eq. 3-40)}$$

and the variance of ε determined from the linear regression fitting procedure is 4670.

Figure 3-84 shows a plot of how the median potential difference ΔE given by Equation (3-39) varies with pH. Also shown are the ±3σ and ±4σ confidence intervals.

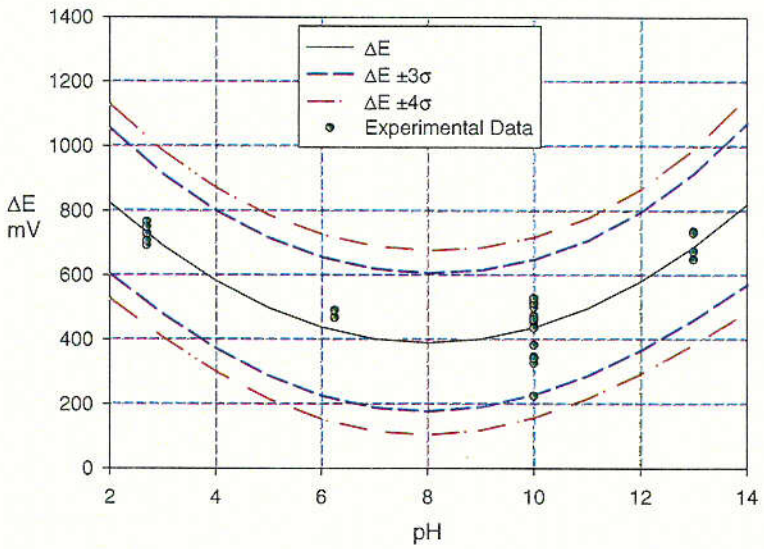

Source: CRWMS, M&O 2000n, Section 6.3.1

Figure 3-84. Plot of ΔE vs. pH for Alloy 22 from Equation (3-39) Showing the ±3σ and ±4σ Confidence Intervals and the CP Experimental Data

The abstraction results in Figure 3-84 shows that localized corrosion of Alloy 22 can not initiate at any pH based on the 4σ confidence interval and based on extrapolation of the repository-relevant experimental data used in the analysis.

3.2.3.3 Localized Corrosion Model for Drip Shield

The CP data for the DS (Titanium Grade 7) was first used to fit ΔE to a function of absolute temperature, T, the base 10 logarithm of the chloride ion concentration (mol/L), and solution pH, i.e.,

$$\Delta E = d_0 + d_1 \cdot T + d_2 \cdot log(Cl^-) + d_3 \cdot pH + \gamma \qquad \text{(Eq. 3-41)}$$

C-34

however, it was found that ΔE exhibited little dependence on absolute temperature or the base 10 logarithm of the chloride ion concentration. Therefore, the CP data for the DS (Titanium Grade 7) ΔE to a function of solution pH only i.e.,

$$\Delta E = f_0 + f_1 \cdot pH + \varepsilon \qquad \text{(Eq. 3-42)}$$

Linear regression gave the following estimates for the parameters in Equation (3-46): $f_0 = 1670$ and $f_1 = -52.2$. The covariance matrix (s) and correlation matrix (C) resulting from the fitting procedure was determined to be:

$$s = \begin{bmatrix} 2040 & -230 \\ -230 & 31.9 \end{bmatrix} \quad C = \begin{bmatrix} 1 & -0.904 \\ -0.904 & 1 \end{bmatrix} \qquad \text{(Eq. 3-43)}$$

and the variance of ε determined from the linear regression fitting procedure is 1080.

Figure 3-85 shows a plot of how the median potential difference ΔE given by Equation (3-42) varies with pH. Also shown are the ±3σ and ±4σ confidence intervals.

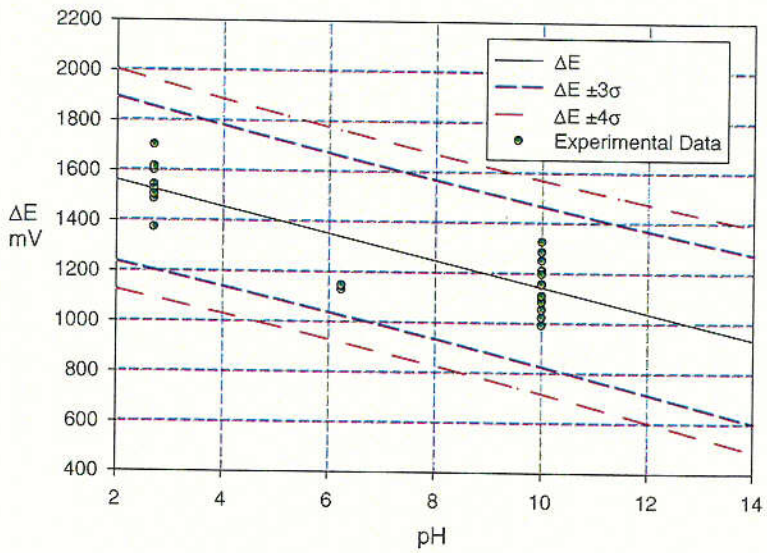

Source: CRWMS, M&O 2000n, Section 6.4.1

Figure 3-85. Plot of ΔE vs. pH for Titanium Grade 7 from Equation (3-42) Showing the ±3σ and ±4σ Confidence Intervals and the CP Experimental Data

The abstraction results shown in Figure 3-85 indicate that localized corrosion of Titanium Grade 7 can not initiate even at a pH of 14 based on the 3σ and 4σ confidence intervals based on extrapolation of the repository-relevant experimental data used in this analysis.

3.2.4 Abstraction of Slip Dissolution Stress Corrosion Cracking Model

In the current waste package degradation analysis, two alternative stress corrosion cracking (SCC) models, the slip dissolution (or film rupture) model and the threshold stress intensity

C-35

factor (K_{ISCC}) model, are considered (CRWMS M&O 2000f, Section 3.2). In the threshold stress intensity factor model, the threshold stress intensity factor (K_{ISCC}) is used to determine when SCC will occur. Provided that an initial flaw and corrosive environment is present, a SCC failure will occur when the applied stress intensity factor K_I is greater than or equal to the threshold stress intensity factor K_{ISCC} (i.e., $K_I \geq K_{ISCC}$). The slip dissolution model assumes that incipient cracks or defects grow continuously when the oxidation reaction that occurs at the crack tip ruptures the protective film via an applied strain in the underlying matrix. The rate at which the crack grows is a function of the crack tip strain rate and environmental and material chemistries. The theory and fundamentals of the SCC models are described in detail in the process model analysis (CRWMS M&O 2000f, Sections 6.3 and 6.4). As recommended in the process model analysis (CRWMS M&O 2000f, Section 6.4), the slip dissolution model was used to access the SCC degradation of the waste package outer barrier (WPOB) (also see Section 3.1.7.2). This section discusses the approach and methodology used in the abstraction development for the slip dissolution model and the associated parameters.

3.2.4.1 Abstraction Approach and Methodology

The purpose of this analysis is to develop abstractions for the parameters that are associated with the slip dissolution model. In the waste package degradation (WAPDEG) analysis this model is employed to calculate the growth rate of cracks initiated by stress corrosion cracking (SCC). The theory and fundamentals of the model are discussed in detail in the process model analysis (CRWMS M&O 2000f, Section 6). The waste package degradation analysis employs a stochastic approach to model the initiation and propagation of SCC cracks. The major efforts in the abstraction discussed in this section are to develop an approach to represent the uncertainty and variability associated with the SCC initiation and crack propagation processes, and to implement them in the waste package degradation analysis. As discussed in the following section, the associated parameters in the model include two model parameters (A and n), stress intensity factor (K_I), threshold stress, and incipient crack density and size. The nominal-case SCC analysis also includes pre-existing manufacturing defects in the closure-lid welds. Abstractions for the manufacturing defects and the residual stress and stress intensity factor in the closure-lid welds are discussed in Sections 3.2.5 and 3.2.6, respectively. The current abstractions for the model parameters (A and n), threshold stress, and incipient cracks expand the process model analysis results to represent and quantify the uncertainty and variability associated with the parameters (CRWMS M&O 2000f). The abstraction assumes that statistical sampling of the associated model parameter values within their probable range capture the effects of the complex processes affecting the SCC crack initiation and growth rate.

3.2.4.2 Crack Growth Rate Model

The crack growth rate in the slip dissolution model is determined by the following expression in Section 3.1.7.8.2 (CRWMS M&O 2000f, Section 6.4.4).

$$V_t = \overline{A}(K_I)^{\overline{n}} \qquad \text{(Eq. 3-44)}$$

where V is the crack growth rate in mm/s, and K_I is the stress intensity factor in MPa(m)$^{1/2}$. Parameters, $\overline{A}$ *and* $\overline{n}$, in the above equation are expressed as follows (CRWMS M&O 2000f, Section 6.4.4; also see Section 3.1.7.8.2).

$$\overline{A} = 7.8\text{x}10^{-2}\text{n}^{3.6}\left(4.1\text{x}10^{-14}\right)^{n} \quad \text{(Eq. 3-45)}$$

$$\overline{n} = 4n \quad \text{(Eq. 3-46)}$$

Parameter "n" (referred to also as the repassivation potential slope) is a function of environmental and materials parameters such as solution conductivity, corrosion potential, and alloy composition (i.e., chromium depletion in the grain boundary) (CRWMS M&O 2000f, Section 6.4.2). The variability in the crack growth rate may be represented with potentially varying exposure conditions (n) and stress intensity factor (K_I) among waste packages and also on different locations over a single waste package. However, due to a lack of data, n is considered independent of exposure conditions and alloy composition. In the waste package degradation analysis described in the following section (Section 3.2.5), the value of the parameter is sampled from a range (i.e., from 0.75 to 0.84 as discussed in the next paragraph). Impact of this approach needs to be assessed as additional data and analysis is developed. However, the effect of n on the failure time by SCC is less than the stress intensity factor (K_I) (see Section 3.2.4.5 below). As discussed in Section 3.2.5, the stress intensity factor profile (as a function of depth in the closure-lid weld) varies along the circumference of the closure-lid welds, but the variability is not significant. It is assumed that there is no variability in the profile among waste packages.

The uncertainty associated with the crack growth rate is represented with the uncertainties in the model parameters, i.e., n and K_I. As discussed in Section 3.2.5, the uncertainties associated with the K_I profiles are represented with normal distribution bounded at three standard deviations from the mean profile. Because of a lack of data, the uncertainty associated with n is coarsely defined: uniform distribution between the lower bound 0.75 and the upper bound 0.84 (CRWMS M&O 2000f, Section 6.4.4). The lower bound value for n will be verified from the on-going work (CRWMS M&O 2000f, Section 3.2).

3.2.4.3 Threshold Stress for Crack Growth Initiation

The threshold stress is defined as the minimum stress at which cracks start growing at a rate determined by Equation (3-47). The threshold stress may be represented as a fraction of the yield strength of the material, which varies with temperature (CRWMS M&O 1999f, p. 33). Because the upper limit of the temperature at which corrosion initiates (or stable liquid water can form) is 120.59 °C (CRWMS M&O 2000a, Section 4.1.8, Table 7), the yield strength of Alloy 22 at 125 °C is used. The yield strength was calculated by linearly interpolating the yield strengths at 93 °C (338 MPa) and 204 °C (283 MPa) (CRWMS M&O 1999f, p. 33). The resulting yield strength used for the threshold stress is 322.3 MPa (46.72 ksi). Although the yield strength increases as temperature decreases, the value at 125 °C is used for all the waste package temperatures after corrosion initiates in the repository. This is because there is only a small change in the yield strength of Alloy 22 from 125 °C to the ambient temperature. Potentially marginal variability in the yield strength and thus the threshold stress are ignored in the current analysis.

As suggested in the process model analysis (CRWMS M&O 2000f, Section 6.5.2), the uncertainty in the threshold stress is conservatively represented as 20 to 30 percent of the yield

strength, and uniform distribution is assumed for the uncertainty range. Thus, the resulting uncertainty range for the threshold stress is 64.46 to 96.60 MPa with the assumed uniform distribution between the two values. In the SCC analysis of waste package closure-lid weld with WAPDEG, for each realization (or each run), the threshold stress is sampled from the range with the assumed uniform distribution, and the sampled threshold stress is used for all the closure-lid weld patches of the waste packages under consideration (CRWMS M&O 2000g, Section 6.3.13).

3.2.4.4 Incipient Cracks and Manufacturing Defects

In the SCC process the crack initiation is associated with microscopic crack formation at localized corrosion or mechanical defect sites that are associated with pitting, intergranular attack, scratches, weld defects, planar dislocations, secondary phase precipitates, or design notches (CRWMS M&O 2000f, Section 6.4.2). The crack growth rate increases as the microscopic cracks coalesce, and approaches a steady-state value when a crack can be detected (CRWMS M&O 2000f, Section 6.4.1). The current analysis assumes that a crack depth range of about 20 μm to 50 μm represents the minimum crack depth for which the Slip Dissolution model can be applied. Those cracks are referred to as "incipient" cracks. Exponential distribution with a maximum size of 50 μm and a medium size of 20 μm was suggested for the incipient crack size distribution (CRWMS M&O 2000f, Section 6.5.2). Because the effect of differing incipient crack sizes within the suggested range on crack growth rate is much less than the model parameters (n and K_I), the maximum crack size (50 μm) is used for all the incipient cracks considered in the SCC analysis.

The SCC analysis using the slip dissolution model also considers manufacturing defects in the closure-lid welds. As discussed in Section 3.2.6, in the WAPDEG analysis, the size of the manufacturing defects are sampled for the closure-lid weld patches, and the sampled defect flaws are included in the analysis with the slip dissolution model. Because manufacturing defects are much larger than the incipient cracks, the closure-lid weld patches with manufacturing defects are likely to fail initially by SCC (CRWMS M&O 2000g, Section 6.4).

3.2.4.5 Slip Dissolution Model Analysis

Bounding analyses were performed to examine the model responses for the SCC failure time of the outer lid (25-mm thick) and inner lid (10-mm thick) as a function of the model parameters (n and K_I). The analyses considered two bounding values (0.75 and 0.84) for n (CRWMS M&O 2000f, Sections 3.2 and 6.4.4) and a range of values for the stress intensity factor that is expected in the closure-lid welds (CRWMS M&O 2000f, Attachment I). The threshold stress for crack growth initiation and pre-existing manufacturing defect were not considered in this bounding analysis. The results are shown in Figure 3-86. As shown in the figure, the stress intensity factor is the dominant parameter in the model, and the time to failure by SCC increases exponentially as the stress intensity factor decreases. The failure time by SCC is less than 100 years for the stress intensity factors greater than 20 MPa($m^{1/2}$). The failure time increases to well above 1,000 years if the stress intensity factor is kept below 6 MPa($m^{1/2}$). The analysis demonstrates that, once a SCC crack initiates, it penetrates the closure-lid thickness fast. It also demonstrates importance of stress mitigation in the closure-lid welds to avoid premature failures of waste packages by SCC.

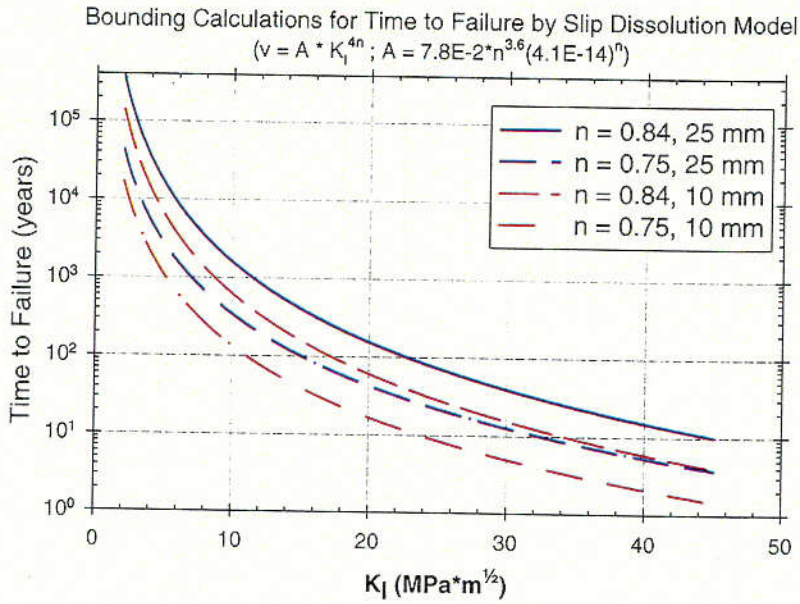

Source: CRWMS, M&O 2000j, Section 6.5

Figure 3-86. Bounding Calculations for the Model Responses for the Time to Failure of the Outer and Inner Closure Lids by SCC Calculated with the Slip Dissolution Model Using the Bounding Values for Parameter *n* for a Range of the Stress Intensity Factor Values

3.2.5 Abstraction of Stress and Stress Intensity Factor Profile in Waste Package Closure Welds

This section discusses the approaches and assumptions used to develop abstracted models for stress and stress intensity factor profiles as a function of depth in the closure-lid welds of WPOB. Two alternative model abstractions are discussed. These are referred to as the realistic-case abstraction and the alternative conservative abstraction, respectively. The resulting abstracted models represent uncertainty and variability of the profiles and used as input to the SCC analysis in the closure lid welds using the integrated WAPDEG (CRWMS M&O 2000g).

3.2.5.1 Approaches and Assumptions used in Realistic-Case Abstraction

The WPOB has dual closure lids (referred to as the outer (25-mm thick) and inner lid (10-mm thick), respectively) (see Figure 1-1). The process model analyses calculated the stress and stress intensity factor profiles along the circumference of the welds for each of the closure lids (CRWMS M&O 2000f). The results were analyzed to develop abstracted models to represent uncertainty and variability of the profiles in the closure-lid welds. In addition, the abstraction was to present the profiles in a format that is suitable for implementation in the integrated WP degradation model (WAPDEG). Details of the abstraction approaches are discussed elsewhere (CRWMS M&O 2000j).

Major assumptions employed in the realistic-case abstraction are described below.

- The hoop stress (and the corresponding stress intensity factor for radial cracks) is the prevailing stress in the closure-lid welds that could lead to SCC through-wall cracks in the closure-lid weld of WPs. Thus, the current abstraction is limited to the profiles for the hoop stress and corresponding stress intensity factor for radial crack.

- The hoop stress (and corresponding stress intensity factor profiles for radial cracks) in the inner lid welds are for a plane that is inclined at about 53 degrees from a plane normal to the outer surface of the inner lid. Because the SCC analysis in the integrated WAPDEG model assumes that cracks propagate normal to the lid surface, the profiles were projected to a plane normal to the outer surface of the lid. The crack orientation used in the abstraction is in the radial direction, which is normal to the hoop stress. As discussed above, the radial crack is considered in the abstraction because the hoop stress was found to be the dominant stress in the closure-lid welds. The hoop stress is likely to be close to the first principal (or maximum) stress. It is assumed the SCC analysis with the projected profiles properly represents the hoop stress and stress intensity factor profiles for the inclined plane.

- The hoop stress and corresponding stress intensity factor profiles as a function of depth in the closure lid welds from the process model analyses (CRWMS M&O 2000f) represent the mean profiles.

- The hoop stress and stress intensity factor profiles vary along the circumference of the closure lid welds, and those represent the variability in the profiles on a given waste package. The angular variation in the hoop stress, $\sigma_t(x)$, where x is the thickness, is given by,

$$\sigma_t(x,\theta) = \sigma_s(x) - (17.236892)\cdot(1-\cos(\theta)) \qquad \text{(Eq. 3-47)}$$

- where θ is angle around the circumference of the waste package closure-lid welds ($\theta = 0$ point arbitrarily chosen). $\sigma_t(x)$ is the mean hoop stress defined in Section 6.3.1 of CRWMS M&O 2000j.

- It is assumed that the same degree of the profile variability is applied equally to all the waste packages in the repository, and there is no variability in the profiles among waste packages.

- The uncertainty range in the hoop stress (and corresponding stress intensity factor profiles based on the hoop stress) is bounded between ± 5% of the yield strength and centered around the mean hoop stress profile. This uncertainty range is sampled through the use of a random variable, z, sampled from standard normal distribution bounded within three standard deviations (± 3 s.d.'s). The hoop stress is multiplied by an uncertain scaling factor, $rscale(\theta,z)$ of the form,

$$rscale(\theta,z) = \frac{\sigma_t(Thck,\theta) + z\cdot\left(\frac{YS\cdot F}{3}\right)}{\sigma_t(Thck,\theta)} \qquad \text{(Eq. 3-48)}$$

where *Thck* is the lid thickness, and *F* is the uncertainty range bound (0.05 or 5%).

- As a crack propagates in the closure lid welds or the weld is thinned by GC, the residual stresses in the welds may re-distribute in such a way that the SCC initiation and crack growth are mitigated (CRWMS M&O 2000f). Such stress re-distribution or relaxation is not considered in the current abstraction. This is a conservative approach.

3.2.5.2 Realistic-Case Abstraction Results for Stress and Stress Intensity Factor Profiles

The abstraction results for the uncertainty range of the hoop stress as a function of depth in the outer closure lid welds (25-mm thick) are given in Figure 3-87. The stress profiles are at a reference location (0° angle) on the circumference of the lid welds. As will be shown later in Figure 3-89, the reference location on the lid weld circumference was selected in such a way that it has the highest hoop stress. The figure shows that the hoop stress in the outer lid weld is compressive at the surface and becomes tensile at a depth of about 8 mm. The uncertainty becomes larger with the weld depth. This is because the stress uncertainty is obtained by multiplying the mean stress by the uncertainty scaling factor in Equation (3-49) and the mean stress increases with the depth. The corresponding stress intensity factor profiles as a function of radial crack depth are shown in Figure 3-88. The stress intensity factor is negative at the surface and becomes positive at a depth of about 12 mm, thus no SCC crack will initiate until the 12-mm thick layer is removed. As with the hoop stress, the uncertainty of the stress intensity factor increases with the weld depth. Figures 3-89 and 3-90 show respectively the hoop stress as a function of depth and the corresponding stress intensity factor as a function of radial crack depth, both at 0°, 90°, and 180° angle along the circumference of the outer-lid welds for a given WP. The reference location designated at 0° angle has the largest hoop stress, and the location at 180° angle has the least hoop stress. As shown in the figures, the variability of the both profiles along the weld circumference in a WP is minor.

The abstraction results for the uncertainty range of the hoop stress as a function of the projected depth in the inner closure lid welds (10-mm thick) are given in Figure 3-91. The stress profiles are at a reference location (0° angle) on the circumference of the lid welds. The hoop stress in the inner lid welds is compressive at the surface, transits to tensile state at a projected depth of about 2-mm, and then back to compressive state at a projected depth of about 8.5-mm. The uncertainty in the profiles is larger for the tensile region in the weld depth. The corresponding stress intensity factor profiles as a function of the projected radial crack depth are shown in Figure 3-92. The stress intensity factor is negative at the surface and becomes positive at a projected depth of about 5 mm, thus no SCC crack will initiate until the (projected) 5-mm thick layer is removed. The uncertainty of the stress intensity factor increases slightly with the weld depth beyond the depth it becomes positive. Figures 3-93 and 3-94 show respectively the hoop stress as a function of the projected depth and the corresponding stress intensity factor as a function of the projected radial crack depth, both at 0°, 90°, and 180° angle along the circumference of the inner-lid welds for a given WP. As shown in the figures, the variability of the both profiles along the weld circumference in a WP is minor.

3.2.5.3 Alternative Conservative Abstraction for Stress and Stress Intensity Factor Profiles

The alternative conservative abstraction uses the same assumptions as the realistic-case abstraction with the exception that:

- The uncertainty range in the hoop stress (and corresponding stress intensity factor profiles based on the hoop stress) is bounded between ± 30% of the yield strength (*YS*) and centered around the mean hoop stress profile. This uncertainty range is sampled through the use of a random variable, *z*, sampled from a triangular distribution with a minimum of –3, a maximum of 3 and a most likely value of zero. An uncertain factor (ΔS) is added to the hoop stress of the form,

$$\Delta S = z \cdot \left(\frac{YS \cdot F}{3} \right) \qquad \text{(Eq. 3-49)}$$

where *F* is the uncertainty range bound (0.30 or 30%).

The abstraction results for the uncertainty range of the hoop stress as a function of depth in the outer closure lid welds (25-mm thick) are given in Figure 3-95. The stress profiles are at a reference location (*0°* angle) on the circumference of the lid welds. The figure shows that the hoop stress in the outer lid welds is compressive at the surface and becomes tensile at a depth between 6 and 10 mm depending on the level of uncertainty used. The corresponding stress intensity factor profiles as a function of radial crack depth are shown in Figure 3-96. The stress intensity factor is negative at the surface and becomes positive at a depth between 3 and about 20 mm depending on the level of uncertainty used. No SCC crack growth will initiate until this layer is removed.

The abstraction results for the uncertainty range of the hoop stress as a function of the projected depth in the inner closure lid welds (10-mm thick) are given in Figure 3-97. The stress profiles are at a reference location (*0°* angle) on the circumference of the lid welds. The hoop stress in the inner lid welds is compressive at the surface, transitions to tensile state at a projected depth between 1 and 2 mm, and then back to compressive state at a projected depth between 6.8 and 9.8 mm. The corresponding stress intensity factor profiles as a function of the projected radial crack depth are shown in Figure 3-98. The stress intensity factor is negative at the surface and becomes positive at a projected depth of about 1.3 mm to 3mm, thus no SCC crack will initiate until this layer is removed. The uncertainty of the stress intensity factor increases slightly with the weld depth beyond the depth it becomes positive. Overall, the increased range of uncertainty of the input parameters to the stress corrosion cracking model should result in an increase in the range of SCC crack failure times.

3.2.6 Abstraction for Manufacturing Defects in Waste Package Closure Welds

This section describes the approaches and assumptions employed in developing abstracted models for the probability and size of manufacturing defects in the waste package closure-lid welds. The abstraction results and their implementation in the waste package degradation (WAPDEG) model for stress corrosion cracking (SCC) analysis are discussed in this section.

3.2.6.1 Approaches and Assumptions

The analyses are to develop abstracted models representing the frequency of occurrence and size of defects potentially found in waste package closure-lid welds. Flaw density and flaw size distributions are obtained from other analyses (see Section 3.1.2; CRWMS M&O 2000m). The

flaw density is used as the parameter for a Poisson distribution used to represent the frequency of occurrence of flaws in a given length of closure weld. The flaw sizes are given as a probability density function on each closure-lid weld.

Major assumptions employed in the abstraction are described below. Further details of the assumptions used in the abstraction analyses are discussed in CRWMS M&O (2000k).

- Only surface-breaking flaws are considered.
- Flaws occur randomly and its occurrence is represented by a Poisson distribution as suggested by the process model analysis (CRWMS M&O 2000m).
- The mean flaw density (Poisson distribution parameter) of the closure weld is from CRWMS M&O (2000m) (0.6839 flaws/meter of one-inch thick weld).
- The fraction of surface breaking flaws is uniformly distributed between the minimum (0.0013) and maximum (0.0049) fractions used to determine the average fraction quoted in CRWMS M&O (2000m). The use of the uniform distribution is a reasonable representation of the uncertainty in expressing this value.
- Pre-inspection flaw sizes are log-normally distributed, with distribution parameters (dependent on the weld thickness) as given in CRWMS M&O (2000m).
- The probability of non-detection is given as a function of flaw size as provided in CRWMS M&O (2000m). The model is dependent on the detection threshold (p), the location parameter (b), and the scale parameter (ν). The location parameter (b) and the scale parameter (ν) are taken to be uncertain with a uniform distribution. The ranges for these distributions are determined from the values identified in the literature as quoted in CRWMS M&O (2000m). This is reasonable, as the manufacturing and detection processes for welds on the waste container are not specified to date. The best that may be modeled at this time are values based on similar industrial manufacturing practices as reported in CRWMS M&O (2000m).
- Results of the residual stress analyses for the closure-lid welds have indicated that the hoop stress (and the radial crack driven by the hoop stress) is the dominant stress that could lead to SCC through-wall cracks in the closure-lid weld (CRWMS M&O 2000f). As a conservative approach, all the surface-breaking manufacturing defects are considered radial cracks and assumed to have a semi-circular shape.

3.2.6.2 Abstraction Results for the Probability and Size of Defect Flaws

Initial (pre-inspection) mean flaw densities and flaw sizes used in the analyses for this calculation were from CRWMS M&O (2000m). Calculation of the outer surface-breaking mean flaw density begins with the base mean flaw density of 0.6839 flaws/meter of weld for a one inch thick stainless steel Tungsten Inert Gas weld (this density was measured from an actual weld performed under shop conditions) subject to radiographic (RT) and dye-penetrant (PT) tests (CRWMS M&O 2000m). To convert this value to a flaw density for an uninspected weld, the

base flaw density is increased by the sum of the flaw reduction factors provided for the RT and PT tests. The adjustment for the RT exam increases the total flaw density by a factor of 12.8 while the PT exam, which detects only surface-breaking flaws, increases the density of only the surface-breaking flaws by a factor of 31.4 (CRWMS M&O 2000m). Next the effect of weld thickness on flaw density is used to adjust for the actual weld thickness on the closure weld. For the 25-mm thick closure weld, the flaw reduction factor (R) is 97.3% (865 divided by 889) (CRWMS M&O 2000m). Multiplying this result by this circumference of the closure-lid weld results in the flaw density per closure weld (or per waste package). A final multiplication by the fraction of surface breaking flaws results in the final mean flaw density of surface breaking flaws per waste-package closure weld.

The resulting cumulative probability for defect flaws for the outer (25-mm thick) and inner (10-mm thick) closure-lid welds are shown in Figure 3-99. Each of the cumulative probabilities in the figure is from 100 realizations with random sampling of the location parameter (b) and the scale parameter (ν) and represent the actual defect probability used in the waste package SCC analysis (CRWMS M&O 2000g). The abstraction results show that at 100th percentile about 18% of waste packages have at least one defect for both the outer and inner closure-lids. At 50th percentile, about 8% of waste packages have at least one defect in the outer closure-lid, and about 7% of waste packages have at least one defect in the inner closure-lid. Figure 3-100 shows several probability density functions for defect sizes in the closure lid welds for various combinations of values for the defect location parameter (b) and the scale parameter (ν). The same probability density functions are used for both the outer and inner lid welds. As shown in Figure 3-100, the size of most defects is between 1 mm and 3 mm. A few defects could have the size up to 4 mm.

3.2.6.3 Implementation of Closure Weld Flaw Abstraction Results in Waste Package Degradation Analysis

The number of flaws that appear on a patch is sampled stochastically as a Poisson random variable. For each flaw that occurs, a flaw size is randomly assigned to it by sampling from the calculated flaw size cumulative distribution function. This flaw's location and size are then used in the SCC analysis. The abstracted results are then input to the waste package degradation model (WAPDEG) to analyze its effect on waste package performance (CRWMS M&O 2000g).

The approach used in this abstraction is that, as these distributions accommodate the variability observed in the occurrence, frequency and size of flaws, some of the parameters that determine these distributions need to be treated as uncertain. The instances of where uncertainty is included are for: (1) the flaw detection distributions (parameters b and ν) and (2) the fraction of surface breaking flaws. The parameters are treated as follows. The b and ν parameters of the detection distribution are allowed to uniformly range between 1.6 to 5 mm and 1 to 3, respectively. The fraction of surface breaking flaws in CRWMS M&O (2000m) is the average of three observations (0.13%, 0.40%, and 0.49%) and is 0.34%. Instead of using the average value of 0.34%, the fraction of surface breaking flaws should be allowed to uniformly range from 0.13 to 0.49%. For a given realization of WAPDEG analysis, the model parameters (defect location parameter (b), defect scale parameter (ν), and fraction of surface-breaking defect fraction) are sampled independently to estimate the probability of a defect occurrence. Then, as discussed above, the number of defects that appear on a patch is sampled stochastically as a

Poisson random variable. Sensitivity analyses with the proposed distributions of the model parameters are needed to analyze the affect of not knowing the correct (deterministic) value of the parameters.

3.2.6.4 Alternative Conservative Abstraction for Defect Probability and Size

Because, as general corrosion proceeds, embedded defects can become surface breaking defects, consideration of pre-existing surface breaking defects only may not be conservative. As an alternative conservative abstraction, both surface breaking defects and embedded defects within the outer ¼ region of the weld surface are considered. Three observations (34.81%, 36.17%, and 36.32%) for the sum of the fraction of surface breaking flaws and the fraction of flaws embedded within the outer ¼ region of the surface (DTN: MO9910SPAFWPWF.001) are used in the alternative conservative abstraction. It is assumed that the flaw fraction is uniformly distributed between the minimum (0.3481) and maximum (0.3632) fractions (DTN: MO9910SPAFWPWF.001). The use of the uniform distribution is a reasonable representation of the uncertainty in expressing this value. The same process as for the case with the surface breaking defect only (Sections 3.2.6.2 and 3.2.6.3) was performed to develop the alternative abstraction, except for the increased flaw fraction range.

The cumulative probability for the average number of defects per waste package in the welds of the outer (25-mm thick) and inner (10-mm thick) lids of waste package outer barrier, considering both surface breaking and flaws embedded within the outer ¼ of the surface, is presented in Figure 3-101. As shown in the figure, with the alternative abstraction, almost 100% of waste packages have at least one defect. At the 50^{th} percentile the outer-lid weld has an average of 18 defects per waste package, and the value for the inner-lid weld is about 15 defects per waste package. An upper bound value for the outer-lid and inner-lid weld is about 40 defects per waste package. The same conditional probability density functions of defect sizes in Figure 3-100 are used with the current alternative abstraction. Because the number of defects per waste package is increased by a factor of about 40, there would be a fairly good probability to sample large defects. A few defects could have the size as large as 5 mm or larger.

Use of the current alternative abstraction in the SCC analysis described in Section 3.2.5 is highly conservative because most embedded defects would be oriented that would not lead to radial cracks. The SCC analysis considers the hoop stress is the dominant stress in the close-lid welds and drives radial crack propagation.

3.2.7 Drip Shield and Waste Package Degradation Analyses

This section reports WAPDEG analysis results for the waste package (WP) and drip shield (DS) degradation. The conceptual model and model logic flow employed in the WAPDEG model are described in Section 3.2.1. The section includes the results for two cases that are likely to represent the "end-members" of potential range of major corrosion model parameter values that could affect long-term performance of waste package and drip shield in the repository. These cases are referred to as (1) realistic case and (2) alternative conservative case.

The WAPDEG model, an integrated model used for WP and DS degradation analysis, is based on a stochastic simulation approach and provides a description of waste package degradation,

which occurs as a function of time and repository location for specific design and thermal-hydrologic modeling assumptions. The corrosion modes that were included in the analyses are:

- Humid-air phase general corrosion of drip shield
- Aqueous phase general corrosion of drip shield
- Localized (pitting and crevice) corrosion of drip shield
- Humid-air phase general corrosion of waste package outer barrier
- Aqueous phase general corrosion of waste package outer barrier
- Localized (pitting and crevice) corrosion of waste package outer barrier
- Stress corrosion cracking (SCC) of closure-lid welds of waste package outer barrier.

In addition, the following corrosion parameters were abstracted and included in the analyses:

- Relative humidity threshold for corrosion initiation of drip shield and waste package outer barrier
- Corrosion potential-based threshold for localized corrosion initiation of drip shield and waste package outer barrier
- Probability of the occurrence and size of manufacturing defects in closure-lid welds of waste package outer barrier
- Stress and stress intensity factor profiles in the closure-lid welds of waste package outer barrier incorporating stress mitigation techniques
- Threshold stress intensity factor (K_{ISCC}) for waste package outer barrier used with the threshold stress intensity factor model
- Threshold stress for the initiation of SCC crack growth for waste package outer barrier used with the slip dissolution model
- Corrosion enhancement factor for aging and phase instability of waste package outer barrier
- Corrosion enhancement factor for MIC of waste package outer barrier.

For the SCC analysis of the waste package closure-lid welds in the WAPDEG analysis, the slip dissolution model has been adopted over the threshold stress intensity factor model (see Section 3.2.4). The threshold stress intensity factor model has also been incorporated in the WAPDEG model, and a switch from the slip dissolution model to the threshold stress intensity factor model and vice versa can be made with a flag for the model selection. For the SCC analysis with the slip dissolution model, the following should be met before initiating a SCC crack propagation in a patch: (1) the stress intensity factor (K_I) should be positive, and (2) the stress state must be greater than or equal to the threshold stress. In the WAPDEG analysis, for those patches with a compressive stress zone (or layer) in the outer surface, the compressive stress zone is removed by general corrosion, and this delays the application of the slip dissolution

model for the crack propagation rate. The delay time depends on the compressive zone thickness and the general corrosion rate sampled for the patch.

In addition, pre-existing manufacturing defects in a patch are assumed all surface-breaking, and grow at the general corrosion rate sampled for the patch. This is based on the modeling assumption that the same exposure condition that a patch experiences during a given time step is also applicable to the interior of defects in the patch. Growth of the defects at the general corrosion rate of the patch is a conservative assumption. Therefore, patches with pre-exisiting defects would be subject to SCC earlier than other patches without defect.

The corrosion enhancement factors for the MIC and aging and phase instability are applied to the general corrosion rate of the waste package outer barrier. No MIC and aging and phase instability factor is applied to localized corrosion rate because no localized corrosion occurs.

For the corrosion models and parameters for which data and analyses are available to quantify their uncertainty and variability, they were represented explicitly in the WAPDEG analysis. Variability in the degradation of the waste packages to be modeled is represented by allocating the total variability variance of the individual corrosion models and their parameters to waste package-to-waste package variability and to patch-to-patch variability within a single waste package. For other corrosion models and parameters that their uncertainty and variability are not quantifiable and that the variance in their value is considered representing a mix of the uncertainty and variability, the fraction of the total variance to separate each other was treated as an uncertain parameter and sampled randomly for each realization. The Gaussian variance partitioning techniques was used to separate the uncertainty and variability from the total variance (see Section 3.2.2.2 for detailed discussions).

Because, except the RH threshold for corrosion initiation, temperature and RH do not affect significantly waste package and DS degradation, a representative set of T and RH histories were used in the current analysis. Also, no separate analysis was conducted for different waste-type waste packages (i.e., commercial spent nuclear fuel waste packages, high-level waste waste-packages, etc.), which could give rise to varying thermo-hydrologic conditions to the DS and waste packages. In addition, the threshold for localized corrosion initiation of DS and waste package outer barrier that requires the presence of drips is much higher than the conditions expected in the repository. Other corrosion models are not dependent on dripping conditions (i.e., drip vs. no-drip). Therefore, no separate analyses were conducted for different dripping conditions. The stainless steel inner layer of waste package was not considered in the analysis. Details of the approaches and assumptions associated with the analyses are described in the supporting report (CRWMS M&O 2000g).

In the Total System Performance Assessment-Site Recommendation analysis, waste package degradation was analyzed with multiple realizations of WAPDEG for the uncertainty analysis of the uncertain corrosion parameters—each WAPDEG realization corresponding to a complete WAPDEG run to represent the degradation variability for a given number of waste package and drip shield pairs. Accordingly, the WAPDEG analysis outputs are reported as a group of "curves" that represent the potential range of the output parameters. The nominal case analysis for waste package and DS degradation constitutes 100 realizations of WAPDEG simulation (or 100 WAPDEG runs) that uses 100 input vectors for uncertain corrosion model parameters and

the simulation parameters that were sampled from their respective range. The major simulation parameters used in the analysis are summarized below:

- Temperature, relative humidity, and contacting solution pH histories in the presence of backfill
- 400 waste package and drip shield pairs
- 20-mm thick waste package outer barrier (Alloy 22) (Note: defense waste co-disposal waste package and naval fuel waste package have a 25-mm thick outer barrier.)
- 15-mm thick drip shield (Titanium)
- 1000 patches per waste package
- 500 patches per drip shield.

The WAPDEG analysis results (i.e., waste package and drip shield failure time and number of crack, pit and patch penetrations) are reported as a group of "degradation profile curves" that represent the potential range of the output parameters. The analysis results will be presented for the upper bound (100^{th} percentile), lower bound (0^{th} percentile), median, mean, and 95^{th}, 75^{th}, 25^{th} and 5^{th} percentiles as a function of time for the following output parameters:

- Waste package first breach (or failure)
- Drip shield first breach (or failure)
- Waste package first crack penetration
- Waste package first patch penetration.

Confidence bounds (or intervals) are produced based on a statistical analysis of the Monte Carlo results. These bounds reflect the uncertainty in the actual percentile value due to the finite number of Monte Carlo realizations. As the actual percentile value is not known, the value is estimated with this estimate itself being a random variable with a distribution (based on the binomial distribution). For the CDF curve the bounds represent a confidence limit (from the estimator distribution) at each percentile level based on the number of realizations, the percentile level, and the values realized. The larger the number of realizations the narrower the confidence interval. The median percentile values are constructed such that, in repeated sampling, the percentile will be above (or below) this median value 50 percent of the time. The 90 percentile confidence interval (given by the 5^{th} and 95^{th} percentile values) will, in repeated sampling, contain the percentile of interest 90 percent of the time.

Note that localized corrosion does not initiate for both the waste package (Alloy 22 outer barrier) and drip shield because the exposure conditions on the drip shield and waste package surface are not severe enough to initiate localized corrosion (i.e., the corrosion potential is less than the critical corrosion potential) (see Section 3.1.6). Therefore no pit or crevice penetration is reported. Also note that the drip shield is assumed not subject to stress corrosion cracking, thus there is no crack penetration failure of drip shield. Thus, for drip shield, the first patch breach time profile is the same as the failure time profile.

3.2.7.1 Realistic Case Analysis Results

Figure 3-102 shows the upper bound (100^{th} percentile), lower bound (0^{th} percentile), median, mean, and 95^{th}, 75^{th}, 25^{th} and 5^{th} percentile confidence intervals of the failure profile of waste packages with time. The upper bound profile, which is the upper extreme of the probable range of the failure time, indicates that the earliest possible failure time of waste package is about 51,000 years. Note that an extremely low probability is associated with the estimated earliest possible failure time. It can be shown by comparing with the upper bound profile in Figure 3-104 (showing the first crack penetration profiles of waste packages with time) that the initial failure is by a SCC crack penetration. The median estimate of the failure time of the upper bound profile is about 120,000 years. The failure time of the median profile is about 80,000 years. The second waste package failure time of the upper bound and median profiles is about 59,000 and 86,000 years respectively. The time to fail 10 percent of waste packages for the two profiles is about 80,000 and 97,000 years respectively.

Figure 3-103 shows the failure profiles of drip shields with time. Because the drip shields are not subject to stress corrosion cracking and localized corrosion, the failure profiles shown in the figure are all by general corrosion only. Both the upper and under sides of drip shield are exposed to the exposure conditions in the emplacement drift and are subject to corrosion. In addition, the both sides experience the same exposure conditions regardless of whether the drip shields are dripped on or not. Thus, in the analysis, the general corrosion rate for the drip shields is sampled twice independently, one for the patches on the upper side and the other for the patches on the under side. This results in reduced variability in the degradation profiles and thus fast failure rate (i.e., many drip shields failing over a short time period). This is shown in the upper bound profile, in which the drip shield failure starts at about 24,000 years and 50 percent of the drip shields fail within a couple of thousand years after the initial failure. Similar trends are also seen with the 95^{th}, 75^{th} and median profiles. In terms of the number of patch penetration openings per failed drip shield with time (not shown here; see CRWMS M&O 2000g, Figure 19), the upper bound profile shows that as the drip shields fail, a large number of patches are perforated over a relatively short time period (a few thousand years). A similar trend is seen for the 95^{th} percentile profile. However, a lot more spread of the failure profile is shown for the other profiles. There is no correlation for the uncertainty and variability split of general corrosion rate between the drip shield and waste package outer barrier.

Figures 3-104 and 3-105 show respectively the first crack penetration and patch penetration profiles of waste packages with time. The first crack penetration time of the upper and 95^{th} percentile profiles is about 51,000 and 61,000 years respectively (Figure 3-104), and the first patch penetration time of the upper and 95^{th} percentile profiles is about 62,000 and 64,000 years respectively (Figure 3-105). Comparison of the first crack and patch penetration profiles with the failure profiles indicates that the initial failure of the waste packages is likely by a SCC crack penetration in the waste package closure lid welds. For the 75^{th} percentile profiles in the figures, the first crack and patch penetration times are about the same (about 72,000 years). For the remaining profiles, the first crack and patch penetration times are reversed.

3.2.7.2 Alternative Conservative Case Analysis Results

The alternative conservative case analysis was to evaluate the effects of alternative conservative model abstractions of several key corrosion model parameters. Those parameters are SCC-related parameters and general corrosion parameters and documented in Sections 3.2.2, 3.2.4, 3.2.5, and 3.2.6. Table 3-13 lists those parameters and their values used in the realistic case and alternative conservative case analyses. As can be seen from the parameter value or its range in the table, this alternative conservative case is likely to represent the wrost case combination of those parameters from the perspective of initial waste package failure time.

Figure 3-106 shows the upper and lower bounds, median, mean, and 95th, 75th, 25th and 5th percentile confidence intervals of the failure profile of waste packages with time. The upper bound profile shows that the earliest possible failure time of waste package is about 12,000 years, much earlier than the realistic case (about 50,000 years, Figure 3-102). Note that the estimated earliest possible failure time has a very low probability. Comparing with the upper bound profile in Figure 3-108 (first crack penetration profiles of waste packages) and Figure 3-109 (first patch penetration profiles of waste packages), it shows that the initial failure is by a SCC crack penetration. The initial failure time of the 95th percentile profile is about 25,000 years. The median estimate of the failure time of the upper bound profile is about 30,000 years, compared to about 120,000 years with the realistic case. The failure time of the median profile is about 50,000 years. The time to fail 10 percent of waste packages for the upper bound and 95th percentile profiles is about 22,000 and 35,000 years respectively.

Figure 3-107 shows the failure profiles of drip shields with time. As with the realistic case analysis (Figure 3-103), the failure profiles shown in the figure are all by general corrosion only. Both the upper and under sides of drip shield are exposed to the exposure conditions in the emplacement drift and are subject to corrosion. In addition, the both sides experience the same exposure conditions regardless of whether the drip shields are dripped on or not. Thus, in the analysis, the general corrosion rate for the drip shields is sampled twice independently, one for the patches on the upper side and the other for the patches on the under side. This results in reduced variability in the degradation profiles and thus fast failure rate (i.e., many drip shields failing over a short time period). As shown in the figure, for the upper bound profile, the drip shield failure starts at about 20,000 years, and 50 percent of the drip shields fail within a thousand years after the initial failure. Similar trends are also seen with the 95th, 75th, mean and median profiles. A little earlier failure times and a tighter overall "spread" of failures of the drip shields are due to the increased general corrosion rate to account for the effect of silica scale deposit on the sample coupons (see Section 3.2.2.5).

Figures 3-108 and 3-109 show respectively the first crack penetration and patch penetration profiles of waste packages with time with the alternative conservative case. The first crack penetration time of the upper and 95th percentile profiles is about 12,000 and 20,000 years respectively (Figure 3-108), and the first patch penetration time of the upper and 95th percentile profiles is about 32,000 and 40,000 years respectively (Figure 3-109). Comparison of the first crack and patch penetration profiles with the failure profiles (Figure 3-106) shows that the initial failures of the waste packages are by a SCC crack penetration in the waste package closure lid welds.

3.2.7.3 Analysis Summary

The waste package and drip shield degradation analyses for the two "end-member" cases (i.e., realistic case and alternative conservative case) have shown that, based on the current corrosion model abstractions and assumptions, both the drip shields and waste packages do not fail within the regulatory time period (10,000 years). From the perspective of initial waste package failure time, the analysis results are encouraging because the alternative conservative case is likely to represent the wrost case combination of key corrosion model parameters that significantly affect long-term performance of waste packages in the repository. In particular, with the realistic case, the waste package service lifetime is predicted to extend far beyond the regulatory time period (failure beginning at about 50,000 years).

The candidate materials for the drip shield (Titanium Grade 7) and the waste package outer barrier (Alloy 22) are highly corrosion resistant. Under the expected repository exposure conditions, these materials are not expected to be subject to the degradation processes that, if initiated, could lead to failure in a short time period. Those degradation modes are localized corrosion (pitting and crevice corrosion), stress corrosion cracking (SCC), and hydrogen induced cracking (HIC) (applicable to drip shield only). Both the drip shield and waste package degrade by general corrosion at very low passive dissolution rate. The current experimental data and detailed process-level analyses, upon which the model abstractions that have been incorporated in the WAPDEG analysis are based, have also indicated that, except the closure-lid welds of waste package, the candidate materials would not be subject to those rapidly penetrating corrosion modes under the expected repository conditions. Complete stress mitigation may not be possible for the closure-lid welds. Because of the potential residual stresses, the closure-lid welds may be subject to SCC. Once a SCC crack initiates, it penetrates the closure-lid thickness in a very short time (see Section 3.2.4.5). Thus stress mitigation in the closure-lid welds is a key design element to avoid premature failures of waste packages by SCC.

The estimated long life-time of the waste packages in the current analysis is attributed mostly to the following two factors: (1) the stress mitigation to the substantial depths in the dual closure-lid welds, which delays the onset of SCC crack propagation until the compressive zone layer is corroded; and (2) the very low general-corrosion rate applied to the closure-lid welds to corrode the compressive stress zones, which renders a long delay time before initiating SCC crack propagation. Substantial uncertainties are associated with the SCC current analyses, especially stress mitigation on the closure-lid welds. The uncertainties associated with the uncertainty range in hoop stress and associated stress intensity factor used in the current SCC analyses will be re-evaluated to further quantify and reduce uncertainties as additional data and analyses are developed. In addition, the alternative conservative abstraction including embedded manufacturing defects in the WPOB closure-lid welds is highly conservative because most embedded defects would be oriented that would not lead to radial cracks. Another major uncertainty in the current analysis is the general corrosion rate applied to the closure-lid welds. The general corrosion model will be refined as additional data and analyses are developed.

Table 3-13. Corrosion Model Parameters Evaluated in the Waste Package and Drip Shield Degradation Analysis for Realistic and Alternative Conservative Cases

Model Parameter	Realistic Case Analysis	Alternative Conservative Case Analysis
WPOB General Corrosion	- 2-year data from the Long-Term Corrosion Testing Facility (LTCTF).	- 2-year data from the LTCTF. - Corrected for potential measurement bias from silica scale deposit on the sample coupons.
DS General Corrosion	- 1-year data from the LTCTF.	- 1-year data from the LTCTF - Corrected for potential measurement bias from silica scale deposit on the sample coupons.
Stress and Stress Intensity Factor (K_I) Uncertainty Range in WPOB Closure-Lid Welds	- ± 5% of yield strength. - Assume nornal distribution bounded at 3 standard deviations around the mean. - Calculate using Eqn. (3-49)	- ± 30% of yield strength. - Assume triangular distribution bounded at the min. and max. and with the mode at the mean. - Calculate using Eqn. (3-50)
Threshold Stress for Crack Propagation	- 20 to 30% of yield strength - Assume uniform distribution between the min. and max.	- 20 to 30% of yield strength - Assume uniform distribution between the min. and max.
Manufacturing Defects Probability in WPOB Closure-Lid Welds	- Include surface breaking defects only.	- Include surface breaking defects and embedded defects in the outer ¼ region of the weld.
Aging and Phase Instability Enhancement Factor for WPOB	- Range from 1.0 to 2.5 applied to WPOB general corrosion rate. - Assume uniform distribution between the min. and max. - Applied to entire surface	- Range from 1.0 to 2.5 applied to WPOB general corrosion rate. - Assume uniform distribution between the min. and max. - Applied to closure-lid welds only.

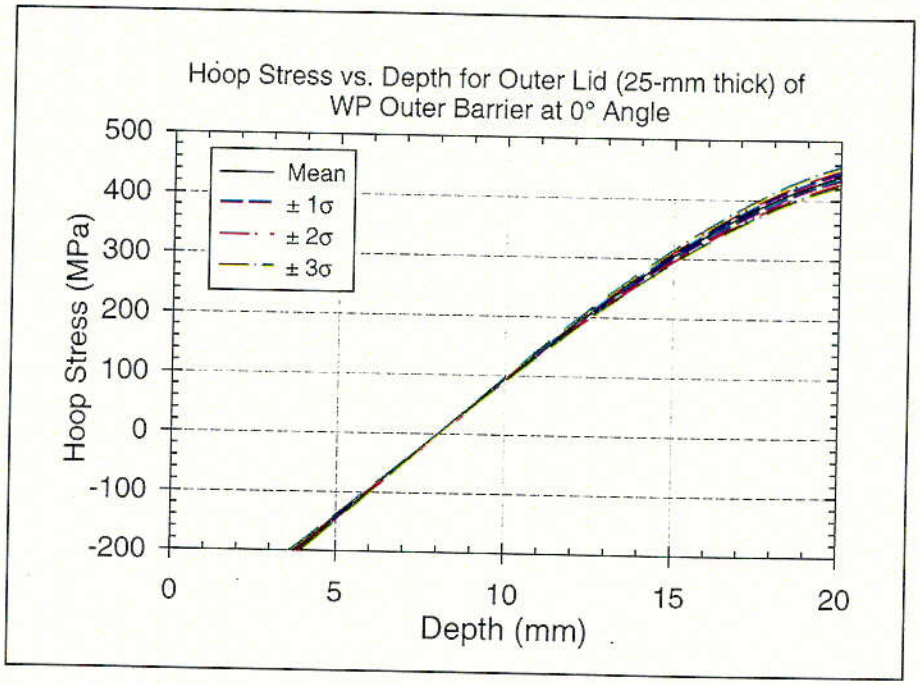

Source: CRWMS, M&O 2000j. Section 6.3.3

Figure 3-87. Hoop Stress as a Function of Depth in the Alloy 22 Outer-Lid Welds (25-mm thick) at the Reference Location on the Outer-Lid Weld Circumference and the Uncertainty Range

CB7

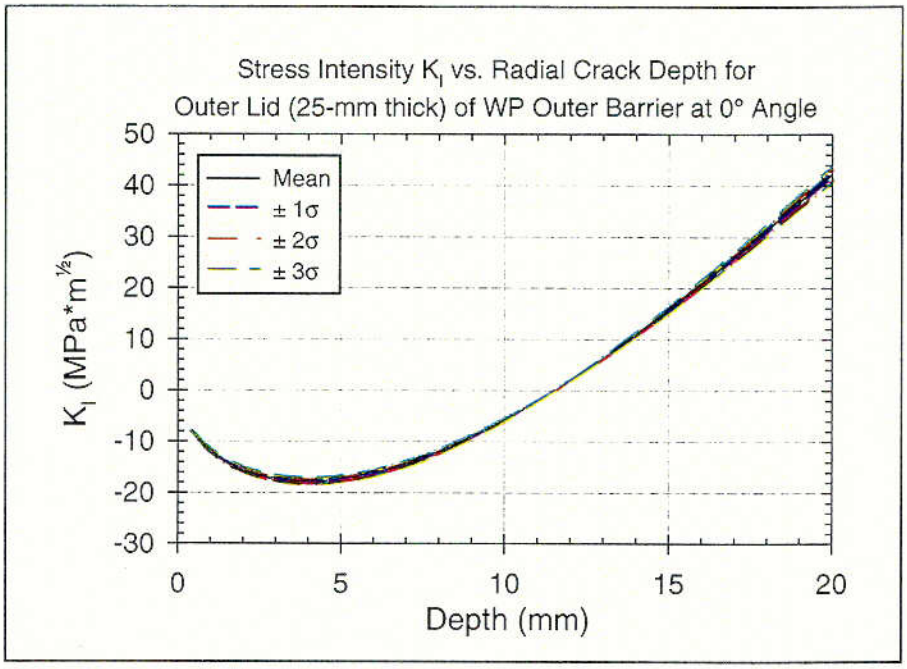

Source: CRWMS, M&O 2000j, Section 6.3.3

Figure 3-88. Stress Intensity Factor as a Function of Radial Crack in the Alloy 22 Outer-Lid Welds (25-mm thick) at the Reference Location on the Outer-Lid Weld Circumference and the Uncertainty Range

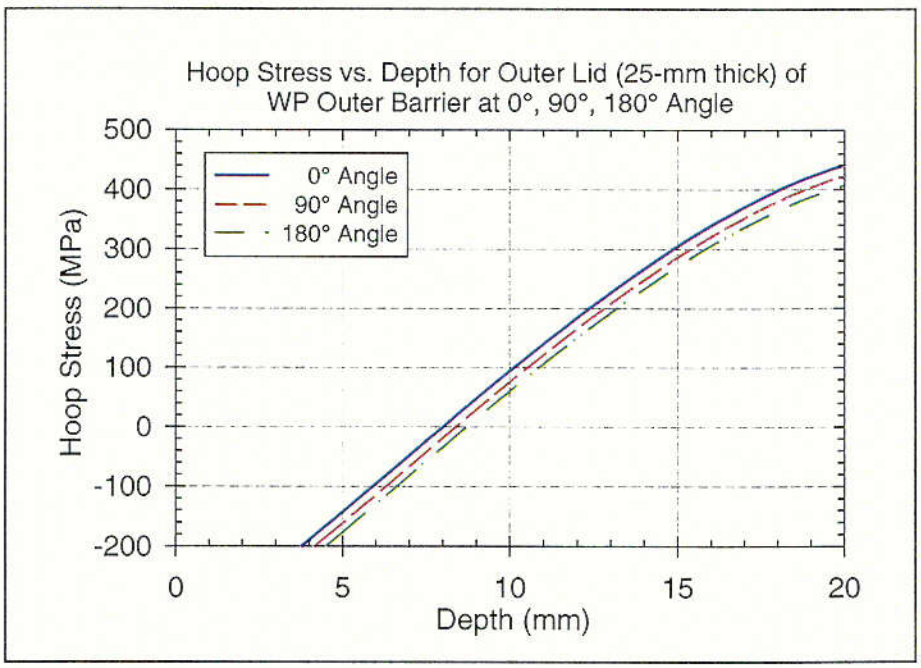

Source: CRWMS, M&O 2000j, Section 6.3.3

Figure 3-89. Hoop Stress as a Function of Depth in the Alloy 22 Outer-Lid Welds (25-mm thick) at 0°, 90° and 180° Angles Along the Circumference of the Outer-Lid Weld

C-38

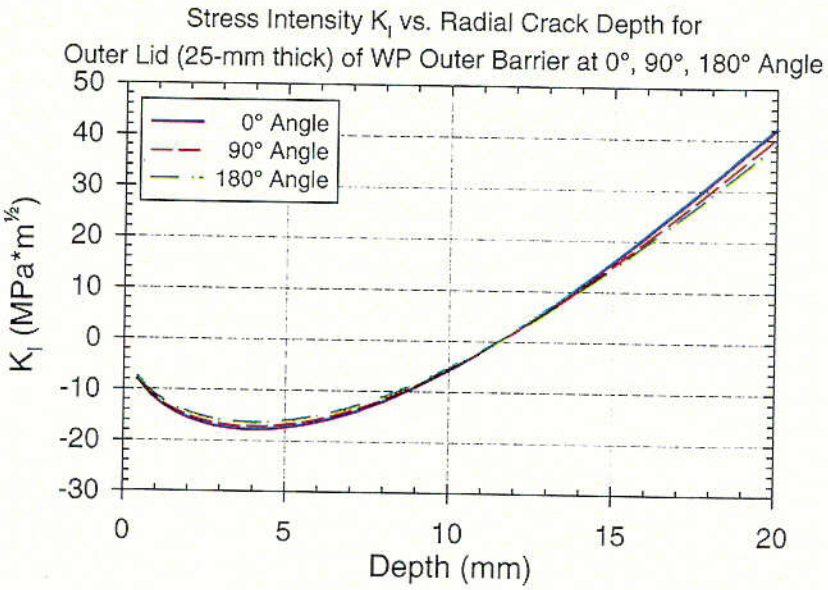

Source: CRWMS M&O 2000j, Section 6.3.3

Figure 3-90. Stress Intensity Factor as a Function of Radial Crack Depth in the Alloy 22 Outer-Lid Welds (25-mm thick) at 0°, 90° and 180° Angles Along the Outer-Lid Weld Circumference

L-39

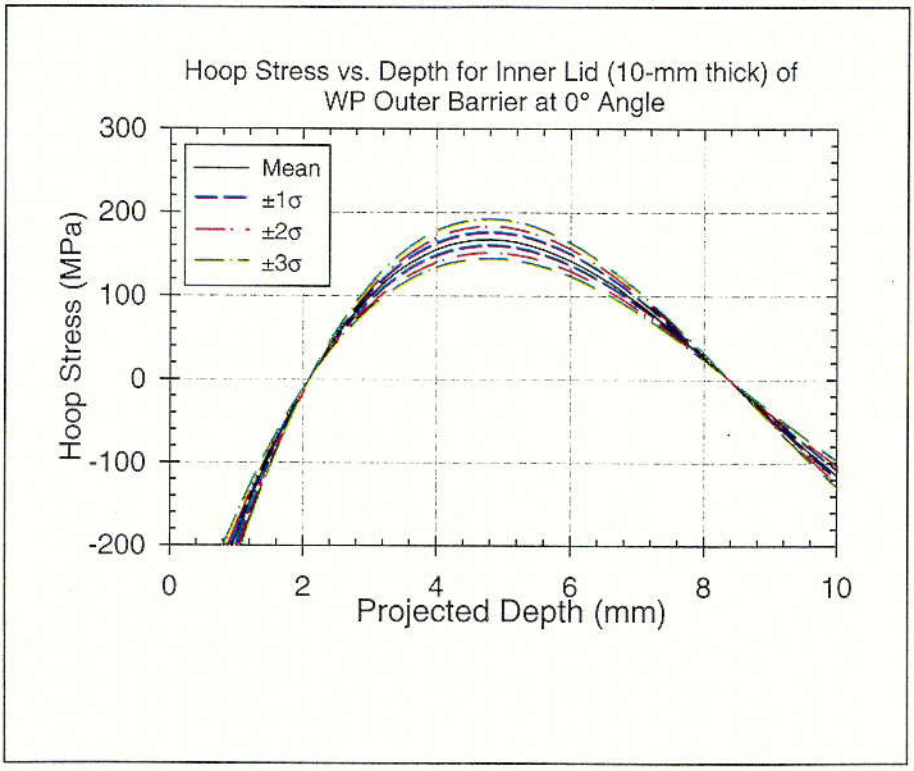

Source: CRWMS M&O 2000j, Section 6.3.3

Figure 3-91. Hoop Stress as a Function of the Projected Depth in the Alloy 22 Inner-Lid Welds (10-mm thick) at the Reference Location on the Inner-Lid Weld Circumference and the Uncertainty Range

C-40

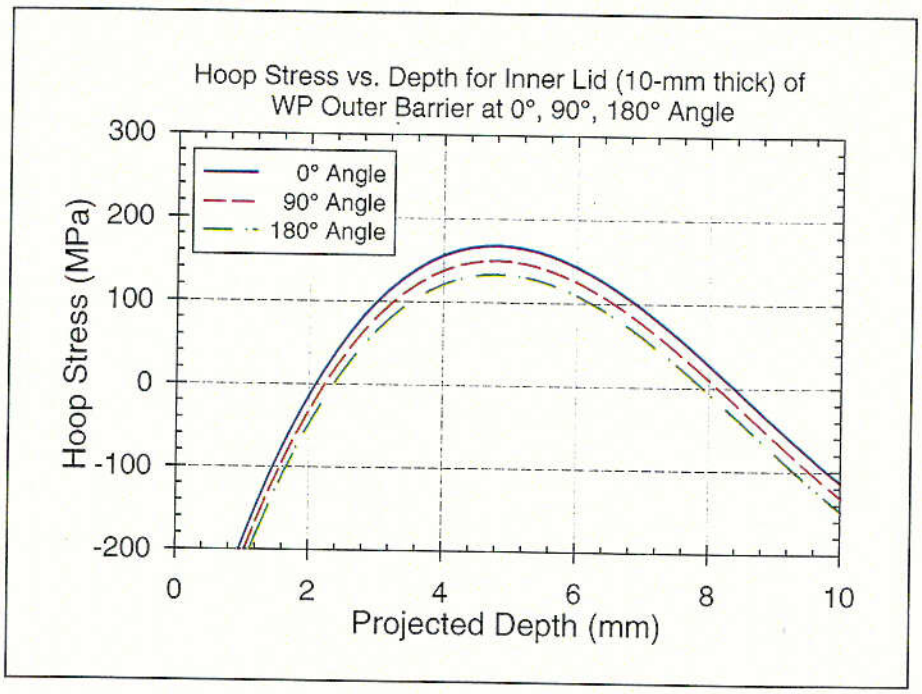

Source: CRWMS M&O 2000j, Section 6.3.3

Figure 3-92. Hoop Stress as a Function of the Projected Depth in the Alloy 22 Inner-Lid Welds (10-mm thick) at 0°, 90° and 180° Angles Along the Circumference of the Inner-Lid Weld

C-41

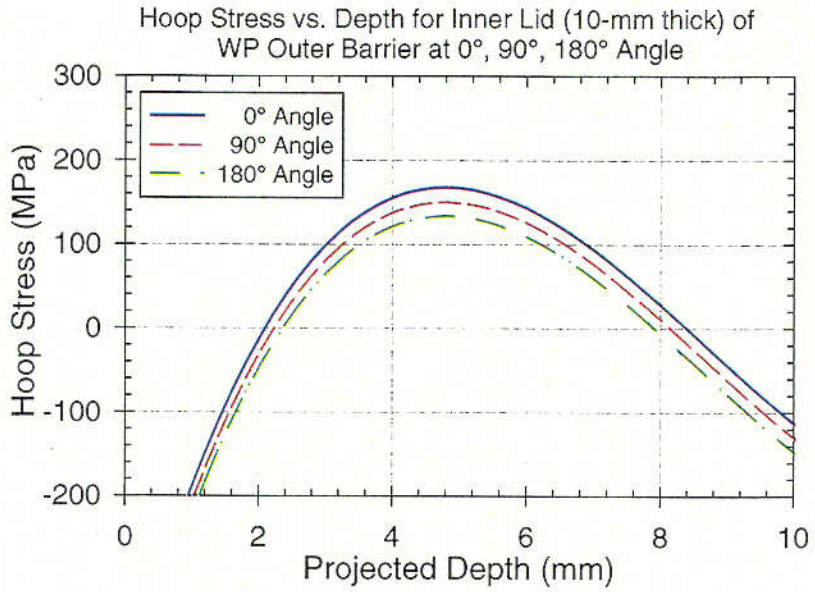

Source: CRWMS M&O 2000j, Section 6.3.3

Figure 3-93. Stress Intensity Factor as a Function of the Projected Radial Crack Depth in the Alloy 22 Inner-Lid Welds (10-mm thick) at the Reference Location on the Inner-Lid Weld Circumference and the Uncertainty Range

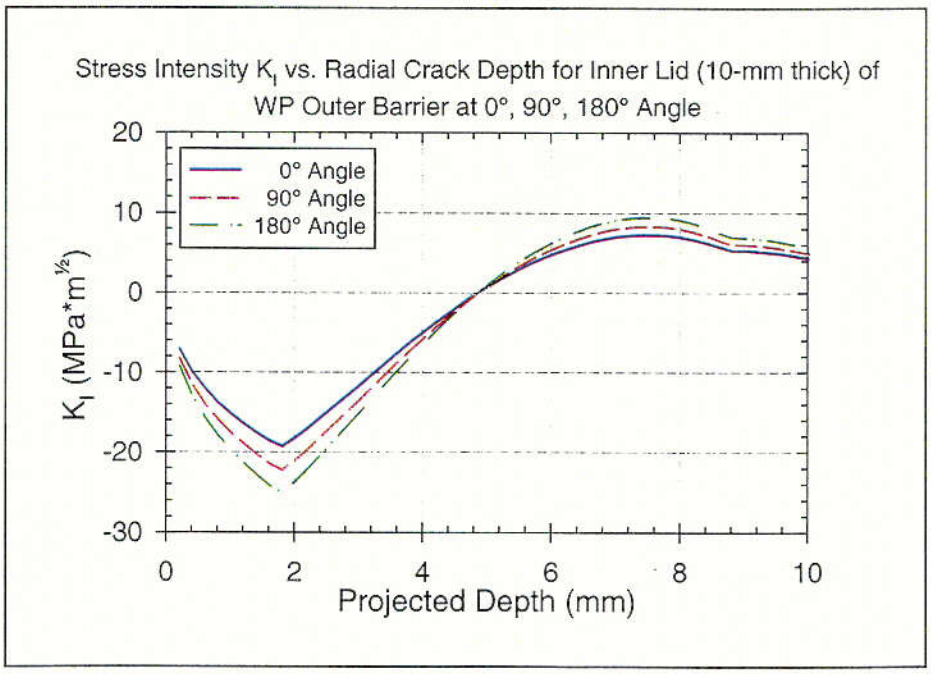

Source: CRWMS M&O 2000j, Section 6.3.3

Figure 3-94. Stress Intensity Factor as a Function of the Projected Radial Crack Depth in the Alloy 22 Inner-Lid Welds (10-mm thick) at 0°, 90° and 180° Angles Along the Inner-Lid Weld Circumference

C-42

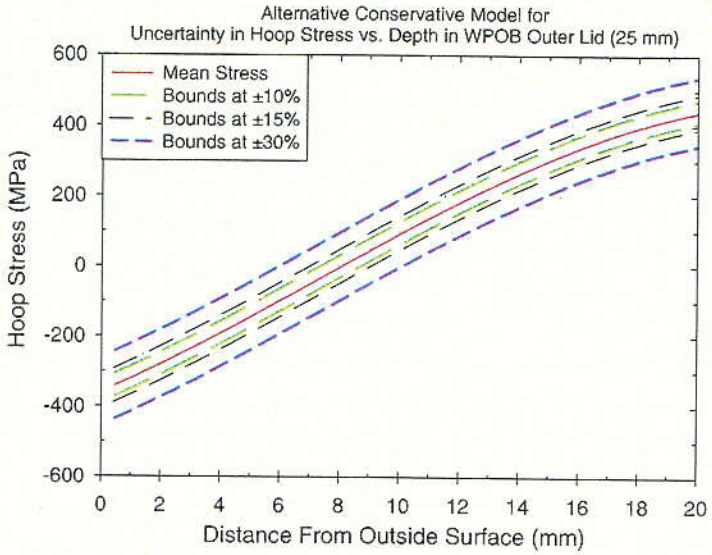

Figure 3-95. Hoop Stress as a Function of Depth in the Alloy 22 Outer-Lid Welds (25-mm thick) at the Reference Location on the Outer-Lid Weld Circumference using Uncertainty Bounds of ± 10, 15, and 30%

C-43

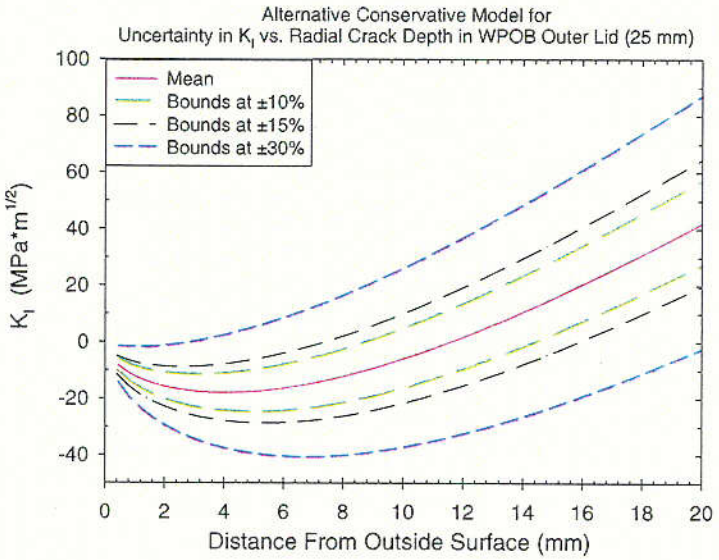

Figure 3-96. Stress Intensity as a Function of Depth in the Alloy 22 Outer-Lid Welds (25-mm thick) at the Reference Location on the Outer-Lid Weld Circumference using Uncertainty Bounds of ± 10, 15, and 30%

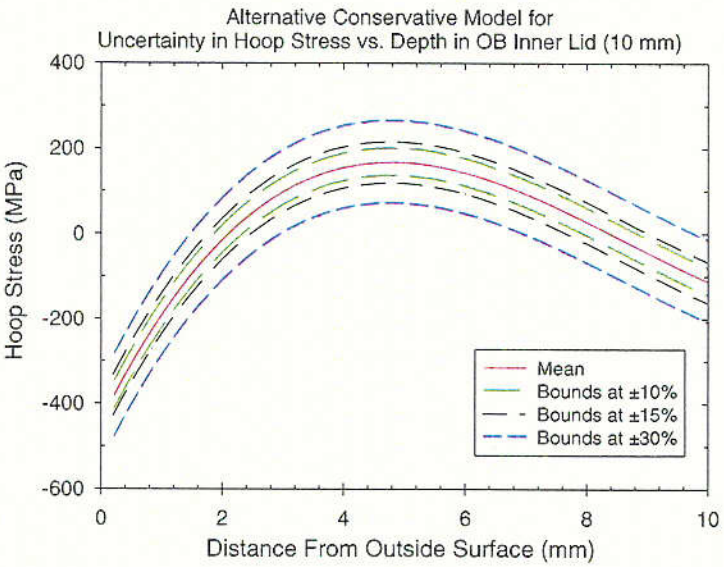

Figure 3-97. Hoop Stress as a Function of Depth in the Alloy 22 Inner-Lid Welds (10-mm thick) at the Reference Location on the Outer-Lid Weld Circumference using Uncertainty Bounds of ± 10, 15, and 30%

C-44

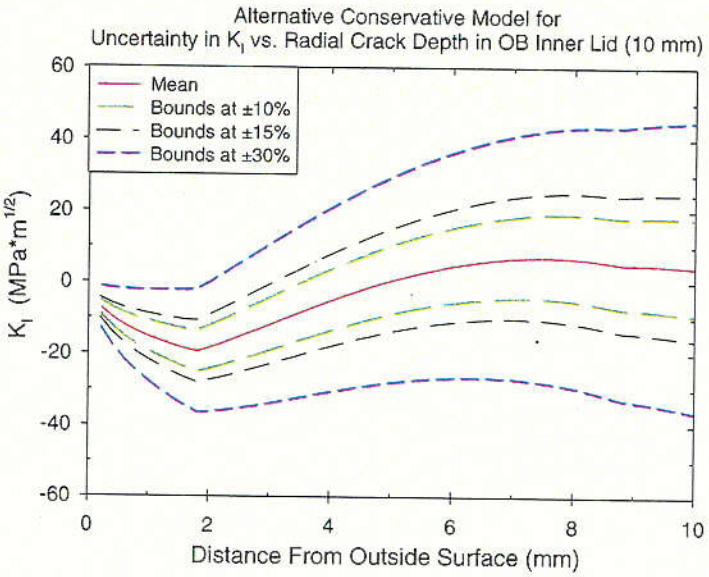

Figure 3-98. Stress Intensity as a Function of Depth in the Alloy 22 Inner-Lid Welds (10-mm thick) at the Reference Location on the Outer-Lid Weld Circumference using Uncertainty Bounds of ± 10, 15, and 30%

C-45

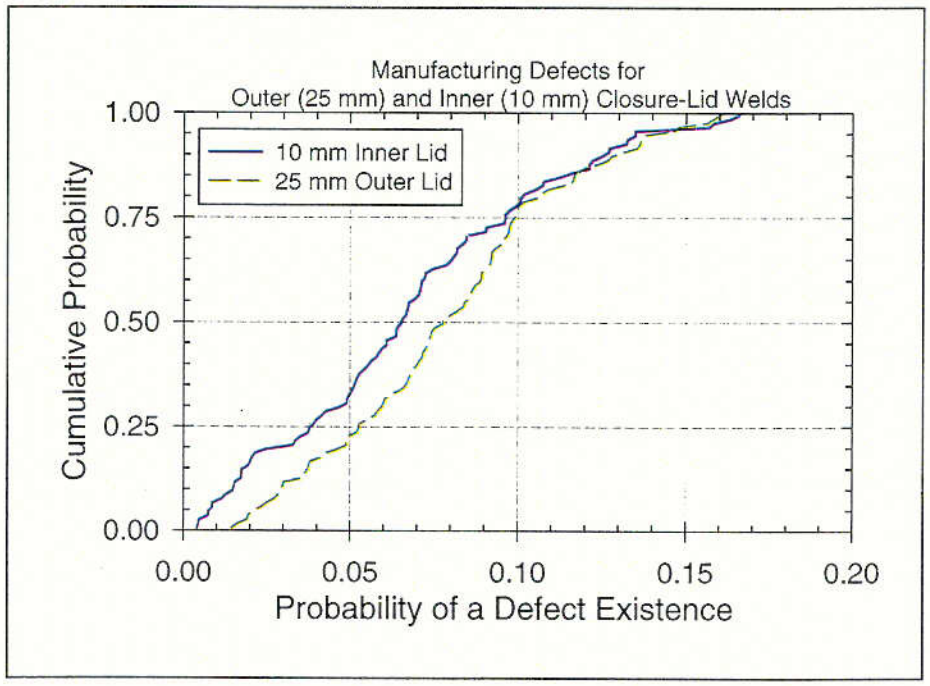

Source: CRWMS M&O 2000j, Section 6.2.2

Figure 3-99. Cumulative Probability for the Occurrence of Defects in the Welds of the Outer (25-mm thick) and Inner (10-mm thick) Lids of Waste Package Outer Barrier (Surface breaking flaws only)

C45-1

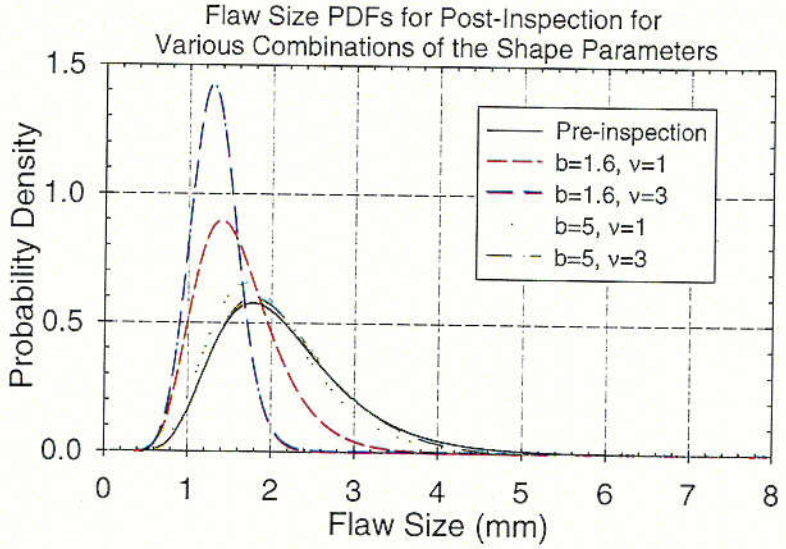

Source: CRWMS M&O 2000j, Section 6.2.2

Figure 3-100. Conditional Probability Density Functions of Defect Sizes in the Closure Lid Welds for Various Combinations of Values for the Location and Scale Parameters (*b* & *v*)

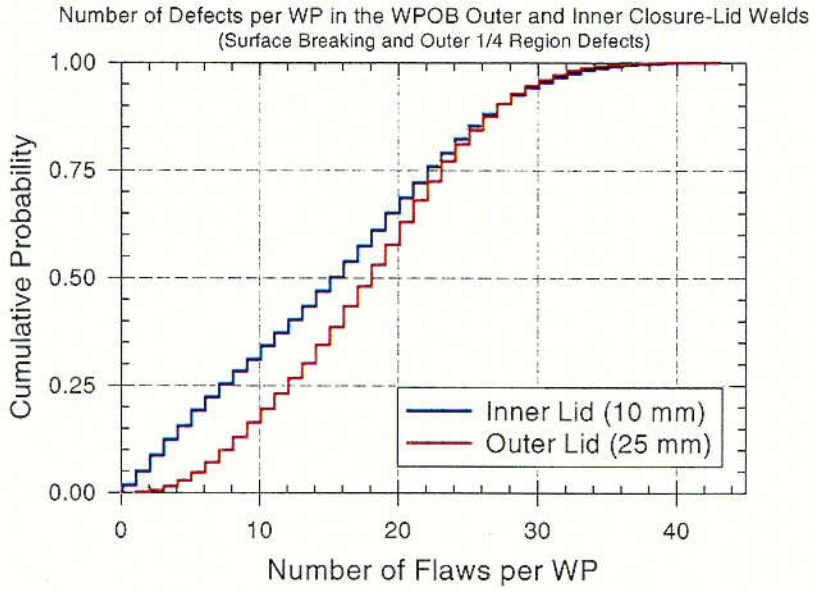

Figure 3-101. Cumulative Probability for the Average Number of Defects per Waste Package in the Welds of the Outer (25-mm thick) and Inner (10-mm thick) Lids of Waste Package Outer Barrier Including Surface Breaking and Embedded Defects

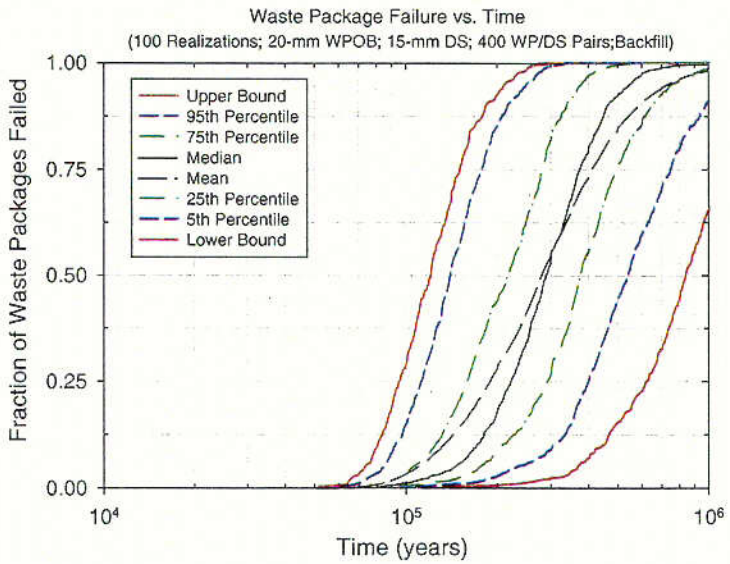

Figure 3-102. The Upper and Lower Bounds, Median, Mean, and 95th, 75th, 25th and 5th Percentile Confidence Intervals of the First Breach Profile of Waste Packages with Time

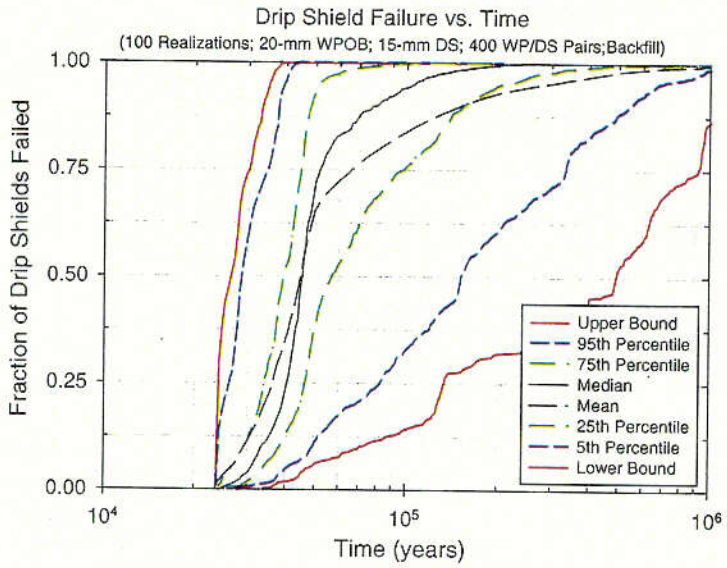

Source: CRWMS M&O 2000g, Section 6.4

Figure 3-103. The Upper and Lower Bounds, Median, Mean, and 95th, 75th, 25th, and 5th Percentile Confidence Intervals of the First Breach Profile of Drip Shield with Time

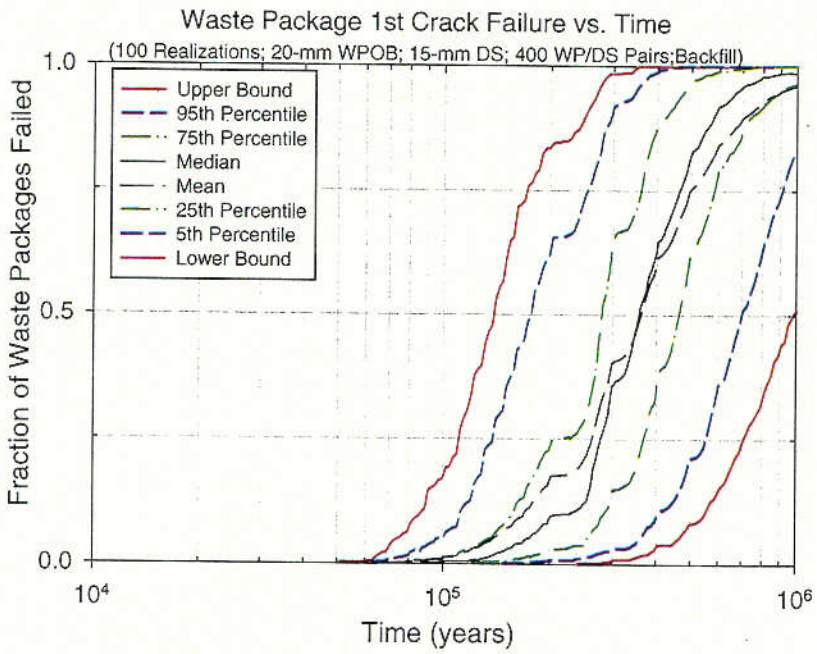

Source: CRWMS M&O 2000g, Section 6.4

Figure 3-104. The Upper and Lower Bounds, Median, Mean, and 95th, 75th, 25th, and 5th Percentile Confidence Intervals of the First Crack Breach Profile of Waste Packages with Time

C-48

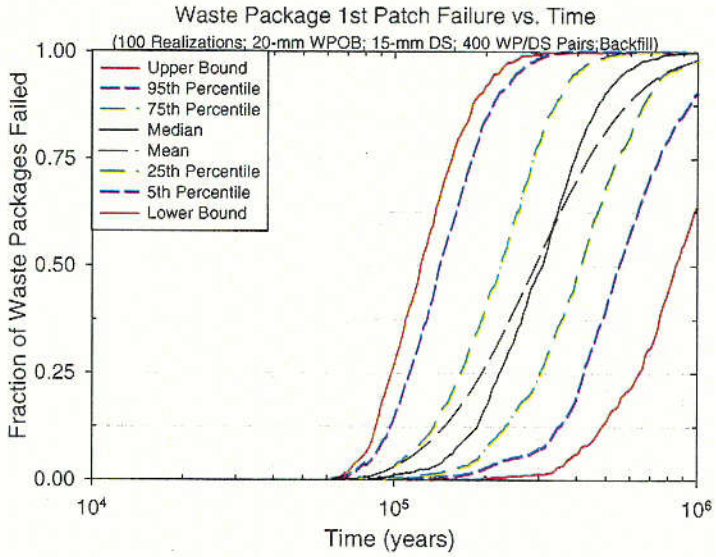

Figure 3-105. The Upper and Lower Bounds, Median, Mean, and 95th, 75th, 25th, and 5th Percentile Confidence Intervals of the First Patch Breach Profile of Waste Packages with Time

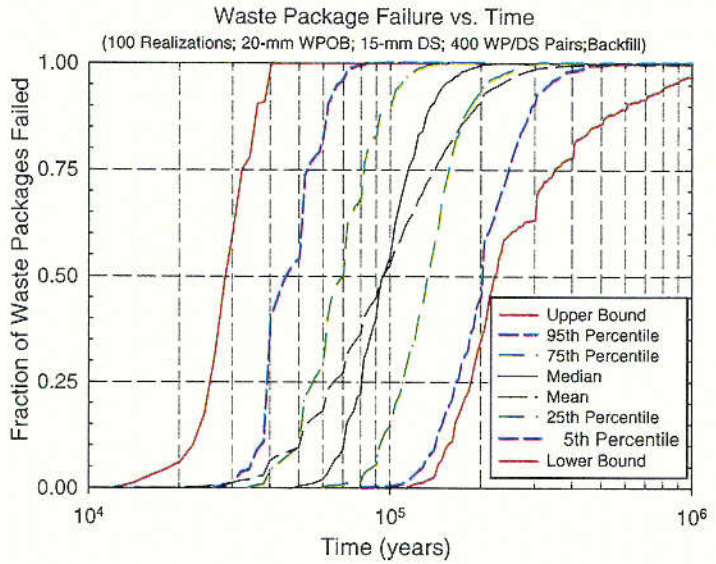

Figure 3-106. The Upper and Lower Bounds, Median, Mean, and 95th, 75th, 25th, and 5th Percentile Confidence Intervals of the First Breach Profile of Waste Packages with Time

C-49

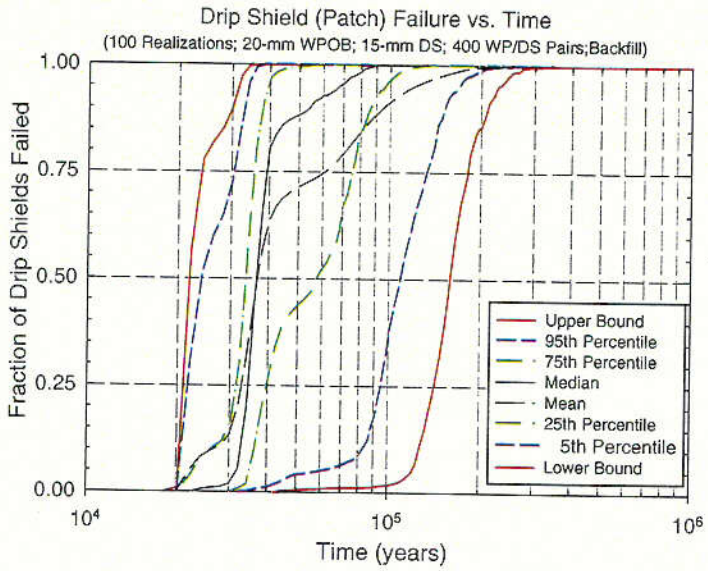

Figure 3-107. The Upper and Lower Bounds, Median, Mean, and 95th, 75th, 25th and 5th Percentile Confidence Intervals of the First Breach Profile of Drip Shield with Time

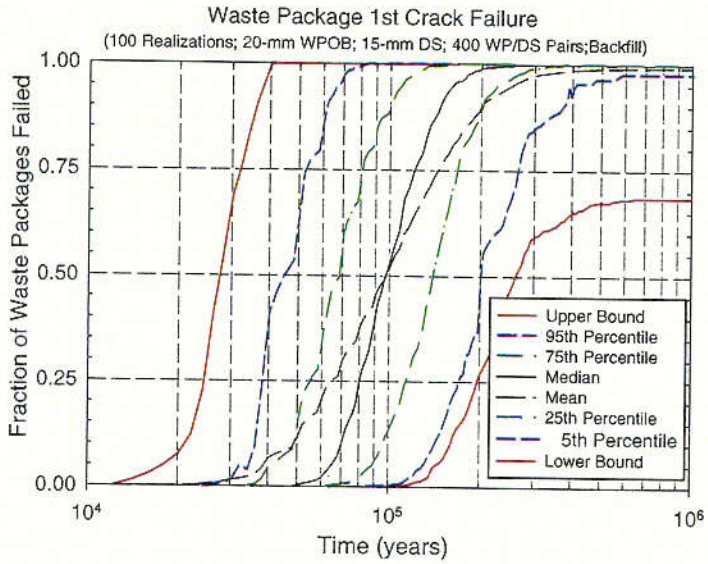

Figure 3-108. The Upper and Lower Bounds, Median, Mean, and 95th, 75th, 25th and 5th Percentile Confidence Intervals of the First Crack Breach Profile of Waste Packages with Time

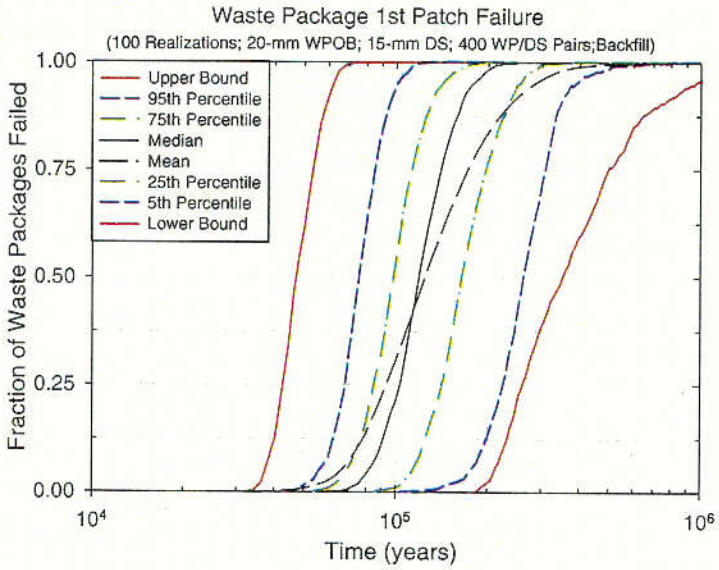

Figure 3-109. The Upper and Lower Bounds, Median, Mean, and 95th, 75th, 25th and 5th Percentile Confidence Intervals of the First Patch Breach Profile of Waste Packages with Time

C-51

INTENTIONALLY LEFT BLANK

4. RELATIONSHIP TO NRC ISSUE RESOLUTION STATUS REPORTS

4.1 SUMMARY OF THE KEY TECHNICAL ISSUES

As part of the review of site characterization activities, the NRC has undertaken an ongoing review of information on Yucca Mountain site characterization activities to allow early identification and resolution of potential licensing issues. The principal means of achieving this goal is through informal, pre-licensing consultation with the U.S. Department of Energy (DOE). This approach attempts to reduce the number of, and to better define, issues that may be in dispute during the NRC licensing review, by obtaining input and striving for consensus from the technical community, interested parties, and other groups on such issues.

The NRC has focused pre-licensing issue resolution on those topics most critical to the postclosure performance of the potential geologic repository. These topics are called Key Technical Issues (KTIs). Each KTI is subdivided into a number of subissues. The KTIs are:

- Activities Related to Development of the EPA Standard
- Container Lifetime and Source Term
- Evolution of the Near-field Environment
- Igneous Activity
- Radionuclide Transport
- Repository Design and Thermal-Mechanical Effects
- Structural Deformation and Seismicity
- Thermal Effects on Flow (TEF)
- TSPA and Integration
- Unsaturated Zone (UZ) and Saturated Zone (SZ) Flow Under Isothermal Conditions.

Identifying KTIs, integrating their activities into a risk informed approach, and evaluating their significance for postclosure performance helps ensure that NRC's attention is focused on technical uncertainties that will have the greatest affect on the assessment of repository safety.

Early feedback among all parties is essential to define what is known, what is not known and where additional information is likely to make a significant difference in the understanding of future repository safety. The Issue Resolution Status Reports (IRSRs) are the primary mechanism that the NRC staff uses to provide feedback to the DOE on the status of the KTI subissues. IRSRs focus on NRC acceptance criteria for issue resolution and the status of issue resolution, including areas of agreement or when the staff has comment or questions. Open meetings and technical exchanges between NRC and DOE provide additional opportunities to discuss issue resolution, identify areas of agreement and disagreement and plans to resolve any disagreements.

Each KTI is subdivided into a number of subissues. For most subissues, the NRC staff has identified technical acceptance criteria that the NRC may use to evaluate the adequacy of information related to the KTIs. The NRC has also identified two cross cutting programmatic criteria that apply to all IRSRs related to the implementation of the QA Program and the use of expert elicitation.

Chapter 4 documents DOE's approach to addressing the acceptance criteria and work performed that is related to the criteria. The following sections provide a summary level discussion of the related KTIs by subissues and specific NRC acceptance criteria.

4.2 RELATION OF THE WASTE PACKAGE PMR TO THE KEY TECHNICAL ISSUES

The WP PMR provides technical information and analyses that relate to three of the KTIs and their associated IRSRs. These include the *Issue Resolution Status Reports Key Technical Issue: Container Life and Source Term* (NRC 1999a), the *Issue Resolution Status Report Key Technical Issue: Total System Performance Assessment and Integration* (NRC 2000), and the *Repository Design and Thermal-Mechanical Effects* (NRC 1999b). Several subissues of these KTIs that relate directly to the WP PMR are discussed in the following sections. Table 4-1 summarizes these KTIs and their subissues that relate directly to this PMR, the related acceptance criteria and PMR approach. In addressing each acceptance criteria, it is assumed that the criteria apply to the DS performance as well.

4.2.1 Container Life and Source Term

The primary issue of the KTI on *Issue Resolution Status Report Key Technical Issue: Container Life and Source Term* (NRC 1999a) is adequacy of the EBS design to provide reasonable assurance that containers will be adequately long-lived, and radionuclide releases from the EBS will be sufficiently controlled, and that the container design and packaging of spent nuclear fuel (SNF) and HLW glass will make a significant contribution to the overall repository performance. The site-specific proposed 10 CFR 63 (Dyer 1999) regulation, currently in the public commenting period, is a performance-based regulation. The current CLST IRSR is mainly focused on the containers and WFs as the primary engineered barriers, but it also considers other engineered sub-system enhancements (i.e., DS, backfill) incorporated as options in the EBS design. For the purpose of this IRSR, the NRC defines the physical boundary of the EBS by the walls of the WP emplacement drifts. The CLST IRSR identifies six subissues and associated general and specific acceptance criteria deemed important to the resolution of this KTI:

1. The effects of corrosion processes on the lifetime of the containers
2. The effects of phase instability of materials and initial defects on the mechanical failure and lifetime of the containers
3. The rate at which radionuclides in SNF are released from the EBS through the oxidation and dissolution of spent fuel
4. The rate at which radionuclides in HLW glass are leached and released from the EBS
5. The effect of in-package criticality on WP and EBS performance
6. The effects of alternate EBS design features on container lifetime and radionuclide release from the EBS.

The IRSR provides acceptance criteria for resolution of each of these subissues from the standpoint of performance of the container materials. Subissues 1, 2, and 5, 6 are related to the WP PMR. The following paragraphs address each of the subissues. Also, specific acceptance criteria related to each of these subissues are discussed in Table 4-1, along with the approach to addressing the criteria and sections of the PMR that describe these approaches. In addressing each acceptance criterion, it is assumed that the criterion applies to DS performance as well.

4.2.1.1 Container Life and Source Term Issue Resolution Status Report General Criteria

In addition to the specific acceptance criteria addressed in Table 4-1, the CLST IRSR includes a set of generic acceptance criteria dealing with expert elicitation and all aspects of data collection, qualification, verification, documentation of uncertainties and limitations in both data and process models. All these general acceptance criteria fall into two NRC's programmatic criteria for QA and the use of expert elicitation. These programmatic criteria apply to all subissues, thus, they are addressed generically for all subissues.

The acceptance criteria for QA addresses DOE's implementation of an adequate QA program. The WP PMR and supporting AMRs were developed in accordance with project procedures for documenting data, analyses, models, and/or computer codes and preparing and reviewing technical reports (see Section 1.4). The programmatic criterion for expert elicitation specifies that DOE conduct expert elicitation in accordance with NUREG-1563 (Kotra et al. 1996) or other acceptable approaches. The WP PMR addresses the NRC's programmatic criteria for QA. No expert elicitation results or data have been used in preparation of this PMR.

4.2.1.2 Container Life and Source Term Issue Resolution Status Report Subissue 1

Subissue 1 considers failure of outer and inner overpacks as a result of various corrosion processes affecting both WP materials, such as dry-air oxidation, humid-air and uniform aqueous corrosion, LC, MIC, SCC and HIC. Models for these corrosion processes have been developed and incorporated into the WP degradation model and are discussed in various parts of the WP PMR. Acceptance criteria related to this subissue and the PMR approach that address the acceptance criteria are provided in Table 4-1.

4.2.1.3 Container Life and Source Term Issue Resolution Status Report Subissue 2

Subissue 2 (NRC 1999a, Sections 4.2 and 5.2) examines long-term degradation of mechanical properties of container materials as a result of prolonged exposures of the WPs (thousands of years) at elevated temperatures. Mechanical failure due to phase instability of WP materials is highly dependent on material chemical composition and processing history. Examples of material instability that can degrade mechanical properties include segregation of metalloid elements such as phosphorus and sulfur, precipitation of carbides of intermetallic phases, and long-range ordering (LRO). Fabrication defects that may lead to early failure of container materials are also the subject of this subissue, as well as the effects of damage due to disruptive events, such as seismicity, faulting, and igneous activity.

Acceptance criteria related to this subissue and the PMR approach that addresses the acceptance criteria are provided in Table 4-1.

4.2.1.4 Container Life and Source Term Subissue 5

Subissue 5 addresses the effects of in-package criticality on WP and engineered barrier subsystem performance. In-package criticality is not addressed in this PMR. However, the related acceptance criteria are addressed in DOE's *Disposal Criticality Analysis Methodology Topical Report* (YMP 1998) and its supporting references.

4.2.1.5 Container Life and Source Term Issue Resolution Status Report Subissue 6

Subissue 6 addresses performance of the alternative EBS design features such as the DS and backfill. The concerns addressed by the NRC in the IRSR relate to the DS design to be fabricated from titanium alloys. These materials can suffer from thermal embrittlement. Both temper embrittlement of steels and thermal embrittlement of titanium alloys occur as a result of a thermally activated redistribution of barely soluble impurities from grain interiors to GB. Titanium alloys have been long recognized for being highly resistant to corrosion as a result of their ability to form a protective oxide film when in contact. The pH and chloride concentrations have been found to have a relatively minor influence on the passive dissolution rate of some titanium alloys, although data are limited in this area. A review of the literature indicates that some of titanium alloys are susceptible to crevice corrosion. Insufficient experimental data are available for titanium-palladium alloys such as Titanium Grade 7 in relevant environments to state with absolute certainty whether or not these materials will undergo crevice corrosion over a period of 10,000 years. It is generally accepted in the material science community that the addition of palladium to titanium does improve the crevice corrosion resistance of such materials. However, given the lack of data for titanium-palladium alloys, further investigation of crevice corrosion is warranted (NRC 1999a).

Environmentally assisted cracking (EAC) of titanium-palladium alloys has not been extensively investigated. Many titanium alloys are susceptible to EAC due to hydrogen embrittlement associated with the precipitation of hydrides ahead of the crack tip. However, the titanium-palladium alloys may be highly resistant to EAC, especially those that have low equivalent oxygen content. The addition of palladium to titanium has also been thought to enhance EAC resistance because hydrogen evolution as H_2 would preferentially take place at Pd-rich sites, thereby decreasing the available atomic hydrogen that could be absorbed into the titanium lattice. It is unclear if this mechanism is operable. Thus, the NRC notes in the CLST IRSR that further DOE investigation of the EAC behavior of titanium-palladium alloys is needed, with particular emphasis on methodologies that would enable monitoring and measurement of slow crack propagation rates (NRC 1999a).

The performance modeling of the DS is addressed in this PMR and the effects and performance of the backfill are addressed in the PMR on EBS. Acceptance criteria related to this subissue and the PMR approach that addresses the acceptance criteria are provided in Table 4-1.

4.2.2 Total System Performance Assessment and Integration

The overall goal of the TSPA Integration KTI (NRC 2000) is to delineate staff's systematic approach for determining compliance with an overall system performance objective. The objective of this KTI is to describe an acceptable methodology for conducting performance

assessments of repository performance and using these assessments to demonstrate compliance with the overall performance objective and requirements for multiple barriers. The TSPAI IRSR identifies four subissues and associated acceptance criteria deemed important to the resolution of this KTI:

1. System Description and Demonstration of Multiple Barriers
2. TSPA Methodology: Scenario Analysis
3. TSPA Methodology: Model Abstraction
4. Demonstration of the Overall Performance Objective

Subissues 1, 2, and 3 are related to the WP PMR. The acceptance criteria for each subissue address fundamental elements of the DOE's TSPA model for the Yucca Mountain site. The following paragraphs address each of the subissues. Also, related acceptance criteria applicable to the WP PMR are discussed in Table 4-1, along with the approach to addressing the criteria. Programmatic acceptance criteria related to the QA and expert elicitation are addressed generically in Section 4.2.1.1 and are not repeated here or in Table 4-1.

4.2.2.1 Subissue 1, System Description and Demonstration of Multiple Barriers

This subissue relates to the transparency and traceability of the analysis that allows for an adequate understanding of DOE's approach and results of the TSPA. Sufficient transparency and traceability of the TSPA analyses and results will convince the NRC that compliance with regulatory criteria will be achieved. The following aspects of transparency and traceability are addressed under this subissue: TSPA document style, structure, and organization FEPs identification and screening; abstraction methodology; data use and validity; assessment results; and code design, data flow, and supporting documentation. Acceptance criteria pertaining to these aspects of the transparency and traceability and the PMR approach in addressing the acceptance criteria are provided in Table 4-1.

4.2.2.2 Subissue 2, Total System Performance Assessment Methodology: Scenario Analysis

This subissue focuses on the attributes of an acceptable methodology for identifying, screening, and selecting FEPs for inclusion in the TSPA. FEPs that could effect future system performance are used to formulate scenarios. This includes construction of scenario classes, assignment of probabilities to scenario classes, and their incorporation into the TSPA. This is a key factor in ensuring the completeness of the TSPA. A systematic method was applied to identify and screen FEPs for WP degradation. A description of this method is provided under Section 1.6. The results of the FEPs screening analyses are also summarized in Table 1-2.

This subissue includes five elements related to the scenario analysis: identification of initial set of processes and events, classification of processes and events, screening of processes and events, formation of scenarios, and screening of scenario classes. Acceptance criteria for these elements and the PMR approach in addressing the acceptance criteria are provided in Table 4-1.

4.2.2.3 Subissue 3, Total System Performance Assessment Methodology: Model Abstraction

This subissue focuses on the information and technical approaches needed to develop defensible model abstractions and their integration into TSPA. The WP degradation model addresses several elements of this subissue that are related to the engineered barrier degradation, mechanical disruption of engineered barriers, and quantity and chemistry of water contacting WPs and WFs. Some of the acceptance criteria for elements listed above that are directly related to the WP PMR and the PMR approach in addressing the acceptance criteria are provided in Table 4-1.

4.2.3 Repository Design and Thermal-Mechanical Effects

The primary focus of the repository design and thermal-mechanical effects (RDTME) KTI is the review of design, construction, and operation of the geologic repository operations area (GROA) with respect to the preclosure and postclosure performance objectives, taking into consideration long-term thermal-mechanical (TM) processes. Consideration of the time-dependent TM coupled response of a jointed rock mass is central to potential repository design and necessary for performance assessment (PA) at the Yucca Mountain (YM) site. Consequently, that is the focus of the preclosure and postclosure elements of this KTI (NRC 1999b, Section 2.1).

The RDTME KTI identifies four subissues and their associated components and acceptance criteria. Only Subissue 3, Thermal-mechanical Effects on Underground Facility Design and Performance, and its major component regarding effect of seismically induced rockfall on WP performance is directly related to this PMR. Table 4-1 addresses the acceptance criterion for rockfall effects and the WP PMR approach.

Table 4-1. Issue Resolution Status Reports, Subissues, Technical Acceptance Criteria, and PMR Approach

NRC Technical Acceptance Criteria	PMR Approach
IRSR: Container Life and Source Term	
SUBISSUE 1 – The Effect of Corrosion Processes on the Lifetime of the Containers	
1. DOE has identified and considered likely modes of corrosion for container materials, including dry-air oxidation, humid-air corrosion, and aqueous corrosion processes, such as GC, LC, MIC, SCC and HIC, as well as the effect of galvanic coupling.	All likely modes of corrosion have been considered and modeled in this PMR (See Section 1.5). The constituent models of this PMR include process models for dry-air oxidation, humid-air corrosion, stress corrosion cracking, HIC, and aqueous corrosion processes, such as GC, LC, and microbial influenced corrosion. Galvanic coupling effects have been minimized.
2. DOE has identified the broad range of environmental conditions within the WP emplacement drifts that may promote the corrosion processes listed previously, taking into account the possibility of irregular wet and dry cycles that may enhance the rate of container degradation.	The corrosion models in this PMR include environmental thresholds that can be used to switch between dominant modes of corrosion. For example, as the WP temperature drops and the RH increases, the mode of attack changes from dry-air oxidation to humid-air or aqueous-phase corrosion. A comparison of the corrosion and threshold potentials is used to determine whether or not LC will occur. WAPDEG uses bounding conditions that envelop wet and dry cycles (see Section 3.2.3) depending upon the condition at a given time step.
3. DOE has demonstrated that the numerical corrosion models used are adequate representations, taking into consideration associated uncertainties, of the expected long-term behaviors and are not likely to underestimate the actual degradation of the containers as a result of corrosion in the repository environment.	Uncertainties are accounted for in corrosion rates. The rate at the 50^{th} percentile is approximately 50 nm y^{-1}, the rate at the 90^{th} percentile is approximately 100 nm y^{-1}, and the maximum rate is 731 nm y^{-1}. About 10 percent of the values fall between 100 and 750 nm y^{-1} (Section 3.1.5). The effects of thermal aging over extended periods of time (10,000 years) is being accounted for in the overall corrosion model for the WPOB (Section 3.1.4).
4. DOE has considered the compatibility of container materials, the range of material conditions, and the variability in container fabrication processes, including welding, in assessing the performance expected in the containers intended waste isolation.	The effects of welding and thermal aging on the corrosion resistance of the WP materials have been accounted for. A fully aged sample of Alloy 22 exhibits a less noble corrosion potential, shifted in the cathodic direction by approximately: 63 mV in the case of SAW at 90°C; 109 mV in the case of SCW at 90°C; and by more than 100 mV in the case of BSW at 100°C. It is assumed that E_{corr} is corrected to account for fully aged material by subtracting approximately 100 mV from values calculated for the base metal. The shift in $E_{critical}$ (threshold potential 1) is approximately 100 mV in most cases. Thus, the difference $E_{critical}$-E_{corr} is virtually unchanged. The effect of thermal aging on the corrosion rate is accounted for in an enhancement factor, G_{aged}, and is based upon a ratio of the non-equilibrium current densities for base metal and aged material. The value of G_{aged} for base metal is approximately one ($G_{aged} \sim 1$), whereas the value of G_{aged} for fully aged material is larger ($G_{aged} \sim 2.5$). Material with less precipitation than the fully aged material would have an intermediate value of G_{aged} ($1 \leq G_{aged} \leq 2.5$) (Section 3.1.4).

Table 4-1. Issue Resolution Status Reports, Subissues, Technical Acceptance Criteria, and PMR Approach (Continued)

NRC Technical Acceptance Criteria	PMR Approach
IRSR: Container Life and Source Term	
SUBISSUE 1 – The Effect of Corrosion Processes on the Lifetime of the Containers	
5. DOE has justified the use of data collected in corrosion tests not specifically designed or performed for the Yucca Mountain repository program for the environmental conditions expected to prevail at the Yucca Mountain site.	The WP degradation process models are based on bounding environmental conditions (temperature, humidity, chemistry, etc.) expected in the proposed repository (See Section 3.1.3). The threshold RH used to determine whether vapor phase attack is by DOX or HAC is based upon the deliquescence point of salt deposits that could form on the WP surface due to aerosol transport. Measurements of GC rates in the vapor and aqueous phases, electrochemical potentials, and other relevant performance data were in test media that can be directly related to water chemistry expected on the WP surface during the service life of Alloy 22. These water chemistries are based upon evaporative concentrations of the standard J-13 well water chemistry. Crevice chemistry is being measured in situ, with and without the presence of buffer ions. In the aqueous phase, a range of temperature extending from room temperature to 120°C is being investigated. The high-temperature limit is based upon the boiling point of a near-saturation water chemistry without buffer. The expected boiling point of the aqueous phase on the WP surface is expected to be lower. In addition to the data generated from long-term and short-term corrosion tests, the process model development also includes data generated outside the YMP. These data in general include testing in environments not directly applicable to the YMP and therefore are used as corroborative information.

Table 4-1. Issue Resolution Status Reports, Subissues, Technical Acceptance Criteria, and PMR Approach (Continued)

NRC Technical Acceptance Criteria	PMR Approach
6. DOE has conducted a consistent, sufficient, and suitable corrosion testing program at the time of the LA submittal. In addition, DOE has identified specific plans for further testing to reduce any significant area(s) of uncertainty as part of the performance confirmation program.	The DOE has established a corrosion test program that addresses all anticipated modes of corrosive attack of the WP. There is a clear linkage between the experimental data being collected and modules in the predictive WAPDEG code that serves as the heart of the TSPA. Data and modules have been developed for each key element of the EDA II design: the WPOB (Alloy 22); the inner structural support (stainless steel 316NG); and the protective DS (Titanium Grade 7). Companion AMRs provide data and modules for the stainless steel 316NG and the Titanium Grade 7 alloy (PMR Section 3.1.4 through 3.1.8). Studies include exposure of over 18,000 samples of candidate WP material in the Long Term Corrosion Test Facility (LTCTF). A large number of pre- and post-exposure measurements of dimension and weight allow establishment of distribution functions for representation of the GC rate. Microscopic examination of samples from the LTCTF and other corrosion tests is done with Scanning Electron Microscopy (SEM), Atomic Force Microscopy (AFM), X-Ray Diffraction (XRD), X-Ray Photoelectron Spectroscopy, Secondary Ion Mass Spectrometry (SIMS), and other state-of-the-art surface analytical techniques. Potentiodynamic and potentiostatic electrochemical tests are conducted with base metal, thermally aged material and simulated welds. Thermally aged material is fully characterized with the transmission electron microscope (TEM) as discussed by Summers and Turchi (CRWMS M&O 2000b). The present test results provide sufficient confidence for the current design. In addition, the Project will continue testing of materials both in the laboratory and in the field. This part of the testing program is covered in the *Performance Confirmation Plan* (CRWMS M&O 2000q). This acceptance criterion pertains directly to the principal factors of the postclosure safety case associated with the degradation and performance of the WP and DS. These principal factors are also associated with one of the performance confirmation factors and will be addressed through testing and analysis identified in the *Performance Confirmation Plan* (CRWMS 2000q). The information obtained in the performance confirmation program is to confirm the corrosion rates and will serve to reduce residual uncertainties regarding long-term corrosion behavior including those arising from corrosion mechanisms not detected in the baseline testing program. See Section 5.3.1.8 and Appendix G of the *Performance Confirmation Plan* (CRWMS M&O 2000q).

Table 4-1. Issue Resolution Status Reports, Subissues, Technical Acceptance Criteria, and PMR Approach (Continued)

NRC Technical Acceptance Criteria	PMR Approach
7. DOE has established a defensible program of corrosion monitoring and testing of the engineered sub-system components during the performance confirmation period to assure they are functioning as intended and anticipated.	This acceptance criterion pertains directly to the principal factors of the postclosure safety case associated with the degradation and performance of the WP and DS. These principal factors are also associated with one of the performance confirmation factors and will be addressed through testing and analysis identified in the *Performance Confirmation Plan* (CRWMS M&O 2000q). The baseline for performance confirmation to address this factor will be information available from site characterization and pre-emplacement testing. Because the DS will not be installed until permanent closure, performance confirmation testing will be confined to laboratory testing to confirm corrosion rates fall within the limits considered in the licensing review (see Section 5.3.1.8 and Appendix G of the Performance Confirmation Plan) and prototype testing (see Sections 5.3.2, 5.3.5.4, and Appendix G of the Performance Confirmation Plan). This information will be considered in evaluating whether the DSs would operate as anticipated and intended (i.e., by comparing with design criteria). Other engineered subsystem components determined not to be important to post-closure safety case will not be addressed in the performance confirmation program. In the current version of the plan, testing to monitor and confirm expectations regarding the effects of other introduced materials to the EBS environment is included in the program. See Section 5.3.1.7 and Appendix G.
SUBISSUE 2 - The effects of phase instability of materials and initial defects on the mechanical failure and lifetime of the containers	
1. DOE has identified and considered the relevant mechanical failure processes that may affect the performance of the proposed container materials.	As described in this report, all likely degradation modes, including HIC and SCC as two possible mechanical failure modes have been considered. Both modes have been included in WAPDEG, and are described in the report (Sections 3.1.7 and 3.1.8, respectively).
2. DOE has identified and considered the effect of material stability on mechanical failure processes for the various container materials as a result of prolonged exposure to the expected range of temperatures and stresses, including the effects of chemical composition, microstructure, thermal treatments, and fabrication processes.	This PMR presents data showing that Alloy 22 has adequate phase stability to serve as a WP material, provided that the temperature is not allowed to exceed 260°C. Expected range of temperature and stresses, chemical composition, microstructure, thermal treatments, and fabrication processes are all related to the material stability and have been considered in modeling in Section 3.1.4 of the PMR.
3. DOE has demonstrated that the numerical models used for container materials stability and mechanical failures are effective representations, taking into consideration associated uncertainties, of the expected materials behavior and are not likely to underestimate the actual rate of failure in the repository environment.	Uncertainties, assumptions, and limitations of the specific models are addressed in the related AMRs. As indicated in Section 3.2.1, the WAPDEG analysis also takes into account quantifiable uncertainties and variability of the degradation model for the possible ranges of corrosion parameters and exposure conditions. The WAPDEG model includes modules for DOX, HAC, APC, SCC and HIC. Also, both GC and LC are considered. The possibility of using either localized thermal annealing or laser peening is considered as a means of mitigating SCC in the WP closure weld.
4. DOE has considered the compatibility of container materials and the variability in container manufacturing processes, including welding, in its WP failure analyses and in the evaluation of radionuclide release.	The design now used prevents galvanic coupling of Titanium Grade 7 with carbon steel, thereby preventing any hydrogen charging of the DS due to the cathodic reduction of hydrogen ions on the titanium surface. Variabilities in processes used for weld stress mitigation are accounted for in the SCC models for both laser peening and induction annealing techniques (See Section 3.1.7).

Table 4-1. Issue Resolution Status Reports, Subissues, Technical Acceptance Criteria, and PMR Approach (Continued)

NRC Technical Acceptance Criteria	PMR Approach
5. DOE has identified the most appropriate methods for nondestructive examination (NDE) of fabricated containers to detect and evaluate fabrication defects in general and, particularly, in seam and closure welds.	An NDE protocol is under development and will be used for DS and WP inspection. Such inspection will limit the size of manufacturing defects as a means of helping prevent SCC and HIC. Materials used in WP construction will be tested electrochemically, to assure that those materials being used are not unexpectedly susceptible to LC.
6. DOE has justified the use of material test results not specifically designed or performed for the Yucca Mountain repository program for environmental conditions (i.e., temperature, stress, and time) expected to prevail at the proposed Yucca Mountain repository.	Various AMRs supporting this report, such as the AMR on degradation of stainless steel (CRWMS M&O 2000e), provide discussion for the use of material test results from published data not specifically designed or performed for the Yucca Mountain repository program for environmental conditions expected to prevail at the proposed Yucca Mountain repository.
7. DOE has conducted a consistent, sufficient, and suitable material testing program at the time of the LA submittal. In addition, DOE has identified specific plans for further testing to reduce any significant area(s) of uncertainty as part of the performance confirmation program.	This acceptance criterion pertains directly to the principal factors of the postclosure safety case associated with the degradation and performance of the WP and DS. These principal factors are also associated with performance confirmation factors and will be addressed through testing and analysis identified in the *Performance Confirmation Plan* (CRWMS M&O 2000q). The baseline for performance confirmation to address them will be information available from site characterization and pre-emplacement testing. This information will include the basis for estimates of the effects of thermal and stress perturbations. The information obtained in the performance confirmation program is to confirm these estimates and will serve to ascertain whether these elements are functioning as intended and anticipated, i.e., meet the design criteria established for them. See Section 5.3.1.8 and Appendix G of the *Performance Confirmation Plan* (CRWMS M&O 2000q).
8. DOE has established a defensible program of monitoring and mechanical testing of the engineered sub-systems components, during the performance confirmation period, to assure they are functioning as intended and anticipated, in the presence of thermal and stress perturbations.	This acceptance criterion pertains directly to the principal factors of the postclosure safety case associated with the degradation and performance of the WP and DS. These principal factors are also associated with performance confirmation factors and will be addressed through testing and analysis identified in the *Performance Confirmation Plan* (CRWMS M&O 2000q). The baseline for performance confirmation to address them will be information available from site characterization and pre-emplacement testing. This information will include the basis for estimates of the effects of thermal and stress perturbations. The information obtained in the performance confirmation program is to confirm these estimates and will serve to ascertain whether these elements are functioning as intended and anticipated, i.e., meet the design criteria established for them. See Section 5.3.1.8 and Appendix G of the *Performance Confirmation Plan* (CRWMS M&O 2000q).
SUBISSUE 5 - The effect of in-package criticality on WP and EBS performance	
Subissue 5 addresses the effects of in-package criticality on WP and engineered barrier subsystem performance. In-package criticality is not addressed in this PMR. However, the related acceptance criteria are addressed in DOE's *Disposal Criticality Analysis Methodology Topical Report* (YMP 1998) and its supporting references.	

Table 4-1. Issue Resolution Status Reports, Subissues, Technical Acceptance Criteria, and PMR Approach (Continued)

NRC Technical Acceptance Criteria	PMR Approach
SUBISSUE 6 - The effects of alternate EBS design features on container lifetime and radionuclide release from the EBS	
1. DOE has identified and considered the effects of backfill, and the timing of its emplacement, on the thermal loading of the repository, WP lifetime (including container corrosion and mechanical failure), and the release of radionuclides from the EBS.	Even though the EDA-II design includes backfill, the effects of the backfill are not considered in determining the environment on the surface DS and WP.
2. DOE has identified and considered the effects of ceramic coating on WP lifetime, including negative consequences as a result of breakdown of the ceramic coating (cracking, spalling, or delamination) in response to the action of environment, manufacturing defects, mechanical impacts and stresses arising from a multiplicity of sources, and the potential for enhanced LC of the containers that might occur at cracks are perforations in the ceramic coating layers.	This criterion is no longer applicable, as the current design for the repository does not include ceramic coatings.
3. DOE has identified ceramic coating materials with outer overpack materials and the combined effect of ceramic coating with backfill on container lifetime.	See response to Criterion 2.
4. DOE has identified and considered the effects of DSs (with backfill) on WP lifetime, including extension of the humid-air corrosion regime, environmental effects, breakdown of DSs and resulting mechanical impacts on WP, the potential for crevice corrosion at the junction between the WP and the DS, and the potential for condensate formation and dripping on the underside of the shield.	The effects of the DS have been considered and evaluated in the analysis of WP performance. This aspect is discussed in Section 3.2.3 of this document. The analysis conservatively assumes that the environment on the surface of the WP is not affected by the presence of the DS. Degradation model for the WP takes into account potential for crevice corrosion and degradation due to mechanical failure and assumes exposure to drift environment with no protection by DS against water dripping. The effects of the backfill with respect to changes in water chemistry are also not assumed since the current design does not include backfill.
5. DOE has evaluated the effect of design changes in container wall thickness that may increase γ-radiolysis of the water contacting WPs and, therefore, enhance the possible occurrence of LC processes.	Experiments have been performed with Alloy 22 to accurately mimic the effects of gamma radiolysis. It is known that gamma radiolysis of aqueous electrolytes produces hydrogen peroxide, and that that hydrogen peroxide increases the open circuit corrosion potential of stainless steels. There has been concern that such effects could push the corrosion potential close to the threshold potential for the initiation of LC. Laboratory experiments have shown that the maximum increase in corrosion potential due to hydrogen peroxide in concentrated repository ground waters is approximately 200 mV, and insufficient to exceed the threshold for initiation of LC (See Section 3.1.6).
6. DOE has identified the chemical composition of the water in the environment surrounding the WP and its evolution with time.	This has been done through both evaporative concentration and thermodynamic calculation.

Table 4-1. Issue Resolution Status Reports, Subissues, Technical Acceptance Criteria, and PMR Approach (Continued)

NRC Technical Acceptance Criteria	PMR Approach
7. DOE has justified the use of test results for the DSs, ceramic coatings, and backfill materials not specifically collected for the Yucca Mountain site for the environmental conditions expected to prevail at the proposed Yucca Mountain repository	At the present time, the ceramic coating is not part of the DS or WP design.
8. DOE has conducted a consistent, sufficient, and suitable corrosion testing program at the time of the LA submittal. In addition, DOE has identified specific plans for further testing to reduce any significant area(s) of uncertainty as part of the performance confirmation program.	The design concept for the EBS includes Alloy 22 material for the WPOB and Titanium Grade 7 for the DS. Alternative EBS materials in each case are being evaluated as part of the design developmental testing, which will provide baseline information for the performance confirmation program for the selected materials. Only selected materials will be considered for continued evaluation in performance confirmation after submittal of the LA. Additional testing on alternative EBS materials may be conducted in mock-up/simulation testing to support assessment of design enhancements; however, this testing would only be considered as part of the performance confirmation program if an alternative material(s) were incorporated into the design through a license amendment and corresponding change to the performance confirmation program. As indicated, testing of the two different materials selected for the WP and DS will be conducted in the performance confirmation program (see Section 5.3.1.8 of the *Performance Confirmation Plan*) (CRWMS M&O 2000q).
IRSR: TOTAL SYSTEM PERFORMANCE ASSESSMENT AND INTEGRATION	
SUBISSUE 1 – System Description and Demonstration of Multiple Barriers	
Transparency and Traceability of the Analysis	
TSPA Documentation Style, Structure, and Organization	
Criterion T1 - Documents and reports are complete, clear, and consistent.	The WP PMR was carefully structured to be complete, clear, and consistent. The review of the draft document included checks for completeness, clarity and consistency.
Criterion T2 - Information is amply cross referenced.	The WP PMR contains ample references to data sources, codes, assumptions, and conclusions.
Features, Events, and Processes Identification and Screening	
Criterion T1 - The screening process by which FEPs were included or excluded from the TSPA is fully described.	Section 1.6 of this PMR summarizes excluded and included FEPs including the rationale for these decisions.
Criterion T2 - Relationships between relevant FEPs are fully described.	Section 1.6 of this PMR describes the relationship between primary and secondary FEPs. The FEPs AMR provides additional documentation including the TSPA disposition of FEPs, IRSR issues relevant to specific FEPs, and analysis and discussion on specific FEPs.

Table 4-1. Issue Resolution Status Reports, Subissues, Technical Acceptance Criteria, and PMR Approach (Continued)

NRC Technical Acceptance Criteria	PMR Approach
Abstraction Methodology	
Criterion T1 - The levels and method(s) of abstraction are described starting from assumptions defining the scope of the assessment down to assumptions concerning specific processes and the validity of given data.	For each model in the WPD PMR, descriptions are provided of process models and, if the models are abstracted, descriptions of the abstractions of the models. The description includes a summary of data and assumptions used to construct models. The AMRs describing the models and the abstracted models provide additional details regarding data and assumptions.
Criterion T2 - A mapping (e.g., a road map diagram, a traceability matrix, a cross-reference matrix) is provided to show what conceptual features (e.g., patterns of volcanic events) and processes are represented in the abstracted models, and by what algorithms.	The WPD PMR provides a sufficient basis for the decisions and assumptions that were made during the abstraction process.
Criterion T3 - An explicit discussion of uncertainty is provided to identify which issues and factors are of most concern or are key sources of disagreement among experts.	The WPD PMR (Section 3.1.9) provides a discussion of uncertainties and limitations for the major process models included in the report. The AMRs describing the abstracted models provide additional details regarding uncertainties and limitations.
Data Use and Validity	
Criterion T1 - The pedigree of data from laboratory tests, natural analogs, and the site is clearly identified.	Section 1.4 of this PMR summarizes the QA status of the data and software used in the component models.
Criterion T2 - Input parameter development and basis for their selection is described.	The WPD PMR discusses input parameter development and the basis for using the parameters. The AMRs describing the models provide additional details regarding input parameter development and the basis for input selection.
Criterion T3 - A thorough description of the method used to identify performance confirmation program parameters.	The *Performance Confirmation Plan* (CRWMS M&O 2000q) specifically addresses the methodology for identifying and selecting parameters that are important to performance based upon TSPA sensitivity analyses and the repository safety strategy. Methods used to collect information for each parameter will be described by the performance confirmation plan or relevant supporting documents to support the license application. Performance confirmation test selection and rationale is also described in the plan based upon the significance of the parameter being measured, and the ability of the test to distinguish construction, emplacement, or time dependent changes in the parameter significant to performance.
Assessment Results	
Criterion T1 - PA results (i.e., the peak expected annual dose within the compliance period) can be traced back to applicable analyses that identify the FEPs, assumptions, input parameters, and models in the PA.	The TSPA-SR summarizes features, processes, conceptual models, and their implementation into the TSPA. This discussion will be based in part on information provided by the WPD PMR.

Table 4-1. Issue Resolution Status Reports, Subissues, Technical Acceptance Criteria, and PMR Approach (Continued)

NRC Technical Acceptance Criteria	PMR Approach
Criterion T2 - The PA results include a presentation of intermediate results that provide insight into the assessment (e.g., results of intermediate calculations of the behavior of individual barriers).	TSPA-SR provides performance analysis results for the total system and will include intermediate results for the components of the system.
Code Design and Data Flow	
Criterion T1 - The flow of information (input and output) between the various modules is clearly described.	TSPA-SR provides a description of information flow between component models including couplings between information and data, conceptual and process-level models, and abstracted models.
Criterion T2 - Supporting documentation (e.g., user's manuals, design documents) clearly describes code structure and relationships between modules.	TSPA-SR describes the TSPA code and provides a reference to supporting documentation such as the user's guide.
SUBISSUE 2 – Total System Performance Assessment Methodology: Scenario Analysis	
Identification of an Initial Set of Processes and Events Data	
Criterion T1 - DOE has identified a comprehensive list of processes and events that: (1) are present or might occur in the Yucca Mountain region and (2) includes those processes and events that have the potential to influence repository performance.	Section 1.6 of this PMR describes the FEP in this PMR. The AMR supporting this section (CRWMS M&O 2000s) provides a list of the processes and events applicable to this PMR. The AMR provides a description of the screening arguments and dispositions for the FEPs and has been thoroughly reviewed by subject matter experts. In addition, the AMR describes the development of the FEPs database, including a description of the FEPs process in sufficient detail to demonstrate the comprehensiveness of the database.
Classification of Processes and Events	
Criterion T1 - DOE has provided adequate documentation identifying how its initial list of processes and events has been grouped into categories.	Section 1.6 of this PMR describes the FEP in this PMR. The AMR supporting this section (CRWMS M&O 2000s) provides documentation and justification for screening arguments and dispositions. Documentation is maintained of all mapping of FEPs into primary and secondary categories. For comprehensiveness, traceability is maintained from the secondary to the related primary FEPs. The AMR also describes the development of the FEPs database, including identifying and classifying relevant FEPs.
Criterion T2 - Categorization of processes and events is compatible with the use of categories during the screening of processes and events.	Section 1.6 of this PMR describes the FEP in this PMR. The AMR supporting this section, (CRWMS M&O 2000s), provides documentation and justification for screening arguments and dispositions. Documentation is maintained of all mapping of FEPs into primary and secondary categories. For comprehensiveness, traceability is maintained from the secondary to the related primary FEPs. The AMR also describes the development of the FEPs database, including identifying and classifying relevant FEPs.

Table 4-1. Issue Resolution Status Reports, Subissues, Technical Acceptance Criteria, and PMR Approach (Continued)

NRC Technical Acceptance Criteria	PMR Approach
Screening of Presses and Events	
Criterion T1 - Categories of processes and events that are not credible for the Yucca Mountain repository because of waste characteristics, repository design, or site characteristics are identified and sufficient justification is provided for DOE's conclusions.	Section 1.6 of this PMR describes the FEP in this PMR. The AMR supporting this section (CRWMS M&O 2000s) provides documentation and justification for screening arguments and TSPA dispositions. Documentation includes a statement of the screening decision for each FEP. Justification is provided for each excluded FEP including the criterion on which it was excluded and the technical basis for the screening argument.
Criterion T2 - The probability assigned to each category of processes and events is consistent with site information, well documented, and appropriately considers uncertainty.	Section 1.6 of this PMR describes the FEP in this PMR. The AMR supporting this section (CRWMS M&O 2000s) provides documentation and justification for screening arguments and dispositions. Probability estimates for FEPs are based on technical analysis of the past frequency of similar events consistent with site information, well documented, and appropriately considers uncertainty.
Criterion T3 - DOE has demonstrated that processes and events screened from the PA on the basis of their probability of occurrence, have a probability of less than one chance in 10,000 of occurring over 10,000 years.	Section 1.6 of this PMR describes the FEP in this PMR. The AMR supporting this section (CRWMS M&O 2000s) provides documentation and justification for screening arguments and TSPA dispositions. Justification is provided for each excluded FEP including the criterion on which it was excluded and the technical basis for the screening argument. For excluded FEPs, documentation includes the criterion on which it was excluded and the technical basis for the screening argument. The probability assigned to FEPs may be one of the screening criteria. FEPs may be excluded only if they can be shown to have a probability of occurrence of less than 10^{-8}/year.
Criterion 4 - DOE has demonstrated that categories of processes and events omitted from the PA on the basis that their omission would not significantly change the calculated expected annual dose, do not significantly change the calculated expected annual dose.	Section 1.6 of this PMR describes the FEP in this PMR. The AMR supporting this section (CRWMS M&O 2000s) provides documentation and justification for screening arguments and TSPA dispositions. For omitted categories, documentation includes the criterion on which it was excluded and the technical basis for the screening argument.
Formation of Scenarios	
Criterion 1 - DOE has provided adequate documentation identifying: (i) whether processes and events have been addressed through consequence model abstraction or scenario analysis and (ii) how the remaining categories of processes and events have been combined into scenario classes.	Section 1.6 of this PMR describes the FEP in this PMR. The AMR supporting this section (CRWMS M&O 2000s) provides documentation and justification for screening arguments and TSPA dispositions. FEPs that have not been excluded are identified as either expected FEPs or disruptive FEPs. Expected FEPs will be included in the TSPA-SR nominal scenario, which is simulated by the base case model described in the TSPA-SR documentation. Disruptive scenarios are constructed from expected FEPs and combinations of disruptive FEPs.
Criterion 2 - The set of scenario classes is mutually exclusive and complete.	Section 1.6 of this PMR describes the FEP in this PMR. The AMR supporting this section (CRWMS M&O 2000s) provides documentation and justification for screening arguments and TSPA dispositions. In addition, the AMR describes the development of the FEPs database including a description of the construction and screening of scenarios.

Table 4-1. Issue Resolution Status Reports, Subissues, Technical Acceptance Criteria, and PMR Approach (Continued)

NRC Technical Acceptance Criteria	PMR Approach
Screening of Scenario Classes	
Criterion 1 - Scenario classes that are not credible for the YM repository because of waste characteristics, repository design, or site characteristics - individually or in combination - are identified and sufficient justification is provided for DOE's conclusions.	TSPA provides justification for screening arguments and TSPA disposition. Scenarios are screened using the same regulatory, probability, and consequence criteria used for screening individual FEPs. Documentation of this process includes identification of any scenarios that have been screened from the analysis and the technical basis for that screening decision.
Criterion 2 - The probability assigned to each scenario class is consistent with site information, well documented, and appropriately considers uncertainty.	TSPA provides justification for screening arguments and TSPA disposition. Probability estimates for scenario classes are based on analyses similar to probabilities assigned for individual FEPs.
Criterion 3 - Scenario classes that combine categories of processes and events may be screened from the PA on the basis of their probability of occurrence, provided: (i) the probability used for screening the scenario class is defined from combinations of initiating processes and events and (ii) DOE has demonstrated that they have a probability of less than one chance in 10,000 of occurring over 10,000 years.	TSPA provides justification for excluding scenario classes. The probability assigned to scenario classes is one of the screening criteria. Scenario classes may be excluded from the TSPA only if they can be shown to have a probability of occurrence of less than 10^{-8}/year. Justification is provided for each excluded scenario class, including the criterion on which it was excluded and the technical basis for the screening argument. In addition, the AMR describes the development of the FEPs database including a description of screening and specifying scenarios for TSPA analysis.
Criterion 4 - Scenario classes may be omitted from the PA on the basis that their omission would not significantly change the calculated expected annual dose, provided DOE has demonstrated that excluded categories of processes and events would not significantly change the calculated expected annual dose.	TSPA provides justification for excluding scenario classes. For excluded scenario classes, documentation includes the criterion on which it was excluded and the technical basis for the screening argument. In addition, the AMR describes the development of the FEPs database including a description of screening and specifying scenarios for TSPA analysis.
SUBISSUE 3 – Total System Performance Analysis Methodology: Model Abstraction	
Engineered Barrier Degradation	
Criterion T1 - Data and Model Justification Sufficient data (field, laboratory or natural analog data) are available to adequately define relevant parameters and conceptual models necessary for developing the WP corrosion abstraction in TSPA. Where adequate data do not exist, other information sources such as expert elicitation have been appropriately incorporated into the TSPA.	The TSPA model requires estimates of corrosion and threshold potentials, both of which are determined through electrochemical testing. Thus far, CP has been done in a wide variety of repository-relevant test solutions, including SDW, SCW, SAW, SCMW, SSW, and BSW. The CP tests are now being conducted in these media with artificial crevices. Experiments have been performed to quantify the extent that pH can be lowered inside crevices, formed between the Alloy 22 WPOB and the 316NG SSSM. The TSPA model also requires estimates of GC rates. Testing in the LTCTF is continuing. Two-year test data has become available and is included in this PMR. These two-year test data are an integral part of the WAPDEG simulation (Sections 3.1.5 and 3.2).

Table 4-1. Issue Resolution Status Reports, Subissues, Technical Acceptance Criteria, and PMR Approach (Continued)

NRC Technical Acceptance Criteria	PMR Approach
Criterion T2 - Data Uncertainty Parameter values, assumed ranges, probability distributions, and bounding assumptions used in the WP corrosion abstraction, such as the critical RH, material properties, pH, and chloride concentration are technically defensible and reasonably account for uncertainties and variabilities.	Model abstractions for various corrosion modes include the aspects of this criterion and documented in the supporting AMRs and Section 3-2 of this PMR.
Criterion T3 - Model Uncertainty Alternative modeling approaches consistent with available data and current scientific understanding are investigated and results and limitations appropriately factored into the WP corrosion abstraction.	Where possible, alternative models are considered. For example, consider methods A and B in the SCC model. Method A is based upon the concept of a threshold stress intensity factor. Method B is based upon the slip dissolution or film rupture model used in the BWR industry. Both are accounted for in the PMR and TSPA calculation. Also consider methods A and B in the LC model. Method A is based upon the concept of exceeding a threshold electrochemical potential for the initiation of LC (crevice corrosion). Method B is based upon the concept of exceeding a threshold temperature of the initiation of LC (crevice corrosion).
Criterion T4 - Model Support WP corrosion abstraction output is justified through comparison to output of detailed process models or empirical observations (laboratory testings, natural analogs, or both).	Output from WAPDEG is being compared to experimental measurements used as the basis of calculations to verify that correct and reasonable results are obtained.
Criterion T5 - Integration Important design features, physical phenomena and couplings, and consistent and appropriate assumptions are incorporated into the WP corrosion abstraction.	The WP degradation model assumes conservative environmental and exposure conditions. WAPDEG code incorporates bounding conditions for the various corrosion modes that envelop effects of design features and couplings.
Mechanical disruption of Engineered Barrier	
Criterion T4 - Model Support Mechanical disruption of the engineered barriers abstraction output is justified through comparison to output of detailed process models or empirical observations (laboratory testing, natural analogs, or both).	Abstraction of mechanical failure of WP due to disruptive events is not in the scope of this PMR. However, will be addressed in addressed in the Disruptive Events PMR.

Table 4-1. Issue Resolution Status Reports, Subissues, Technical Acceptance Criteria, and PMR Approach (Continued)

NRC Technical Acceptance Criteria	PMR Approach
Criterion T5 - Integration Important design features, physical phenomena and couplings, and consistent and appropriate assumptions are incorporated into the mechanical disruption of the engineered barriers abstraction.	Abstraction of mechanical failure of WP due to disruptive events is not in the scope of this PMR. However, will be addressed in addressed in the Disruptive Events PMR.
Quantity and chemistry of water contacting WPs and WFs	
Criterion T1 - Sufficient data (field, laboratory, or natural analog data) are available to adequately define relevant parameters and conceptual models necessary for developing the quantity and chemistry of water contacting WPs and waste forms abstraction in a TSPA. Where adequate data do not exist, other information sources such as expert elicitation have been appropriately incorporated into the TSPA.	Laboratory experiments have been conducted to determine the type of waters that may contact the WP and the drip shield. Evaporative concentration of these waters have been performed to determine bounding concentrations of the solution that is likely to form on the surfaces of the WP and the drip shield. The results of these studies were documented in an AMR (CRWMS M&O 2000a) and in Section 3.1.3. This information has been abstracted for use in the integrated model in WAPDEG. The waste form aspects of this criterion are addressed in the Waste Form PMR. No expert elicitation was used.
Criterion T2 - Parameter values, assumed ranges, probability distributions, and bounding assumptions used in the quantity and chemistry of water contacting WPs and waste forms abstraction, such as the pH, carbonate concentration, chloride concentration, and amount of water flowing in and out of the breached WP, are technically defensible and reasonably account for uncertainties and variability.	The parameters used for defining the chemistry of water contacting the WPs are based on bounding assumptions. The threshold humidity required for maintaining an aqueous film on the surface deposits (the deliquescence point of NaNO3) formed the bounding condition for the relative humidity. The bounding chemistry was assumed to be that expected from the evaporative concentration of the expected Yucca Mountain waters. (CRWMS M&O 2000a, PMR section 3.1.3). The expected quantity of water contacting the WP is not included in the AMR as the corrosion models are not affected by this parameter. The waste form aspects of this criterion are addressed in the Waste Form PMR.
Criterion T3 – Alternative modeling approaches consistent with available data and current scientific understanding are investigated and results and limitations appropriately factored into the quantity and chemistry of water contacting WPs and waste forms abstraction.	The chemistry of the waters contacting the WPs was bounded by the assumptions of evaporative concentration of the water and therefore alternative models are not included in the AMR. Alternative models based on this bounding chemistry for the various degradation modes for the WP and the drip shield were evaluated in each of the specific AMRs and also briefly discussed in Section 3.1.11 of this PMR. The waste form aspects of this criterion are addressed in the Waste Form PMR.
Criterion T4 - Output of quantity and chemistry of water contacting WPs and waste forms abstraction are supported by comparison to output of detailed process models or empirical observations (laboratory testing, natural analogs, or both).	Chemistry of the contacting water was determined by laboratory testing. No process model was developed for this data but the results of this testing were used for developing corrosion test data and process models for material degradation. The quantity of water contacting the WP was not addressed as the degradation models assume bounding chemistries and are independent of the quantity. The waste form aspects of this criterion are addressed in the Waste Form PMR.
Criterion T5 - Important design features, physical phenomena and couplings, and consistent and appropriate assumptions are incorporated into the quantity and chemistry of water contacting WPs and waste forms abstraction.	The analysis for the environment on the surface of the WP is bounding and is based on laboratory testing and is documented in the AMR (CRWMS M&O 2000a) does not take into account the benefits of the design features such as the backfill, and the drip shield. This is to provide a conservative approach. The quantity of the water contacting the WP is not addressed in the PMR.

Table 4-1. Issue Resolution Status Reports, Subissues, Technical Acceptance Criteria, and PMR Approach (Continued)

NRC Technical Acceptance Criteria	PMR Approach
IRSR: REPOSITORY DESIGN AND THERMAL-MECHANICAL EFFECTS, REV. 2	
Subissue 3 – Thermal-Mechanical Effects on Underground Facility design and Performance	
Component 2: Effects of Seismically Induced Rockfall on WP	
Criterion 1 – Approved quality assurance and control procedures and standards are applied to collection, development, and documentation of data, methods, models, and codes.	This PMR and its supporting AMRs were developed in accordance with project procedures for documenting data, analyses, models, and/or computer codes and preparing and reviewing technical reports (see Section 1.4).
Criterion 2 – If used, expert elicitation is conducted and documented in accordance with the guidance in NUREG-1563 or other acceptable approaches.	No expert elicitation results or data have been used in preparation of this PMR.
Criterion 5 – The analytical model used in the estimation of impact load due to rockfall on the WP is: (I) based on reasonable assumptions and site data; (ii) consistent with the underground facility (emplacement drift geometry and backfill) and WP design; and (iii) defensible with respect to providing realistic or bounding estimates of impact loads and stresses.	The rockfall impact analysis for WP is based on reasonable assumptions on site data and on engineered barrier system design. The analyses does not include the presence of backfill. A separate analyses for drip shield has also been performed. The analyses use bounding assumptions with respect to rock size distribution.

5. SUMMARY AND CONCLUSIONS

Performance of a potential monitored geologic repository at Yucca Mountain for high-level radioactive waste depends on both the natural barrier system and the EBS and on their interactions. As a major component of the EBS, the WP contributes to isolation of high-level radioactive waste during the postclosure period and reduces the uncertainties associated with the performance of the repository. It is expected that the WP protected by a DS will be exposed to processes and conditions in the repository environment that will eventually have an impact on its postclosure performance. Some of the important conditions contributing to WP degradation include: humidity and temperature in the emplacement drift, chemistry of the water dripping onto the WP, and corrosion properties of the WPOB. As part of the performance-based risk-informed evaluation of postclosure repository performance, it is important to understand and account for degradation processes that will impact the WP lifetime. This document describes how WP and DS degradation processes are modeled, analyzed, and combined into an overall degradation model; the results from the model are incorporated into the assessment of the postclosure repository total system performance. This PMR also addresses KTIs and IRSRs of the NRC and the approach to the resolution of the issues. In addition, issues on repository performance raised by other agencies such as NWTRB are addressed.

A variety of anticipated modes of WP degradation under the most important environmental conditions including thermal, hydrological, and geochemical conditions have been considered and analyzed as part of an integrated degradation process model. The WP degradation process model consists of individual process models or analyses and associated abstraction models. These models address the environment on the degradation of the WP and DS and consider various degradation modes including early material failure due to manufacturing and fabrication defects, phase stability and aging, GC, LC, stress corrosion cracking, and hydrogen-induced cracking. A generic integrated model constructed based on abstracted results from individual component models is then applied to the WP and DS materials to determine their overall performance. A detailed discussion of the WP and DS degradation processes within the NFE and the analytical results from the process-level models are documented in the individual AMRs. Following is a list of the process-level models:

- Environment on the Surface of DS and WPOB
- Mechanisms for Early Failures
- Aging and Phase Stability of WPOB
- GC and LC of WPOB
- GC and LC of DS
- SCC of the DS, the WPOB and the Stainless Steel Structural Material
- Hydrogen-Induced Cracking (HIC) of DS
- Degradation of Stainless Steel Structural Material.

Abstraction of Models–Abstraction results from the detailed process-level models listed above are used as input to the WP degradation (WAPDEG) model for evaluation of the performance of the WPOB and DS materials. These abstractions include thresholds for corrosion initiation and degradation rate with the associated uncertainty and variability. The WAPDEG analysis results are further abstracted as input to the TSPA-SR analysis. The abstractions include the time-histories of WP failures including the number of penetrations on WPs and the size distribution of penetration openings on WPs including the associated uncertainties. The TSPA-SR uses the results of the abstraction and synthesis of WP degradation information in PA to determine WP lifetime and potential impact on long-term repository performance.

Analysis Results–Abstracted results from the process models described above, along with abstracted results for the drift environment were used as input in the integrated degradation model, WAPDEG. The WAPDEG model, an integrated degradation model, is used for WP and DS degradation analysis and to determine the failure time. This integrated model is based on a stochastic simulation approach and provides a description of waste package and DS degradation, as a function of time and repository location for specific design and thermal-hydrologic modeling assumptions. Each WAPDEG realization corresponds to a complete WAPDEG run for a given number of waste packages. Accordingly, the WAPDEG analysis outputs are reported as a group of "curves" representing the potential range of the output parameters. The nominal case analysis for WP and DS degradation constitutes 100 realizations of WAPDEG simulation that uses 100 input vectors for uncertain corrosion model parameters and simulation parameters that were sampled from their respective ranges.

Except for the RH threshold for corrosion initiation, the temperature and RH do not affect WP and DS degradation. For this reason, representative sets of temperature and RH histories were used in the analysis. In addition, the threshold for LC initiation of the DS and WPOB requires the presence of drips and is much higher than the conditions expected in the repository. Therefore, LC is not expected. The analysis assumed WP failure when the Alloy 22 outer barrier has breached. Therefore, the stainless steel inner structural layer of WP was not considered in the analysis, as this component is not viewed as a corrosion barrier.

The WP and DS degradation analyses have shown that based on the current corrosion model abstractions and assumptions presented in this PMR, both the DSs and WPs do not fail within the regulatory time period (10,000 years). In particular, the WP service lifetime is predicted to extend far beyond the regulatory time period (failure beginning at about 50,000 years). The materials selected for the DS (Titanium Grade 7, an analog of Titanium Grade 16, which has been used for experiments) and the WPOB (Alloy 22) are highly corrosion resistant and, under the repository exposure conditions, are expected to be immune to the degradation processes that, if initiated, could lead to failure in a shorter time period. Those degradation modes are LC (pitting and crevice corrosion), SCC, and HIC (applicable to the DS only). Both the DS and WP degrade by GC at very low passive dissolution rates. The current experimental data and detailed process-level analyses, upon which the model abstractions incorporated in the WAPDEG analysis are based, have also indicated that the candidate materials would not be subject to those rapidly penetrating corrosion modes under the expected repository conditions, except for possibly the closure-lid welds of the WP, if SCC were to occur there. To preclude SCC, weld stress mitigation will be implemented on a dual-lid WP closure weld design.

The estimated long life-time of the WPs in the current analysis is attributed mostly to 1) the depth of the stress mitigation in the dual-closure-lid welds and 2) the very low general-corrosion rate of the closure-lid welds, which requires a very long time to corrode away the compressive stress zones, thus providing a very long delay time before initiating SCC crack growth.

This document may be affected by technical product input information that requires confirmation. Any changes to the document that may occur as a result of completing the confirmation activities will be reflected in subsequent revisions. The status of the input information quality may be confirmed by review of the Document Input Reference System (DIRS) database.

INTENTIONALLY LEFT BLANK

6. REFERENCES

6.1 DOCUMENTS CITED

ASM International 1987. *Corrosion.* Volume 13 of *Metals Handbook.* 9th Edition. Metals Park, Ohio: ASM International. TIC: 209807.

Budnitz, B.; Ewing, R.C.; Moeller, D.W.; Payer, J.; Whipple, C.; and Witherspoon, P.A. 1999. *Peer Review of the Total System Performance Assessment-Viability Assessment Final Report.* Las Vegas, Nevada: Total System Performance Assessment Peer Review Panel. ACC: MOL.19990317.0328.

Cohon, J.L. 1999a. Reaction to Information Presented by the DOE, September 14-15, 1999 Nuclear Waste Technical Review Board Meeting. Letter from J.L. Cohon (NWTRB) to L.H. Barrett (DOE/OCRWM), November 10, 1999. ACC: MOL.20000321.0152.

Cohon, J.L. 1999b. Comments on the Scientific Program, June 1999 Nuclear Waste Technical Review Board Meeting. "Letter from J.L. Cohon (NWTRB) to L.H. Barrett (OCRWM), August 3, 1999." ACC: MOL.20000317.0405.

CRWMS M&O 1994. *Total System Performance Assessment - 1993: An Evaluation of the Potential Yucca Mountain Repository.* B00000000-01717-2200-00099 REV 01. Las Vegas, Nevada: CRWMS M&O. ACC: NNA.19940406.0158.

CRWMS M&O 1995. *Total System Performance Assessment - 1995: An Evaluation of the Potential Yucca Mountain Repository.* B00000000-01717-2200-00136 REV 01. Las Vegas, Nevada: CRWMS M&O. ACC: MOL.19960724.0188.

CRWMS M&O 1996. *Waste Package Materials Selection Analysis.* BBA000000-01717-0200-00020 REV 00. Las Vegas, Nevada: CRWMS M&O. ACC: MOL.19961203.0112.

CRWMS M&O 1998a. *Total System Performance Assessment - Viability Assessment Base Case.* B00000000-01717-0210-00011 REV 01. Las Vegas, Nevada: CRWMS M&O. ACC: MOL.19981202.0279.

CRWMS M&O 1998b. "Waste Package Degradation Modeling and Abstraction." Chapter 5 of *Total System Performance Assessment-Viability Assessment (TSPA-VA) Analyses Technical Basis Document.* B00000000-01717-4301-00005 REV 01. Las Vegas, Nevada: CRWMS M&O. ACC: MOL.19981008.0005.

CRWMS M&O 1999a. *Monitored Geologic Repository Project Description Document.* B00000000-01717-1705-00003 REV 00 DCN 01. Las Vegas, Nevada: CRWMS M&O. ACC: MOL.19991117.0160.

CRWMS M&O 1999b. *Development Plan for Waste Package Degradation Process Model Report.* TDP-WIS-MD-000030 REV 00. Las Vegas, Nevada: CRWMS M&O. ACC: MOL.19991220.0375.

CRWMS M&O 1999c. *Classification of the MGR Uncanistered Spent Nuclear Fuel Disposal Container System.* ANL-UDC-SE-000001 REV 00. Las Vegas, Nevada: CRWMS M&O. ACC: MOL.19990928.0216.

CRWMS M&O 1999d. *1101213PM7 Waste Package Analyses & Models - PMR.* Activity Evaluation, September 21, 1999. Las Vegas, Nevada: CRWMS M&O. ACC: MOL.19991012.0219.

CRWMS M&O 1999e. *Requirements Document for WAPDEG 4.0.* STN: 10000-4.0-00, SDN: 10000-RD-4.0-00. Las Vegas, Nevada: CRWMS M&O. ACC: MOL.19991025.0069.

CRWMS M&O 1999f. *Waste Package Material Properties.* BBA000000-01717-0210-00017 REV 00. Las Vegas, Nevada: CRWMS M&O. ACC: MOL.19990407.0172.

CRWMS M&O 2000a. *Environment on the Surfaces of the Drip Shield and Waste Package Outer Barrier.* ANL-EBS-MD-000001 REV 00. Las Vegas, Nevada: CRWMS M&O. ACC: MOL.20000328.0590.

CRWMS M&O 2000b. *Aging and Phase Stability of Waste Package Outer Barrier.* ANL-EBS-MD-000002 REV 00. Las Vegas, Nevada: CRWMS M&O. ACC: MOL.20000410.0407.

CRWMS M&O 2000c. *General Corrosion and Localized Corrosion of Waste Package Outer Barrier.* ANL-EBS-MD-000003 REV 00. Las Vegas, Nevada: CRWMS M&O. ACC: MOL.20000202.0172.

CRWMS M&O 2000d. *General Corrosion and Localized Corrosion of the Drip Shield.* ANL-EBS-MD-000004 REV 00. Las Vegas, Nevada: CRWMS M&O. ACC: MOL.20000329.1185.

CRWMS M&O 2000e. *Degradation of Stainless Steel Structural Material.* ANL-EBS-MD-000007 REV 00. Las Vegas, Nevada: CRWMS M&O. ACC: MOL.20000329.1188.

CRWMS M&O 2000f. *Stress Corrosion Cracking of the Drip Shield, the Waste Package Outer Barrier and the Stainless Steel Structural Material.* ANL-EBS-MD-000005 REV 00. Las Vegas, Nevada: CRWMS M&O. ACC: MOL.20000504.0312.

CRWMS M&O 2000g. *WAPDEG Analysis of Waste Package and Drip Shield Degradation.* ANL-EBS-PA-000001 REV 00. Las Vegas, Nevada: CRWMS M&O. ACC: MOL.20000526.0332.

CRWMS M&O 2000h. *Hydrogen Induced Cracking of Drip Shield.* ANL-EBS-MD-000006 REV 00. Las Vegas, Nevada: CRWMS M&O. ACC: MOL.20000329.1179.

CRWMS M&O 2000i. *Calculation of General Corrosion Rate of Drip Shield and Waste Package Outer Barrier to Support WAPDEG Analysis.* CAL-EBS-PA-000002 REV 00. Las Vegas, Nevada: CRWMS M&O. ACC: MOL.20000319.0047.

CRWMS M&O 2000j. *Abstraction of Models of Stress Corrosion Cracking of Drip Shield and Waste Package Outer Barrier and Hydrogen Induced Corrosion of Drip Shield.* ANL-EBS-PA-000004 REV 00. Las Vegas, Nevada: CRWMS M&O. ACC: MOL.20000526.0326.

CRWMS M&O 2000k. *Calculation of Probability and Size of Defect Flaws in Waste Package Closure Welds to Support WAPDEG Analysis.* CAL-EBS-PA-000003 REV 00. Las Vegas, Nevada: CRWMS M&O. ACC: MOL.20000424.0676.

CRWMS M&O 2000l. Not used.

CRWMS M&O 2000m. *Analysis of Mechanisms for Early Waste Package Failure.* ANL-EBS-MD-000023 REV 01. Las Vegas, Nevada: CRWMS M&O. ACC: MOL.20000223.0878.

CRWMS M&O 2000n. *Abstraction of Models for Pitting and Crevice Corrosion of Drip Shield and Waste Package Outer Barrier.* ANL-EBS-PA-000003 REV 00. Las Vegas, Nevada: CRWMS M&O. ACC: MOL.20000526.0327.

CRWMS M&O 2000o. *Abstraction of Models for Stainless Steel Structural Material Degradation.* ANL-EBS-PA-000005 REV 00. Las Vegas, Nevada: CRWMS M&O. ACC: MOL.20000526.0337.

CRWMS M&O 2000p. *Incorporation of Uncertainty and Variability of Drip Shield and Waste Package Degradation in WAPDEG Analysis.* ANL-EBS-MD-000036 REV 00. Las Vegas, Nevada: CRWMS M&O. ACC: MOL.20000526.0333.

CRWMS M&O 2000q. *Performance Confirmation Plan.* TDR-PCS-SE-000001 REV 01. Las Vegas, Nevada: CRWMS M&O. ACC: MOL.20000302.0312.

CRWMS M&O 2000r. *Drift Scale Thermal Analysis.* CAL-WIS-TH-000002 REV 00. Las Vegas, Nevada: CRWMS M&O. ACC: MOL.20000420.0401.

CRWMS M&O 2000s. *FEPs Screening of Processes and Issues in Drip Shield and Waste Package Degradation.* ANL-EBS-PA-000002 REV 00. Las Vegas, Nevada: CRWMS M&O. ACC: MOL.20000526.0334.

CRWMS M&O 2000t. *Emplacement Drift System Description Document.* SDD-EDS-SE-000001 REV 00. Las Vegas, Nevada: CRWMS M&O. ACC: MOL.20000121.0119.

CRWMS M&O 2000u. *Waste Package Operations Fabrication Process Report.* TDR-EBS-ND-000003 REV 00. Las Vegas, Nevada: CRWMS M&O. ACC: MOL.20000217.0244.

CRWMS M&O 2000v. *Disruptive Events FEPs.* ANL-WIS-MD-000005 REV 00. Las Vegas, Nevada: CRWMS M&O. ACC: MOL.20000501.0227.

CRWMS M&O 2000w. *Repository Safety Strategy: Plan to Prepare the Postclosure Safety Case to Support Yucca Mountain Site Recommendation and Licensing Considerations.* TDR-WIS-RL-000001 REV 03. Las Vegas, Nevada: CRWMS M&O. ACC: MOL.20000119.0189.

CRWMS M&O 2000x. *Internal Pressurization Due to Fuel Rod Rupture in Waste Packages.* CAL-EBS-ME-000005 REV 00. Las Vegas, Nevada: CRWMS M&O. ACC: MOL.20000315.0671.

Deutsch, C.V. and Journel, A.G. 1992. *GSLIB Geostatistical Software Library and User's Guide.* New York, New York: Oxford University Press. TIC: 224174.

DOE (U.S. Department of Energy) 1995. *The Nuclear Waste Policy Act, As Amended. With Appropriations Acts Appended.* DOE/RW-0438, Rev. 1. Washington, D.C.: U.S. Department of Energy, Office of Civilian Radioactive Waste Management. ACC: HQO.19950124.0001.

DOE (U.S. Department of Energy) 1998. *Total System Performance Assessment.* Volume 3 of *Viability Assessment of a Repository at Yucca Mountain.* DOE/RW-0508. Washington, D.C.: U.S. Department of Energy, Office of Civilian Radioactive Waste Management. ACC: MOL.19981007.0030.

DOE (U.S. Department of Energy) 2000. *Quality Assurance Requirements and Description.* DOE/RW-0333P, Rev. 10. Washington, D.C.: U.S. Department of Energy, Office of Civilian Radioactive Waste Management. ACC: MOL.20000427.0422.

Dyer, J.R. 1999. "Revised Interim Guidance Pending Issuance of New U.S. Nuclear Regulatory Commission (NRC) Regulations (Revision 01, July 22, 1999), for Yucca Mountain, Nevada." Letter from J.R. Dyer (DOE/YMSCO) to D.R. Wilkins (CRWMS M&O), September 3, 1999, OL&RC:SB-1714, with enclosure, "Interim Guidance Pending Issuance of New NRC Regulations for Yucca Mountain (Revision 01)." ACC: MOL.19990910.0079.

Erbing Falkland, M.L. 2000. "Duplex Stainless Steels." *Uhlig's Corrosion Handbook.* Revie, R.W., ed. 2nd Edition. 651-666. New York, New York: John Wiley & Sons. TIC: 247904. Copyright Requested Library Tracking Number-247904.

Haynes International. 1993. Haynes 625 Alloy. Kokomo, Indiana: Haynes International. TIC: 239935.

Khaleel, M.A.; Chapman, O.J.V.; Harris, D.O.; and Simonen, F.A. 1999. "Flaw Size Distribution and Flaw Existence Frequencies in Nuclear Piping." *Probabilistic and Environmental Aspects of Fracture and Fatigue: The 1999 ASME Pressure Vessels and Piping Conference. PVP-386,* 127-144. New York, New York: American Society of Mechanical Engineers. TIC: 245621.

Kotra, J.P.; Lee, M.P.; Eisenberg, N.A.; and DeWispelare, A.R. 1996. *Branch Technical Position on the Use of Expert Elicitation in the High-Level Radioactive Waste Program.* NUREG-1563. Washington, D.C.: U.S. Nuclear Regulatory Commission. TIC: 226832.

Lu, J. ed. 1996. *Handbook of Measurement of Residual Stresses.* Lilburn, Georgia: Fairmont Press. On Order Library Tracking Number-247903.

Mohr, W.C. 1996. "Internal Surface Residual Stresses in Girth Butt-Welded Steel Pipes ." *Residual Stresses in Design, Fabrication, Assessment and Repair, PVP-Vol. 321,* 37-44. New York, New York: American Society of Mechanical Engineers. TIC: 247502.

NRC (U.S. Nuclear Regulatory Commission) 1999a. *Issue Resolution Status Report Key Technical Issue: Container Life and Source Term.* Rev. 2. Washington, D.C.: U.S. Nuclear Regulatory Commission. TIC: 245538.

NRC (U.S. Nuclear Regulatory Commission) 1999b. *Issue Resolution Status Report Key Technical Issue: Repository Design and Thermal-Mechanical Effects.* Rev. 02. Washington, D.C.: U.S. Nuclear Regulatory Commission. ACC: MOL.20000306.0670.

NRC (U.S. Nuclear Regulatory Commission) 2000. *Issue Resolution Status Report Key Technical Issue: Total System Performance Assessment and Integration.* Rev. 2. Washington, D.C.: U.S. Nuclear Regulatory Commission. TIC: 247614.

Pasupathi, V. 2000. Documentation of Literature on Residual Stress Measurements. Interoffice correspondence from V. Pasupathi (CRWMS M&O) to G.M. Gordon, May 19, 2000, LV.WP.VP.05/00-070, with enclosures. ACC: MOL.20000522.0146.

Shcherbinskii, V.G. and Myakishev, V.M. 1970. "Statistical Distribution of Welding Defects with Respect to Azimuth." No. 4, July-August, 1970, 1971 *Central Scientific Research Institute of Technical Engineering, translated from Defektoskopiya.* UDC 620.179.16. 143-144. New York, New York: Plenum Publishing Corporation. Copyright Requested Library Tracking Number-247890.

YMP (Yucca Mountain Project) 1998. *Disposal Criticality Analysis Methodology Topical Report.* YMP/TR-004Q, Rev. 0. Las Vegas, Nevada: Yucca Mountain Site Characterization Office. ACC: MOL.19990210.0236.

6.2 CODES, STANDARDS, REGULATIONS, AND PROCEDURES

64 FR 46976. 40 CFR 197: Environmental Radiation Protection Standards for Yucca Mountain, Nevada; Proposed Rule. Readily Available

ASME (American Society of Mechanical Engineers) 1995. "Materials." Section II of *1995 ASME Boiler and Pressure Vessel Code.* New York, New York: American Society of Mechanical Engineers. TIC: 245287.

ASTM B 443 - 93. 1995. *Standard Specification for Nickel-Chromium-Molybdenum-Columbium Alloy (UNS N06625)* Plate, Sheet, and Strip 1.* Philadelphia, Pennsylvania: American Society for Testing and Materials. TIC: 237693.

ASTM B 575-99a. 1999. *Standard Specification for Low-Carbon Nickel-Molybdenum-Chromium, Low-Carbon Nickel-Chromium-Molybdenum, Low-Carbon Nickel-Chromium-Molybdenum-Copper, Low-Carbon Nickel-Chromium-Molybdenum-Tantalum, and Low-Carbon Nickel-Chromium-Molybdenum-Tungsten Alloy Plate, Sheet, and Strip.* West Conshohocken, Pennsylvania: American Society for Testing and Materials. TIC: 247534.

ASTM C 1174-97. 1997. *Standard Practice for Prediction of the Long-Term Behavior of Materials, Including Waste Forms, Used in Engineered Barrier Systems (EBS) for Geological Disposal of High-Level Radioactive Waste.* West Conshohocken, Pennsylvania: American Society for Testing and Materials. TIC: 246015.

ASTM G 1-90 (Reapproved 1999). 1990. *Standard Practice for Preparing, Cleaning, and Evaluating Corrosion Test Specimens.* West Conshohocken, Pennsylvania: American Society for Testing and Materials. TIC: 238771.

ASTM G 5 - 94. *Standard Reference Test Method for Making Potentiostatic and Potentiodynamic Anodic Polarization Measurements.* Philadelphia, Pennsylvania: American Society for Testing and Materials. TIC: 231902.

ASTM G 61-86 (Reapproved 1998). 1987. *Standard Test Method for Conducting Cyclic Potentiodynamic Polarization Measurements for Localized Corrosion Susceptibility of Iron-, Nickel-, or Cobalt-Based Alloys.* West Conshohocken, Pennsylvania: American Society for Testing and Materials. TIC: 246716.

ASTM G1-81. 1987. *Standard Practice for Preparing, Cleaning, and Evaluating Corrosion Test Specimens.* Philadelphia, Pennsylvania: American Society for Testing and Materials. TIC: 246089.

AP-2.14Q, Rev. 0, ICN 1. *Review of Technical Products.* Washington, D.C.: U.S. Department of Energy, Office of Civilian Radioactive Waste Management. ACC: MOL.20000405.0477.

AP-3.10Q, Rev. 02, ICN 1. *Analyses and Models.* Washington D.C.: U.S. Department of Energy, Office of Civilian Radioactive Waste Management. ACC: MOL.20000512.0066.

AP-3.11Q, Rev. 1, ICN 0. *Technical Reports.* Washington, D.C.: U.S. Department of Energy, Office of Civilian Radioactive Waste Management. ACC: MOL.20000516.0008.

AP-3.15Q, Rev. 1, ICN 1. *Managing Technical Product Inputs.* Washington, D.C.: U.S. Department of Energy, Office of Civilian Radioactive Waste Management. ACC: MOL.20000218.0069.

AP-SIII.2Q, Rev. 0, ICN 2. *Qualification of Unqualified Data and the Documentation of Rationale for Accepted Data.* Washington, D.C.: U.S. Department of Energy, Office of Civilian Radioactive Waste Management. ACC: MOL.19991214.0625.

QAP-2-0 Rev. 5, ICN 1. *Conduct of Activities.* Las Vegas, Nevada: CRWMS M&O. ACC: MOL.19991109.0221.

QAP-2-3, Rev. 10. *Classification of Permanent Items.* Las Vegas, Nevada: CRWMS M&O. ACC: MOL.19990316.0006.

6.3 SOURCE DATA

MO9910SPAFWPWF.001. Weld Flaws of Waste Packages. Submittal date: 10/22/1999.

INTENTIONALLY LEFT BLANK